The Hong Kong Polytechnic University

Department of Civil and Structural Engineering

Photodegradation of indoor air pollutants by photocatalyst TiO_2

by

AO CHIO-HANG

A thesis submitted in partial fulfillment of the requirements for Degree of Doctor of Philosophy

February, 2005

CERTIFICATE OF ORIGINALITY

I hereby declare that this thesis is my own work and that, to the best of my knowledge and belief, it reproduces no material previously published or written nor material which has been accepted for the award of any other degree or diploma, expect where due acknowledgement has been made in the text.

____________________________ (Signed)

Ao Chio-Hang ________________ (Name of student)

ABSTRACT

Indoor air quality received great attention after the energy crisis in the 70's. Buildings were designed to be more airtight to save energy consumption. Consequently, employees complained about increasing sickness such as headache and irritating eyes. Later, studies showed that these sickness are related to the elevated indoor air pollutant concentrations, which is known as Sick Building Syndrome (SBS).

Traditional gaseous pollutant removal method such as physical adsorption or air scrubbing is not suitable for indoor air purification since the quantity and the concentration of the pollutant in indoor air is too low. The aforementioned methods are costly and require frequent replacement.

Photocatalysis offers a new alternative for gaseous pollutant removal. It actually oxidizes pollutant into harmless compound such as H_2O and CO_2. Furthermore, it works under room temperature and atmospheric pressure. However, the use of photocatalysis for indoor air purification is rare.

This study aims to investigate the use of photocatalysis for indoor air purification. Common indoor air pollutants such as nitrogen monoxide (NO), nitrogen dioxide (NO_2), carbon monoxide (CO), sulfur dioxide (SO_2), volatile organic compounds (VOCs) and formaldehyde (HCHO) were selected as target compounds with reference to its typical indoor air pollutant concentration. Sensitive analyses were conducted with the aforementioned pollutants, either separately or concurrently, under different residence time, humidity levels, initial concentrations, irradiation time and ultra violet lamp intensities in a continuously flow reactor and photocatalyst TiO_2. Inhibitory and promotion effect was observed between concurrent photodegradation of multiple pollutants. The photodegradation rate,

in general, decreased with decreasing residence time, decreasing ultra violet intensity and increasing humidity levels. The adverse effect of humidity levels is the largest amount the sensitive analyses.

To rectify the humidity levels problem, photocatalyst TiO_2 was modified but the result was not significant. TiO_2 was then immobilized on an activated carbon filter (TiO_2/AC). Results showed that the pollutant removal efficiency, especially VOCs, was significantly increased even at high humidity levels.

Apart from using glass fiber filter and activated carbon filter as coating substrate, TiO_2 was also coated on stainless steel by liquid phase deposition (LPD). The TiO_2 thin film was calcinated under different temperatures. Surface characterization methods such as Fourier Transform Infrared Spectroscopy (FTIR), X-ray diffraction (XRD), Scanning Electron microscope (SEM), Photoluminescence Spectra (PL), and X-ray Photoelectron Spectroscopy (XPS) were applied to characterize the photocatalyst calcinated under different temperatures. The as-prepared TiO_2 thin films contained not only Ti and O elements, but also a small amount of F, N and Fe elements. No activity was observed when the TiO_2 was calcinated at a temperature under 400 °C since the TiO_2 thin film was composed of amorphous TiO_2. The amount of Fe^{3+}, which was contributed by the diffusion from substrate, affected the photoactivity of the TiO_2 thin film. An optimum content of Fe^{3+} was observed for the photodegradation of NO.

The pollutant removal efficiency of the TiO_2/AC filter was further evaluated by placing it inside a commercially available air cleaner. The air cleaner was tested inside an environmental chamber. Results also showed that the pollutant removal efficiency of the TiO_2/AC filter is higher and faster than TiO_2 only. Furthermore, the TiO_2/AC filter with a set of ultra violet lamps was installed in the air duct inside an office to investigate the pollutant removal efficiency in a practical field. Results showed that pollutant removal, including bacteria was observed.

The use of photocatalytic technology is suitable for indoor air purification. To increase its efficiency for practical application, it is necessary to combine photocatalyst with adsorbent. This method is successful and evaluated by the laboratory-scale reactor, practical application such as air cleaner and on-site testing (commercial office). Thus, the use of photocatalyst and adsorbent showed a promising direction for indoor air purification in which the pollutant concentration is low and high humidity levels are often encountered.

PUBLICATIONS ARISING FROM THE THESIS

International journal

1. Lee, S.C., Li, W.M., **Ao, C.H.** (2002). Investigation of indoor air quality at residential homes in Hong Kong-case study. *Atmospheric Environment, 36,* 225-237.
2. **Ao, C.H.,** Lee, S.C., Mak, C.L., Chan, L.Y. (2003). Photodegradation of volatile organic compounds (VOCs) and NO for indoor air purification using TiO_2: promotion versus inhibition effect of NO. *Applied Catalysis B: Environmental, 42,* 119-129.
3. **Ao, C.H.,** Lee, S.C., Yu, J.C. (2003). Photocatalyst TiO_2 supported on glass fiber for indoor air purification: effect of NO on the photodegradation of CO and NO_2. *Journal of Photochemistry and Photobiology A: Chemistry, 156,* 171-177.
4. **Ao, C.H.,** Lee, S.C. (2003). Enhancement effect of TiO_2 immobilized on activated carbon filter for the photodegradation of pollutants at typical indoor air level. *Applied Catalysis B: Environmental, 44, 191-205.*
5. **Ao, C.H.,** Lee, S.C. (2004). Combination effect of activated carbon with TiO_2 for the photodegradation of binary pollutants at typical indoor air level. *Journal of Photochemistry and Photobiology A: Chemistry, 161,* 131-140.
6. **Ao, C.H.,** Lee, S.C., Zou, S.C., Mak, C.L. (2004). Inhibition effect of SO_2 on NO_x and VOCs during the photodegradation of synchronous indoor air pollutants at parts-per-billion (ppb) level by TiO_2. *Applied Catalysis B: Environmental, 49,* 187-193.

7. **Ao, C.H.,** Lee, S.C., (2005). Indoor air purification by photocatalyst TiO_2 immobilized on an activated carbon filter installed in an air cleaner. *Chemical Engineering Science,* 60, 103-109.

8. **Ao, C.H.,** Lee, S.C., Yu, J.Z., Yu, J.H., (2004). Photodegradation of formaldehyde by photocatalyst TiO_2: Effects on the presences of NO, SO_2 and VOCs. *Applied Catalysis B: Environmental,* 54, 41-50.

9. Li, F.B., Li, X.Z., **Ao, C.H.,** Lee, S.C., Hou, M.F., (2004). Enhanced Photocatalytic Degradation of Volatile Organic Compounds (VOCs) by Lanthanide Ions Doped TiO_2 for Indoor Air Purification. *Chemosphere,* in press.

10. Li, F.B., Li, X.Z., **Ao, C.H.,** Hou, M.F., Lee, S.C., (2004). Higher Photocatalytic Activity for NO Conversion of TiO_2 by Hydrothermal Processes for Air Pollution Control. *Applied Catalysis B: Environmental*, 54, 275-283

11. Yu, H.G., Yu, J.G., Cheng, B., **Ao, C.H.,** Lee, S.C., (2005). Effects of Substrates on the Composition and Microstructure of TiO_2 Thin Films Prepared by the LPD method. *Key Engineering Materials*, 280-283, 795-800.

International conference paper

Ao, C.H., Lee, S.C., (2002). Application of heterogeneous photodegradation of indoor air level NO_x under U.V. irradiation. *The 9th International Conference on Indoor Air Quality and Climate (Indoor Air 2002),* Monterey, California, 706-711.

Ao, C.H., Lee, S.C., (2002). Removal of indoor air ppb level volatile organic compounds (VOCs) and NO_x by heterogeneous photocatalysis. *Better Air Quality in Asian and Pacific Rim Cities (BAQ 2002)*, Hong Kong SAR, PS-37-1 - PS-37-5.

Ao, C.H., Lee, S.C., (2003). Removal of multiple air pollutants by the photocatalyst TiO_2 loaded on adsorbent. *International Conference on Pollution in the Metropolitan and Urban Environment (POLMET 2003),* Hong Kong SAR, section 7A.

Ao, C.H., Lee, S.C., (2004). Application of environmental nanotechnology: Titanium dioxide (TiO_2) coated on activated carbon filter in a commercial air cleaner. *International Symposium on Environmental Nanotechnology 2004*, Taipei, Taiwan, 139-142.

ACKNOWLEDGEMENTS

I would like to thank my supervisor, Dr. S.C. Lee, for his unanimous and sincere support and supervision throughout this project. Without his guidance and advice, the completion of this thesis is unachievable. Sincere thanks to our laboratory technician, Mr. W.F. Tam, is inevitable for his technical. Dr. Ho Kin Fai, my former colleague is acknowledged for his precious suggestion for this project. Dr. L.Y. Chan, my co-supervisor, is also acknowledged for his support and suggestion.

I would also like to thank Mrs. Anson and Charles Griffith for the help of the use of English for technical writing. Special thanks are given to the support from my Church and Opus Dei. The support from my family and Catherine Lau is gratefully acknowledged.

Finally, the financial support from the Hong Kong Polytechnic University (GW-047) is acknowledged.

TABLE OF CONTENTS

Certificate of Originality	I
Abstract	II
Publications arising from the thesis	IV
Acknowledgements	VII
Table of Contents	VIII
List of Figures	XVIII
List of Tables	XXIII

CHAPTER 1 INTRODUCTION

1.1 Background	1
1.2 Objectives	4

CHAPTER 2 LITERATURE REVIEW

2.1 Photocatalysis	6
2.1.1 Background	6
2.1.2 Mechanism	7
2.1.3 Kinetics	9
2.1.4 Reactor	15
2.1.4.1 Fluidized bed reactor	17
2.1.4.2 Annular reactor	20
2.2 Synthesis of photocatalyst	21
2.2.1 Liquid phase deposition (LPD)	21
2.2.2 Sol-gel method	25
2.3 Methods for improving activity of photocatalyst	29

2.3.1 Metals and ions doping 30

2.3.2 Photocatalyst loaded on adsorbent 32

2.4 Effects of common indoor environmental parameters on pollutant photodegradation 36

2.4.1 Effects of temperature 36

2.4.2 Effects of initial pollutant concentration 37

2.4.3 Effects of residence time 38

2.4.4 Effects of humidity levels 40

2.5 The impact of indoor air pollutants on health and removal by photocatalysis 43

2.5.1 Nitrogen oxides (NO_x) 45

2.5.2 Volatile organic compounds (VOCs) 48

2.5.3 Carbon monoxide (CO) 56

2.5.4 Sulfur dioxide (SO_2) 59

2.5.5 Formaldehyde (HCHO) 60

2.5.6 Airborne bacteria 63

2.6 Photodegradation of multiple pollutants 65

CHAPTER 3 METHODOLOGY

3.1 Introduction 67

3.2 Target pollutants 67

3.2.1 Common indoor air pollutants 67

3.2.2 Pollutant concentration and analytical methods 68

3.2.3 Photodegradation of multiple pollutants 70

3.3 Photocatalytic activity evaluation 71

3.3.1 Photocatalytic activity evaluated in a laboratory scale reactor 71

3.3.1.1 Reagents 71

3.3.1.2 Experimental setup 73

3.3.2 Photocatalytic activity evaluated in an air cleaner 77

3.3.2.1 Configuration of the air cleaner 77

3.3.2.2 Experimental setup 79

3.3.3 Photocatalytic activity evaluated in an air duct inside an office building 80

3.3.3.1 Site description 80

3.3.3.2 Experimental setup 82

3.4 Photocatalyst 83

3.4.1 P25 (Degussa) 84

3.4.2 Photocatalyst syntheses by sol-gel method 87

3.4.3 Photocatalyst syntheses by liquid phase deposition (LPD) 87

3.5 Coating substrate 88

3.5.1 Glass fiber 88

3.5.2 Activated carbon filter 89

3.5.3 Stainless steel 89

3.6 Quality assurance and quality control 89

3.6.1 Instrumentation 90

3.6.2 Calibration 90

3.6.3 Sampling 95

3.6.3.1 Laboratory scale reactor 95

3.6.3.2 Air cleaner and air duct inside an office 96

Chapter 4 Removal of indoor air pollutants by photocatalyst loaded on glass fiber filter

4.1 Introduction 97

4.2 Characterization of photocatalyst loaded on glass fiber filter 97

4.3 Nitrogen oxide (NO) 99

4.3.1 Photodegradation of NO 99

4.3.2 Effects of the amount of TiO_2 loaded on the glass fiber filter 102

4.3.3 Effects of initial concentrations 105

4.3.4 Effects of residence time 108

4.3.5 Effects of humidity levels 109

4.3.6 Photodegradation of NO by photocatalyst synthesized by sol-gel method 113

4.3.6.1 Characterization of photocatalyst synthesized by sol-gel method 113

4.3.6.2 Characteristic of the photocatalyst 114

4.3.6.3 Photodegradation of NO by photocatalyst synthesized by sol-gel method at different residence time 116

4.3.6.4 Photodegradation of NO by photocatalyst synthesized by sol-gel method at different humidity levels 117

4.3.6.5 Photodegradation of NO with photocatalyst T1, 119

T2 and P25

4.4 Carbon monoxide (CO) 121

4.4.1 Photodegradation of CO 121

4.5 Sulfur dioxide (SO_2) 122

4.5.1 Photodegradation of SO_2 122

4.5.2 Effects of humidity levels 124

4.6 Benzene, Toluene, Ethylbenzene and o-Xylene (BTEX) 127

4.6.1 Photodegradation of BTEX 127

4.6.2 Effects of initial concentrations 131

4.6.3 Effects of residence time 133

4.6.4 Effects of humidity levels 135

4.6.5 Photodegradation of BTEX by photocatalyst synthesized by sol-gel method 137

4.7 Formaldehyde (HCHO) 139

4.7.1 Photodegradation of HCHO 139

4.7.2 Effects of initial concentrations 141

4.7.3 Effects of residence time 144

4.7.4 Effects of humidity levels 145

4.8 Quantum yield 148

4.9 Summary 150

Chapter 5 Removal of indoor air pollutants by photocatalyst loaded on activated carbon filter

5.1 Introduction 152

5.2 Characterization of photocatalyst loaded on activated carbon filter 152

5.3 Nitrogen oxide (NO) 154

5.3.1 Adsorption of NO 154

5.3.2 Removal of NO by AC, TiO_2 and TiO_2/AC filter 156

5.3.3 Long term activity and deactivation 160

5.4 Benzene, Toluene, ethylbenzene and o-Xylene (BTEX) 161

5.4.1 Adsorption of BTEX 161

5.4.2 Removal of BTEX by AC, TiO_2 and TiO_2/AC filter 163

5.5 Summary 171

Chapter 6 Removal of multiple indoor air pollutants by photocatalyst loaded on glass fiber filter and activated carbon filter

6.1 Introduction 172

6.2 Concurrent photodegradation of NO and BTEX by TiO_2 filter 172

6.2.1 Effects of residence time 172

6.2.2 Effects of humidity levels 175

6.2.3 Effects of initial concentrations 178

6.3 Concurrent photodegradation of NO and BTEX by TiO_2 filter and TiO_2/AC filter 182

6.3.2 Binary adsorption of NO and BTEX 182

6.3.3 Effects of residence time 185

6.3.4 Effects of humidity levels 188

6.4 Concurrent photodegradation of NO and CO by TiO_2 filter 191

6.5 Concurrent photodegradation of NO and NO_2 by TiO_2 filter 192

6.6 Concurrent photodegradation of NO and SO_2 by TiO_2 filter 194

6.6.1 Effects of humidity levels 194

6.7 Concurrent photodegradation of NO and SO_2 by TiO_2 filter and TiO_2/AC filter 198

6.7.1 Adsorption of SO_2 by TiO_2/AC filter HCHO and VOCs 198

6.7.2 Effects of humidity levels 199

6.8 Concurrent photodegradation of NO and HCHO by TiO_2 filter 202

6.8.1 Effects of initial concentrations 202

6.8.2 Effects of residence time 203

6.8.3 Effects of humidity levels 204

6.9 Concurrent photodegradation of HCHO and NO by TiO_2 filter 207

6.10 Concurrent photodegradation of HCHO and SO_2 by TiO_2 filter 209

6.11 Concurrent photodegradation of HCHO and BTEX by TiO_2 filter 211

6.12 Summary 214

Chapter 7 Application of TiO_2 photocatalyst TiO_2 for indoor air pollution control

7.1 Introduction 217

7.2 Indoor air pollutants removal by commercial air cleaner installed with TiO_2 filter & TiO_2/AC filter 217

7.2.1 Leakage test of the environmental chamber 218

7.2.2 NO removal by the air cleaner without TiO_2 and TiO_2/AC filter 219

7.2.3 NO removal of the air cleaner with TiO_2 filter using UVA and UVC lamp 221

7.2.4 NO removal of the air cleaner with TiO_2 filter and 222

TiO$_2$/AC filter

7.2.5 Intermediate generated from the photodegradation of NO 224

7.2.6 Toluene removal of the air cleaner with TiO$_2$ filter and TiO$_2$/AC filter 227

7.3 Indoor air pollutants removal via air duct installed with TiO$_2$/AC filter 229

7.3.1 Background concentrations inside the office 229

7.3.2 Pollutant concentrations after installing TiO$_2$/AC filter inside the air duct 229

7.4 Summary 231

Chapter 8 Conclusion 233

References 239

Appendix I Analytical equipments & procedures

1. Carbon monoxide (CO) 285
2. Nitrogen monoxide (NO) and nitrogen dioxide (NO$_2$) 285
3. Sulfur dioxide (SO$_2$) 286
4. Non-Methane Hydrocarbon (NMHC) 287
5. Volatile organic compounds (VOCs) 288
6. Aldehydes 289
7. Nitrate ion, sulfate ion and formic acid 292
8. Intermediates generated from the photodegradation of VOCs 292

Appendix II TiO$_2$ photocatalyst coated on stainless steel

1. Introduction 294

2. Characterization of photocatalyst 294

   2.1 Fourier Transform Infrared Spectroscopy (FTIR) 294

   2.2 X-ray diffraction (XRD) 296

   2.3 Scanning Electron microscope (SEM) 398

   2.4 Photoluminescence Spectra (PL) 300

   2.5 X-ray Photoelectron Spectroscopy (XPS) 302

3. Photodegradation of NO by TiO$_2$ synthesized by LPD method 308

4. Summary 315

List of Figures

Figure	Title	Page
2.1	Reciprocal initial rate versus reciprocal initial reactant concentration.	11
2.2	L-H plot for acetone decomposition.	12
2.3	Inverse of reaction rate of ozone photooxidation vs. water vapor concentration in the gaseous phase.	15
2.4	Schematic diagram of a typical photocatalytic experiment using standard gas as pollutant source.	16
2.5	Schematic diagram of a typical photocatalytic experiment using liquid VOCs as pollutant source.	16
2.6	Schematic diagram of fluidized bed reactor used by Dibble and Raupp.	19
2.7	Schematic diagram of a typical annular flow reactor with internal illumination.	19
2.8	Schematic diagram of a typical annular flow reactor with external illumination.	20
2.9	Schematic diagram of TiO_2 thin film and powder synthesis by LPD method.	23
2.10	Preparation of TiO_2 thin film by sol-gel method.	28
2.11	Preparation of TiO_2-SiO_2 powder by sol-gel method.	34
2.12	Primary (a) and secondary (b) benzene photodegradation pathways	55
2.13	Primary (a) and secondary (b) toluene photodegradation pathways	56
3.1	NIST certificate of formaldehyde standard gas.	72
3.2	Schematic diagram of the experimental setup.	74
3.3	Laboratory scale continuous flow reactor.	75
3.4	Front view of the commercial air cleaner.	78
3.5	Top view of the commercial air cleaner.	78
3.6	Top view of the commercial air cleaner installed with the TiO_2/AC filter.	79
3.7	Floor plan of the sampling site and sampling locations.	81
3.8	TiO_2/AC filter installed in an air duct.	82
3.9	UV lamps installed inside the air duct.	82
3.10	Specifications of photocatalyst TiO_2 Degussa P25.	86
3.11	Schematic diagram of CO calibration.	90
3.12	CO calibration curve.	92
3.13	Calibration systems for the GC/MS.	92
3.14	Formaldehyde calibration curve.	94
3.15	Sulfate ion calibration curve.	95
4.1	Scanning electron micrographs of (a) fiber, (b) fiber coated with TiO_2, (c) top and (d) cross-section.	98
4.2	Typical photodegradation profile of NO; 200 ppb NO; humidity level 2100 ppmv; residence time 0.6 min.	100

4.3	Effects of TiO_2 weight percentage on NO conversion and NO_2 generation; 500 ppb NO; humidity level 2100 ppmv; residence time 0.6 min.	104
4.4	L-H plots for NO photodegradation; humidity level 2100 ppmv; residence time 3.7 min.	108
4.5	Effects of residence on NO conversion and NO_2 generation; 200 ppb NO; humidity level 2100 ppmv.	109
4.6	Effects of humidity levels on NO conversion and NO_2 generation; 200 ppb NO; residence time 1.2 min.	112
4.7	Inverse of reaction rate of NO photodegradation vs. humidity levels. Experimental conditions: residence time 1.2 min, 200 ppb HCHO.	113
4.8	XRD patterns of photocatalyst T1.	114
4.9	DSC-TG analyses of photocatalyst T1.	115
4.10	Variation of NO_x at different residence time. Experimental conditions: 200 ppb NO; humidity 2100 ppmv.	117
4.11	Variation of NO_x at different levels of humidity. Experimental conditions: 200 ppb NO; Residence time 3.8 min.	118
4.12	Sulfate ion (SO_4^{2-}) concentration under different relative humidity levels at an initial concentration of 200 ppb SO_2. Experimental conditions: Residence time 1.2 min.	127
4.13	Photodegradation of 35 ppb BTEX. Experimental conditions: Residence time 11.4 min; humidity level 2100 ppmv.	131
4.14	Photodegradation of BTEX under different initial concentrations. Experimental conditions: residence time 3.8 min; humidity levels 2100 ppmv.	133
4.15	Photodegradation of BTEX under different residence time Experimental conditions: humidity level 2100 ppmv; 20 ppb BTEX.	134
4.16	Photodegradation of BTEX under different humidity levels Experimental conditions: residence time 1.2 min; 20 ppb BTEX.	136
4.17	Photodegradation of formaldehyde under different initial concentrations. Experimental conditions: 50 ppb HCHO; humidity level 2100 ppmv; residence time 3.8 min.	143
4.18	L-H plot of formaldehyde photodegradation. Experimental conditions: humidity level 2100 ppmv, residence time 3.8 min.	143
4.19	Impact on HCHO conversion under different residence time. Experimental conditions: 50 ppb HCHO; humidity level 2100 ppmv.	145
4.20	Impact on HCHO conversion and HCOOH yield under different humidity levels. Experimental conditions: 50 ppb HCHO; residence time 1.2 min.	146
4.21	Inverse of reaction rate of formaldehyde photodegradation vs. humidity levels. Experimental conditions: residence time 1.2 min, 50 ppb HCHO.	147
5.1	Scanning electron micrographs of (a) activated carbon, (b) glass fiber comprehend with activated carbon, (c) intimate	153

	contact of TiO_2 and activated carbon (d) inner layer of activated carbon coated with TiO_2.	
5.2	Amount of NO adsorbed in the dark under different residence times. Experimental conditions: Humidity level 2100 ppmv, 200 ppb NO.	155
5.3	Amount of NO adsorbed in the dark under different humidity levels. Experminetal conditions: Residence time 1.2 min, 200 ppb NO.	155
5.4	NO and NO_2 conversion under different residence time. Experimental conditions: Humidity level 2100 ppmv, 200 ppb NO.	158
5.5	NO and NO_2 conversion under different humidity levels. Experimental conditions: Residence time 1.2 min, 200 ppb NO.	159
5.6	Long term activity of TiO_2 and TiO_2/AC. Experimental conditions: Residence time 1.2 min, humidity level 22000 ppmv, 200 ppb NO.	161
5.7	Amount of BTEX adsorbed in the dark under different residence times. Experimental conditions: Humidity level 2100 ppmv, 20 ppb BTEX.	162
5.8	Amount of BTEX adsorbed in the dark under different humidity levels. Experimental conditions: Residence time 1.2 min, 20 ppb BTEX.	163
5.9	Benzene removal under different residence time. Experimental conditions: humidity level 2100 ppmv, 20 ppb BTEX.	165
5.10	Toluene removal under different residence time. Experimental conditions: humidity level 2100 ppmv, 20 ppb BTEX.	165
5.11	Ethylbenzene removal under different residence time. Experimental conditions: humidity level 2100 ppmv, 20 ppb BTEX.	166
5.12	o-Xylene removal under different residence time. Experimental conditions: humidity level 2100 ppmv, 20 ppb BTEX.	166
5.13	Benzene conversion under different humidity levels. Experimental conditions: residence time 1.2 min, 20 ppb BTEX.	169
5.14	Toluene conversion under different humidity levels. Experimental conditions: residence time 1.2 min, 20 ppb BTEX.	169
5.15	Ethylbenzene conversion under different humidity levels. Experimental conditions: residence time 1.2 min, 20 ppb BTEX.	170
5.16	o-Xylene conversion under different humidity levels. Experimental conditions: residence time 1.2 min, 20 ppb BTEX.	170
6.1	Variation of BTEX conversion under the presence of NO at different residence time. Experimental conditions: 20 ppb BTEX & 200 ppb NO; humidity level 2100 ppmv.	174

6.2	Variation of NO_x conversion under the presence of BTEX at different residence time. Experimental conditions: 20 ppb BTEX & 200 ppb NO; humidity level 2100 ppmv.	181
6.3	Variation of BTEX conversion under the presence of NO at different humidity levels. Experimental conditions: 20 ppb BTEX & 200 ppb NO; residence time 1.2 min.	177
6.4	Variation of NO_x conversion under the presence of BTEX at different humidity levels. Experimental conditions: 20 ppb BTEX & 200 ppb NO; residence time 1.2 min.	177
6.5	Amount of NO adsorbed with and without the presence of BTEX under different residence time. Experimental conditions: 200 ppb NO; 20 ppb BTEX; humidity level 2100 ppmv.	183
6.6	Amount of BTEX adsorbed with and without the presence of NO under different residence time. Experimental conditions: 200 ppb NO; 20 ppb BTEX; humidity level 2100 ppmv.	183
6.7	Amount of NO adsorbed with and without the presence of BTEX under different humidity levels. Experimental conditions: 200 ppb NO; 20 ppb BTEX; residence time 1.2 min	184
6.8	Amount of BTEX adsorbed with and without the presence of NO under different humidity levels. Experimental conditions: 200 ppb NO; 20 ppb BTEX; residence time 1.2 min.	185
6.9	NO conversion using TiO_2 and TiO_2/AC with and without the presence of BTEX under different residence time. Experimental conditions: 200 ppb NO; 20 ppb BTEX; humidity level 2100 ppmv.	187
6.10	NO_2 generation using TiO_2 and TiO_2/AC with and without the presence of BTEX under different residence time. Experimental conditions: 200 ppb NO; 20 ppb BTEX; humidity level 2100 ppmv.	188
6.11	NO conversion using TiO_2 and TiO_2/AC with and without the presence of BTEX under different humidity levels. Experimental conditions: 200 ppb NO; 20 ppb BTEX; residence time 1.2 min.	189
6.12	NO_2 generation using TiO_2 and TiO_2/AC with and without the presence of BTEX under different humidity levels. Experimental conditions: 200 ppb NO; 20 ppb BTEX; residence time 1.2 min.	190
6.13	Conversion of NO with and without the presence of SO_2 at an initial concentration of 200 ppb NO & SO_2. Experimental conditions: Residence time 1.2 min; humidity level 2100 ppmv.	194
6.14	Conversion of NO_2 with and without the presence of SO_2 at an initial concentration of 200 ppb NO & SO_2. Experimental conditions: Residence time 1.2 min; humidity level 2100 ppmv.	195
6.15	SO_2 removal using TiO_2 and TiO_2/AC under different humidity levels. Experimental conditions: 200 ppb SO_2; residence time 1.2 min.	199

6.16	NO conversion using TiO_2 and TiO_2/AC with and without the presence of SO_2 under different humidity levels. Experimental conditions: 200 ppb NO; 200 ppb SO_2; residence time 1.2 min.	200
6.17	NO_2 generation using TiO_2 and TiO_2/AC with and without the presence of SO_2 under different humidity levels. Experimental conditions: 200 ppb NO; 200 ppb SO_2; residence time 1.2 min.	201
6.18	Impact on NO_x conversions with and without the presence of HCHO under different initial NO concentrations. Experimental conditions: 50 ppb HCHO; residence time 3.8 min; humidity level 2100 ppmv.	102
6.19	Impact on NO_x conversions with and without the presence of HCHO under different residence time. Experimental conditions: 50 ppb HCHO; 200 ppb NO; humidity level 2100 ppmv.	203
6.20	Impact on NO_x conversions with and without the presence of HCHO under different humidity levels. Experimental conditions: 50 ppb HCHO; 200 ppb NO; residence time 1.2 min.	204
6.21	Impact on HCHO conversion with and without the presence of NO under different humidity levels. Experimental conditions: 50 ppb HCHO; 200 ppb NO; residence time 1.2 min.	207
6.22	Impact on HCHO conversion with and without the presence of SO_2 under different humidity levels. Experimental conditions: 50 ppb HCHO; 200 ppb SO_2; residence time 1.2 min.	209
6.23	Impact on HCOOH yield with and without the presence of SO_2 under different humidity levels. Experimental conditions: 50 ppb HCHO; 200 ppb SO_2; residence time 1.2 min.	210
6.24	Impact on HCHO conversion with and without the presence of BTEX under different humidity levels. Experimental conditions: 50 ppb HCHO; 20 ppb BTEX; residence time 1.2 min.	211
6.25	Impact on HCOOH yield with and without the presence of BTEX under different humidity levels. Experimental conditions: 50 ppb HCHO; 20 ppb BTEX; residence time 1.2 min.	214
7.1	Leakage test of the environmental chamber using NO.	219
7.2	Leakage test of the environmental chamber using toluene.	219
7.3	NO removal using the air cleaner settings.	221
7.4	NO removal using TiO_2 filter with UVA lamp and UVC lamp.	222
7.5	NO removal using TiO_2 filter and TiO_2/AC filter.	224
7.6	Intermediate generated from the photodegradation of NO under different experimental conditions.	226
7.7	Toluene removal by the air cleaner with AC+HEPA, TiO_2 filter and TiO_2/AC filter.	228

List of Tables

Table	Title	Page
2.1	k and K values obtained from Fig. 2.1.	11
2.2	L-H parameters obtained from the photodegradation of 12 pollutants.	14
2.3	Effects of initial pollutant concentration on conversion.	37
2.4	Effects of residence time on conversion.	38
2.5	Effects of humidity levels on conversion.	40
2.6	Sources of common indoor air VOCs.	49
2.7	Most frequently found VOCs in indoor environment.	50
2.8	VOCs for good class classification in Hong Kong.	50
2.9	Range of BTEX in Hong Kong.	52
2.10	Acute health effects from formaldehyde exposure.	61
3.1	Selected concentration of the target pollutants and analytical methods.	69
3.2	Summary of photodegradation of multiple indoor air pollutants.	70
3.3	Summary of reactant gas acquired from compressed gas cylinder.	72
4.1	Effects of initial concentrations of NO and NO_2 photo-steady-state concentration and NO_x conversion; humidity level 2100 ppmv; residence time 3.7 min.	106
4.2	Variation of NO_x using photocatalyst T1, T2 and P25 at different residence time. Experimental conditions: 200 ppb NO; humidity:2100 ppmv.	120
4.3	Variation of NO_x using photocatalyst T1, T2 and P25 at different levels of humidity. Experimental conditions: 200 ppb NO; residence time 3.8 min.	120
4.4	Photodegradation of CO under different experimental conditions.	121
4.5	Photodegradation of SO_2 under different experimental conditions. Experimental conditions: humidity level 2100 ppmv; residence time 3.7 min.	122
4.6	Photodegradation of BTEX using photocatalyst T1, T2 and P25.	138
4.7	Photodegradation and photolysis of formaldehyde. Experimental conditions: 50 ppb HCHO; humidity level 2100 ppmv; residence time 3.8 min.	141
6.1	Variation of BTEX and NO_x at different NO initial concentrations.	178
6.2	Variation of BTEX and NO_x at different BTEX initial concentrations.	181
6.3	BTEX conversions with and without the presence of NO using TiO_2 and TiO_2/AC under different residence time. B: benzene; T: toluene; E: ethylbenzene; X: o-xylene; Experimental conditions: 200 ppb NO; 20 ppb BTEX;	187

	humidity level 2100 ppmv.	
6.4	BTEX conversions using TiO_2 and TiO_2/AC with and without the presence of NO under different levels of humidity. B: benzene; T: toluene; E: ethylbenzene; X: o-xylene; Experimental conditions: 200 ppb NO; 20 ppb BTEX; residence time 1.2min.	190
6.5	Photodegradation of NO co-injected with CO.	192
6.6	Photodegradation of NO co-injected with NO_2.	193
6.7	Sulfate ion (SO_4^{2-}) and nitrate ion (NO_3^-) from the photodegradation of SO_2 and NO; humidity level 2100 ppmv; residence time 1.2 min.	197
6.8	HCOOH yield with and without the presence of NO under different humidity levels. Experimental conditions: 50 ppb HCHO; 200 ppb NO; residence time 1.2 min.	208
6.9	Summary of reactions between different pollutants.	215
7.1	NO, NO_x and NMHC removal efficiency using TiO_2 filter and TiO_2/AC filter.	228
7.2	Background pollutant concentrations inside the office.	229
7.3	Pollutant concentrations inside the office after installing the TiO_2/AC filter.	230
7.4	Pollutant concentrations inside the office after installing the TiO_2/AC filter.	231

Chapter 1 INTRODUCTION

1.1 Background

In general, 80% of people spend their time in indoor environment (Roberts and Nelson, 1995). The quality of indoor air has a direct impact on human health in terms of lengthened exposure to pollutants by inhalation. Subsequent to the oil crisis in 1970s, buildings were designed to be more energy efficient and better insulation (Jones, 1998). This mean that a lower air exchange rate is used and the pollutant concentration accumulated are often higher than outdoor environment.

The accumulation of elevated pollutant concentration causes adverse health impact on the occupant. Occupants having a complex range of vague and often subjective health complaints such as headache, burning eyes and fatigue. This phenomenon is known as 'sick building syndrome' (SBS) (Horvath, 1997), and these complaints lessened when the occupants leaving the building. Indeed, problems associated with shortcomings in indoor air may be one of the most common environmental health issues most doctors now face (Seltzer, 1995). Moreover, study (Wallace, 1997) showed that SBS symptoms may have a greater impact on public health and cost to the economy than some major disease due to widespread absenteeism and lowered productivity amongst affected workers. For example, it has been estimated that the annual cost of headaches amongst the employees of the US Environmental Protection Agency may be as high as $2 million. Thus, it can be observed that it is necessary to reduce the pollutant level in indoor environment.

In general, there are three mitigation measures to reduce the SBS, namely source control, ventilation and air cleaning. The first two methods are usually impossible as the source is unreachable and the ventilation is often ungovernable by building occupants. Thus, air cleaning is a feasible and convenient method for the individual occupant to improve indoor air quality.

In view of the current indoor air pollutants, there are two major categories namely, particle pollutants and gaseous pollutants. Particle pollutants are particles generated from smoking (Cooper, 1980) and cooking (Pandey et al., 1989). The particle can be effectively removed by the installation of high efficiency particulate air (HEPA) filter. It has a minimum removal efficiency of 99.7% when tested at an aerosol of 0.3μm diameter (U.S. Department of Energy). Gaseous pollutants generated from large varieties of indoor activities and also related to its ventilation system in correlation to the outdoor pollutant concentration. Traditional remediation technique such as adsorption is not suitable and cost-effective for such low concentration pollutants (Khand and

Ghoshal, 2000). This filter, without adequate replacement, could even become a source of volatile organic compounds (VOCs) in the ventilation system (Schleibinger and Ruden 1999).

Advanced oxidation process (AOP) such as photocatalysis is a promising technology for air purification. Photodegradation occurs at room temperature and pressure and actually oxidizes pollutants to H_2O and CO_2, and no additional carrier gas is needed (Obuchi et al., 1999; Noguchi and Fujishima, 1998; Mills and LeHunte, 1997; Matos et al., 1998; Yu et al., 2002). The photocatalyst, such as titanium dioxide (TiO_2), is also relatively inexpensive. In addition, it showed high removal rate in many pollutants such as hydrocarbons (Alberici and Jardim, 1997; Einaga et al., 1999), chlorinated hydrocarbons (Shen and Ku, 2002; d'Hennezel and Ollis, 1997), carbonyls (Peral and Ollis, 1992; Yang et al., 2000), sulfur dioxide (Shang et al., 2002), nitrogen oxides (Hashimoto et al., 2001) and odor compounds (Nishikawa and Takahara, 2001; Martyanov and Klabunde, 2003). The aforementioned studies, however, used a concentration of several hundreds parts per million (ppm), which is seldom found in normal and polluted indoor environment such as offices and residential homes. The effect of photodegradation on the parts per billion (ppb) levels of indoor air pollutants is seldom reported. Also, the above studies were conducted using only single pollutant, in which multiple pollutants simultaneously exist in the environment.

In addition, to the best of my knowledge, no study reported the important factors such as humidity levels, residence time and initial concentrations for indoor air purification using photocatalysis. In view of this research deficiency in the area of photocatalysis, there is a requisite to study photocatalysis for indoor air purification.

1.2 Objectives

The aim of this study is to investigate the use of photocatalysis for indoor air purification under simulated indoor environment. To truly and effectively benefit the humanities, it is necessary to bring this technology for practical use. Hence, the objectives of this study are:

i) Conduct photocatalysis study for indoor air purification by using common indoor air pollutants with reference to its indoor air concentrations;

ii) Identify which factors that affect the performance of photocatalysis for indoor air purification by conducting sensitive analyses such as variations of initial pollutant concentrations, residence time and humidity levels;

iii) Conduct simultaneous photodegradation of multiple common indoor air pollutants to determine if there is any reciprocal effects;

iv) Rectify the problems encountered, if any, for indoor air purification by photocatalysis;

v) Evaluate the pollutant removal efficiency by the photocatalysis technique developed in a practical application such as a commercial air cleaner; and

vi) Evaluate the pollutant removal efficiency by the photocatalysis technique developed in a real indoor environment such as a commercial office.

Chapter 2 LITERATURE REVIEW

2.1 *Photocatalysis*

2.1.1 Background

The initial interest of the photoinduced redox reactions was first discovered by Fujishima and Honda in 1972 (Fujishima and Honda, 1972). They used an n-type TiO_2 semiconductor electrode, which was connected through an electrical load to a platinum black counter electrode and exposed to near-UV light. Photocurrent flowed from the platinum counter electrode to the TiO_2 electrode through the external circuit. The current direction showed that the oxidation reaction occurred at the TiO_2 electrode and the reduction reaction occurred at the platinum electrode (Fujishima et al., 2000). This work prompted extensive research on producing hydrogen from water as a means of solar energy conversion. Later, this redox reaction was utilized in organic and inorganic compounds for environmental protection. In 1977, for example, Frank and Bard investigated the decomposition of cyanide in water by heterogeneous photocatalysis (Frank and Bard, 1977).

2.1.2 Mechanism

Semiconductor is used rather than metal in photocatalysis because it lacks a continuum of interband states to assist the recombination of the electron-hole pair. The void region which extends from the top of the filled valence band to the bottom of the vacant conduction band is called the bandgap. The bandgap also defines the wavelength sensitivity of the semiconductor to irradiation (Fox and Dulay, 1993). The initial step of photocatalysis is the adsorption of photons by a molecule to produce highly reactive electronically excited states. The photon needs to have an energy of $h\nu$ matches or greater than its bandgap energy, E_g, of the semiconductor. An electron is promoted from the valence band to the conduction band, leaving a positive hole in the valence band. The valence band holes are powerful oxidants, whereas the conduction band electros are good reductants. The electron-hole pair can recombine and dissipate into heat energy in the volume of the semiconductor particle or on the surface (Hoffmann et al., 1995). It can also react with electron donors and acceptors adsorbed on the semiconductor surface or within the surrounding electrical double layer of the charged particles. To reduce the recombination of electron-hole pair, charge carrier trapping is needed (Linsebigler et al., 1995). This can be done by trapping the photogenerated electron, the photogenerated hole or both. Oxygen in the air is an efficient conduction band electron trap, and suppressed electron-hole recombination. The superoxide O_2^- formed is highly active and can attack either organics or adsorbed intermediates. Study (Gerischer and Heller 1992) showed that the photocatalytic activity is adversely affected without the presence of oxygen, which is possibly due to the back interfacial electron transfer from active species present on the photocatalyst surface. It is also suggested that the photoactivity of anatase phase TiO_2 is higher than the rutile phase because rutile phase has a lower capacity to adsorb oxygen (Serpone and Pelizzetti, 1989).

For the heterogeneous photocatalysis in air, where abundant of oxygen and water vapor are presence, the reactions can be summarized as follows (Komazaki et al., 1999; Zhao and Yang, 2003):

TiO_2 generates a positive hole and electron upon illumination of UV light.

$$TiO_2 \xrightarrow{hv} h^+ + e^- \qquad (2.1)$$

Water vapor in the air adsorbs on the surface of the TiO_2 and dissociates into hydrogen ions and hydroxide ions.

$$H_2O \longrightarrow H^+ + OH^- \qquad (2.2)$$

The positive hole (h^+) reacts with the hydroxide ion (OH^-) to generate hydroxyl radical on the TiO_2 surface.

$$h^+ + OH^- \longrightarrow OH \cdot \qquad (2.3)$$

Oxygen acts as the charge carrier trapping and reacts with the electron.

$$e^{-} + O_2 \longrightarrow O_2^{-} \qquad (2.4)$$

Peroxyl ion may also form by the reaction of superoxide and hydrogen ions.

$$H^{+} + O_2^{-} \longrightarrow HO_2 \cdot \qquad (2.5.)$$

2.1.3 Kinetics

The Langmuir-Hinshelwood (L-H) model has been widely used to describe the kinetics of gas-solid phase reaction in heterogeneous photocatalysis. The model assumes that (Fox and Dulay, 1993):

i) At equilibrium the number of surface adsorption sites is fixed;

ii) Only one substrate may bind at each surface site;

iii) The heat of adsorption by the substrate is identical for each site and is independent of surface coverage;

iv) There is no interaction between adjacent adsorbed molecules;

v) The rate of surface adsorption of the substrate is greater than the rate of any subsequent chemical reactions; and

vi) No irreversible blocking of active sites by binding to product occurs.

The surface coverage (θ) is related to the apparent adsorption equilibrium constant (K) by the following equation:

$$\theta = \frac{KC_o}{(1 + KC_o)} \qquad (2.6)$$

The rate of product formation can be expressed as a L-H kinetic rate expression.

$$r = \frac{kKC_o}{1 + KC_o} \qquad (2.7)$$

where k is the apparent reaction rate constant occurring at the active site of the photocatalyst surface and C_o is the initial concentration of the pollutant. By rearranging equation 2.7, a linear form of the L-H model can be obtained.

$$r = \frac{kKC_o}{1 + KC_o} \longrightarrow \frac{1}{r} = \frac{1 + KC_o}{kKC_o} \longrightarrow \frac{1}{r} = \frac{1}{kKC_o} + \frac{KC_o}{kKC_o}$$

$$\frac{1}{r} = \frac{1}{kKC_o} + \frac{1}{k} \qquad (2.8)$$

A standard means of using the L-H model is to test the linearity of the data by plotting the inverse of reaction rate versus the initial concentration, which requires both a positive slope $(kK)^{-1}$ and intercept $(k)^{-1}$ (Serpone and Pelizzetti, 1989).

Fig. 2.1 shows an example of the use of L-H model for heterogeneous photocatalysis. By plotting the reciprocal of the reaction rate versus the reciprocal of the initial concentration, a good linearity of the data is observed. In addition, the values of the rate constant k and the equilibrium constant K (Table 2.1) can be obtained by the intercept and the slope of the graph, respectively. This L-H model has also been used by different researches to predict the photodegradation of acetaldehyde (Sopyan et al., 1996), toluene (Duan et al., 2002), acetone (Kim and Hong, 2002), benzyl alcohol (Cunningham and Srijaranai, 1991) and chlorinated phenols (Al-Ekabi and Serpone, 1988).

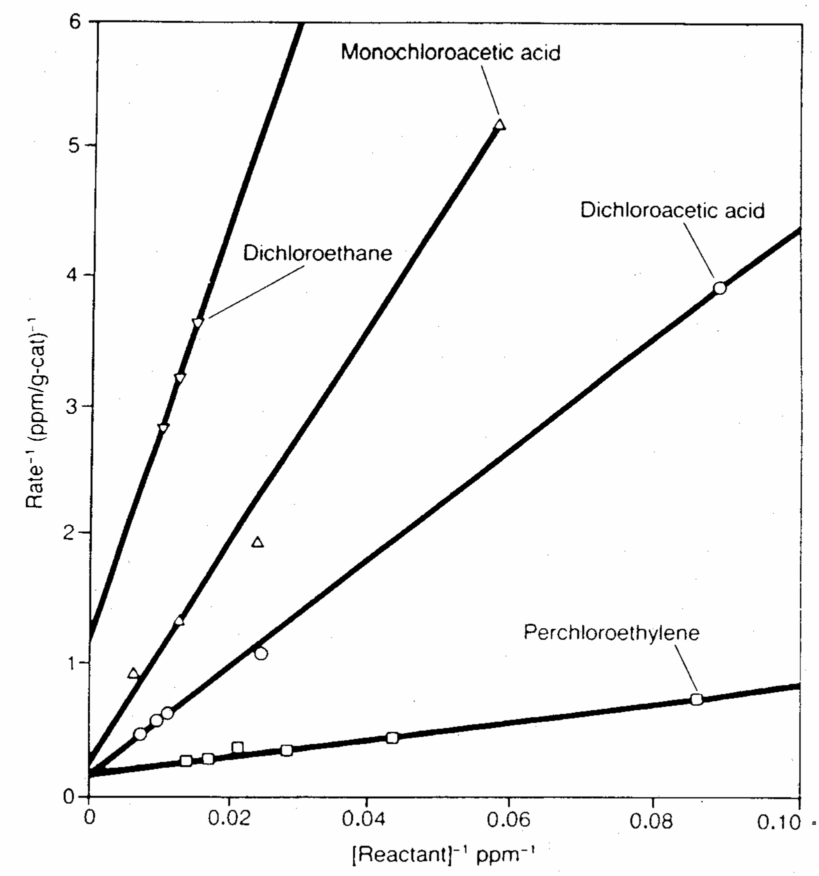

Figure 2.1 Reciprocal initial rate versus reciprocal initial reactant concentration(Serpone and Pelizzetti, 1989).

Reactant	k (ppm /min g)	K $(ppm)^{-1}$
Monochloroacetic acid	5.5	0.002
Dichloroethane	1.6	0.02
Dichloroacetic acid	8.5	0.003
Perchloroethylene	6.8	0.02

Table 2.1 k and K values obtained from Fig. 2.1(Ollis, 1985).

L-H model can also modeled the contact time of the pollutant by integrating equation 2.7.

$$r = -\frac{dC}{dt} = \frac{kKC}{1+KC}$$

$$-\int dt = \int \left(\frac{1}{kKC} + \frac{1}{k}\right) dC$$

$$\ln\frac{C_o}{C} + K(C_o - C) = kKt \qquad (2.9)$$

By rearranging equation 2.9, a linear plot of $(V/Q)(C_o\text{-}C)^{-1}$ versus $\ln(C_o/C)(C_o\text{-}C)^{-1}$ can be obtained to ventilate the L-H model, as shown in equation 2.10 (Zhang et al., 1994; Alberici and Jardim,1997; Cho et al., 2004).

$$\ln\frac{C_o}{C} + K(C_o - C) = kK\frac{V}{Q}$$

$$\frac{V}{Q} = \frac{1}{kK}\ln\left(\frac{C_o}{C}\right) + \frac{1}{k}(C_o - C)$$

$$\frac{V/Q}{(C_o - C)} = \frac{1}{k} + \frac{1}{Kk}\frac{\ln(C_o/C)}{(C_o - C)} \qquad (2.10)$$

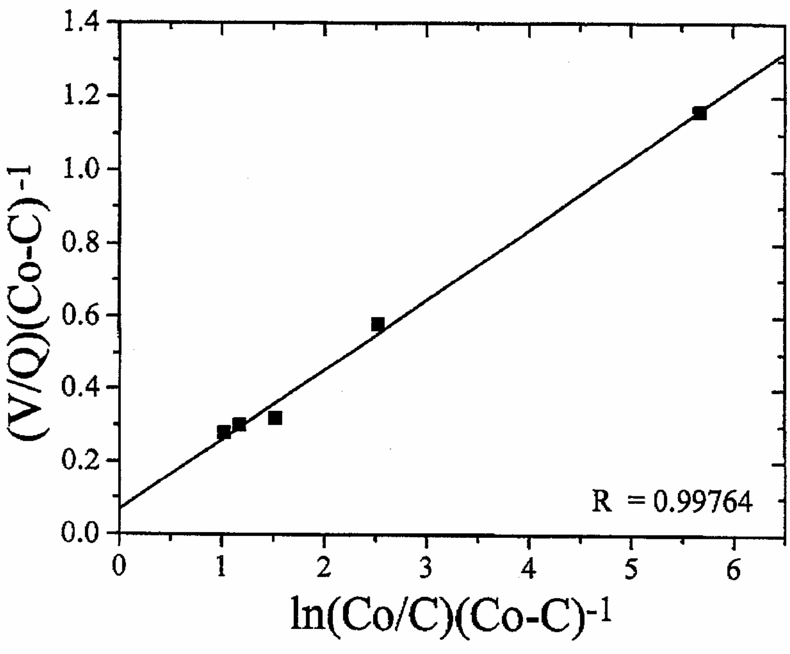

Figure 2.2 L-H plot for acetone decomposition(Alberici and Jardim,1997).

Fig. 2.2 (Alberici and Jardim,1997) shows the photodegradation of acetone is in good agreement with this integral rate-law analysis. The half life value, that is the time required to reduce the initial pollutant concentration by half, is obtained in equation 2.9 when $C=0.5C_o$, as shown in equation 2.11.

$$\ln\frac{C_o}{C} + K(C_o - C) = kKt \qquad (2.9)$$

$$\frac{1}{kK}\ln\frac{C_o}{C} + \frac{1}{k}(C_o - C) = t$$

When $C=0.5C_o$,

$$\frac{1}{kK}\ln\frac{C_o}{0.5C_o} + \frac{1}{k}(C_o - 0.5C_o) = t_{0.5}$$

$$\frac{1}{kK}\ln 2 + \frac{1}{k}0.5C_o = t_{0.5}$$

$$t_{0.5} = \frac{0.693}{kK} + \frac{0.5C_o}{k} \qquad (2.10)$$

This result showed that both the values of *k* and K affect the photodegradation rate of the pollutant. A larger value of k or K does not necessary mean a higher photodegradation rate, but the combination of both is important. For example, as shown in Table 2.2, methanol and isopropanol has the maximum value of adsorption constant K, whereas isooctane is the minimum. The adsorption constant of methanol was 40 times higher than isooctane. However, combining the value of the reaction constant k, it can be observe that the half life value of methanol is only double that of isooctane.

Compounds	C_{in} (ppmv)	k ($g/m^3 min$)	K (m^3/g)	$k \cdot K$ (min^{-1})	$t_{1/2}$ (min)
Methanol	650	9.09	0.75	6.82	0.15
Trichloroethylene	538	28.05	0.21	5.89	0.17
Acetone	590	14.68	0.35	5.14	0.19
Methyl ethyl ketone	441	10.13	0.44	4.53	0.22
Dimethoxymethane	570	15.47	0.29	4.49	0.22
Isooctane	492	173.31	0.017	2.95	0.24
Methyl isopropyl ketone	455	7.02	0.32	2.24	0.43
Isopropanol	750	4.14	0.63	2.61	0.50
t-Butyl methyl ether	605	5.78	0.33	1.90	0.57
Methylene chloride	398	20.72	0.054	1.12	0.65
Chloroform	442	25.79	0.032	0.82	0.89
Tetrachloroethylene	618	11.27	0.08	0.90	0.97

Table. 2.2 L-H parameters obtained from the photodegradation of 12 pollutants(Alberici and Jardim,1997).

Peral and Ollis (1992) showed that the photodegradation rate is depended on the water vapor in the feed stream, and the relationship can be described in the following equation.

$$r = \frac{r_o}{1 + K_H [H_2O]^{\beta}} \qquad (2.11)$$

where r_o is the reaction rate under the condition that the feed stream is absolutely free of water, and K_H is the influential factor related to the water vapor in the flowing stream. By rearranging equation 2.11 into equation 2.12, the inverse of the reaction rate is plotted against the water vapor concentration, as shown in Fig. 2.3 (Cho et al., 2004).

$$\frac{1}{r} = \frac{1}{r_o} + \frac{K_H}{r_o}[H_2O]^{\beta} \qquad (2.12)$$

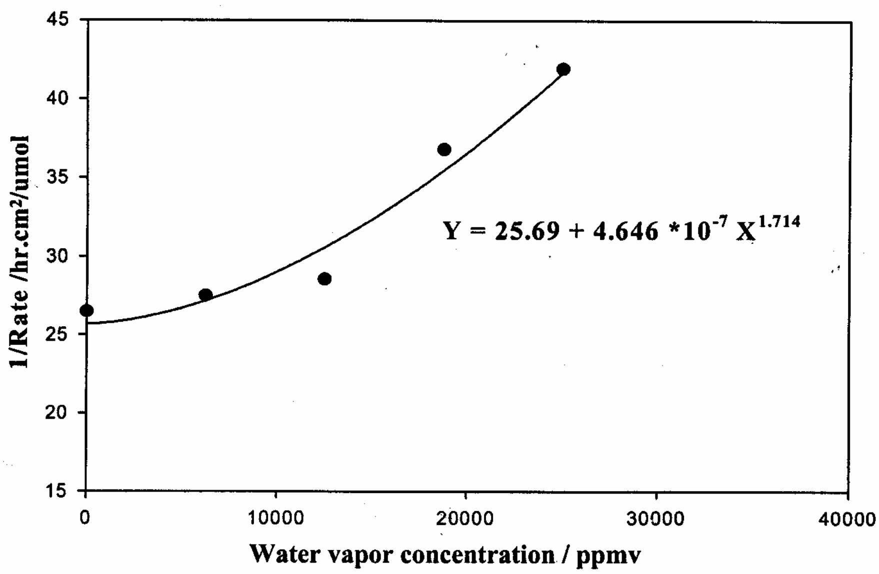

Figure 2.3 Inverse of reaction rate of ozone photooxidation vs. water vapor concentration in the gaseous phase(Cho et al., 2004).

2.1.4 Reactor

Reactor provides a physical boundary for the photocatalytic reaction between the pollutants and the photocatalyst. In aqueous phase, most of the studies used a batch flow reactor. The reactor usually is a glass breaker with pollutants of known concentration suspended with powdered catalyst (Gomez et al., 2003; Arana et al., 2001; Colon et al., 2003). Alternatively, the powdered catalyst can be replaced by immobilized catalyst thin film (Yu et al., 2000; Matsuda et al., 2001a, Ma et al., 2001). The reactor usually is continuously stirred and bubbled with air or oxygen. Ultraviolet light is provided on top of the breaker or surrounding the breaker. Only a few studies reported the use of a plug flow reactor for the photodegradation of pollutant in aqueous phase (Zhang et al., 1994).

On the contrary, most of the photodegradation studies on gaseous phase pollutant are conducted in a continuous flow reactor, though few studies conducted in a batch flow reactor (Yu et al., 2002, Wang and Ray, 2000). Despite the different configurations of the reactor, in general it consists of a sampling inlet and outlet, ultraviolet lamp(s) (internal or external), and a sample holder for mounting the photocatalyst.

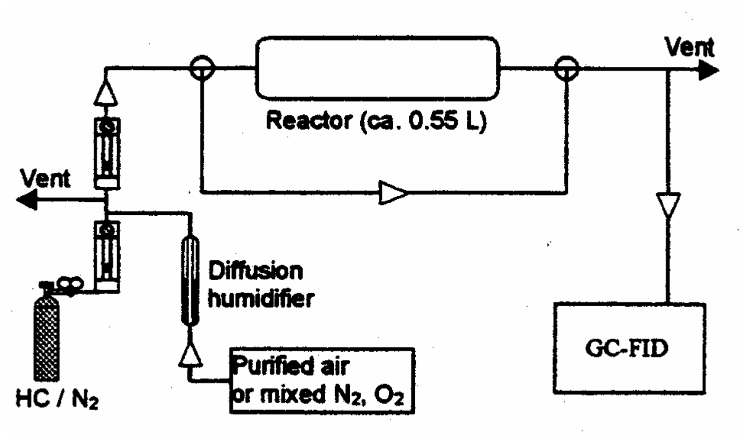

Figure 2.4 Schematic diagram of a typical photocatalytic experiment using standard gas as pollutant source (Sakamoto et al., 1999).

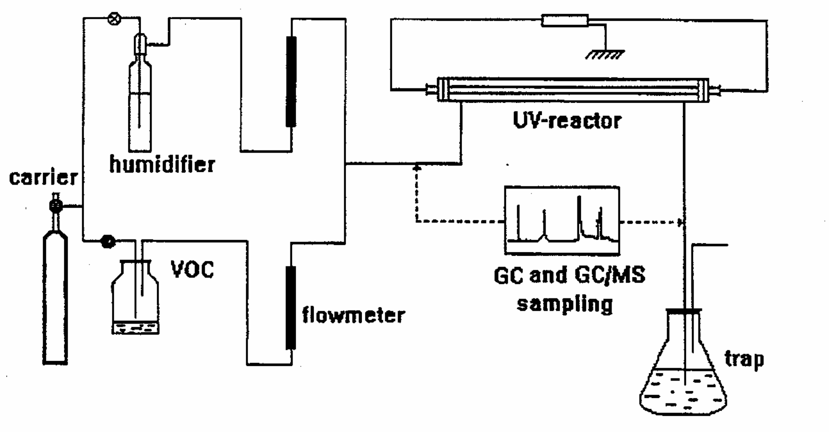

Figure 2.5 Schematic diagram of a typical photocatalytic experiment using liquid VOCs as pollutant source(Alberici and Jardim, 1997).

Apart from the reactor itself, it is worthwhile to mention the supporting equipment for the photodegradation experiment. As shown in Fig. 2.4 and Fig. 2.5, the major difference of the experimental apparatus is that one used standard gas and the other used liquid VOCs as the pollutant source. The function of the experimental apparatus is briefly explained as follows:

i) Carrier: Provide gas flow (inlet stream) for the experiment.

ii) Humidifier: Provide desire humidity level.

iii) Flow meter: Control desire flowrate.

iv) Standard gas/Liquid VOCs: Provide desire pollutant and concentration.

v) GC-FID: Analysis equipment, for analyze the concentration of VOCs.

vi) Reactor: Provide physical boundary for photocatalytic reaction.

vii) Ultraviolet lamp: Provide energy for activation of photocatalytic reaction.

viii) Vent: Discharge of excess flow for safety purpose.

For batch flow reactor, an air pump is needed for air recirculation. The pumping speed can control the residence time of the pollutant inside the reactor.

The following are some typical reactors commonly used for gaseous phase photocatalysis.

2.1.4.1 Fluidized bed reactor

A schematic fluidized bed reactor (Dibble and Raupp, 1992) used for trichloroethylene photodegradation is shown in Fig. 2.6. This reactor has an advantage of high throughput, low pressure drop and efficient reactant-catalyst contacting. TiO_2 was used as photocatalyst impregnated on silica gel for fluidization. Illumination was provided by ultraviolet lamp located outside the reactor. As shown in Fig. 2.7, the inlet gas passed through from the bottom of the reactor. The buoyancy of the inlet air caused the catalyst bed fluidization and trichloroethylene was photodegradated. Dibble and Raupp (1992) reported that the illumination irradiance strongly influenced reactor performance. The conversion increased from 20% to 95% when the light source decreased from 3.5 cm to 0.5 cm from the surface of the flat plate. Recently, Nam et al., (2000) reported the use of fluidized reactor with ultraviolet lamp located inside the reactor to maximize illumination. In addition, air nozzles were used at the inlet to increase the uniformity of the air flow. Lim et al., (2000) reported the use of mirror box surrounding the reactor to maximize the use of the reflected and deflected light. Matsuda et al., 2001 also reported the use of fluidized bed reactor for nitrogen oxide photodegradation. They showed that the removal of nitrogen oxide is proportional to the specific surface area of the photocatalyst. An optimal particle diameter was observed during the fluidization. An oversized particle diameter would cause break down of the particle and lower the conversion.

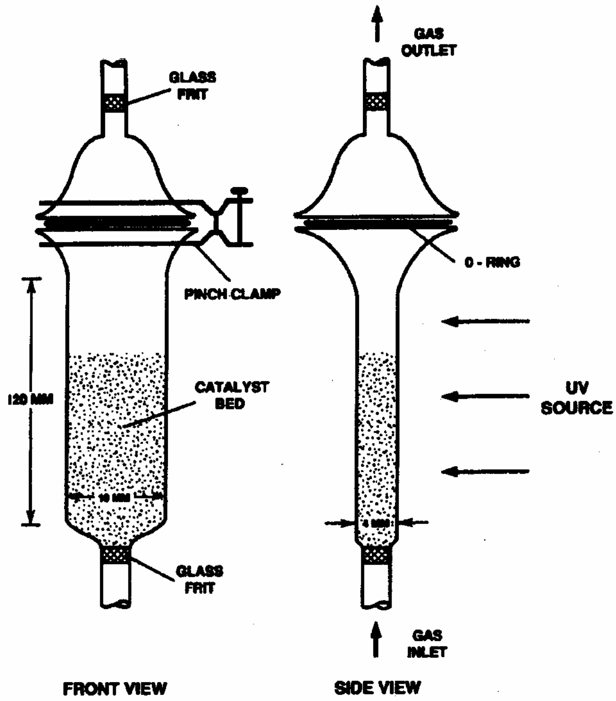

Figure 2.6 Schematic diagram of fluidized bed reactor used by Dibble and Raupp (Dibble and Raupp, 1992).

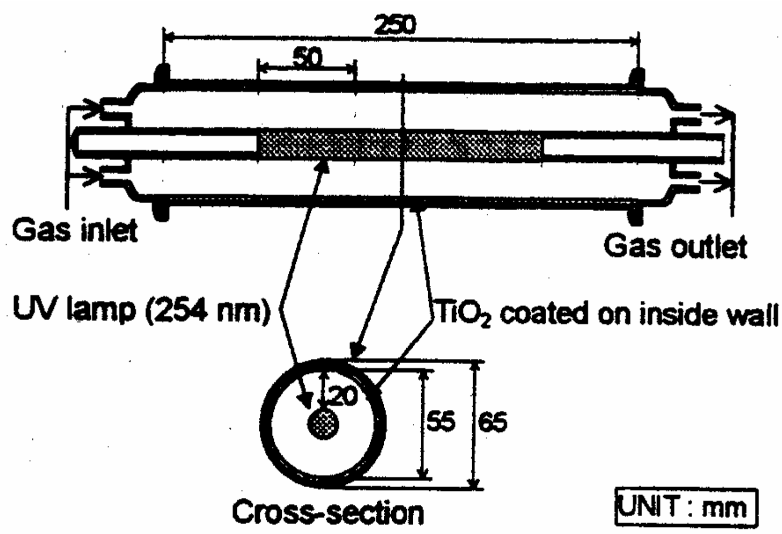

Figure 2.7 Schematic diagram of a typical annular flow reactor with internal illumination(Sakamoto et al., 1999).

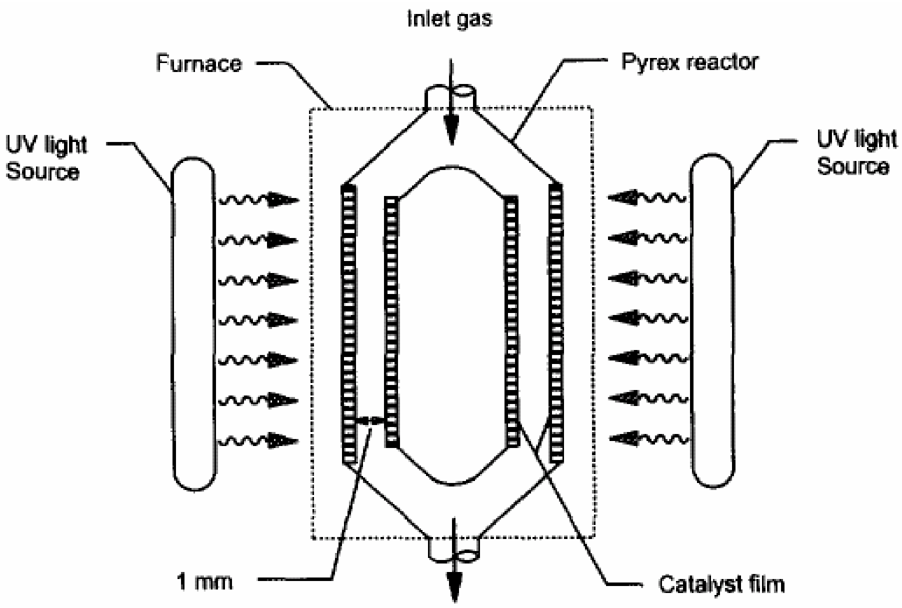

Figure 2.8 Schematic diagram of a typical annular flow reactor with external illumination(Larson et al., 1995).

2.1.4.2 Annular reactor

It is one of the most commonly used configurations for photocatalytic reaction. The photocatalyst usually coated on the internal surface of the reactor. The rector is usually made of transparent material such as glass to facilitate coating and illumination. Illumination can be provided internally (Fig. 2.7) or externally (Fig. 2.8). For external illumination, the photocatalyst has to be transparent enough to allow illumination. Frequently, the photocatalyst is located parallel to the flow to reduce pressure drop. This reactor has the advantage of virtually no pressure drop and the amount of photocatalyst used can be easily controlled. A very high flow velocity can be obtained. The geometry of the photocatalyst is also versatile, depending only on the shape of the reactor. Alternatively, the photocatalyst is first coated on a thin film and mounted inside the reactor. This configuration is usually applied for the evaluation a series of synthetic (or modified) photocatalyst. This simple configuration allows a fast and effective photocatalyst evaluation. Compare to the fluidized bed reactor, annular reactor is more commonly used for its easy configuration and versatility in catalyst preparation.

2.2 Synthesis of photocatalyst

TiO_2 photocatalyst can be synthesized by many methods such as liquid phase deposition (LPD) (Yu et al., 2003; Deki et al., 1996), sol-gel (Duan et al., 2002; Zhang et al., 2003; Negishi et al., 1998), chemical vapor deposition (Powell et al., 1996), magnetron sputtering (Okimura et al., 1996) and pulsed laser deposition (Garapon et al., 1996). For environmental application such as pollution remediation, sol-gel method is most commonly investigated. Recently, LPD has received much attention for the synthesis of photocatalyst.

2.2.1 Liquid Phase Deposition (LPD)

LPD is a process in which metal oxide thin film could be directly deposited on the immersed substrate by utilizing chemical equilibrium reaction between the metal fluoro-complex ion and the metal oxide in the aqueous solution (Deki et al., 1996). Metal oxide or hydroxide thin films are formed by means of a ligand-exchange equilibrium reaction of a metal-fluoro complex ion and an F^- consuming reactor act as scavengers for F^-. Using this method, various oxide thin films such as titanium oxide (Deki et al., 1996), silicon oxide (Hishinuma et al., 1991), vanadium oxide (Deki et al., 1997) and iron oxyhydroxide (Deki et al., 1997a) were synthesized. This method has the advantage of coating large area of substrate and complex morphology. In addition, this method allows low temperature crystallization, which enables the use of low melting point substrate such as plastic and glass fiber.

Titanium dioxide, for example, is synthesized by using a parent solution called ammonium hexa-fluorotitanate [$(NH_4)_2TiF_6$] (Deki et al., 1996) or titanium fluoride [TiF_4] (Shimizu et al., 1999). Ammonium hexa-fluorotitanate was first dissolved in water forming $[TiF_6]^{2-}$ and fluoric acid [HF]. Boric acid [H_3BO_3] dissolved in water was used as an F^- scavenger. The solution of ammonium hexa-fluorotitanate and boric acid was added together forming the parent coating solution. Upon the addition of boric acid, it reacted readily with F^- ions forming more stable BF_4^- ion, which promoted the consumption of non-coordinated F^- ion. This caused reaction 2.13 shifted to the right hand side forming more metal-fluorocomplex ions $[TiF_{6-n}(OH)_n]^{2-}$. The reactions are summarized as follows (Yu et al., 2003):

$$[TiF_6] + nH_2O \Leftrightarrow [TiF_{6-n}(OH)_n]^{2-} + nHF \tag{2.13}$$

$$H_3BO_3 + 4HF \Leftrightarrow HBF_4 + 3H_2O \tag{2.14}$$

$$[TiF_{6-n}(OH)_n]^{2-} \xrightarrow{H_2O} [TiF_{5-n}(OH)_{n+1}]^{2-} + H^+ + F^- \tag{2.15}$$

$$[TiF_{5-n}(OH)_{n+1}]^{2-} + H^+ + F^-$$

$$\xrightarrow{(5-n)H_2O} [Ti(OH)_6]^{2-} + (6-n)F^- + (6-n)H^+ \tag{2.16}$$

$$[Ti(OH)_6]^{2-} + 2H^+ \longrightarrow TiO_2 + 4H_2O \tag{2.17}$$

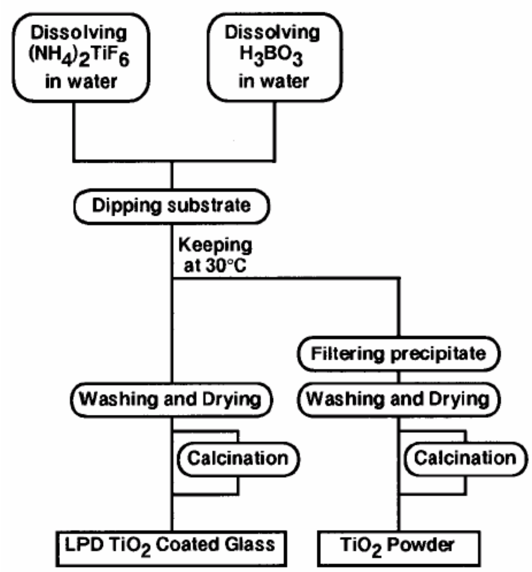

Fig 2.9 Schematic diagram of TiO_2 thin film and powder synthesis by LPD method(Kishimoto et al., 1998).

If the concentration of the parent solutions is too low, it is metastable because of its extremely low reaction rate. On the contrary, if the concentration is too high, it is highly supersaturated and precipitation takes place through homogeneous nucleation. The concentrations of the ammonium hexa-fluorotitanate and boric acid were carefully selected in order to achieve a status between highly supersaturated and metastable in order to obtain thin film formation through heterogeneous nucleation on the substrate (Shimizu et al., 1999). Fig. 2.9 shows an illustrative LPD deposition process.

The TiO_2 thin film prepared by LPD process is considerably different from that prepared by sol-gel method. For instance, Shimizu et al. (1999) and Kishimoto et al. (1998) showed that the as deposited thin film contained anatase phase without calcination. On the contrary, it is well known that calcination at 400~500 °C is needed for thin film prepared by sol-gel method in order to be crystallized (Yu et al., 2000). At a calcination temperature of 700°C, only anatase phase was observed on TiO_2 thin film prepared by LPD process, whereas both anatase and rutile phase were observed prepared by sol-gel method. The higher phase transformation temperature from anatase to rutile can be ascribed to the formation of Ti-O-Fe bonds in the thin film. The Fe-O species at the interface of TiO_2 crystallites inhibit the formation of rutile phase by preventing the nucleation that is necessary for the phase transformation to rutile.

Different researchers used different LPD preparation process for TiO_2 thin film. However, both studies showed a maximum photocatalytic activity at an optimal temperature. Kishimoto et al. (1998) showed that the highest acetaldehyde decomposition rate when the calcination temperature is 300 °C. The optimal photocatalytic activity is related to the physical and chemical properties of the TiO_2 such as crystallite size, BET surface area, pore size distributions and total pore volume. Yu et al. (2003) further showed that the highest methyl orange decomposition rate at a calcination temperature of 700°C is related to the Si content diffused from the substrate and the combination rate of electron-hole pair.

The preparation of TiO_2 from LPD process can be varied by the concentration of the parent solutions, pH value, calcination temperature and duration. As in other synthesis methods, metals and adsorbent were added to the TiO_2 thin film to increase its photocatalytic activity. Deki et al. (1996) dispersed Au in the TiO_2 film. Deki et al. (2001) also incorporated silicon oxide into TiO_2 film. These studies showed that the incorporation of other materials in TiO_2 by LPD method is possible. However, in both studies, no photocatalytic activity on pollutant removal was reported.

2.2.2 Sol-gel method

Sol-gel method is a process in which a precursor for preparation of a colloid consists of a metal or metalloid element surrounded by ligands (Brinker and

Scherer, 1990). Metal alkoxide is most commonly used as the starting precursor because it reacts readily with water. This process is called hydrolysis, as shown in the following equation,

$$M(OR)_4 + H_2O \longrightarrow HO - M(OR)_3 + ROH \qquad (2.18)$$

where M is a metal atom and R is a proton or other ligand such as an alkyl. Depending on the amount of water added, hydrolysis may be completed as shown in equation 2.19.

$$M(OR)_4 + 4H_2O \longrightarrow M(OR)_4 + 4ROH \qquad (2.19)$$

In this case, all the OR groups are replaced by OH group. The partially hydrolyzed HO-M(OR)$_3$ may be linked together by a condensation reaction forming a giant polymer structure, as shown in equations 2.20 and 2.21.

$$M(OR)_3 - OH + HO - M(OR)_3 \longrightarrow (OR)_3M - O - M(OR)_3 + H_2O \qquad (2.20)$$

$$M(OR)_3 - OR + HO - M(OR)_3 \longrightarrow (OR)_3M - O - M(OR)_3 + ROH \qquad (2.21)$$

The synthetics of titanium dioxide for environmental pollution remediation are extensively investigated by sol-gel process. This can be observed by an excellent review report prepared by Blake (2001 to 1994) in which it contained more than 1700 references on this subject. In general, metal alkoxide such as titanium isopropoxide (Lin et al., 1998; Negishi et al., 1998; Yu and Wang, 2000) and titanium butoxide (Muralidharan and Agrawal, 1997; Yu et al., 2000) is used as the starting precursor. Using titanium isopropoxide as the starting precursor, for an example, an appropriate amount of water, alcohol and acid are added to the metal alkoxide to form a transparent sol with vigorous stirring to avoid local concentration. Depending on the concentrations of the water and alcohol, the solution may form a transparent sol or participate. Usually, participation is avoided for thin film coating. The coating solution can be coated on the substrate either by dip-coating of spin-coating. In dip-coating, a uniform withdrawn speed is desired in order to obtain a better coating. Similarly, the spinning speed of the spin-coating machine is usually uniform during the coating process. The as-prepared TiO_2 thin film is amorphous. Calcination at around 400°C is needed for the transformation of amorphous to anatase phase. At a higher temperature of around 700°C, the anatase phase is transformed to the more stable rutile phase. Fig. 2.10 shows the preparation of TiO_2 film by sol-gel method (Lin et al., 1998).

Studies showed that, however, crystallize TiO_2 can be formed without high temperature calcination. Tang et al. (2002) reported that by controlling the ratio of titanium isopropoxide, nitric acid and water, TiO_2 participate of rutile phase is obtained. Farias (2001) showed that anatase titania powders were obtained directly by the hydrolysis of titanium butoxide in aqueous saturated solution of calcium chloride and other chloride salts. Kotani and others (2000, 2001) even also showed that anatase TiO_2-SiO_2 thin film can be formed by hot water treatment.

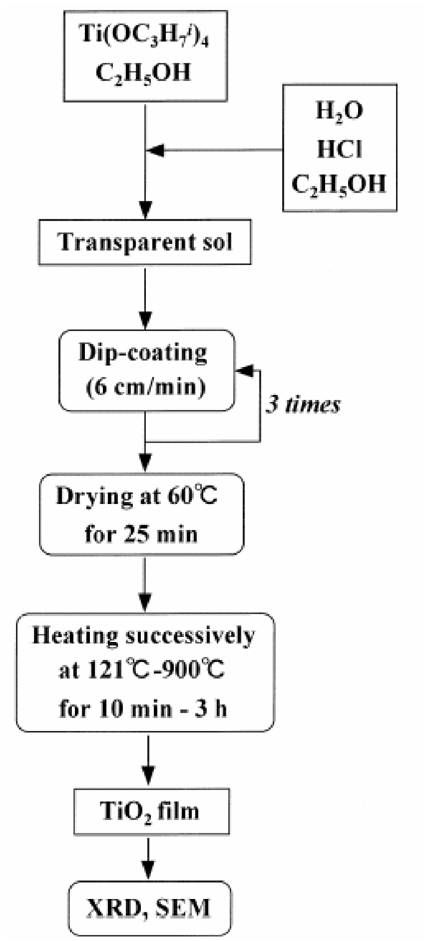

Fig. 2.10 Preparation of TiO_2 thin film by sol-gel method(Lin et al., 1998).

Similar to the LPD process, the preparation method of sol-gel process has a significant effect on the photocatalytic activity of the photocatalyst. Tanaka and Suganuma (2001) showed that the heat treatment effect on the photocatalytic activity of TiO_2. No activity was observed in the as-prepared amorphous TiO_2. Amorphous TiO_2 contained a lot of imperfections such as impurities, dangling bonds, microvoids which lead to electronic states in the band gap and behave as a recombination center. (Ohtani et al., 1997) At a calcination temperature of 600°C, the TiO_2 transferred from anatase to rutile phase, and the photocatalytic activity drastically decreased. The photocatalytic activity of rutile phase TiO_2, in general is lower than anatase phase TiO_2 because rutile phase has a higher electron-hole recombination rate (Fox and Dulay, 1993). As the calcination temperature increased, the surface area of the photocatalyst decreased. In general, a higher surface area has a higher photocatalytic activity due to its larger surface for adsorption (Ohtani et al., 1997; Tanaka and Suganuma, 2001). The crystallinity is also affected by the calcination temperature. Increasing the calcination temperature leads to a higher crystallinity and thus a higher photocatalytic activity due to its lower photo-excited electron-hole recombination rate (Tanaka et al., 1991; Ohtani et al., 1997). It is worthwhile to note that, the increase in surface area and the increase in crystallinity are contradictory with respect to the increasing calcination temperature.

2.3 Methods for improving activity of photocatalyst

The ultimate aim of the modification of photocatalyst is to increase its activity for practical use. The most convenient method, as indicated in the previous section, is to modify the synthetic process to achieve different physical and chemical properties. Common modification parameters are the morphology, crystal phase, crystallinity, surface area, immobilization of photocatalyst, metal and ion-doping and combination with adsorbent. The effects on the photoactivity by the modification of photocatalyst are already mentioned in the previous section. Thus, the following section will be focused on the ion-doping and combination of adsorbent.

2.3.1 Metals and ions doping

The advantage of metal and ions doping is to increase the trapping rate of electrons to inhibit the electron-hole recombination during illumination. In other words, it is a process to induce defect sites into the semiconductor lattice. Common ion dopants are Fe^{3+} (Iron), Cr^{3+} (Chromium), V^{4+} (Vanadium) and Pt (Platinum) (Fox and Dulay, 1993; A.L. Linsebigler et al., 1995; M.R. Hoffmann et al., 1995). Using an electron paramagnetic resonance technique, it is observed that the Ti^{3+} intensity of the Fe^{3+} doped TiO_2 increased during illumination (Gratzel and Howe, 1990). The effect of doping is very sensitive to its concentration. Milis and co-workers (1994) reported that a maximum photoactivity of nitrate removal was achieved when the iron content is 0.5%. Excess iron content decreased the photoactivity which is probably due to the formation of pseudobrookite (F_2TiO_5) (Navio et al., 1992) or the formation of iron spots on the surface which diminish the number of active sites (Schiavello et al., 1984). However, the beneficial effect of doping also depends on the dopant itself. It is reported that the addition of Cr^{3+} is detrimental to photoactivity. It created sites which increase electron-hole recombination (Herrmann et al., 1984). Similar detrimental effects were observed for Mo and V doping (Luo and Gao, 1992).

The beneficial effect of Pt addition to TiO_2 is widely accepted. The enhancement of photoactivity is probably due to an optimal attraction of free electrons of TiO_2 by Pt crystallites (Fox and Dulay, 1993). Cho and co-workers (2004) showed that the addition of Pt increased the photodegradation of ozone especially at high humidity levels. Fu et al. (1995) showed that the removal rate of benzene and the production of CO_2 are higher by platinized TiO_2.

Another important function of doping is to extend the light absorption spectrum from UV region (< 400 nm) to visible light region. Studies showed that by adding neodymium ion (Xie and Yuan, 2004), tungsten oxide (Li et al., 2001a), and cobalt ion (Iwasaki et al., 2000), photodegradation is observed under visible light region. Nevertheless, the photoactivity in general is lower than UV light region.

2.3.2 Photocatalyst loaded on adsorbent

Apart from metal and ion doping, photocatalyst loaded on adsorbent is also a convenient method to increase the photodegradation rate. Carbon, zeolite and silica are most commonly used with TiO_2 as they are the most widely investigated and commonly found adsorbent. The advantage of TiO_2 loaded on adsorbent is to increase the adsorption of pollutant at the initial stage of photo-oxidation.

Studies showed that the combination of adsorbent with TiO_2 can be achieved by different methods. Ibusuki and Takeuchi (1994) showed that a high NO removal was achieved simply by mixing activated carbon and TiO_2 mechanically. Similarly, a higher phenol (Matos et al., 1998) and salicylic acid (Arana et al., 2003) removal was reported by simply adding activated carbon into a TiO_2 suspension. Yoneyama and co-workers (Uchida et al., 1993; Takeda et al., 1995; Torimoto et al., 1996; Torimoto et al., 1997; Takeda et al., 1998) added activated carbon into a TiO_2 colloidal solution formed by sol-gel method using titanium tetraisopropoxide as the precursor solution. Tsumura et al. (2002) combined TiO_2 with carbon by carbonization. 10 g of TiO_2 was mixed with methanol solution of hydroxypropyle cellulose and dried to powder. It is then carbonized by heating at 700°C in a flow of nitrogen for 1 hr. Przepiorski et al. (2001) also carbonized

TiO_2 by mixing raw coal with a solution of bis(2,4-pentanedionato)-titanium oxide and heated to 900°C under nitrogen flow.

Durgakumari et al. (2002) provided an easy method to immobilize TiO_2 on zeolite. Initially, TiO_2 and zeolite were mixed thoroughly using ethanol in agate pestle and mortar. The solvent was removed by evaporation while mixing. It is then dried at 110°C and calcined at 450°C for 6 hr. Xu and Langford (1997) used a more complex method to support TiO_2 on zeolite. A solution of cetyltrimethylammonium was prepared by exchange of cetyltrimethylammonium chloride with aqueous ammonia. Ludox and sodium aluminate were used as the source of silica and alumina, respectively. The reaction mixture was loaded into a polypropylene bottle and heated without stirring at 90-95°C for 3 days. The solid product was filtered, washed with distilled water and dried in air at 100°C overnight. The solid was finally calcined in air at 540°C. Sampath et al. (1994) used a similar sol-gel method reported by Yoneyama and co-workers (Uchida et al., 1993; Takeda et al., 1995; Torimoto et al., 1996; Torimoto et al., 1997; Takeda et al., 1998) to load TiO_2 on zeolite.

The use of silica for immobilization of TiO_2 is widely investigated. Using sol-gel method, a similar procedure is applied as described in Section 2.2.2 with the addition of a silica precursor. Fig. 2.11 shows an illustrative example of preparing TiO_2-SiO_2 (Yu and Wang, 2000). Due to the difference in the hydrolysis rate of Ti-alkoxide and Si-alkoxide which cause phase separation, Yoldas (1989) partially hydrolyzed the Si-alkoxide prior to mixing with the Ti-alkoxide. Alternatively, the hydrolysis rate of Si-alkoxide is altered by adding a chelating agent such as acetylacetone (Zhai et al., 1999).

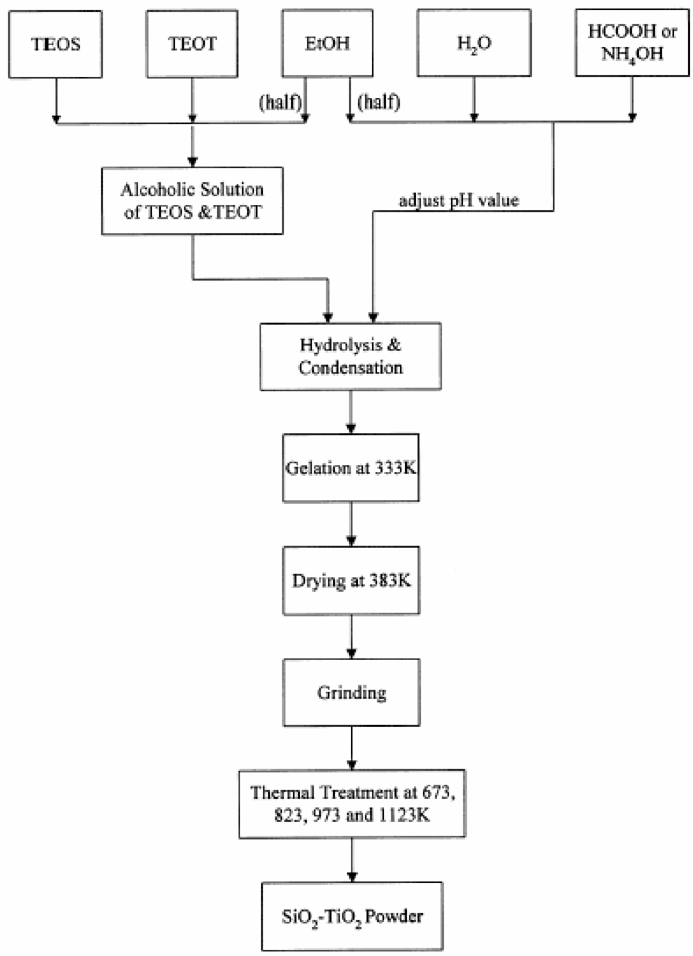

Fig. 2.11 Preparation of TiO_2-SiO_2 powder by sol-gel method(Yu and Wang, 2000).

Xu et al. (1999) provided an alternate way to coat TiO_2 on silica. They dispersed silica powder into a TiO_2 sol prepared by sol-gel method. The powder was finally heated at 450°C in air for 6 hrs. Nishikawa and Takhara (2001) also used SiO_2

beads coated with TiO_2 for adsorption and photocatalytic decomposition of odor compounds, but no details of the synthetic of TiO_2-SiO_2 were reported.

The primary function of loading TiO_2 on adsorbents is to increase its surface area. The BET surface area of TiO_2, in general, is in a range of less than 100 m^2/g. By combing TiO_2 with activated carbon, studies (Tryba et al., 2002; Uchida et al., 1993) showed that the BET surface area can increase to more than 400 m^2/g. Another important function of TiO_2 loaded on adsorbent is the reduction of intermediate during photocatalysis. Study (Torimoto et al., 1996) showed that the intermediates generated from the photodegradation of propyzamide is largely reduced when TiO_2 is loaded on activated carbon. They postulated that the activated carbon is able to adsorb the intermediate from the solution, thereby decrease the amount of intermediate from dissolution.

Liu et al. (1996) demonstrated an innovative use of TiO_2 with activated carbon. They used TiO_2 to generate the spent activated carbon. No reduce in adsorption of activated carbon was observed when coated with TiO_2. A 60% of the virgin capacity of the activated carbon was achieved after regeneration. No initial breakthrough was found for the adsorbent that were regenerated four times.

2.4 Effects of common indoor environmental parameters on pollutant photodegradation

Indoor environment is dynamic and ever-changing. Many factors affect the environment such as temperature, humidity levels, air exchange rate, number of occupants, nearby by outdoor and indoor environments, pollutant levels, etc. Out of the aforementioned factors, the followings are most commonly found that affect the photocatalytic reaction.

2.4.1 Effects of temperature

Photocatalytic reaction, unlike traditional catalytic reaction, does not require heating for activation. Instead, it requires photonic energy for activation. Duan et al. (2002) observed that no effect on toluene decomposition rate under the variation of temperature from 20-50°C. Blake and Griffin (1988) also showed that the photodecomposition rate of 1-Butanol is insensitive to temperature variation. Study (Fu et al., 1995) showed that, however, the removal rate of benzene is affected by the reaction temperature. A higher conversion of benzene is observed in the range of 70-110°C. They elucidated that the high conversion is due to the thermal catalytic reaction of the TiO_2 photocatalyst. Kim et al. (2002) showed that the reaction rate of VOCs is lower at higher temperature (75°C) and is due to the lower adsorption of VOCs on the catalyst.

2.4.2 Effects of initial pollutant concentration

The effect of initial pollutant concentration is controversial. Table 2.3 summarized the relationship between reaction rate and the initial concentration of different pollutants.

Compound	Decrease in reaction rate	Increase in reaction rate
Ozone	N.A.	Cho et al. (2004)
Toluene	Duan et al. (2002), Zhang et al. (2003), Wang and Ray (2000)	Li et al. (1998)[a], Kim and Hong (2002)[b], Obee (1996)[a], Maria et al. (2001)
Vinyl chloride	N.A.	Mohseni and David (2003)
Tetrachloroethylene	Li et al. (1998), Ku et al. (2001)	Kim and Hong (2002)[b], Ku et al. (2001)
Acetone	N.A.	Kim and Hong (2002)[b]
Methanol	N.A.	Kim and Hong (2002)[b]
Benzene	Wang and Ray (2000)	N.A.
Dichloroethene	Wang and Ray (2000)	N.A.
Formaldehyde	N.A.	Noguchi et al. (1998), Obee (1996)[a]

[a]Decreased after a certain concentration.

[b]Increased to a certain concentration and become steady.

Table 2.3 Effects of initial pollutant concentration on conversion.

The reaction rate of ozone, vinly chloride, acetone, methanol and formaldehyde increased with increasing initial concentration, whereas an opposite trend is observed for benzene and dichloroethene. The effect of initial concentration of toluene and tetrachloroethylene showed different results by different studies. For those studies reported an increased reaction rate with increasing initial concentration, the reaction agreed with the L-H model (Kim and Hong 2002; Mohseni and David, 2003). On the contrary, the decrease in reaction rate with increasing pollutant concentration is due to the blockage of active sites by the intermediates (Li et al., 1998; Duan et al., 2002). For the results reported by Obee (1996), the reaction rate increased initially and followed by a decreasing trend which is due to limited and fixed amount of active sites on the TiO_2 surface. In another study, a constant conversion was observed with regards to the variation of initial pollutant concentration (Sakamoto et al., 1999).

2.4.3 Effects of residence time

The effect of residence time is widely studied in the field of photocatalysis. Similar to the effects of initial pollutant concentration, two opposite effects are observed. Table 2.4 summarized the effects and the compounds reported in the literature. All the studies are conducted in a continuous flow reactor expected stated otherwise.

Compound	Conversion decreased with decreasing residence time	Conversion increased with decreasing residence time
Toluene	Sakamoto et al. (1999), Zhang et al. (2003)	Duan et al. (2002)[a], Obee and Brown (1995)[b],

		Maira et al. (2001)[b],
Nitrogen monoxide	Lim et al. (2000)	Devahasdin et al. (2003)[b],
Formaldehyde	N.A.	Obee and Brown (1995)[b]
Trichloroethylene	Shen and Ku (2002)	Wang et al. (1998)[b]
Ozone	Cho et al. (2004)	N.A.
Acetone	Alberici and Jardim (1997)	N.A.
Benzene	Sakamoto et al. (1999)	N.A.
Vinyl chloride	Mohseni and David (2003)	N.A.

[a]Batch flow reactor.

[b]Increased to a certain residence time and become steady.

Table 2.4 Effects of residence time on conversion.

Incongruous results for compounds such as toluene, nitrogen monoxide and trichloroethylene are observed. The increase in conversion by the decrease in residence time is obvious for the batch flow reactor. The increase in recirculation time decreased the irradiation time needed for pollutant removal (Duan et al. 2002). The influence of mass transfer played a significant role in the effect of residence time. When the mass transfer is significant, the degradation rate of the reactant increased with decreasing residence time (Alberici and Jardim, 1997). The conversion of pollutant increased with decreasing residence time and reached a steady state, followed by a decreasing trend with decreasing residence time. The photodegradation rate changed from mass transfer control to kinetic rate control and can be described by the L-H model (see section 2.1.3). On the contrary, studies (first column of Table 2.4) showed that the conversion decreased with increasing residence time. It is probably due to a better gas-solid contact can be obtained at a lower residence time (Cho et al., 2003) and a higher collision numbers of between the pollutant and the TiO_2 surface area is achieved (Sakamoto et al., 1999).

2.4.4 Effects of humidity levels

The effects of humidity levels on photodegradation rate are controversial and were pointed out in several reviews (Zhao and Yang, 2003; Mills and Le Hunte, 1997; Peral et al., 1997). This can be observed by the different effects of humidity level on different pollutants as shown in Table 2.5.

Compound	Conversion decreased with increasing humidity levels	Conversion increased with increasing humidity levels
Toluene	Cao et al. (2000)	Kim and Hong (2002), Li et al. (1998)[b], Einaga et al. (2002), Wang and Ray (2000), Luo and Ollis (1996)[a], You et al. (2001), Obee and Brown (1995)[a], Duan et al. (2002)[a], Sakamoto et al. (1999)[b], Zhang et al. (2003)[a]
m-Xylene	N.A.	Peral and Ollis (1992)[a]
Nitrogen monoxide	Devahasdin et al. (2003)[b]	N.A.
Formaldehyde	N.A.	Obee and Brown (1995)[a]
Trichloroethylene	Li et al. (1998), Wang et al. (1998)	Kim and Hong (2002)[a]
Methanol	N.A.	Kim and Hong (2002)[a]
1-Butene	Cao et al. (1999)	N.A.
Ozone	Cho et al. (2004)	N.A.

Acetone	Kim and Hong (2002), Peral and Ollis (1992),	N.A.
Cyclohexane	N.A.	Einaga et al. (2002)[b]
Cyclohexene	Einaga et al. (2002)	N.A.
1,3-Butadiene	Obee and Brown (1995)	N.A.
Benzene	N.A.	Einaga et al. (2002), Wang and Ray (2000), Lichtin and Sadeghi (1998), d' Hennezel et al. (1998), Sakamoto et al. (1999)[a]
Ethylene	N.A.	Park et al. (1999)

[a]Increased to a certain humidity levels then decreased.
[b]Increased to a certain humidity levels then become steady.

Table 2.5 Effects of humidity levels on conversion.

As shown in Table 2.5, aromatic compounds such as toluene and benzene are most frequently investigated. Toluene and trichloroethylene, for example, reported contradictory effect with increasing humidity levels in different studies. In a single study, the effect of increasing humidity levels varied with different compounds (Obee and Brown, 1995; Kim and Hong, 2002). In addition, the conversion increased to a certain humidity levels and then decreased or reached a steady state. In the case of the conversion increased with increasing humidity levels (3rd column of Table 2.5), the conversion in half of the studies decreased eventually. On the contrary, in the case of the conversion decreased with increasing humidity levels (2nd column of Table 2.5), the conversion consistently decreased with increasing humidity levels.

The above authors elucidated that the decrease in conversion in increasing humidity levels is due to the competitive adsorption of adsorption sites on TiO_2 between pollutant and water vapor. Obee and Brown (1995) conducted a dynamic sorption experiment between water vapor, toluene and formaldehyde, respectively. They showed that the increase in humidity levels decreased the sorption of toluene and formaldehyde significantly. Another possible reason is that the addition of water onto TiO_2 caused structural changes in surface band bending, which enhanced the efficiency of electron-hole recombination and reduced photoefficiency (Anpo et al., 1991). Cao et al. (2000) further showed that the surface of the TiO_2 is strongly hydrophilic and the preferential adsorption of water on the surface is responsible for low degradation rate at high humidity levels.

During photodegradation, water is needed for the generation of hydroxyl radical. Under a high pollutant concentration, water vapor is needed in the feed stream to generate sufficient hydroxyl radical for photodegradation. Thus, an increase in conversion is observed with increasing water vapor concentration to a certain concentration (Kim and Hong, 2002, Peral and Ollis, 1992). However, when excess water vapor is provided, the competition effect between pollutant and water vapor become dominant and decreased the conversion.

Other effects of water vapor reported are catalyst deactivation and mineralization ration. Ameen and Raupp (1999) showed that the deactivation caused by o-Xylene is decreased with increasing water vapor concentrations. The higher water vapor concentrations favor higher production rate of reactive hydroxyl radicals, which serve to attack adsorbed reactant molecules and partial oxidation intermediates, thereby decreasing the surface coverages by these compounds. Kim and Hong (2002) also showed a similar result in toluene photodegradation. They reported that at low humidity level, the color of the photocatalyst changed to brown. With increasing water vapor concentrations, the intermediates which were accumulated on the catalyst surface was desorbed or degradated.

Fu et al. (1995) reported that the amount of CO_2 produced is higher at higher water vapor concentrations from the photodegradation of benzene. Ibusuki and Takeuchi (1986) also showed that the production of CO_2 also increased with increasing water vapor concentrations from the photodegradation of toluene. On the contrary, study (Einaga et al. 2002) showed that the mineralization ratio is not affected by the variation of water vapor concentrations for the photodegradation of cyclohexane, cyclohexene and toluene.

2.5 *The impact of indoor air pollutants on human health and*

removal by photocatalysis

Traditionally, people focused on the outdoor air quality. The frequently invisible nature of indoor air quality problems compared to the highly visible photochemical smog is another reason why people concern outdoor air quality than indoor air quality (Jones, 1999). However, this focus was changed after the oil crisis in 1970s. Buildings were designed to be more air tight to increase its energy efficiency (Jones, 1998). The decrease in ventilation rate, improved insulation and the extensive use of synthetic building materials caused large amount of pollutants generated and accumulated inside the building (Teichman, 1995). Results from the TEAM (Total Exposure Assessment Methodology) studies conducted by the United State Environmental Protection Agency (USEPA) during the 1980s consistently showed that personal exposures to many pollutants in indoor environment are higher than outdoor (Wallace, 1991). Moreover, people generally spend more than 80% of their time in indoor environment (Roberts and Nelson, 1995). From the risk assessment point of view, indoor air quality has a higher impact of total risk exposure.

The concentration of an indoor air pollutant depends on many factors such as the volume of the indoor environment, the rate of generation and removal of the pollutant, the air exchange rate, and outdoor air pollutant concentration (Maroni et al., 1995). Hence, indoor air consists of a wide range of pollutants from biological to non-biological, organic to inorganic and gaseous phase to particulate phase. As a consequence, occupants of some buildings repeatedly describe a complex range of vague and often subjective health complaints, which is known as Sick Building Syndrome (SBS) (Horvath, 1997). Nevertheless, the common indoor air pollutants have not been changed for the past twenty years and their impact on human health is listed in the following section.

2.5.1 Nitrogen oxides (NO_x)

Nitrogen oxides, in general, is defined as the sum of nitrogen monoxide (NO) and nitrogen dioxide (NO_2). It is one of the major compounds which contributed to the photochemical smog in the atmosphere (Cohen and Murphy, 2003). It is an orange-brown color gas in high concentration. At low concentration, it is yellow or invisible and has an odor similar to bleach, but it is less pungent and smells somewhat sweeter than chlorine (Alberts, 1994). NO_x are formed from the combustion of nitrogen and oxygen at high temperature. Typical sources of NO_x are vehicle engine, cooking stoves, outdoor air and even cigarettes smoking (Chan et al., 1990; Samet et al., 1987). The daily variation of NO concentration is tremendous. Study (Weschler and Shields, 1994) showed that the peak NO concentration at the morning can reach as high as 400 ppb, whereas the average daily NO concentration is around 120 ppb. One of the major contributions of NO_x in household is the use of cooking stove. The use of electric stoves generated significantly lower NO_2 than vented gas cooking stove (Samet et al., 1987). Spengler et al. (1981) reported that the transient peak concentration of NO_2 may be as high as 1000 ppb.

The solubility of NO_2 in water is controversial. Study (Lambert, 1997) showed that it is highly soluble in water and a large proportion of inhaled NO_2 is removed in the respiratory system by combing with water in the lungs to form nitric acid and react with lipids and proteins to form nitrite anions and hydrogen ions (Postlethwait and Bidani, 1990). NO_2 within the airways is also converted into vapor phase nitrous acid via heterogeneous reactions (Spicer et al., 1993). An opposite idea was proposed by Alberts (1994), however, that NO_2 is poorly soluble in water and may penetrate to the conducting airways. This low solubility also delayed injury without provoking immediate warning symptoms. Nevertheless, both authors agreed that the exposure of NO_2 causes lung damage. Exposure to high levels (50 ppm) for a short period may produce cough, hemoptysis, dyspnea and chest pain. At a higher concentration (200 ppm), the exposure can produce pulmonary edema, which can be fatal (Rosenstock, 1987).

At typical indoor NO_2 level, exposure can cause eyes, nose and throat irritation (Fernand-Caldas and Fox, 1992). In England, Jarvis et al. (1996) reported that woman using gas cooking stove showed reduced lunch function and increased airway obstruction. Viegi and co-workers (1992) also reported a similar result. They showed that the increased reporting of cough and phlegm was associated with the use of bottled gas for cooking. In addition, studies showed that asthmatic patients are more sensitive to the exposure of NO_2 (Orehek et al., 1976). They reported that the exposure of asthmatic patients to only 0.1 ppm of NO_2 for 1 hour increased air reactivity. Salmone et al. (1996) also showed a slight increase in airway hyper responsiveness when the asthmatics exposed to 600 ppb NO_2.

In 1986, Hori et al. (1986) first demonstrated that NO is rapidly oxidized to NO_2 using photocatalyst TiO_2. Later, several studies proposed the reaction mechanism of NO using photocatalyst TiO_2, as shown in the following equations (Matsuda et al., 2001; Komazaki et al., 1999; Dalton et al., 2002).

$$TiO_2 \xrightarrow{hv} h^+ + e^- \qquad (2.1)$$

$$H_2O \longrightarrow H^+ + OH^- \qquad (2.2)$$

$$h^+ + OH^- \longrightarrow OH\cdot \qquad (2.3)$$

$$e^- + O_2 \longrightarrow O_2^- \qquad (2.4)$$

$$H^{+} + O_2^{-} \longrightarrow HO_2 \cdot \qquad (2.5)$$

$$NO + HO_2 \cdot \rightarrow NO_2 + OH \cdot \qquad (2.22)$$

$$NO_2 + OH \cdot \rightarrow HNO_3 \qquad (2.23)$$

$$HNO_{3(ads)} \rightarrow HNO_{3(aq)} \qquad (2.24)$$

The nitric acid formed on the TiO_2 surface was reported to deactivate the photocatalyst and the amount of nitric acid can be detected by the nitrate ion (NO_3^-) formed (Ibusuki and Takeuchi, 1994; Negishi et al., 1998; Ichiura et al., 2003). To alleviate the deactivation problem causes by the formation of nitric acid, metal compound with high pH value such as calcium oxide was found to be effective. In the absence of oxygen, nitrous oxide (N_2O), oxygen and nitrogen were formed instead of NO_2 (Zhang et al., 1998).

2.5.2 Volatile organic compounds (VOCs)

Volatile organic compounds are defined as a compound that contains at least one carbon and a hydrogen atom in its molecular structure and has a boiling point between 50°C and 260°C (Maroni et al., 1995). Common outdoor VOCs sources are vehicular exhaust and industrial activities (Pfeffer, 1994; Scheff and Wadden, 1993; Vega et al., 2000). The air pollutants emitted by vehicular exhausts are not easily dispersed inside the highly populated areas and readily accumulated to levels that can pose adverse health effects to people living or working there (Perry and Gee, 1994). Daisey et al. (1994) identified that motor vehicle emissions from outdoor air is a major source of VOCs. Indoor VOCs come from varieties of sources. Table 2.6 summarized the sources of VOCs and its species (Maroni et al., 1995). These compounds are widely used in indoor environment because they exhibit the desirable characteristics of good insulation properties, economy, fire resistance, and ease of installation (Burton, 1997). Brooks et al. (1991) reported that over 350 VOCs were found at concentrations higher than 1 ppb. Out of these VOCs, Table 2.7 summarized the most frequently found VOCs in indoor environment (IEH, 1996). Table 2.8 summarized the most frequently found VOCs in indoor environment of Hong Kong (EPD, 2003).

Consumer and commercial products	Aliphatic hydrocarbons (n-decane, branched alkanes), aromatic hydrocarbons (toluene, xylenes), halogenated hydrocarbons (methylene chloride), alcohols, ketones (acetone, methyl ethyl ketone), aldehydes (formaldehyde), esters (alkyl ethoxylate), ethers (glycol ethers), terpenes (limonene, alpha-pinene).
Paints and associated supplies	Aliphatic hydrocarbons (n-hexane, n-heptane), aromatic hydrocarbons (toluene), halogenated hydrocarbons (methylene chloride, propylene dichloride), alcohols, ketones (methyl ethyl ketone), esters (ethyl acetate), ethers (methyl ether, ethyle ether, butyl ether).
Adhesives	Aliphatic hydrocarbons (hexane, heptane), aromatic hydrocarbons, halogenated hydrocarbons, alcohols, amines, ketones (acetone, methyl ethyl ketone), esters (vinyl acetate), ethers.
Furnishings and	Aromatic hydrocarbons (styrene, brominated aromatics),

clothing	halogenated hydrocarbons (vinyl chloride), aldehydes (formaldehyde), ethers, esters.
Building materials	Aliphatic hydrocarbons (n-decane, n-dodecane), aromatic hydrocarbons (toluene, styrene, ethylbenzene), halogenated hydrocarbons (vinyl-chloride), aldehydes (formaldehyde), ketones (acetone, butanone), ethers, esters (urethane, ethylacetate).
Combustion appliances	Aliphatic hydrocarbons (propane, butane, isobutane), aldehydes (acetaldehyde, acrolein).
Potable water	Halogenated hydrocarbons (1,1,1-trichloroethane, chloroform, trichloroethane).

Table 2.6 Sources of common indoor air VOCs(Maroni et al. 1995).

Pollutant	Concentration				
	Percentile				Mean
	10^{th}	50^{th}	90^{th}	98^{th}	
Benzene	2	10	20	30	10
Toluene	30	65	150	250	80
n-Decane	3	10	50	90	20
Limonene	2	15	70		30
o-Xylene	3	5	10		10
1,1,1,-Trichloroethane	2	5	20		10
p-Dichlorobenzene	1	5	20		
1,2,4-Trimethylbenzene		5	20		10
m- and p-Xylene	10	20	40		20
Undecane	3	5	25		10
1,3,5-Trimethylbenzene		2	5		5
Dichloroethane		< 10	< 10	600	
Trichloroethane	1	5	20	30	

Table 2.7 Most frequently found VOCs in indoor environment(IEH, 1996).

Compound	Good Class
Benzene	5 ppbv

Carbon tetrachloride	16 ppbv
Chloroform	33 ppbv
1,2-Dichlorobenzene	83 ppbv
1,4-Dichlorobenzene	33 ppbv
Ethylbenzene	333 ppbv
Tetrachloroethylene	37 ppbv
Toluene	290 ppbv
Trichloroethylene	143 ppbv
Xylene (*o*-,*m*-,*p*-isomers)	333 ppbv

Table 2.8 VOCs for good class classification in Hong Kong (HKEPD, 2003).

The concentration of VOCs in indoor environment depends on many factors such as location, building age and indoor activities. VOCs concentration is much higher in newly constructed buildings anzxd building work or decoration has just competed. For example, Wallace et al. (1991) found that the concentration of decane is 100 times (from 0.49 to 49 ppb) after painting and the use of solvents. In general household, Wallace et al. (1991) showed that the personal maxima exposure of benzene in Los Angeles were 49.2 ppb. Winkle and Scheff (2001) reported that maximum concentration of ethylbenzene in a Southeast Chicago home was 39.5 ppb. In Italy, the concentrations of toluene and benzene were around 10.8 ppb (Carrer et al., 2000). In Hong Kong, the most common VOCs are benzene, toluene, ethylbenzene and xylene (BTEX). Out of these four compounds, different studies conducted by different research groups also showed that the concentration of toluene is the highest (Chao and Chan, 2001, Huo et al., 2003, Lee et al., 2002a). Table 2.9 shows the range of BTEX in Hong Kong (Huo et al., 2003).

Compound	Range (ppb)
Benzene	0.21-13.93
Toluene	1.45-76.76
Ethylbenzene	0-13.11
Xylene (*o*-,*m*-,*p*-isomers)	0.01-3.93

Table 2.9 Range of BTEX in Hong Kong (Huo et al., 2003).

VOCs are the most extensively investigated indoor air pollutant because of its adverse acute and chronic health impact. At evaluated concentrations, VOCs are potent narcotics and depressed the central nervous system (Maroni et al., 1995). Burton (1997) reported that some VOCs at high concentration may impair neurobehavioral function. Otto et al. (1992) showed that individual reported symptoms of headache, drowsiness, fatigue and confusion under the exposure of 22 VOCs at a concentration of 6.3 ppb. At an even higher concentration (12.8 ppb), toluene may cause symptoms of lethargy, dizziness and confusion. These may progress to coma, convulsions, and possibly death at levels in excess of 8750 ppb (Sandmeyer, 1982).

The chronic effect of VOCs is the increase in cancer risk (WHO, 1989). Chloroform, benzene, tetrachloroethylene, toluene, styrene and xylene are suspected to be toxic or carcinogenic (WHO, 1989; Godish, 1989). Wallace

(1991a) estimated that the typical concentration of benzene, vinylidine chloride, p-dichlorobenzene, chloroform, ethylene dibromide, methylene chloride and carbon tetrachloride exceeded the $1x10^{-6}$ risk of cancer by at least a factor of 10. Numerous sicknesses were also reported from chronic exposure of VOCs. Norback et al. (1995) reported a positive association between levels of VOCs and the prevalence of nocturnal breathlessness in Sweden. A strong association between mucous membrane irritation, central nervous system symptoms and the exposure of VOCs were reported amongst office workers (Hodgson et al., 1991). These unspecific and complex symptoms caused by the exposure of VOCs are called the Sick Building Syndrome (SBS) (Maroni, 1995).

The photodegradation of VOCs is extensively investigated in the field of photocatalysis. The topics include photodegradation of different pollutants, reaction mechanism and intermediates, deactivation and kinetics.

The conversion of aromatic hydrocarbon such as benzene and toluene is low (Einaga et al., 2002) and required a longer time to reach photo-steady-state concentration. The lower conversion of aromatic hydrocarbon is due to the intermediate formed and poisoned the photocatalyst. Its conversion depends on various parameters and is discussed in section 2.4. Chlorinated hydrocarbon, in general, has a very high conversion. Methylene chloride and trichloroethylene, for example, achieved 100% conversion reported by different research groups (Lichtin et al., 1996; d’ Hennezel and Ollis, 1997). Chlorine radical was formed from the photodegradation of chlorinated hydrocarbon and this chlorine radical attacked the pollutant and increased the conversion.

Deactivation problem is frequently reported during the photodegradation of aromatic hydrocarbon such as benzene (Fu et al., 1995; d’Hennezel et al., 1998), toluene (Alberici and Jardim, 1997; d’Hennezel et al., 1998; Zhang et al., 2003; Kim and Hong, 2002; Einaga et al., 2002) and o-xylene (Ameen and Raupp, 1999). The deactivation is not only noticed by the decreasing conversion of the pollutant but also observed by the change of the photocatalyst color from white to brown. It is reported that the deactivation problem and be reduced by adding ozone (Zhang et al., 2003), decreasing initial pollutant concentration (Alberici and Jardim, 1997) and increasing humidity levels (Ameen and Raupp, 1999). Deactivation is also reported from the photodegradation of sulfur containing compound such as diethyl sulfide (Kozlov et al., 2003), hydrogen sulfide (Canela et al., 1998) and alcohol such as 2-propanol (Cunningham and Hodnett, 1980;) and 1-butanol (Blake and Griffin). An excellent summary of catalyst deactivation in gas-solid photocatalysis is reported by Sauer and Ollis (1996).

The identification of intermediate is to understand the reaction mechanism and its effect on photodegradation of the target pollutant. Mendez-Roman and Cardona-Martinez (1998) reported that toluene reacted to form benzaldehyde and then reacted to form benzoic acid, which deactivated the surface. Benzyl alcohol and trace amount of formic and acetic acid were identified as intermediates from the photodegradation of toluene and benzene (d' Hennezel et al., 1998). These intermediates were identified from the surface of the photocatalyst but not from the gaseous phase. When the reaction temperature was raised to 260°C, benzene and benzaldehyde were identified as intermediate from the photodegradation of toluene. Similarly, toluene and benzaldehyde were identified as intermediate from the photodegradation of xylene (Blanco et al., 1996). Dichloroacetyl acid and phosgene were identified as the intermediates from the photodegradation of trichloroethylene and caused photocatalyst deactivation (Kim et al., 2000). By identifying the intermediates, the photodegradation mechanism of toluene and benzene was proposed ('d Hennezel et al., 1998), as shown in Fig 2.12 and 2.13.

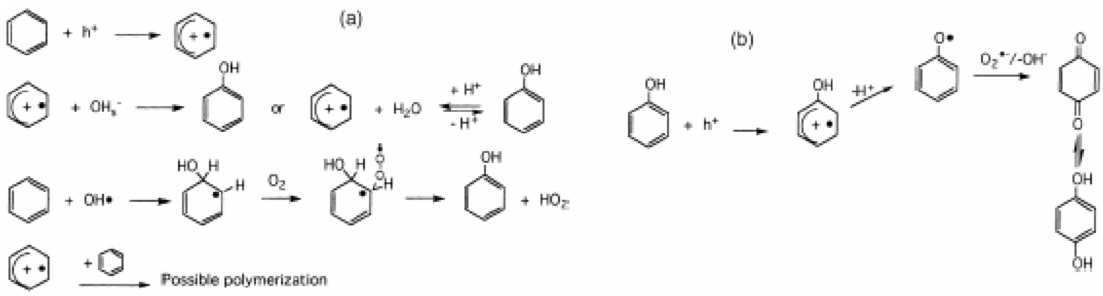

Figure 2.12 Primary (a) and secondary (b) benzene photodegradation pathways((d'Hennezel et al., 1998).

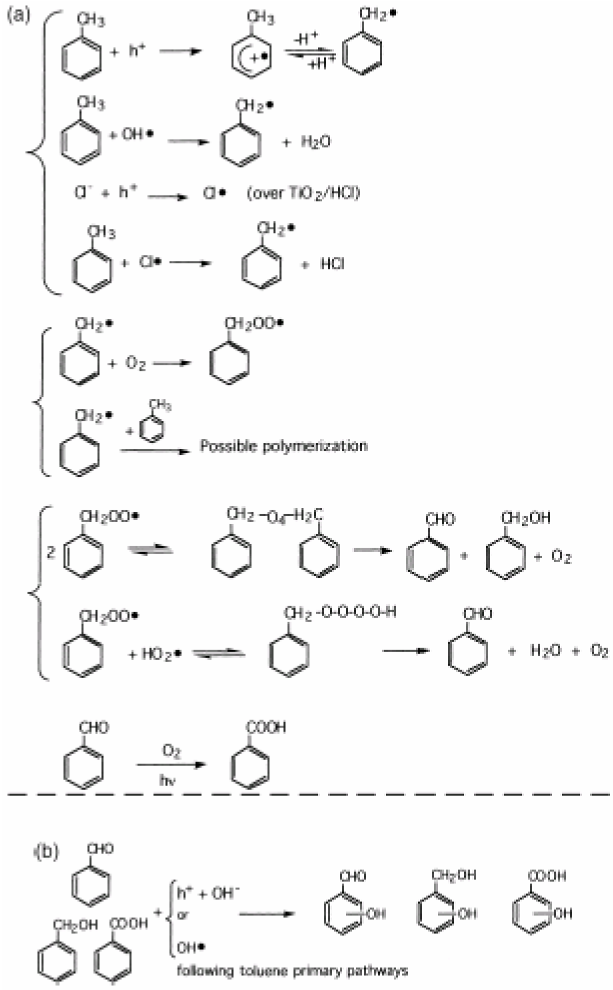

Figure 2.13 Primary (a) and secondary (b) toluene photodegradation pathways([d'Hennezel et al., 1998]).

2.5.3 Carbon monoxide (CO)

Carbon monoxide is a toxic, odorless and colorless gas that may result from incomplete combustion from any carbonaceous material (Alberts, 1994). Common indoor CO sources are heaters (Gold, 1992), gas stoves, attached garage (Alberts, 1994), vehicular emission (Samet et al., 1987) and tobacco smoking (Sterling, 1991). Another source of CO is methylene chloride which metabolized within the body to form CO (Gold, 1992).

The CO concentration in residential area is usually in the range of 2 to 4 ppm (Akland et al., 1985) and increased to a maximum of 12 ppm where gas stoves are in operation (Samet et al., 1987). In Hong Kong, the CO concentration in office was around 1.5 ppm (Lee and Chan, 1998). In shopping mall, the CO concentration is higher and ranged from 0.8 to 4.5 ppm. This is probably due to the close proximity of major entry doors to the public transport drop-off area (Li et al., 2001). The CO concentration is even higher in restaurants. Study showed that the CO concentration ranged from 1.2 to 13.7 ppm. This is due to the operation of cooking stoves for Korean barbecue and Chinese hot pot within the dining area (Lee et al., 2001).

The adverse health effects of CO are usually associated with its high affinity for hemoglobin (Colutas and Lambet, 1991). The affinity for hemoglobin is more than 200 times that of oxygen. Thus, it displaces O_2 binding carboxyhaemoglobin and impairing the release of O_2 to the tissue (Roughoton and Darling, 1994). At low concentrations of CO, it may produce non-specific flu symptoms such as headache, lethargy, nausea and dizziness with 2% to 10% carboxyhaemoglobin level (Baker et al., 1988). An alternation in alertness is reported with a carboxyhaemoglobin level of 3% to 4% (Levesque et al., 1990). Driving skills are impaired at 4% (Wright et al., 1973) and visual acuity may be affected at levels from 5% to 10% of carboxyhaemoglobin levels (Levesque et al., 1990). Similar to nitrogen oxides, patient expose to CO has a particular high risk (USEPA, 1991). Lambert (1994) reported that the probability of occurrence of an episode of myocardial ischemia was 2.1 times higher at 2% of carboxyhaemoglobin than below 1%.

The photodegradation of CO is rarely investigated. Vorontsov et al. (1997) showed that the photocatalytic activity was low using photocatalyst TiO_2 by different preparation methods but platinized TiO_2 showed significant activity. Vorontsov et al. (1999) further showed a higher activity was achieved with lowering of Pt oxidation state. The initial concentration and humidity levels also have a significant effect on the photoactivity of CO (Einaga et al., 2003; Hwang et al., 2003) and followed the L-H model. They showed that the reaction rate increased with increasing initial CO concentration and decreasing humidity levels. CO_2 is the product from the photodegradation of CO, as shown in the following equations (Hwang et al., 2003).

$$h^{+} + O^{2-} \Leftrightarrow O^{-} \qquad (2.25)$$

$$O^{-} + O_2 \Leftrightarrow O_3^{-} \qquad (2.26$$

$$CO + O_3^{-} \longrightarrow CO_2 + O_2^{-} \qquad (2.27)$$

$$CO + O^{-} \longrightarrow CO_2^{-} \qquad (2.28)$$

$$CO + OH \longrightarrow CO_2 + H \qquad (2.29)$$

2.5.4 Sulfur dioxide (SO_2)

Sulfur dioxide is a colorless gas with a strong pungent odor that can be detected at about 0.5 ppm. It is readily soluble in water and can be oxidized within airborne water droplets (Maroni et al., 1995). It is mainly produced from oxidation of sulfur during coal burning or other fuels that contain sulfur (Burr, 1997). In a study conducted in Riyadh, the capital of Saudi Arabia, Al-Rehaili (2002) showed that the indoor and outdoor concentration of SO_2 is closely related. The major sources of SO_2 are power stations, automobiles, industrial activities, indoor combustion in gas stoves and heating. The indoor concentration of SO_2 ranged from 0 to 2.76 ppm. Indoor SO_2 concentration may increase up to 30 ppb in Connecticut, USA (Leaderer et al., 1993). Using kerosene heaters and gas stoves, a mean value of 57 ppb SO_2 concentration is recorded (Leaderer et al., 1984). In China, 200 ppb of SO_2 concentration is reported (UAPCC, 2001). In Hong Kong, the concentration of SO_2 is similar to those reported in US and Europe. Both studies (Lee and Chan, 1998; Chao, 2001) showed that the indoor SO_2 concentration is below 10 ppb.

Adverse health effects due to the exposure of SO_2 are reported. Burr et al. (1981)

observed a higher rate of breathlessness and wheezing amongst miners wives who had open coal fires. Impaired lunch function and a range of other respiratory symptoms are reported to be associated with coal burning (Qin et al., 1993; Jin et al., 1993).

Study (Shang et al., 2002) showed that both homogeneous and heterogeneous reaction occurred on SO_2. With the addition of TiO_2, the reaction rate was considerably higher than homogeneous reaction. After several runs, the catalyst was deactivated and the reaction rate returned to that of homogeneous reaction. When heptane was co-injected with SO_2, the photodegradation rate of SO_2 decreased. Intermediates such as 2-butenoic acid, 2-hydroxyl-propanoic acid, heptoic acid and sulfur acid were found to deactivate TiO_2 surface.

2.5.5 Formaldehyde (HCHO)

Formaldehyde is a colorless gas with a pungent odor detectable at 1 ppm. Formaldehyde is the most commonly found aldehydes in the environment (Anderson et al., 1996). Sources of formaldehyde are building materials (Hines et al., 1993), infiltration from outdoor sources such as vehicular (Gabele, 1990) and industrial (Carlier et al., 1986) emissions, and incense burning (Ho and Yu, 2002). Anderson et al. (1975) reported that the indoor concentration of formaldehyde in

Denmark was 0.5 ppm. Similar findings were reported in Finland by Niemala et al., (1985) and in USA by Breysse (1984). Al-Rehaili (2002) reported that the average indoor formaldehyde concentration was 20 ppb in Saudi Arabia. In Australia, the average indoor formaldehyde concentration is 12.6 ppb (Garrett et al., 1999). In Hong Kong, the average formaldehyde concentration is lower than 20 ppb at home, office and air-conditioned classroom. In shopping mall and restaurant, the formaldehyde concentration is around 40 ppb (Lee et al., 2002a).

The adverse health effects of formaldehyde are widely investigated. It is a well-known irritant of the upper respiratory tact with symptoms such as eye, nose and throat irritation (Godish, 1990; Hanrahan et al., 1984; Ritchie and Lehnen, 1987). Eberlein-Konig et al. (1998) also showed that formaldehyde vapor is also a skin irritant. The acute health effects from formaldehyde exposure are summarized in Table 2.10 (Hines et al., 1993).

Formaldehyde concentration (ppm)	Observed health effects
<0.05	None reported
0.05-1.5	Neurophysiologic effects
0.05-1.0	Odour threshold limit
0.01-2.0	Irritation of eyes
0.10-25	Irritation of upper airway
5-30	Irritation of lower airway and pulmonary effects
50-100	Pulmonary edema, inflammation, pneumonia
>100	Coma, death

Table 2.10 Acute health effects from formaldehyde exposure (Hines et al., 1993).

Formaldehyde is an animal carcinogen (Morgan, 1997). A significant correlation between formaldehyde exposure and nasopharyngeal cancer is reported (Vaughan et al., 1986).

The reaction rate of formaldehyde is comparatively higher than aromatic hydrocarbon such as toluene, which is due to a stronger adsorption affinity and simpler oxidation chemistry (Obee and Brown, 1995; Obee, 1996). In another study (Noguchi et al., 1998) showed that the reaction rate of formaldehyde is also higher than acetaldehyde. This is due to the adsorption strength of formaldehyde is higher than acetaldehyde. The photodegradation of formaldehyde also obeyed the L-H model.

The reaction rate of formaldehyde is affected by its initial concentration and the humidity levels. At low humidity levels and high concentration levels, the reaction rate decreased with decreasing humidity levels. At high humidity levels and high concentration levels, the reaction rate increased with increasing humidity levels. At moderate to high humidity levels and low concentration levels, the reaction rate decreased with increasing humidity levels. The different effects of humidity levels on the initial formaldehyde concentration is related to the dehydroxylation by hydroxyl radical attack of formaldehyde, rehydroxylation through dissociation of water vapor, and competition effect between water vapor and formaldehyde on TiO_2 surface.

Like many photocatalytic reactions, the final oxidation products of formaldehyde are CO_2 and H_2O. Prior to the formation of final oxidation products, formic acid was reported as the frequently found intermediates (Noguchi et al., 1998, Yang et al., 2000) (equations 2.30-2.32).

$$HCHO + OH\cdot \longrightarrow HCO\cdot + H_2O \qquad (2.30)$$

$$HCO\cdot + OH\cdot \longrightarrow HCOOH \qquad (2.31)$$

$$HCOOH + 2h^+ \longrightarrow CO_2 + 2H^+ \qquad (2.32)$$

2.5.6 Airborne bacteria

The sources of airborne bacteria are outdoor air (Wanner et al., 1993) and usually associated with the presence of organic matter such as wood and food in indoor environment (IEH, 1996). The Hong Kong humid and warm climate makes Hong Kong a favorable environment for the growth of airborne bacteria. Many households in Hong Kong are installed with window type air conditioners. If the air conditioners are not frequently cleaned, they can be coated with dust and pathogenic bacteria. One of the contributing factors affecting indoor concentrations of airborne bacteria is the hygienic quality of a residence. Jaffal et al. (1997) found that the houses with low hygienic standards had higher bacteria counts. The age of a residential building, the frequency of housekeeping and ventilation were predominant factors associated with the concentrations of airborne bacteria within a domestic home (Lee and Chang, 1999).

Symptoms such as rhinitis, asthma, humidifier fever are reported from the exposure of airborne bacteria (IEH, 1996). Peat et al. (1998) reported a number of well-defined disease and various less well-defined symptoms associated with bacteria. In UK, Hunter et al. (1996) reported the average colony forming units CFU/m^3 for bacteria is 365.6 at home. In some intensive cases, 917 and 933 CFU/m^3 was found in living rooms and bedrooms, respectively. In USA, Macher et al. (1991) showed that the airborne bacteria level in an apartment is only 198 CFU m/^{3}. In Hong Kong, the airborne bacteria at home, office, air-conditioned classroom, shopping mall and restaurant exceed than those in outdoor environment. In particular, the airborne bacteria level was reported as high as 2220 CFU/m^3 for air-conditioned classroom. The average airborne bacteria of the aforementioned indoor environments are around 750 CFU/m^3 (Lee et al., 2002a).

Photocatalytic sterilization of bacteria is well documented. This effect was first reported by Fujishima and co-workers (Kikuchi et al., 1997; Sunada et al., 1998). 150 μL of E. coli suspension was placed on an illuminated TiO_2 coated glass plate. After 1 hour illumination, all the cells were killed, where as 50% of the cell remained without the presence of TiO_2. In another study, Goswami et al. (1997) reported the use of illuminated TiO_2 for disinfection of indoor air. They reported that higher UV intensity (without the presence of TiO_2) resulted in higher destruction rate of bacteria. The destruction rate was higher under the presence of TiO_2. The destruction rate of bacteria was decreased with increasing humidity levels and decreasing residence time.

2.6 Photodegradation of multiple pollutants

Photodegradation of multiple pollutants is rarely investigated as reported by Ollis (2000). The photodegradation of multiple pollutants, however, is important as studies showed that the conversion of a pollutant is affected by the presence of other pollutants. Sauer et al. (1995) and Luo and Ollis (1996) showed that the presence of 1,1,3-Trichloropropene (TCP) largely promoted the conversion of toluene and decreased the deactivation rate. On the contrary, the increased in toluene concentration decreased the conversion of TCP and increased the deactivation rate. Similar effects were reported for perchloroethylene and toluene mixture. The presence of methylene chloride only slightly promoted the conversion of toluene but no effect was observed between chloroform and carbon tetrachloride with toluene. The promotion mechanism involved the reaction of hydroxyl radical or positive hole with TCP leading to the formation of chlorine radical. The chlorine radical then attacked the toluene and promoted its conversion. The presence of chloroform or carbon tetrachloride did not promote the conversion of toluene because it has no carbon-carbon double bond for chlorine radicals to attack to initiate the reaction. The increase in toluene conversion decreased the promotion effect is probably due to the scavenging of chlorine radicals. In another study (d'Hennezel and Ollis, 1997), the presence of trichloroethylene promoted the conversions of toluene, ethylebenzene, m-xylene, methyl ethyl ketone, acetaldehyde, butyraldehyde, methyl-tert-butyl ether, methyl arcylate, 1,4-dioxane and hexane. The presence of trichloroethylene, however, inhibited the conversions of acetone, methylene chloride, chloroform and 1,1,1-trichloroethane and no effect was reported on benzene and methanol. Similar study was also reported by Lichtin groups (Lichtin et al., 1994, Lichtin et al., 1996). They found that the presence of trichloroethylene promoted the conversions of i-octane, methylene chloride, chloroform, and inhibited the conversions of acetone and acetonitrile. Methanol was also found to inhibit the conversions of methylene chloride and trichloroethylene and vice versa. Tetrachloromethane promoted the conversion of methanol and had little effect on 2-propanol and t-butanol.

Chapter 3 METHODOLOGY

3.1 Introduction

This chapter describes the methodology for the synthesis of photocatalyst on different substrates and the experimental setup for the photo-reactor. The sampling and analytical methods of target pollutants can be also found in this chapter. The procedure of pollutants removal efficiency of the photocatalyst installed in a commercial air cleaner and inside an air duct in an office is also provided. Details of the analytical instruments can be found in Appendix I.

3.2 Target pollutants

3.2.1 Common indoor air pollutants

The target pollutants selected in this study are those commonly found in indoor air. To apply photocatalytic technology for air pollution, indoor air is most suitable because people generally spend more than 80% of their time in indoor air (Roberts and Nelson, 1995) and the pollutant in indoor environment is usually higher than outdoor air (Jones, 1999).

Nitrogen monoxide (NO), nitrogen dioxide (NO_2), sulfur dioxide (SO_2), volatile organic compounds (VOCs), carbon monoxide (CO) and formaldehyde (HCHO) were selected as target pollutants in this study. Studies showed that these pollutants are commonly found in indoor air and has adverse health impact (See Chapter 2). Among numerous compounds which belong to VOCs, benzene, toluene, ethylbenzene and o-xylene (BTEX) were chosen for this study. The reason is that BTEX is the major VOCs found in indoor environments in different countries (IEH, 1996; Van Winkle and Scheff et al., 2001). In Hong Kong, BTEX are also the major VOCs found in the indoor environment, either in mechanically ventilated buildings or in residential homes (Chao and Chan, 2001; Lee et al., 2002a). Thus, BTEX were selected as the target organic pollutant.

3.2.2 Pollutant concentration and analytical methods

The pollutants concentrations were carefully and specifically selected in this study. It is because the pollutant concentration has a vital effect on various aspects of photocatalysis. Deactivation, for instance, are likely to occur at high pollutant concentration (Alberici and Jardim, 1997; Ameen and Raupp, 1999). The photodegradation rate of a pollutant also increased with increasing initial concentration (Maria et al. 2001; Mohseni and David, 2003). In addition, the effects of humidity levels also related to the initial concentration of the pollutant (Obee and Brown, 1995).

Reactant	Concentration	Reference	Method
NO	200 ppb	Weschler and Shields, 1994; Lee and Chan, 1998.	USEPA designated Chemiluminescence method
NO_2	45 ppb	Ryan et al., 1989; Leaderer et al., 1986.	USEPA designated Chemiluminescence method
CO	2 ppm	Akland et al., 1985; Samet et al., 1987.	USEPA designated Gas Filter Correlation method
SO_2	200 ppb	UAPCC, 2001.	USEPA designated Pulsed Fluorescence method
BTEX (each)	20 ppb	Lee et al., 20026; Chao and Chan, 2001;	USEPA TO-14A
HCHO	50 ppb	Garrett et al., 1990; Niemala, 1985.	USEPA TO-11A

Table 3.1 Selected concentration of the target pollutants and analytical methods.

Most of the photocatalytic studies conducted using a concentration of several to thousand parts-per-million (ppm) level (Kim and Hong, 2002; Ku et al., 2001; Wang and Ray, 2000). However, this extreme high pollutant concentration is not found in normal and polluted indoor environment. Thus, the concentration conducted has a significant effect on deactivation, reaction rate and effects of humidity levels. In this study, the concentration of the target pollutants is selected with reference to the typical indoor air pollutant level. Most of the experiments conducted in this study followed the concentration listed in Table 3.1 unless otherwise stated. Intermediates such as anions and formic acid were analyzed by Ion Chromatography (IC) and VOCs intermediates were analyzed by Gas Chromatography / Mass Spectrometer (GC/MS). Details of the analytical instruments and procedures can be found in Appendix I.

3.2.3 Photodegradation of multiple pollutants

To comprehend indoor air purification by photocatalysis, photodegradation of multiple pollutants is vital. Studies (Luo and Ollis, 1996; Lichtin et al., 1996) showed that the presence of a pollutant has a significant effect on the photoactivity of other pollutants. Thus, a series of experiments were conducted to understand the reciprocal effects between indoor air pollutants by photocatalysis. Table 3.2 shows the cases of photodegradation of multiple pollutants.

	NO	CO	NO_2	SO_2	BTEX	HCHO
NO		X	X	X	X	X
CO	X		X	X	X	X
NO_2	X	X		N.A.	N.A.	N.A.
SO_2	X	X	N.A.		X	X
BTEX	X	X	N.A.	X		X
HCHO	X	X	N.A.	X	X	

X = cases performed; N.A. = cases not performed.

Table 3.2 Summary of photodegradation of multiple indoor air pollutants.

3.3 Photocatalytic activity evaluation

The reactor used in the photocatalyst study is most vital. It provides a physical boundary to identify the photoactivity of the photocatalyst on different pollutants. Apart from reactors, the photocatalyst was also installed in an air cleaner and tested in an environmental chamber under static condition. Finally, the photocatalyst was installed in an air duct inside an office to evaluate the performance under real indoor environment. The purpose of different testing conditions is to increase the testing scale from laboratory scale reactor to residential scale air cleaner and finally to actual indoor environment such as office. Testing photocatalyst in different scales provides a comprehensive evaluation of applying photocatalytic technology for indoor air purification.

3.3.1 Photocatalytic activity evaluated in a laboratory scale reactor

3.3.1.1 Reagents

Standard gas was used as the pollutant source. It is acquired from compressed gas cylinder with nitrogen as balanced gas with traceable National Institute of Standards and Technology (NIST) standard. The details of the standard gas are shown in Table 3.3. A typical NIST certificate of formaldehyde acquired from the compressed gas cylinder is shown in Fig. 3.1. The concentration of the standard gas depended on the initial pollutant concentration applied in this study.

Reactant	Concentration (ppmv)	Company
NO	50 ± 1%	BOC gas
CO	100 ± 2%	BOC gas
SO_2	50 ± 1%	BOC gas
BTEX (mixing ratio 1:1:1:1)	1 ± 2%	Spectra gas
HCHO	10 ± 2%	Arkonic gas

Table 3.3 Summary of reactant gas acquired from compressed gas cylinder.

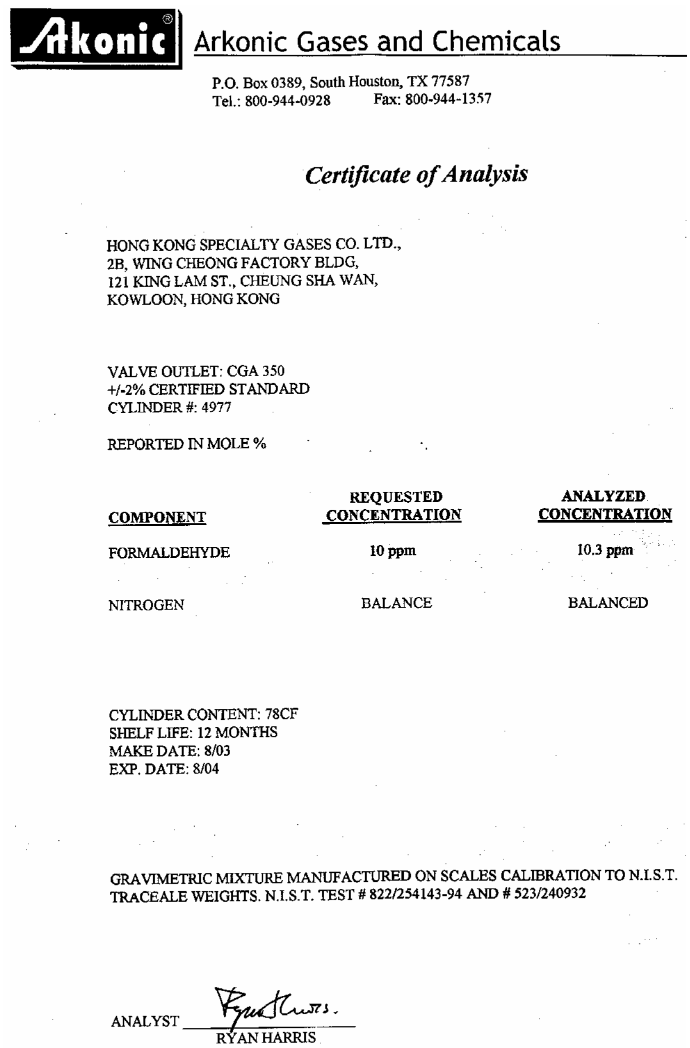

Arkonic Gases and Chemicals

P.O. Box 0389, South Houston, TX 77587
Tel.: 800-944-0928 Fax: 800-944-1357

Certificate of Analysis

HONG KONG SPECIALTY GASES CO. LTD.,
2B, WING CHEONG FACTORY BLDG,
121 KING LAM ST., CHEUNG SHA WAN,
KOWLOON, HONG KONG

VALVE OUTLET: CGA 350
+/-2% CERTIFIED STANDARD
CYLINDER #: 4977

REPORTED IN MOLE %

COMPONENT	REQUESTED CONCENTRATION	ANALYZED CONCENTRATION
FORMALDEHYDE	10 ppm	10.3 ppm
NITROGEN	BALANCE	BALANCED

CYLINDER CONTENT: 78CF
SHELF LIFE: 12 MONTHS
MAKE DATE: 8/03
EXP. DATE: 8/04

GRAVIMETRIC MIXTURE MANUFACTURED ON SCALES CALIBRATION TO N.I.S.T. TRACEALE WEIGHTS. N.I.S.T. TEST # 822/254143-94 AND # 523/240932

ANALYST RYAN HARRIS

Figure 3.1 NIST certificate of formaldehyde standard gas.

The generation of NO_2 was different from other gases. NO_2 was generated from the oxidation of NO under the presence of ozone, as shown in the following equation.

$$NO + O_3 \longrightarrow NO_2 + O_2 \qquad (3.1)$$

In order to achieve complete oxidization of NO, the amount of O_3 was higher than that of NO. The O_3 was generated by a dynamic calibrator (Model 700, Advanced Pollution Instrumentation Inc.). The mixing volume of the calibrator is designed according to USEPA guidelines to ensure complete mixing reaction. For example, 60 ppb of ozone was generated with 45 ppb of NO to obtain 45 ppb NO_2. The concentration of ozone accompanied with NO_2 was also simultaneously monitored by an UV photometer ozone analyzer (Disibi Environmental Corp.).

3.3.1.2 Experimental setup

Fig. 3.2 shows a schematic diagram of the experimental setup for the experiments conducted with the laboratory scale reactor. A reactor with a volume of 18.6 liter (20.1H x 44.2L x 21W cm, Fig. 3.3) with its surface coated by a Teflon film (BYTAC Type AF-21) was used for this study. Illumination was provided by a 6W UV lamp (Cole-Parmler) which emits a primary wavelength at 365 nm and its intensity was determined by a UV meter (Spectroline DRC-100X).

The UV lamp was horizontally placed at the upper part of the reactor, 14 cm from both ends. UV intensity measured in all experiments was 750 μW/cm^2. The TiO_2 coated filter was supported by a Teflon film and fixed horizontally with a vertical distance of 5 cm between the UV lamp. Stainless steel sampling ports and Teflon tubing were used to connect the reactor and the analytical instruments.

1.Zero air generator 2.Humidification chamber
3.Standard gas 4.Calibrator
5.Reactor 6.NOx analyzer
7.O_3 scrubber & DNPH cartridge
8.Summa canister 9. Data recorder
10.HPLC 11.GC/MS

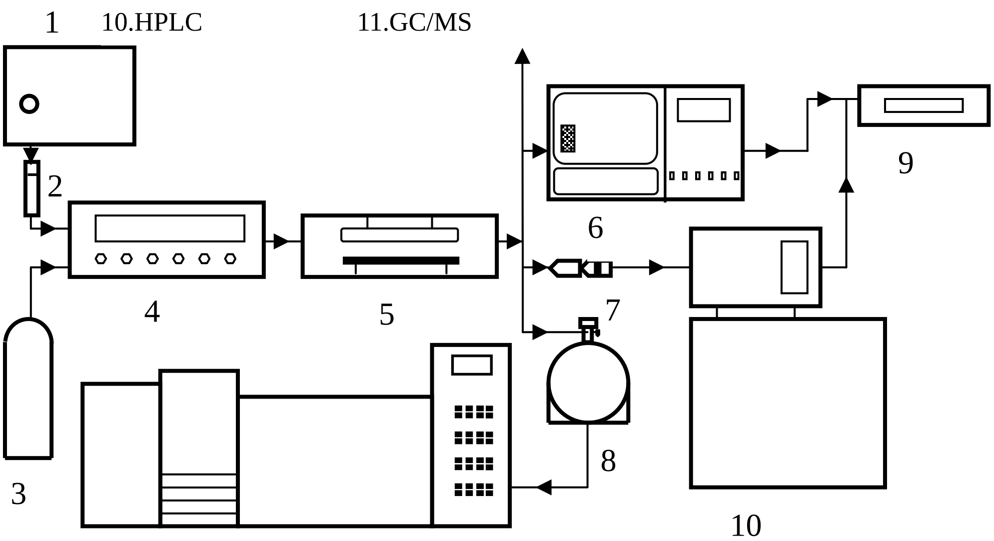

Figure 3.2 Schematic diagram of the experimental setup.

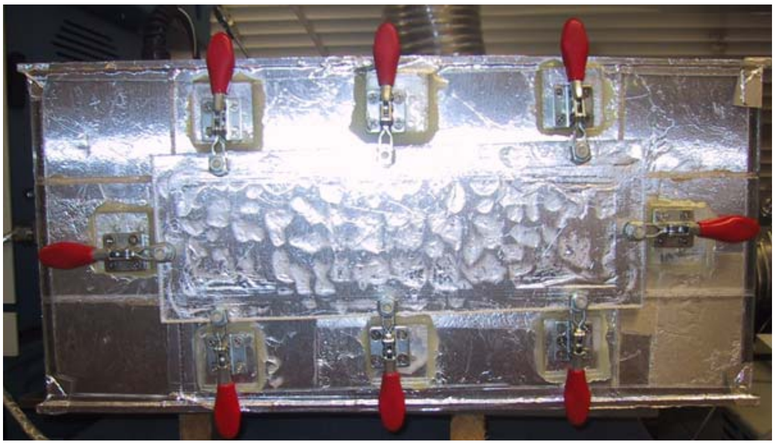

Figure 3.3 Laboratory scale continuous flow reactor.

A zero air generator (Thermo Environmental Inc. Model 111) was used to supply the air stream. The desired humidity of the flow was controlled by passing the zero air stream through a humidification chamber. The reactant stream and the zero air stream were connected to a mass flow calibrator (Advanced Pollution Instrumentation Inc. Model 700). The gas streams were pre-mixed by a gas blender and the desired flow was controlled by a mass flow controller inside the calibrator. After the inlet and the outlet concentration achieved equilibrium (1 hour), the UV lamp was turned on and initiated the reaction. The concentration of NO was continuously measured with a Chemiluminescence NO analyzer (Thermo Environmental Instruments Inc. Model 42c), which monitors NO, NO_2, and NO_x at a sampling rate of 0.7 L/min. SO_2 was continuously measured with a Pulsed Fluorescence SO_2 analyzer (Thermo Environmental Instruments Inc. Model 43b) at a sampling rate of 0.4 L/min. Pre-cleaned Summa canisters were evacuated for VOCs sampling. Constant VOCs sampling time was achieved using a mass flow controller. Samples of VOCs were collected at designated times during the experiment. After collection, the canister sample was first concentrated by a Nutech Cryogenic Concentrator (Model 3550A), and the trapped VOCs were separated and analyzed by Hewlett Packard Gas Chromatograph (Model HP 6890) and quantified by a Mass Selective Detector (Model HP5973). After analysis, the canister was sequentially evacuated and pressurized with humidified zero air until all compounds detected were smaller than 0.2 ppb. TO-14 (Toxi-Mat-14M Certified Standard (Matheson)) standard gas was analyzed using the GC/MS system seven times at 0.2 ppb to obtain the method detection limits (Lee et al., 2002).

The formaldehyde concentration was sampled with a procedure similar to those reported elsewhere (Ho et al., 2002). An acidified 2,4-dintrophenylhydrazine (Waters Sep-Pak DNPH-silica) equipped with a Desert Research Institute (DRI)'s standard carbonyl sampler (Fig. 3.11) was used to collect the formaldehyde according to the USEPA TO-11 method. It is known that the presence of ozone degradated the formed 2,4-DNPH hydrazones and induced bias on the silica cartridges (Arnts and Tejada, 1989). An ozone scrubber (Waters) was equipped before the DNPH-silica cartridge, to prevent any interference caused by the ozone. The flowrate passing through the DNPH-silica cartridge with the ozone scrubber was measured by a soap bubble flow meter (Bios flowmeter, Fig. 3.12) prior to and after the sampling. Typically, the sampling flowrate was 1 L/min and no breakthrough was found. The sampling flowrate used to calculate the formaldehyde concentration is the average flowrate prior and after the sampling. After sampling, all the cartridges were capped and wrapped in pouches provided by Waters. The pouches were stored in a refrigerator at -10°C and were analyzed within one week. Prior to the experiment, the background aldehydes samples were collected at the time when the pollutant was generated. After turning on the UV lamp, samples of the aldehydes were also collected. The reported aldehydes concentrations during the photodegradation process were subtracted from the background aldehydes concentration.

3.3.2 Photocatalytic activity evaluated in an air cleaner

3.3.2.1 Configuration of the air cleaner

The photocatalyst was installed in an air cleaner. The air cleaner consisted of an activated carbon filter, a HEPA filter and a UV lamp (Fig. 3. 4). Illumination was provided by a 6W ultraviolet germicidal lamp (Sankyo Denki, Japan) (Fig. 3.5). The wavelength of the germicidal lamp ranged from 200 to 300 nm with the maximum light intensity at 254 nm (denoted as UVC). The ultraviolet germicidal lamp can be interchanged by a 6W black lamp (Sankyo Denki, Japan), depending on the experimental settings. A centrifugal fan is used to draw air at the front of the air cleaner and exhausted on the top. The flowrate used in all study was 5.1 m^3/min. The TiO_2 filter or the TiO_2/AC filter was mounted 1cm on top of the UV lamp (Fig. 3.6). The UV intensity measured (UVP radiometer, model UVX) at the surface of the TiO_2 filter was 1.49 mW/cm^2 at 365 nm and 2.76 mW/cm^2 at 254 nm using the UVA lamp and UVC lamp, respectively.

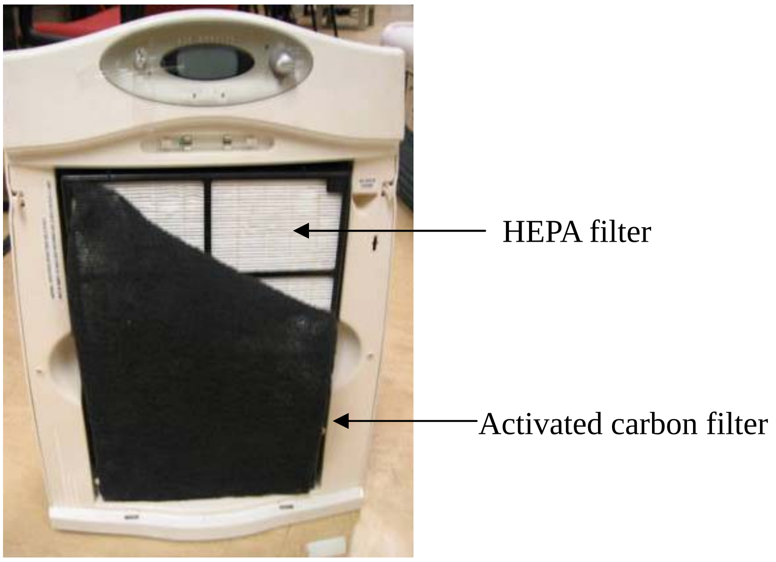

Figure 3.4 Front view of the commercial air cleaner.

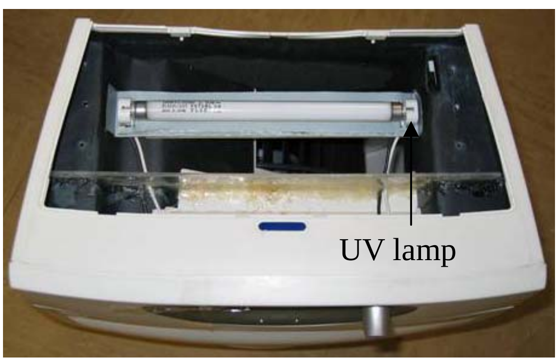

Figure 3.5 Top view of the commercial air cleaner.

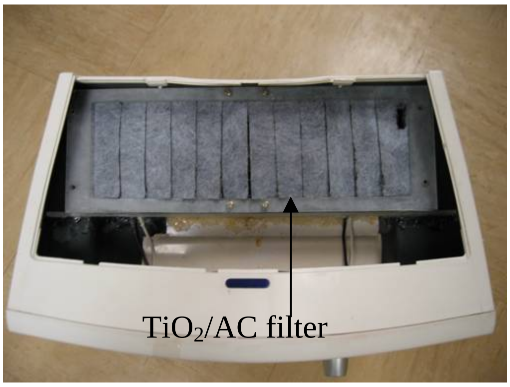

Figure 3.6 Top view of the commercial air cleaner installed with the TiO_2/AC filter.

3.3.2.2 Experimental setup

The air cleaner was placed inside an environmental chamber under static condition. The environmental chamber used in this study was made by electropolished stainless steel with a volume of 2.38 m^3 was (Lee et al., 2003a; Kwok et al., 2003, Lam et al., 2001). The temperature and relative humidity in all studies were 24 ± 1°C and 70% ± 5%, respectively. Four mixing fans were installed at the bottom corners of the chamber to ensure adequate mixing of air. The temperature and relative humidity were continuously monitored by a portable Q-Trak monitor (Model 8550, TSI, MN, USA). After each test, the chamber was cleaned by scrubbing the inner surfaces with deionized and distilled water. The chamber was then conditioned by purging zero air (Thermo Environmental Inc. Model 111) and conditioned to 25°C and 70% relative humidity for at least 24 h prior to testing. The chamber background level was measured before each experiment. NO and toluene were injected inside the chamber via a stainless sampling port. Mixing was allowed for 30 min and sample of the initial concentrations were collected via the stainless steel sampling port with Teflon tubing at the center of the environmental chamber at 0.6m above floor into a Tedlar sampling bag (SKC). The concentration of NO was measured by a Chemiluminescence NO analyzer (Thermo Environmental Instruments Inc. Model 42c), which monitors NO, NO_2, and NO_x at a sampling rate of 0.7 L/min. The concentration of toluene was measured by a Non-Methane Hydrocarbon (NMHC) analyzer equipped with a FID detector (Thermo Environmental Instruments Inc. Model 55) at a sampling rate of 1 L/min. The air cleaner was turned on from an external circuit equipped outside the environmental chamber. Samples were then taken at desired time intervals. The reagents used such as standard gas and photocatalyst are identical to that reported in section 3.3.1.1.

3.3.3 Photocatalytic activity evaluated in an air duct inside an office building

3.3.3.1 Site description

The office is located inside a commercial building in Hong Kong. A typical floor plan of the office is shown in Fig. 3.7. Owing to the continuous activities inside the office, the sampling sites were selected so that the interference caused by the sampling was minimized. The concentrations of NO, NO_2 and NMHC were measured at locations 1 to 5 at a duration of 10 minutes and the airborne bacteria concentration was measured at locations 6 and 7, as shown in Fig 3.7. The office was air conditioned and the door was always closed.

The TiO_2/AC filter was installed inside the air duct at the “FCU-B” location, as shown in Fig. 3.8. The filter size was 12 cm x 50 cm and was constrained by the size of the existing air duct. Illumination was provided by two 6W UVC lamps (Fig. 3.9). The UV intensity measured was 450 $\mu W/cm^2$ on the surface on the TiO_2/AC filter. According to the information provided by the air duct maintenance personnel, the percentage of the fresh air was around 30%.

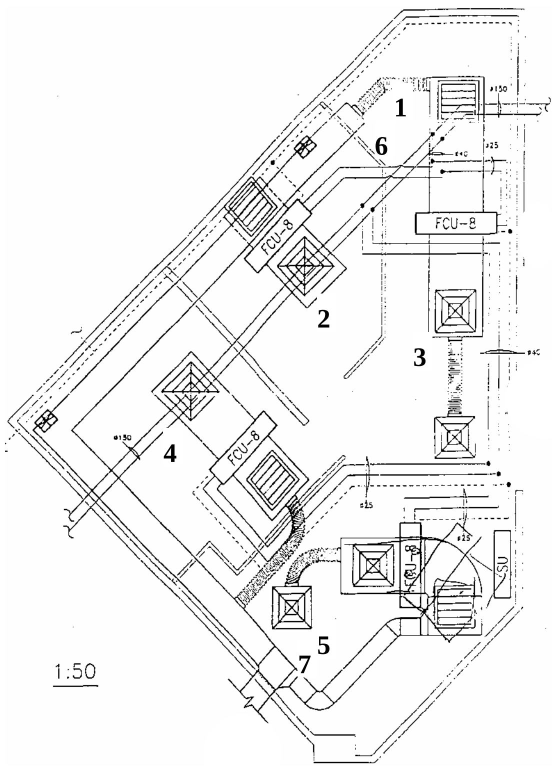

Fig. 3.7 Floor plan of the sampling site and sampling locations.

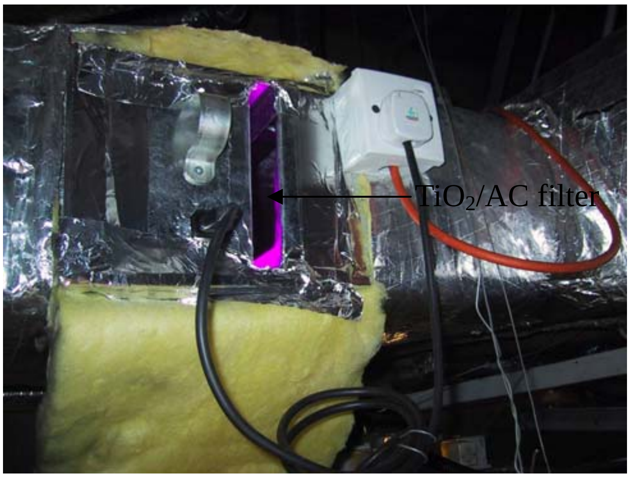

Fig. 3.8 TiO_2/AC filter installed in an air duct.

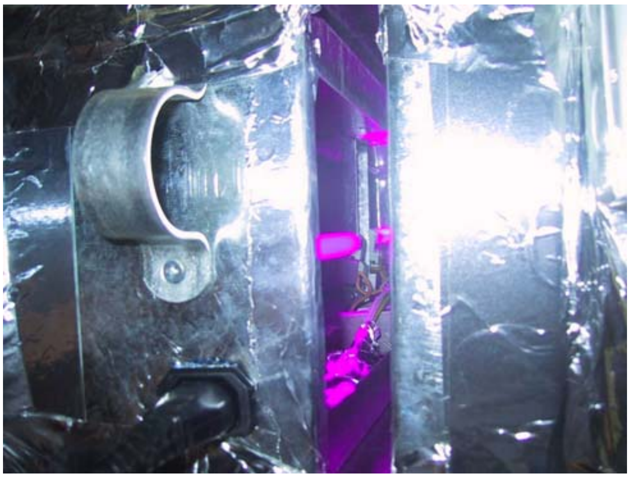

Fig. 3.9 UV lamps installed inside the air duct.

3.3.3.2 Experimental setup

Prior to the installation of the TiO_2/AC filter, a background sampling was conducted to measure the target pollutants level inside the office. The background sampling lasted for 3 days. In each day, a morning (11:00 to 12:00) session and an afternoon (3:00-4:00) session sampling was conducted. Samples of NO, NO_2 and HMHC were collected by a Tedlar sampling bag via a sampling pump (SKC). The concentrations of NO and NO_2 were measured by a Chemiluminescence NO analyzer (Thermo Environmental Instruments Inc. Model 42c) at a sampling rate of 0.7 L/min. The concentration of hydrocarbons was measured by a Non-Methane Hydrocarbon (NMHC) analyzer equipped with a FID detector (Thermo Environmental Instruments Inc. Model 55) at a sampling rate of 1 L/min. A Burkard single stage impactor (Burkard Manufacturing Co. Ltd.) with an agar plate is used to sample the airborne bacteria. Plate count agar filled in the plate was used as a nutrient media. The agar plate was stored in the refrigerator before use. The agar plate prior and after the sampling was placed inside an ice box. The bacteria samples were taken at 10 ml/min for 9 min. The agar plate after sampling was cultured at 25°C for 48 hours. Plate count was conducted to evaluate the total airborne bacterial level (Lee et al., 2003). After the installation of the TiO_2/AC filter, the exact sampling procedures, time and duration were followed.

3.4 Photocatalyst

Semiconductors such as TiO_2, ZnO, ZrO_2, CeO_2, CdS and ZnS can act as photo-sensitizers, which is characterized by the filled valence band and an empty conduction band (Boer, 1990). Under illumination by photos equal or greater than its band-gap energy, an electron is promoted from the valence band to the conduction band and thus creating a highly excited electron-hole pair (Hoffmann et al., 1995).

As observed in many studies, TiO_2 showed the highest activity among other semiconductors. It has a higher adsorptive properties on reactants and better absorptive properties on photons (Herrmann et al., 1999). TiO_2 also satisfies the requirements of photo-sensitizers as suggested by Mills and LeHunte (1997). The requirements are:

a) photoactive;

b) able to utilize visible or UV light;

c) biologically and chemically inert;

d) photostable; and

e) inexpensive.

Fox and Dulay (1993) also showed that TiO_2 has become the benchmark photocatalyst for photocatalytic activity measurement. Hence, only photocatalyst TiO_2 was investigated and other semiconductors are beyond the scope of this study.

3.4.1 P25 (Degussa)

Degussa (P25, T-805), Alderich, Acros and Beijing Chemicals, for example, provide TiO_2 in powder form and can be readily purchased. However, among the available commercial photocatalysts, Degussa (P25) TiO_2 is the most widely used. It was used in studies such as deactivation (Ameen and Raupp, 1999), photocatalytic oxidation of aromatic compounds (Einaga et al., 2002), identification of intermediates (Blount and Falconer, 2002) and photodegradation of binary pollutants (Luo and Ollis, 1996). In order to ease for comparison between this study and other studies, P25 was chosen as the photocatalyst. P25 also provides a stable and known properties of the photocatalyst, which improves the reproducibility of the experiments.

P25 is produced through the high temperature (> 1200°C) flame hydrolysis of $TiCl_4$ in the presence of hydrogen and oxygen. It is then treated with steam to remove HCl (Mills and LeHunte 1997). The specifications of P25 provided by the manufacturer are shown in Fig 3.10.

P25 was used as received without any pretreatment. Water suspension with 5% of TiO_2 was coated on a glass fiber filter (Whatman) as a supporting substrate. It was then calcinated at 120°C for 1 hour with a temperature gradient of 5.5°C per minute. The weight of TiO_2 imposed was determined by the weight difference before and after the coating procedure (denoted as TiO_2 filter). In all experiments, the weight of TiO_2 imposed is 1.64 g ± 5%, which was determined by an analytical balance calibrated annually (Sartorius, analytic) with a resolution of 0.1 mg and a precision of 0.5 mg.

Degussa

Specification

Titanium Dioxide P 25

Degussa AG
KC-FA-AT
Dr. Günther Michael
Tel. +49/6181/59-4583
Fax +49/6181/59-4489

please quote Id.no. with order:
(XX = Space for packaging code)
Material 23.8595.0000.XX
Spec. no. 1261/1

Standard

page 1 of 1
date of print: 09.12.1998
valid from: 21.11.1998

Product specification

	Properties and Test Methods	Units	Target Values (Spec. Limits)
665/T100	**Specific surface area (BET)**	m^2/g	50 (35 - 65)
665/T200 665/T200	**pH** in 4% dispersion		3,5 - 4,5

Characteristic physico-chemical data

	Properties and Test Methods	Units	Typical Values	
665/T701 665/T701	**Tamped density (approximate value)** acc. to DIN ISO 787/XI, Aug. 1983	g/l	130	**(+)**
665/T300 665/T300	**Moisture** 2 hours at 105°C	%	<= 1,5	**(+)**
665/T400 665/T400	**Ignition loss** 2 hours at 1000°C based on material dried for 2 hours at 105°C	%	<= 2,0	**(+)**
665/T581 665/	**TiO_2-content (1)** (1) based on ignited material	%	>= 99,50	**(+)**
665/T563	**Al_2O_3-content (1)**	%	<= 0,300	**(+)**
665/T501	**SiO_2-content (1)**	%	<= 0,200	**(+)**
665/T571	**Fe_2O_3-content (1)**	%	<= 0,010	**(+)**
665/T801	**HCl-content (1)**	%	<= 0,300	**(+)**
665/T900 665/T900	**Sieve residue by Mocker, 45 µm** acc. to DIN ISO 787/XVIII, Apr. 1984	%	<= 0,050	**(+)**
665/T990	**Average primary particle size**	nm	21	**(+)**

(+) No measured value given in quality documents

ZJQ_SPEZ/DEG/09.12.1998/17:09/dss04pf/001 A/K:0000800051/0000000000/0201/20 JQP0003

Figure 3.10 Specifications of photocatalyst TiO_2 Degussa P25.

3.4.2 Photocatalyst syntheses by sol-gel method

The preparation of the synthetic photocatalyst (denoted as T1) is as follows: A metal alkoxide solution of titanium isopropoxide (TTIP, Acros) was used as the starting materials. 10g of TTIP was slowly added at room temperature to a solution of absolute ethanol (EtOH) in a breaker under vigorously stirred for 0.5 h to prevent a local concentration of the TTIP solution. EtOH mixed with nitric acid was added to the solution to promote hydrolysis. Polyethylene glycol (PEG, Acros) 600 was added to the solution and stirred for 1 h. The solution was then ultra sounded for 0.5 h and left for 24 h before being used. The molar ratio of TTIP : EtOH : PEG was 1:15:10, corresponding to 5 wt % of TiO_2 in order to compare the photodegradation using P25 (Mikula et al., 1995; You et al., 2001). Photocatalyst T2 was prepared without the addition of PEG. T1 and T2 was immobilized on glass fiber by dip-coating. The glass fiber was loaded into the solution for 30 min and retracted at a rate of 10 mm/s. The glass fiber was dried at 100 °C for 2 h and then calcinated at 450 °C for 2 hr at a heating rate of 5.5 °C per min in air.

3.4.3 Photocatalyst syntheses by liquid phase deposition (LPD)

The aqueous solutions of ammonium hexafluouotitanate and boric acid were mixed, stirred and used as the treatment solution. The resultant concentration of treatment solution was 0.1 mol/L for ammonium hexfluorotitanate and 0.3 mol/L for boric acid, which is in the concentration range where transparent and uniform films could be obtained (Deki et al., 1996). The stainless steel substrates were dipped into the treatment solution and suspended there vertically for 48 hours. After the substrates were taken out and rinsed with distilled water, the TiO_2 thin films were calcinated at 100, 300, 400, 500, 600, 700, 800 and 900^oC in air for 1 hour, respectively. Alternatively, glass fiber was used instead of stainless steel as the coating substrate. The glass fiber was calcinated at 200 to 500°C in air for 1 hour. Note that the results of pollutant removal by photocatalyst synthesis by LPD method are shown in Appendix II.

3.5 Coating substrate

3.5.1 Glass fiber

Glass fiber was selected as the coating substrate because of its porous nature and allowed air flow passed through across the filter. The filter was provided from Whatman and used without any pretreatment. The highest calcination temperature applied was 500°C. Glass fiber was used as the coating substrate for P25, sol-gel method and LPD method.

3.5.2 Activated carbon filter

Activated carbon filter was used to evaluate the effect of the combination of adsorbent with photocatalyst TiO_2. The same procedure was followed for TiO_2 loaded on activated carbon filter (TiO_2/AC), except an activated carbon filter (23.085g ± 0.5%) was used instead of a glass fiber filter. The activated carbon was used without any pretreatment. The surface area of the glass fiber filter was identical to the activated carbon, which was 20cm x 21cm. The amount of TiO_2 imposed was determined by the weight difference before and after the coating procedure. In all experiments, the weight of TiO_2 imposed was 1.64 g ± 5%, which was identical to the amount of TiO_2 coated on glass fiber filter. Activated carbon was used as the coating substrate with photocatalyst P25 only.

3.5.3 Stainless steel

Stainless steel was used as the coating substrate because it can sustain high calcination temperature. The stainless steel was washed with acetone followed by deionized and distilled water. It is used as the coating substrate for the LPD method.

3.6 Quality assurance and quality control

3.6.1 *Instrumentation*

All the analytical instruments used in this study are those USEPA reference methods except NMHC. This is to ensure that the interference of instrument signal is minimized during analysis. This is especially important when multiple gases were investigated simultaneously in this study.

3.6.2 *Calibration*

For CO, NO, NO_2, SO_2 and NMHC, the instrument was calibrated before each experiment. The calibration was performed through a Teflon sample line filter, which was also used during analysis. The flowrate for calibration was greater than the total flow required by the analyzer and any other flow demand connected to the manifold. All the standard gases used for calibration have a NIST certificate.

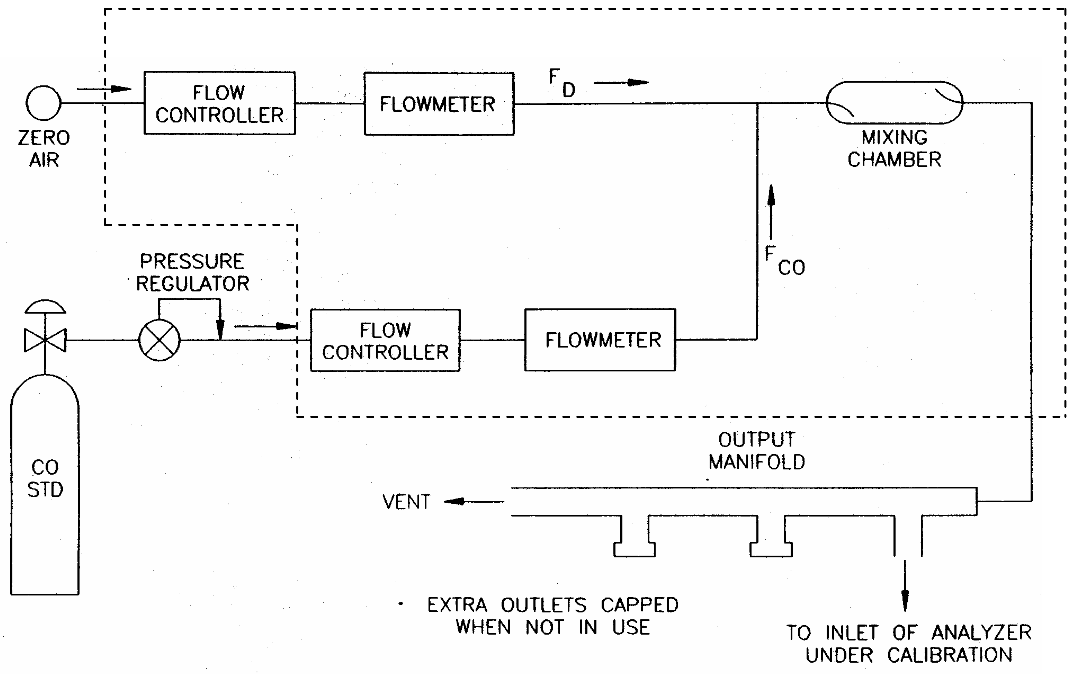

Figure 3.11 Schematic diagram of CO calibration.

A schematic diagram of the calibration is shown in Fig. 3.11. The flow controller and flow meter of the zero air and CO standard gas and the mixing chamber is simply replaced a mass flow calibrator (Advanced Pollution Instrumentation, Inc., model 700). The mass flow calibrator allows the user to select different pollutants and concentrations for calibration. Firstly, the CO analyzer was allowed to sample zero air unit a stable reading was obtained. Then, span adjust was achieved be selecting the desire CO concentrations. In this study, for instance, 2 ppm CO was selected as the target concentration. In a typical calibration, the CO concentration ranged from 0.5 ppm to 2.5 ppm. The CO analyzer was allowed to sample the span concentrations unit a stable reading was achieved. No periodic zero and one point span checks were performed since prior to every experiment, the instrument was calibrated by the aforementioned full range calibration. The response of the CO analyzer was plotted against the corresponding CO concentrations. The experimental points were connected using a straight line and determined by linear regression techniques. The calibration curve, as shown in Fig. 3.12, was used to adjust subsequent experimental data.

The calibrations of other gases like SO_2, NO, and NMHC followed the same procedure and the R^2 value of SO_2, NO, and NMHC were greater than 0.98. A mixture of methane and propane was used as the standard gas for the calibration of NMHC. The calibration of NO_2 utilized a gas phase titrator system (GPT). Ozone was generated and allowed to react with NO to form NO_2. This GPT system is equipped inside the mass flow calibrator.

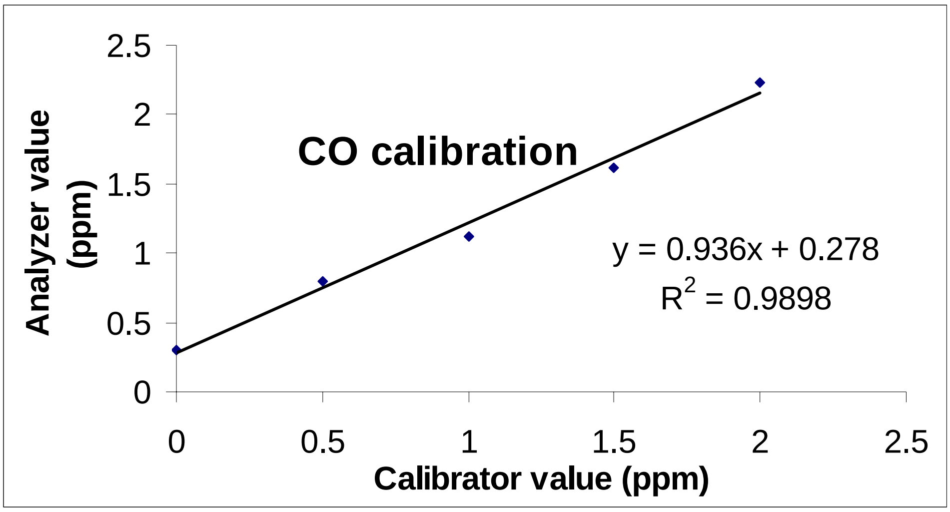

Figure 3.12 CO calibration curve.

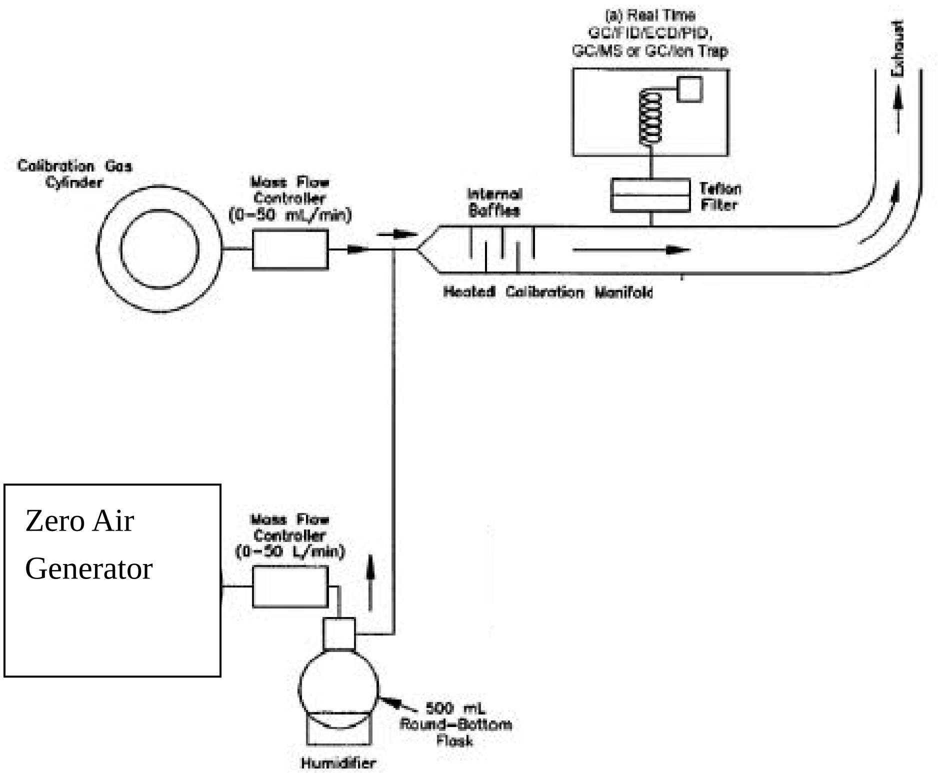

Figure 3.13 Calibration systems for the GC/MS.

The GC/MS system is calibrated by a multipoint dynamic calibration. It consisted of a zero air generator, a humidifier and a VOCs standard gas (Toxi-Mat-14M Certified Standard (Matheson)), as shown in Fig. 3.13. The flowrate from the VOCs standard gas was fixed by a mass flow controller, while the flowrate of the zero air was controlled by a flow controller. The concentrations of the VOCs were calculated by the flowrate and concentration of the VOCs standard gas and zero air. In a typical calibration, an initial VOCs concentration of 40 ppb was applied. The mixture was allowed to flow and equilibrate for 30 min. After the equilibration period, the gas standard mixture was sampled and analyzed by the GC/MS system. Different volumes of gas standard mixture were achieved by injecting 250mL, 125mL and 50mL for multipoint calibration. The calibration was performed on a weekly basis. The liner R^2 of all the VOCs were greater than 0.95. The experimental points were connected using a straight line and determined by a linear regression technique. The calibration data was stored inside the computer and was applied automatically to calculate the concentrations of VOCs.

The aldehydes were calibrated by diluting a standard purchased from Superco (CARB Method 1004 DNPH Mix 2) with acetonitrile (HPLC grade) in a volumetric flask. It was then further diluted by acetonitrile to achieve different aldehydes concentration. Acetonitrile was injected to the HPLC as the zero check. Different concentrations of the standard mixtures were then injected to the HPLC and the corresponding peak was obtained. For all the samples and calibrations, each single injection was repeated twice. If the results were differed by 10%, a third injection was performed. The liner R^2 of all the aldehdyes were greater than 0.95. The experimental points were connected using a straight line and determined by linear regression techniques. The calibration curve, as shown in Fig. 3.14, was used to adjust subsequent experimental data.

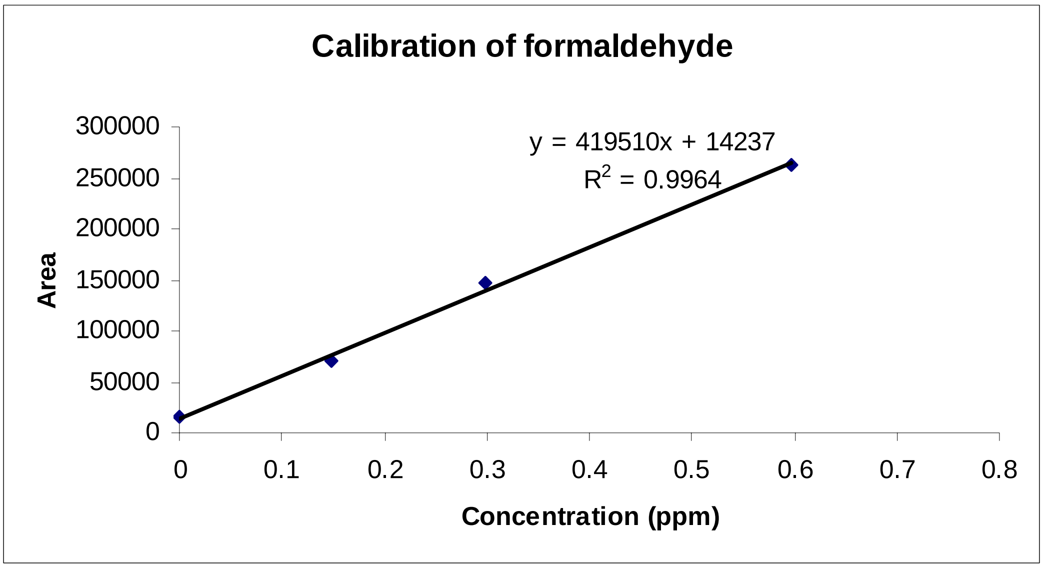

Figure 3.14 Formaldehyde calibration curve.

The concentration of formic acid, nitrate ions and sulfate ions were calibrated by dissolving desired amount of CHO_2Na, $NaNO_3$ and K_2SO_4 into distilled deionized water. For all the samples and calibrations, each single injection was repeated twice and the precision was over 90%. Fig. 3.15 shows a typical calibration curve for sulfate ion. The linear R^2 of sulfate ion, nitrate ion and formic acid were 0.9996, 0.9987 and 0.9992, respectively.

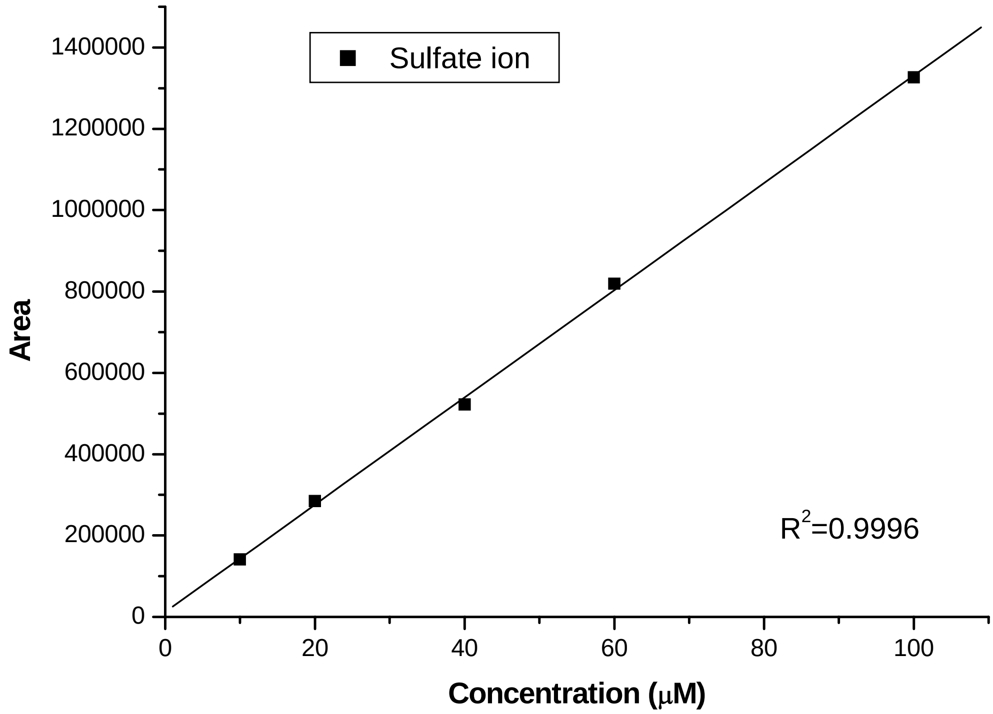

Figure 3.15 Sulfate ion calibration curve.

3.6.3 Sampling

3.6.3.1 Laboratory scale reactor

All the experiments were repeated 4 times and the average value was reported. This is to ensure that the value reported was repeatable between each experiment. For the criteria gases such as CO, SO_2, NO and NO_2, stainless steel sampling port was used to directly connect the Teflon tube between the reactor and the analytical instrument to minimize adsorption of gas.

For VOCs sampling, the canisters used for sampling were cleaned 5 times by sequential evacuating and pressuring with humidified zero air. The background pollutant concentration of the 25% cleaned canister was checked to ensure that all target compounds were less than 0.2 ppbv. For aldehydes sampling, 10 initial and 10 final flowrates through the cartridge were measured by a flowmeter (BIOS) and their average values were used for aldehydes concentration calculation.

3.6.3.2 Air cleaner and air duct inside an office

Direct connection between the air cleaner and air duct inside an office and the analytical instrument was not possible. Thus, samples were collected by a sampling pump (SKC) and drawn to a Tedlar sampling bag (SKC). The sampling bag was then connected to the analytical instrument. Prior to each sampling, the Tedlar bag was cleaned by pumping and evacuating zero air for 5 times. The background concentration of the cleaned Tedlar bag (25%) was analyzed to identify the pollutant concentration inside the air bag after the cleaning procedures.

Chapter 4 Removal of indoor air pollutants by photocatalyst loaded on glass fiber filter

4.1 Introduction

This chapter depicts the use of titanium dioxide (TiO_2) as a photocatalyst loaded on glass fiber filter as a coating substrate for indoor air pollutant removal. NO, BTEX, CO, SO_2, HCHO were selected as target pollutants with reference to their typical indoor air concentrations in this study. Sensitive analyses were conducted for the above pollutants under different residence time, humidity levels and initial pollutant concentrations. Sol-gel method was used to synthesize photocatalyst to improve pollutant conversion. Since the results of pollutant removal by photocatalyst synthesis by LPD method do not fit the general theme of the dissertation, the results are shown in Appendix II.

4.2 Characterization of photocatalyst loaded on glass fiber filter

Fig. 4.1 (a), (b), (c) and (d) show the scanning electron micrographs (Leica Stereoscan 440) of the fiber filter used as the coating substrate and the different views of fiber coated with Degussa (P25) TiO_2. The glass fiber used has a fiber size ranging from 150 nm to 1800 nm, which allowed the TiO_2 to be coated entirely around the fiber, as shown in Fig. 4.1 (a) and (b). The smaller size TiO_2 particles also enabled to be strained, impinged or intercepted between the fibers. From the micrographs, it can be seen that the TiO_2 particles agglomerated after calcination. Fig. 4.1 (c) shows the uppermost TiO_2 layer coated on the fiber. On top of the fiber, TiO_2 agglomerates into pieces around 60μm. It is probably that, this layer with a thickness of 3μm, as shown in Fig. 4.1 (d), is the layer responsible for heterogeneous reaction.

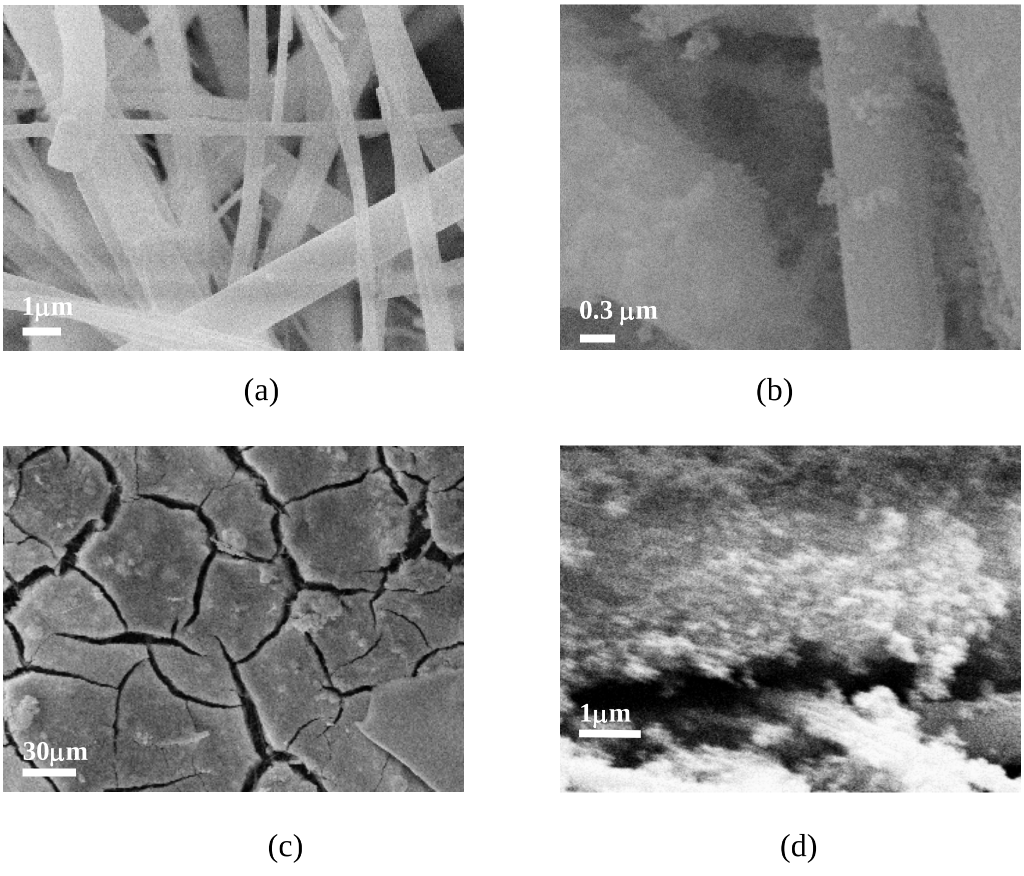

Figure 4.1 Scanning electron micrographs of (a) fiber, (b) fiber coated with TiO_2, (c) top and (d) cross-section.

The Brunauer–Emmett–Teller (BET) surface area of the TiO_2 powder was determined by nitrogen adsorption–desorption isotherm measurements at 77K on a Micromeritics ASAP 2000 nitrogen adsorption apparatus. The BET surface area of the TiO_2 powder and the activated carbon powder was 46 m^2/g, which is in agreement with the specifications provided by Degussa (Fig. 3.22).

4.3 Nitrogen monoxide (NO)

4.3.1 Photodegradation of NO

Prior to the photodegradation of NO, the photolysis of NO was examined. After achieving equilibrium concentration of NO by monitoring the inlet and the outlet concentrations, UV light was turned on with without the presence of the TiO_2 filter inside the reactor. No decrease in NO concentration was observed. The finding in this study is also supported by Hori et al. (1986), Lim et al.,(2000) and Devahasdin et al. (2003). They reported that no conversion of NO by photolysis was observed using a concentration of 20-200 ppm NO. A blank test was also conducted by generating 200 ppb NO to the reactor with the presence of TiO_2 filter and UV lamp turned off. The concentrations of NO and NO_2 did not change under the experimental conditions and similar result was reported by Devahasdin et al. (2003).

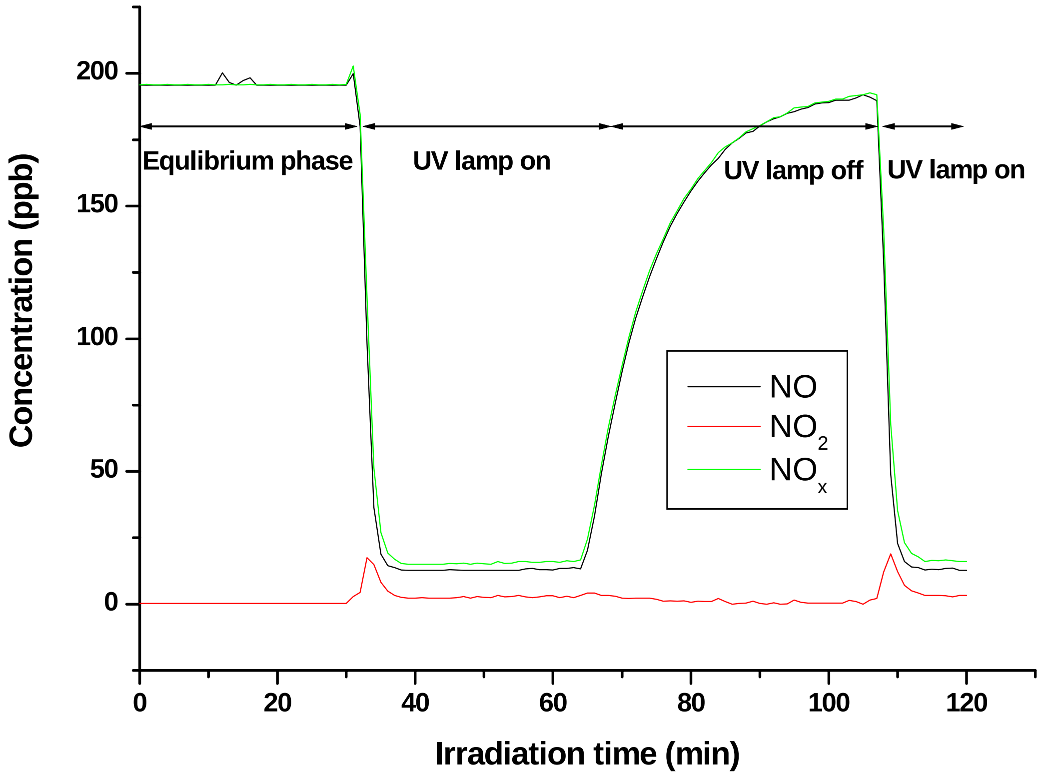

Figure 4.2 Typical photodegradation profile of NO; 200 ppb NO; humidity level 2100 ppmv; residence time 0.6 min.

Fig. 4.2 shows a typical photodegradation profile of NO. The inlet and outlet NO concentration reached equilibrium at the last 30 min, and the UV lamp was turned on. The NO concentration rapidly dropped from 200 ppb to 11.8 ppb in 5 min. Simultaneously, 5 ppb of NO_2 was generated as a side product from NO photodegradation. Deactivation was observed for NO photodegradation. The photo-steady-state concentration of NO remained unchanged, but NO_2 concentration increased to 5.2 ppb at 120 min after reaching its photo-steady-state concentration of 2.7 ppb. The accumulation of HNO_3 deactivated the photodegradation of NO (Ibusuki and Takeuchi, 1994). The photodegradation of NO is expressed in the following equations (Hoir et al., 1986; Negishi et al., 1997; Komazaki et al., 1999; Matsuda et al., 2001; Devahasdin et al., 2003;).

$$TiO_2 \xrightarrow{hv} h^+ + e^- \qquad (4.1)$$

$$H_2O \longrightarrow H^+ + OH^- \qquad (4.2)$$

$$h^+ + OH^- \longrightarrow OH\cdot \qquad (4.3)$$

$$e^- + O_2 \longrightarrow O_2^- \qquad (4.4)$$

$$H^+ + O_2^- \longrightarrow HO_2\cdot \qquad (4.5)$$

$$NO + HO_2\cdot \rightarrow NO_2 + OH\cdot \qquad (4.6)$$

$$NO_2 + OH\cdot \rightarrow HNO_3 \qquad (4.7)$$

$$HNO_{3(ads)} \rightarrow HNO_{3(aq)} \qquad (4.8)$$

Although NO also reacted with OH radical, HO_2 radical, NO_2, and HNO_3 forming other products such as HONO and HNO_2 (Brauer et al., 1993; Pagsberg et al., 1997), NO_2 is the only intermediate observed from the photodegradation of NO under the presence of oxygen (Hori et al., 1986; Hashimoto et al., 2001; Lim et al., 2000;). NO_2 is further photooxidized to HNO_3. Devahasdin et al. (2003) showed that HNO_2 may be formed during the transient period in which HNO_2 is rapidly oxidized to NO_2. Using a FTIR technique, NO was oxidized to NO_2 followed by the formation of nitrate ions (Hashimoto et al., 2001). Dalton et al.

(2002) also showed similar results by using a surface spectroscopic approach. In this study, surface species on the TiO_2 filter were attempted to be identified by the FTIR technique. However, due to the use of low concentration and glass fiber as the coating substrate, the resultant of the signal to noise ratio was too high and no identification was able to be observed. Anpo and co-workers, however, reported that N_2, O_2 and N_2O were the products from the photodegradation of NO under the presence of helium instead of oxygen (Zhang et al., 2001; Hu et al., 2003). In the presence of oxygen, it usually acts as the primary electron acceptor, as shown in equation 4.4 (Hoffmann et al., 1995; Fox and Dulay, 1993). It is also known that the adsorption of O_2 on TiO_2 is much higher than NO due to its high electron affinity and lower electron negativity (Zhang et al., 2001). Thus, in the presence study, oxygen was primary reduced to superoxide (equation 4.4) and nitrogen oxide was oxidized to nitrogen dioxide (equation 4.6). In the system used by Anpo and co-workers, NO was simultaneously oxidized to O_2 and reduced to N_2O and N_2 under the presence of helium only.

4.3.2 Effects of the amount of TiO_2 loaded on the glass fiber filter

The conversion of NO is defined as:

$$Conversion = \frac{[NO]_i - [NO]_f}{[NO]_i} \times 100\% \qquad (4.7)$$

where $[NO]_i$ is the inlet NO concentration and $[NO]_f$ is the photo-steady-state NO concentration at an irradiation time of 120 min. The generation of NO_2 is defined as:

$$Generation = -\frac{[NO_2]_f}{[NO]_i} \times 100\% \qquad (4.8)$$

The negative sign of equation 4.8 indicated that NO_2 was actually generated from the system. The definition of NO and NO_2 conversion is valid using the concept of equation 4.9 (Cohen and Murphy, 2003; Seinfeld and Pandis, 1998):

$$NO_x = NO + NO_2 \qquad (4.9)$$

Using the definition of equation 4.9, the conversion of NO_x at 0.2 weight percentage of TiO_2 is:

$$Conversion = \frac{[NO_x]_i - [NO_x]_f}{[NO_x]_i} x100\%$$

$$= \frac{([NO]_i + [NO_2]_i) - ([NO]_f + [NO_2]_f)}{([NO]_i + [NO_2]_i)} \times 100\%$$

$$= \frac{(500+0) - (52.7+62.8)}{(500+0)} \times 100\%$$

$$= 76.90\%$$

Applying equation 4.7, the conversion of NO and NO_2 at 0.2 weight percentage of TiO_2 was 89.46% and -12.56%. Adding it together (89.46-12.65), the conversion of NO_x is equal to 76.90% and is identical to the above calculations. Hence, equations 4.7 and 4.8 is valid to express the conversion of NO and generation of NO_2.

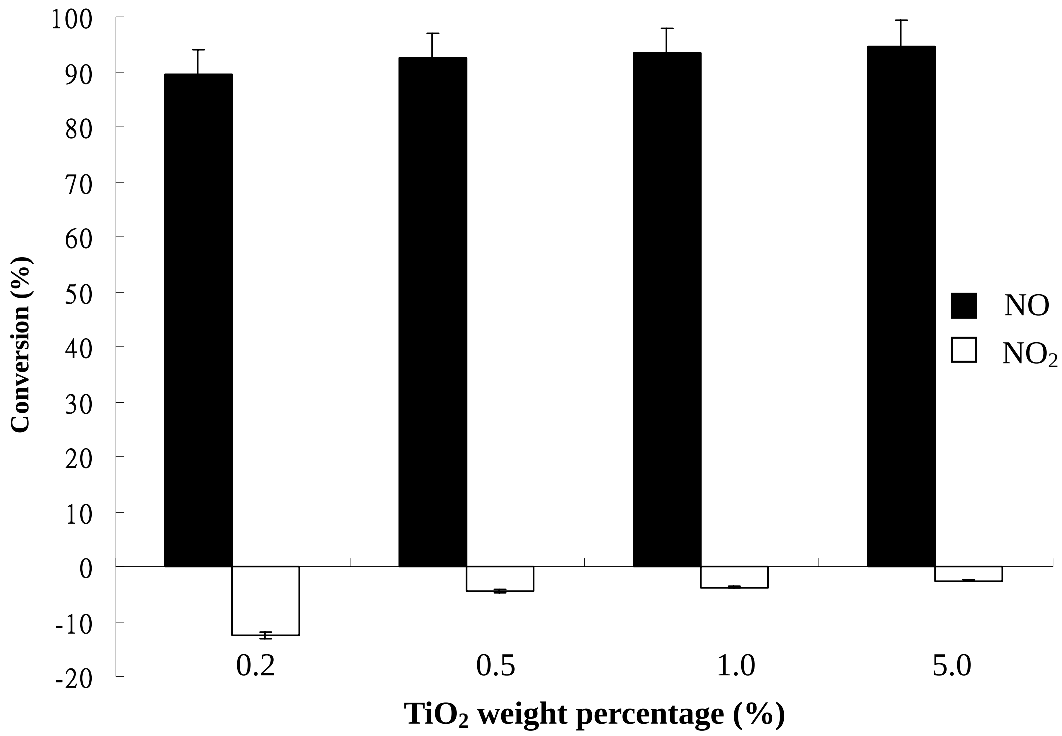

Figure 4.3 Effects of TiO_2 weight percentage on NO conversion and NO_2 generation. Experimental conditions: 200 ppb NO; humidity level 2100 ppmv; residence time 0.6 min.

Fig. 4.3 shows the effect of TiO_2 weight percentage loaded on the glass fiber filter. The conversion of NO increased with increasing TiO_2 weight percentage, whereas the generation of NO_2 decreased. However, this beneficial effect is less significant when the weight of TiO_2 approached to 5%. This result suggested that a higher loading of TiO_2 may form a thicker film where the TiO_2 is inaccessible to the UV irradiation. Similar findings were reported by Li et al. (1998). They reported that the conversion of toluene and trichloroethylene increased with increasing TiO_2 weight and reached a steady state. Using the same coating substrate (glass fiber), You et al. (2001) also reported that the conversion of toluene become constant at a weight of 6% TiO_2 loaded on glass fiber. In this study, at a higher TiO_2 loading, the mechanical stability of the TiO_2 on the glass fiber decreased significantly. Using 200 ppb as the NO initial concentration, the beneficial effect of the increasing TiO_2 weight percentage was less significant. Thus, the percentage of TiO_2 loaded on glass fiber was fixed at 5% in this study.

4.3.3 Effects of initial concentrations

The effects of NO initial concentrations are shown in Table 4.1. The conversion of NO did not vary significantly under different initial NO concentrations. It is noted that, however, the photo-steady-state NO concentration increased with increasing initial NO concentrations. On the other hand, the NO_2 generation and photo-steady-state concentrations also increased with increasing initial NO concentrations. Considering NO and NO_2 together, the NO_x conversion also decreased with increasing initial NO concentrations. The results obtained in this study are different from that reported by Lim et al. (2000) and Devahasdin et al. (2003). They showed that the NO conversion decreased with increased initial NO concentration at a range of 5 to 24 ppm and 50 to 120 ppm, respectively.

Initial NO conc.(ppb)	NO conc. (ppb)	NO_2 conc. (ppb)	NO conversion (%)	NO_2 generation (%)	NO_x conversion (%)
200	19.7	9.7	90.15	-4.85	85.30
500	50.6	25.8	89.88	-5.16	84.72
700	70.2	50.4	89.97	-7.20	82.77
900	89.2	111.9	90.09	-12.43	77.66

Table 4.1 Effects of NO initial concentrations on NO and NO_2 photo-steady-state concentration and NO_x conversion. Experimental conditions: humidity level 2100 ppmv; residence time 3.7 min.

In this study, the conversion of NO did not vary significantly under different initial NO concentrations. Although the difference of the highest and lowest NO concentration is 4.5 times, the concentration increased by 700 ppb only. The increase in NO concentration may not be large enough to impose a significant effect on hydroxyl radical consumption. This postulation is supported by the results reported by Murata et al. (1999). They showed that the conversion of NO decreased significantly when the NO concentration increased from 1 ppm to 10 ppm, whereas the conversion of NO only decreased slightly when the NO concentration increased from 0.1 ppm to 1 ppm. In a typical indoor environment, the NO concentration seldom exceeds 1 ppm. Thus, the concentration applied cover the typical indoor NO variation range.

Langmuir-Hinshelwood (L-H) rate expression has been widely used to describe the gas-solid phase reaction for heterogeneous photocatalysis (Kim and Hong, 2002; Fox and Dulay, 1993; Serpone and Pelizzetti, 1989):

$$r = \frac{kKC}{1 + KC} \qquad (4.10)$$

where k is the rate constant, K is the adsorption constant and C is the NO concentration. By substituting the L-H rate expression into a mass balance equation of a plug flow reactor, the following expression is obtained (Alberici and Jardim, 1997; Zhang et al., 1994):

$$\frac{V}{Q} = \frac{1}{kK}\ln(\frac{C_o}{C}) + \frac{1}{k}(C_0 - C) \qquad (4.11)$$

where V is the volume of the reactor, Q is the flowrate through the reactor and C_o is the initial NO concentration. By rearranging equation 4.11, a linear form is obtained, as shown in equation 4.12:

$$\frac{V/Q}{(C_o - C)} = \frac{1}{k} + \frac{1}{kK}\,\frac{\ln(C_o - C)}{(C_o - C)} \qquad (4.12)$$

If L-H kinetics is valid for a plug flow reactor, then a plot of $(V/Q)/(C_o\text{-}C)$ versus $\ln(C_o/C)/(C_o\text{-}C)$ should be linear. Equation 4.11 was tested by using different C_o and C. As shown in Fig. 4.4, the experimental data is in good agreement with the integral rate law analysis. The values of k and K can be obtained from the intercept and slope of Fig. 4.4. The values of k and K are 384.62 ppb/min and 0.002 ppb^{-1}. Thus, the photocatalytic reaction occurred on the photocatalyst surface but not in the bulk fluid.

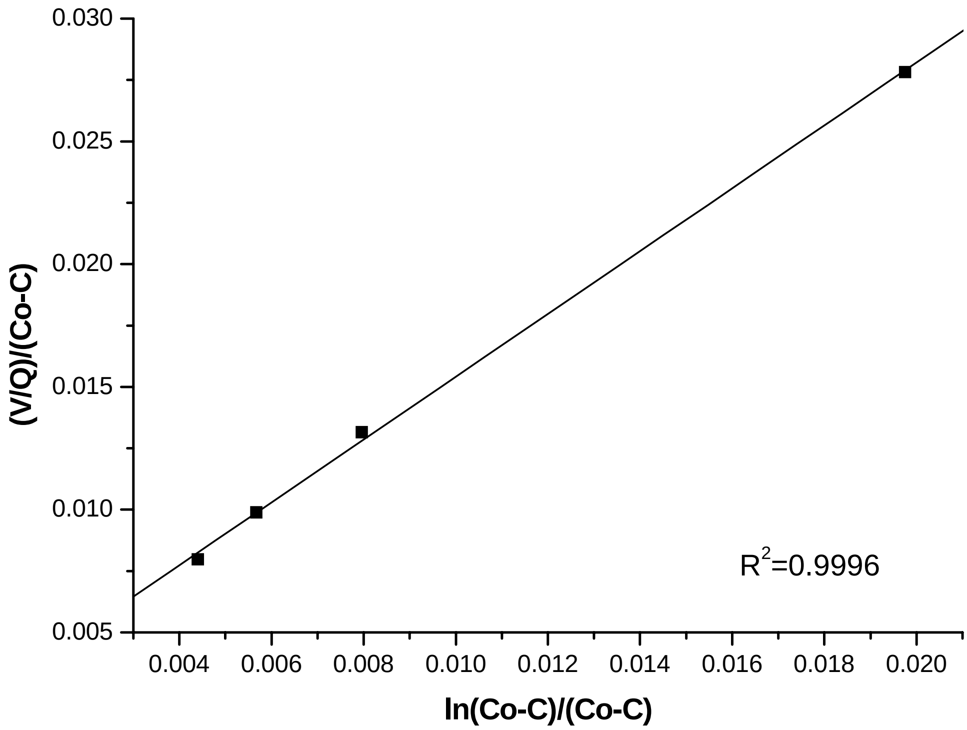

Figure 4.4 L-H plots for NO photodegradation. Experimental conditions: humidity level 2100 ppmv; residence time 3.7 min.

4.3.4 Effects of residence time

Fig 4.5 shows the effects of residence time on the conversion of NO. It is observed that the conversion decreased with decreasing residence time. Residence time is defined as the volume of the reactor divided by the volumetric flowrate (Metcalfe, 1997; Devahasdin et al., 2003). For instance, at a residence time of 3.7 min, the conversion of NO is 90.2% whereas the conversion of NO dropped to 67.8% when the residence time decreased to 0.6 min. Similarly, the NO_2 generation increased from 1.6% to 9.2% when the residence time decreased from 3.7 to 0.6 min. It can be assumed that a longer residence time, a higher rate of contact and length of contact time were achieved between the pollutants and the hydroxyl radicals, resulting in a higher conversion. Similar results were reported by Lim et al. (2000).

4.3.5 Effects of humidity levels

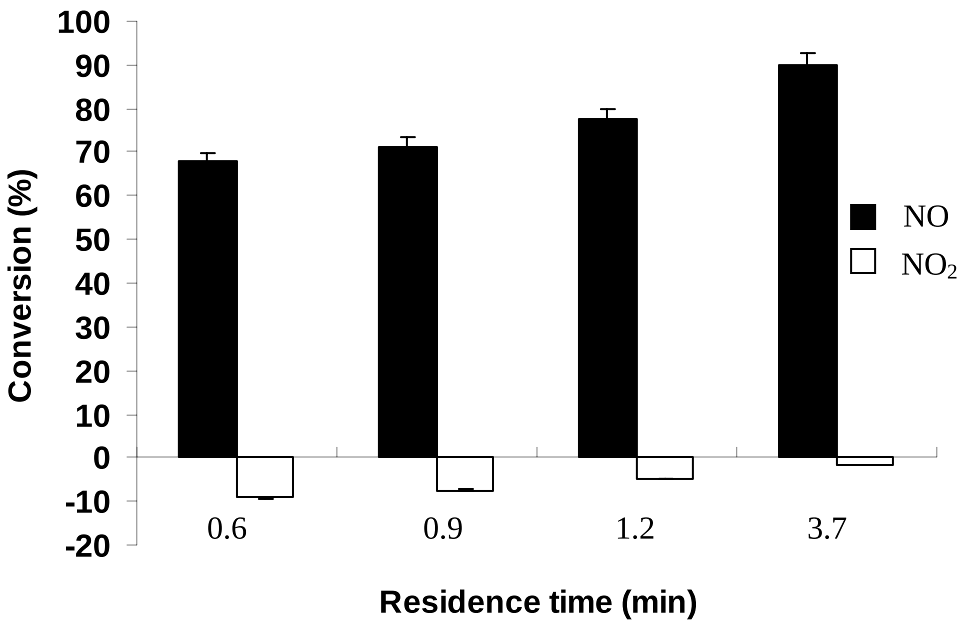

Figure 4.5 Effects of residence on NO conversion and NO_2 generation. Experimental conditions: 200 ppb NO; humidity level 2100 ppmv.

The effects of humidity levels are shown in Fig. 4.6. The conversion of NO and the generation of NO_2 increased with increasing humidity levels. For instance, the conversion of NO decreased from 77.6% to 62.9% when the humidity levels increased from 2100 ppmv to 22000 ppmv whereas the NO_2 generation increased from 4.9% to 25.1%. This shows that the increasing humidity levels not only decreased the primary pollutant conversion but also increased the generation of the intermediate. However, studies showed that the conversion of m-xylene (Peral and Ollis, 1992), benzene (d' Hennezel et al., 1998), trichloroethylene and tetrachloroethylene (Hager et al., 2000) at several hundreds pppm levels increased with increasing humidity levels. Their results suggested that the increase in water vapor increased the hydroxyl radicals formed on the TiO_2 surface due to water dissociation using TiO_2 (P25) as photocatalyst and thus a higher conversion was achieved. On the contrary, the conversions of cyclohexane (Eingaga et al., 2002;), 1-Butene (Cao et al., 1999) and 1-Buanol (Peral and Ollis, 1992) at several hundreds ppm levels decreased with increasing humidity levels. The above authors elucidated that water competed with the pollutant for adsorption sites on the TiO_2 surface. In a single study, Kim and Hong (2002) showed that different compounds reacted differently with increasing humidity levels. Thus, the effect of humidity levels is pollutant dependent and it is not appropriate to compare between different compounds.

The effect of increasing humidity levels on NO was reported by Devahasdin et al. (2003). They showed that the conversion of 40 ppm NO increased with increasing relative humidity and reached a steady conversion at a relative humidity level of 80%. The discrepancy can be explained by the concentration of the pollutant applied. When the pollutant level applied is high, a high humidity levels is necessary to maintain a high hydroxyl radical density from the dissociation of water vapor in air. The equilibrium between the continuous consumption of hydroxyl radical and the replenishment of water is achieved, as in the case reported by Devahasdin et al. (2003). However, in this study the pollutant applied was only 200 ppb and the same high humidity levels was maintained. As a result, the excess water vapor competed with NO for adsorption site on the TiO_2 surface and inhibited the conversion. At the ppb level, the competition for adsorption sites between NO and water vapor is a thousand times more than applying ppm level pollutants and only a small amount of water vapor is sufficient for the generation of OH radicals. Thus, the high humidity levels inhibited the conversion of NO. Anpo et al. (1991) further showed that the addition of water increase the photoluminescence intensity. The increase of the photoluminescence intensity indicated a higher electron-hole recombination rate and thus lowered the conversion.

The effect of humidity on the photodegradation rate may be quantitatively described by the following equation (Peral and Ollis, 1992):

$$r = \frac{r_o}{1 + K_H [H_2O]^{\beta}} \qquad (4.13)$$

where r_o is the reaction rate under the absence of water. By rearranging equation 4.13 into equation 4.14, the inverse of the reaction rate is plotted against the water vapor concentration, as shown in Fig. 4.7.

$$\frac{1}{r} = \frac{1}{r_o} + \frac{K_H}{r_o}[H_2O]^{\beta} \qquad (4.14)$$

From the results obtained in Fig. 4.7, the relationship between the reverse of the reaction rate and water vapor concentration can be described as $1/r = 0.32121 + 0.0005445[H_2O]^{0.55}$, and $\beta = 0.55$, $r_o = 3.113$ μmol/m^2 min, $K_H = 1.695 \times 10^{-3}$ ppm^{-1}.

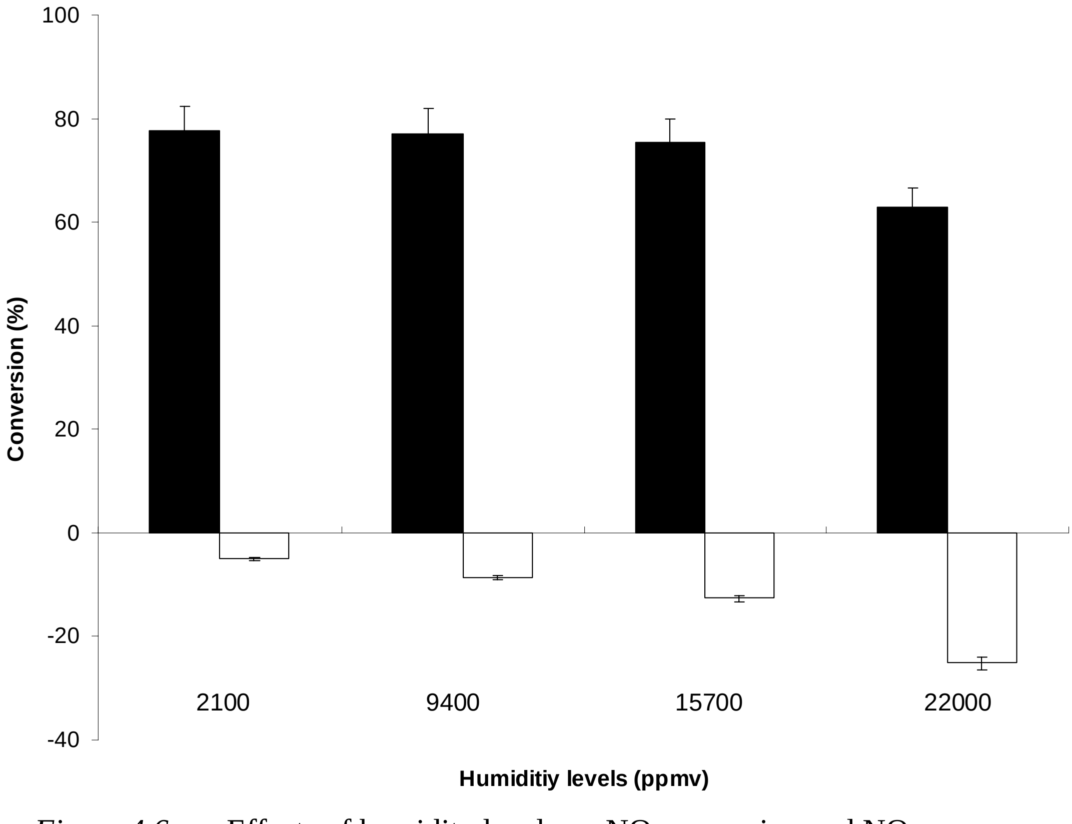

Figure 4.6 Effects of humidity levels on NO conversion and NO_2 generation; 200 ppb NO; residence time 1.2 min.

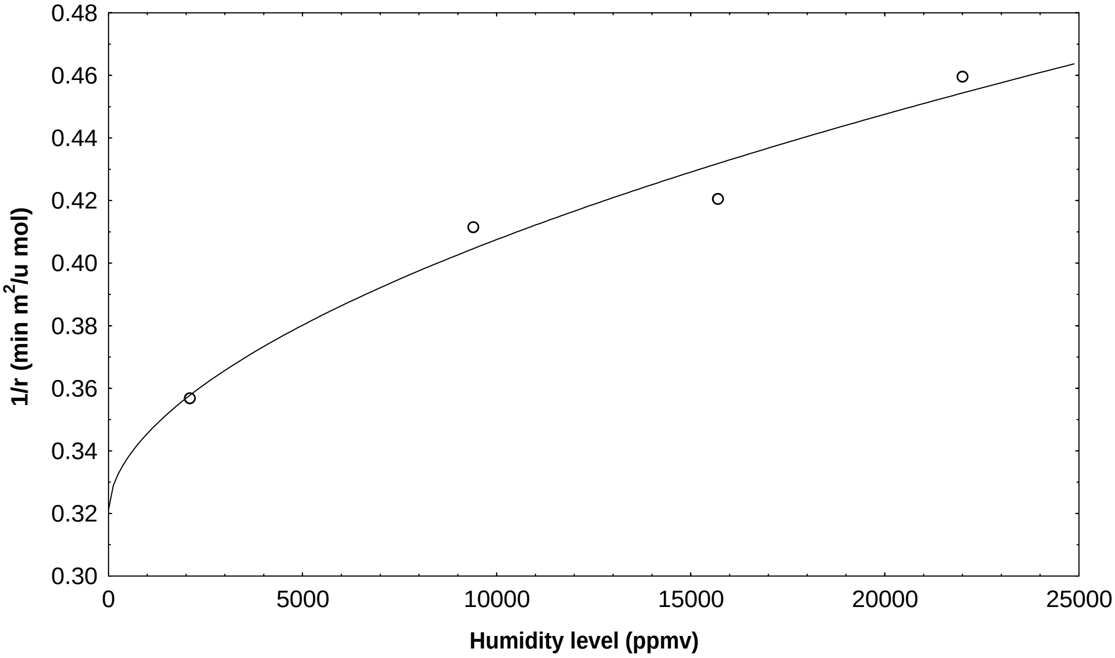

Figure 4.7 Inverse of reaction rate of NO photodegradation vs. humidity levels. Experimental conditions: residence time 1.2 min, 200 ppb NO.

4.3.6 Photodegradation of NO by photocatalyst synthesized by sol-gel method

4.3.6.1 Characterization of photocatalyst synthesized by sol-gel method

A Philips E'xpert X-ray diffractometer employing Cu Kα was used to identify the X-ray diffraction (XRD) pattern and the phase presented. An accelerating voltage of 35 kV and a current of 20mA with a scan rate of 0.05° 2θ /s were used. The crystallite size was calculated by applying the Scherrer formula. Differential Scanning Calorimetry (DSC) and thermal gravity (TG) analysis was preformed using a NETZSCH instrument. A 10 mg sample was used and the heating rate was 10°C/min in flowing air. The Brunauer–Emmett–Teller (BET) surface area was determined by nitrogen adsorption–desorption isotherm measurements at

77K on a Micromeritics ASAP 2000 nitrogen adsorption apparatus. The samples were degassed at 180°C before measurement.

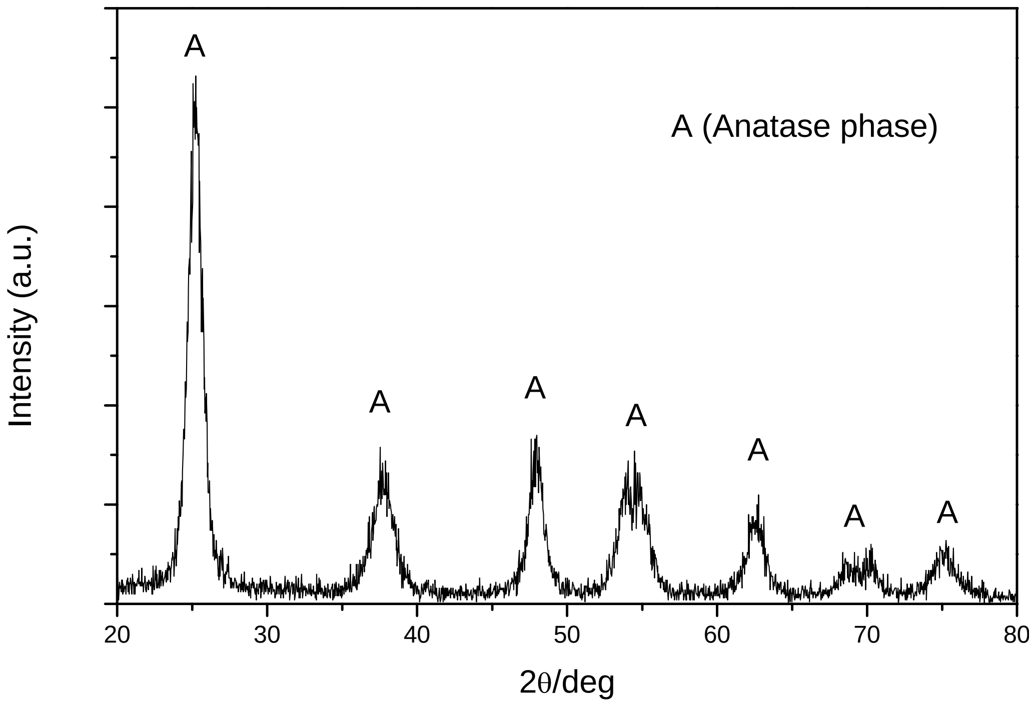

Figure 4.8 XRD patterns of photocatalyst T1.

4.3.6.2 Characteristic of the photocatalyst

The X-ray diffraction pattern of T1 deposited on glass fiber was too weak for phase identification. Fig. 4.8 shows the XRD pattern of T1 powders with the same method prepared for T1 deposited on the glass fiber. The pattern was compared with the 21-1272 anatase ASTM card and 21-1276 rutile card. Only the anatase phase was found. Even when the powder was heated to 900 °C, no rutile phase and only anatase phase was found. The average crystallite size of T1 and P25 was estimated to be 9.8 nm and 18.8 nm using the Scherrer equation (Music et al., 1997).

Fig. 4.9 shows the result of TG-DSC. Two weight loss regions were observed. From room temperature to 260°C, a steep slope is observed and the weight loss corresponds to the desorption of absorbed water and alcohol. From 250°C to 500°C, a flat slope is observed and the weight loss corresponds to the residual organic and chemisorbed water. From the DSC curve, an exothermic peak was observed to be at 426 °C which corresponded to the crystallization of TiO_2 from amorphous phase to anatase phase (Montoya et al., 1992). The result also agreed with the XRD result and only the anatase phase was observed when the sample was calcinated at 450°C.

As with of applying coated TiO_2 glass fiber for XRD detection, only powders of T1 with the same preparation was used to identify the BET surface area. The BET surface area of T1 and P25 is 96 m^2/g and 46 m^2/g respectively.

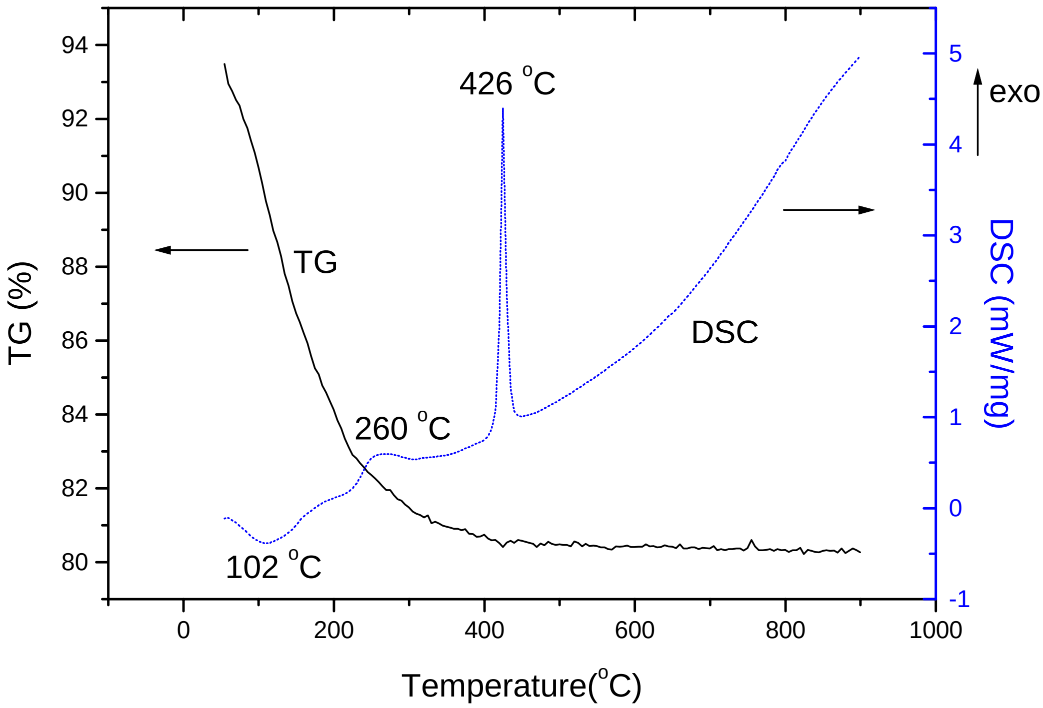

Figure 4.9 DSC-TG analyses of photocatalyst T1.

4.3.6.3 Photodegradation of NO by photocatalyst synthesized by sol-gel method at different residence time

Fig. 4.10 shows the photodegradation of 200 ppb NO at a humidity level of 2100 ppmv. Results showed that the conversion of NO_x decreased with decreasing residence time for photocatalyst T1 and P25. The conversion of NO_x using photocatalyst T1 and P25 decreased from 94.5% to 70.2% and 92.2% to 69.2% when the residence time decreased from 11.4 min to 2.9 min. At a longer residence time, a higher rate of collision frequency between the hydroxyl radicals and the pollutants is expected and therefore the conversion of NO_x is higher (Lim et al., 2000). The higher conversion of NO_x using photocatalyst T1 is probably due to a higher BET surface area and a smaller crystal size (Hashimoto et al., 2000; Zhang et al., 2001). The BET surface area of T1 is nearly double that of P25. Under a low level of humidity, a higher BET surface area provides a larger adsorption site on the catalyst surface for NO to be adsorbed. Similar findings were also reported. Photocatalysts having a larger BET surface area have a higher conversion for organic compounds in the gaseous phase (Mikula et al., 1995) and phenol in the aqueous phase (Montoya et al., 1992).

Study (Maira et al., 2001) also showed the photodegradation rate is also dependent on the crystal size. Maria and others (2001) showed that a smaller crystal size has a higher conversion of toluene with or without water. The result suggested that using EPR spectra, a smaller crystal size would have a more of edges and corner sites for the formation of Ti^{3+} center and form superoxide ions. It can be seen from the XRD data, photocatalyst T1 has a crystal size of 9.8 nm which is half the crystal size of P25. It is plausible that the smaller crystal size of T1 contribute the higher conversion of T1.

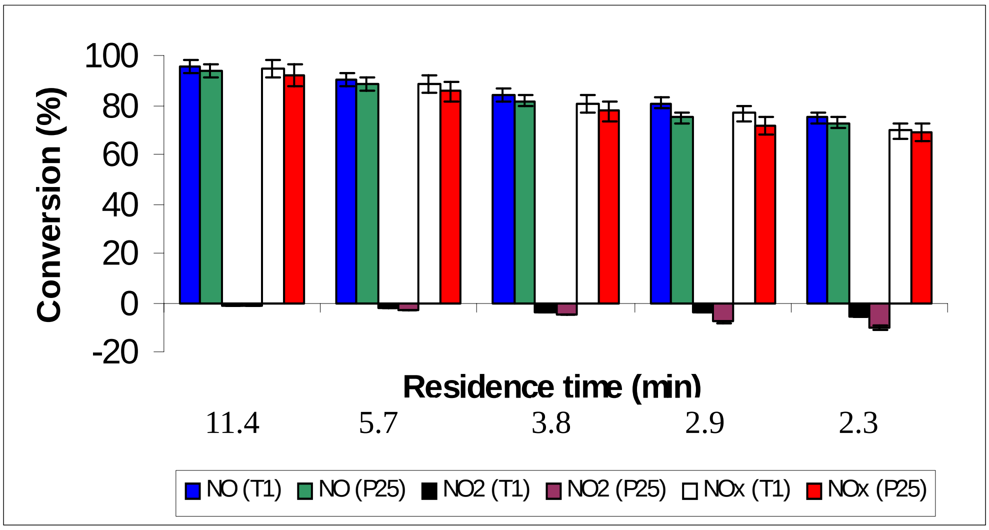

Figure 4.10 Variation of NO_x at different residence time.
Experimental conditions: 200 ppb NO; humidity 2100 ppmv.

4.3.6.4 Photodegradation of NO by photocatalyst synthesized by sol-gel method at different humidity levels

Fig. 4.11 shows the photodegradation of 200 ppb NO at a residence time of 3.8 min. Previously we reported that water vapor competed with NO, at ppb levels, for the adsorption site. It is clearly shown in the figure that the NO_x conversion using photocatalyst T1 and P25 decreased with increasing humidity levels. Note that the affect on T1 is smaller than P25. It is presumed that the larger BET surface area of T1 has a larger adsorption site for the conversion of NO to NO_2, with the result that the NO_2 concentration exiting the outlet stream is smaller. As the humidity level increased, the conversion difference between T1 and P25 also increased. The increase in the BET surface area successfully improved the conversion of NO_x under the current experimental conditions. As discussed in the previous section, the smaller crystal size may also affect the conversion of NO. However, as the photocatalyst T1 has a larger BET surface area and a crystal size smaller than P25, it is difficult to distinguish at this stage whether the higher conversion of T1 is due to the smaller crystal size or the larger BET surface area. In order to evaluate the vital parameter for higher conversion, T1 was prepared without the addition of PEG 600 (denoted as T2). T2 has a similar crystal size of 10.2 nm and a BET surface area of 37 m^2/g.

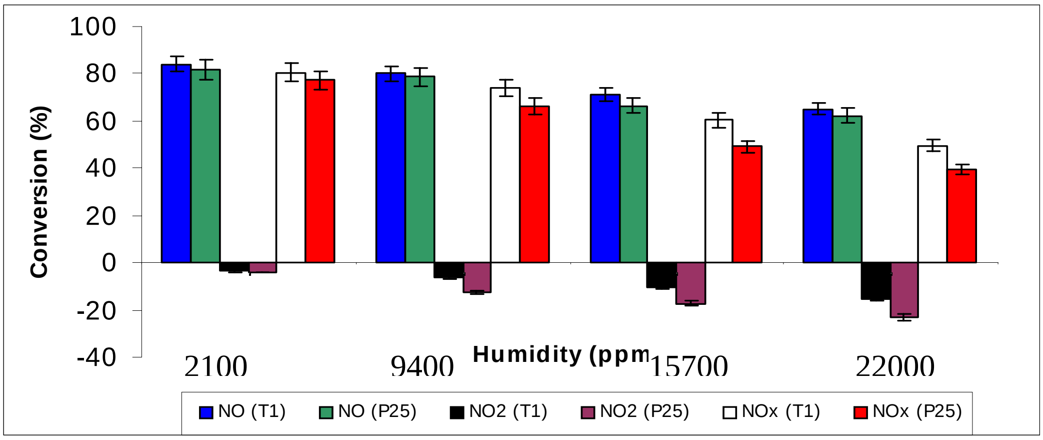

Figure 4.11 Variation of NO_x at different levels of humidity. Experimental conditions: 200 ppb NO; Residence time 3.8 min.

4.3.6.5 Photodegradation of NO with photocatalyst T1, T2 and P25

The effect of crystal size and BET surface area was investigated to identify the vital parameters for photodegradation of NO at ppb level. As shown in Table 4.2, the NO conversion of T2 under different residence time is lower than T1 and P25. This is probably due to the lower BET surface area of the photocatalyst T2. T2 has a BET surface area of 37 m^2/g, which is smaller than T1 and P25. The difference in NO conversion, however, is not significant, as the BET surface area of T2 is only slightly smaller than P25. The results of a comparison of photocatalysts T1 and T2, indicated that the difference between NO conversion was larger and a fact that can be attributed to larger BET surface area. Table 4.3 shows the conversion of NO under different levels of humidity. The conversion of NO also follows this trend, with respect to the BET surface area of the photocatalyst, in the following order: T1 > P25 > T2. Under high levels of humidity, the competition effect of water vapor indicated the significant effect of the BET surface area.

The effect of crystal size is not significant under the current experimental conditions. Although T2 has a smaller crystal size (10.2 nm) than that of P25 (18.8 nm), T2 has a lower NO conversion than that of P25. The results presented in this study are contradicted with the results presented by Maria and others

(2001). This discrepancy is probably owing to the effect of water vapor and the different pollutant levels applied. These researchers conducted a toluene photodegradation at ppm levels with different crystal size photocatalyst. At ppb levels, the competition for adsorption sites between pollutants and water vapor is a thousand times when ppm levels is applied. The above results suggested that the BET surface area is more vital than the crystal size of the photocatalyst for the photodegradation of ppb level pollutants at high levels humidity.

Residence time (min)	Conversion (%)			Generation (%)			Conversion (%)		
	NO (T1)	NO (T2)	NO (P25)	NO_2 (T1)	NO_2 (T2)	NO_2 (P25)	NO_x (T1)	NO_x (T2)	NO_x (P25)
11.40	95.50	92.10	93.50	-1.02	-1.87	-1.35	94.48	90.23	92.15
5.70	90.23	87.27	88.33	-2.18	-2.63	-2.95	88.05	84.64	85.35
3.80	84.17	80.36	81.65	-3.63	-4.33	-4.87	80.54	76.03	77.45
2.85	80.88	73.58	74.75	-4.20	-8.50	-7.99	76.68	65.08	71.95
2.30	75.78	72.28	72.75	-5.61	-12.29	-10.29	70.18	59.99	69.20

Table 4.2 Variation of NO_x using photocatalyst T1, T2 and P25 at different residence time. Experimental conditions: 200 ppb NO; humidity:2100 ppmv.

Humidity level (ppmv)	Conversion (%)			Generation (%)			Conversion (%)		
	NO (T1)	NO (T2)	NO (P25)	NO_2 (T1)	NO_2 (T2)	NO_2 (P25)	NO_x (T1)	NO_x (T2)	NO_x (P25)
2100	84.17	73.08	81.65	-3.63	-6.22	-4.2	80.54	66.86	77.45
9400	80.23	70.94	78.65	-6.22	-17.51	-12.4	74.01	53.43	66.25
15700	71.08	62.76	66.45	-10.76	-24.13	-17.45	60.32	38.63	49.00
22000	64.98	50.99	62.25	-15.36	-28.97	-22.95	49.62	22.02	39.30

Table 4.3 Variation of NO_x using photocatalyst T1, T2 and P25 at different levels of humidity. Experimental conditions: 200 ppb NO; residence time 3.8 min.

4.4 Carbon monoxide (CO)

4.4.1 Photodegradation of CO

The concentration of CO conducted in this study is 2 ppm, which is a typical indoor CO level (Akland et al., 1985). No removal of CO was observed by photolysis and blank test. Table 4.4 shows the photodegradation of CO using photocatalyst T1. As shown in the table, no conversion of CO was found under different levels of humidity and residence time. This is probably due to the amount adsorbed on the TiO_2 is rather low. Takahama et al. (1997) showed that no CO was photodegradated at 50 ppm. In this study, only an indoor CO level of 2 ppm was applied thus that reason no CO conversion was observed.

Experimental conditions	Initial concentration CO (ppm)	Conversion (%)
Humidity 2100 ppmv; R.T. 11.4 min	2	0
Humidity 22000 ppmv; R.T. 3.8 min	2	0

Table 4.4 Photodegradation of CO under different experimental conditions.

The result obtained in this study is not surprising. The conversion of CO is favorite at high concentration and the presence of Pt-deposited photocatalyst. Takahama et al. (1997) showed that the Pt-deposited photocatalyst TiO_2 achieved 80% CO conversion at 50 ppmv whereas no conversion was reported using bare TiO_2. Hwang et al. (2003) also reported similar results. Using three different commercial TiO_2, they showed that the CO conversion (30 ppmv) for naked TiO_2

was insignificant, whereas significant conversion was observed using platinized TiO_2. The conversion of CO was more significant when the concentration increased to 500 ppmv. Einaga et al. (2003) elucidated that the effect of Pt was to increase the adsorption of CO on the TiO_2 surface.

Experimental conditions		Initial SO_2 conc. (ppb)	SO_2 conc. (ppb) at 120 min
U.V. lamp off			
	TiO_2 powder (P25)	200	198
	Blank filter	200	51
	TiO_2 filter (P25)	200	46
U.V. lamp on			
	TiO_2 powder (P25)	200	199
	Blank filter	200	52
	TiO_2 filter (P25)	200	44

Table 4.5 Photodegradation of SO_2 under different experimental conditions. Experimental conditions: humidity level 2100 ppmv; residence time 3.7 min.

4.5 Sulfur dioxide (SO_2)

4.5.1 Photodegradation of SO_2

Prior to the photodegradation of SO_2, a photolysis test was conducted. No change in SO_2 concentration was observed passing through the reactor when only UV irradiation was presented. Table 4.5 shows the photodegradation of SO_2 at a humidity level of 2100 ppmv and at a residence time of 3.7 min both with and without the presence of UV irradiation. Around 75% of the SO_2 was adsorbed on the blank glass fiber filter. When the filter was imposed with TiO_2, the amount of SO_2 adsorbed between the blank filter and the TiO_2 filter is insignificant. Upon UV irradiation, the concentration of SO_2 was similar to the amount adsorbed on the blank filter. Thus, no photodegradation was found on the TiO_2 filter.

To further evaluate the photodegradation of SO_2, the same amount of TiO_2 powder was imposed on a Teflon plate having the same surface area of the glass fiber filter. Results showed that no adsorption in the dark or photodegradation of SO_2 under UV irradiation was found within the limit of the experimental error. This showed that SO_2 is primarily adsorbed on the glass fiber filter but not on TiO_2. No photodegradation of SO_2 was observed despite the kind of substrate used. The results of this study are different from those reported by Shang et al. (2002). The latter reported that both homogeneous and heterogeneous photooxidation reactions were observed when using a 400 W high-pressure mercury lamp and 4000 ppm SO_2. This discrepancy is probably due to the differences arising from the application of SO_2 concentration and the UV lamp. In this study, a 6 W UV lamp was used and the energy provided is probably not large enough to initiate the homogeneous reaction (Seinfeld and Pandis, 1998). No heterogeneous photodegradation was observed in this study is probably due to the SO_2 concentration conducted is too low to be adsorbed on TiO_2. Since the concentration conducted in this study is only 200 ppb whereas 4000 ppm was used by Shang et al. (2002), no photocatalytic heterogeneous reaction is due to the low adsorption of SO_2 on TiO_2 because only ppb levels of SO_2 were conducted in this study.

4.5.2 Effects of humidity levels

Fig. 4.12 shows the concentration of the sulfate ion (SO_4^{2-}) on the TiO_2 filter during the photodegradation of 200 ppb SO_2 at a residence time of 1.2 min at different humidity levels. The blank SO_4^{2-} concentration of the filter is 39 μg/filter and is subtracted from the SO_4^{2-} concentration presented in Fig. 4.11. The formation of SO_4^{2-} increased with increasing humidity levels. When the humidity level increased from 2100 ppmv to 22000 ppmv, the amount of SO_4^{2-} also increased from 433 μg/filter to 1395 μg/filter. SO_2 generated from the inlet stream was oxidized as SO_4^{2-} species and was deposited on the filter. As shown in the same figure, the pH value of the TiO_2 filter decreased from 10.02 to 9.61 when the humidity increased from 2100 ppmv to 22000 ppmv. The results showed that the acidity on the TiO_2 glass fiber filter increased with increasing humidity levels. This is probably due to the adsorption of SO_2 on the filter converted into sulfuric acid. Sulfur dioxide is a highly soluble gas and absorbs water on the TiO_2 filter. It is then dissociated into hydrogen ion (H^+) and bisulfite (HSO_3^-) ion. The bisulfite is then further dissociated into sulfite ion (SO_3^{2-}) and reacted with oxygen forming sulfate ion (SO_4^{2-}), as shown in equation (4.15) to (4.18) (Meszaros et al., 1981).

$$SO_2 + H_2O \Leftrightarrow SO_2 \cdot H_2O \qquad (4.15)$$

$$SO_2 \cdot H_2O \Leftrightarrow H^+ + HSO_3^- \qquad (4.16)$$

$$HSO_3^- \Leftrightarrow H^+ + SO_3^{2-} \qquad (4.17)$$

$$2SO_3^{2-} + O_2 \rightarrow 2SO_4^{2-} \qquad (4.18)$$

Reactions (4.15) to (4.18) proceed without the presence of catalyst, thought it is reported that the presence of iron catalyst increased the rate of reaction (Hegg and Hobbs, 1978).

Another possible pathway of SO_4^{2-} ion formation is the reactions between SO_2 and HO_2 radicals, as shown in equation (4.19) to (4.22) (Seinfeld and Pandis, 1998; Graedel, 1978).

$$SO_2 + HO_2 \cdot \longrightarrow SO_3 + OH \cdot \qquad (4.19)$$

$$SO_3 + H_2O \longrightarrow H_2SO_4 \qquad (4.20)$$

$$H_2SO_4 \longrightarrow H^+ + HSO_4^- \qquad (4.21)$$

$$HSO_4^- \longrightarrow H^+ + SO_4^{2-} \qquad (4.22)$$

Reactions (4.19) to (4.22) are likely not the sulfate ion formation pathway as sulfate ion was found even without the presence of UV light and TiO_2. The formation of sulfate ion from reactions (4.15) to (4.18) in this study is similar to the formation of acid rain. Studies (Wang and Deng, 2001; Gimeno et al., 2001; Henry and Heinke, 1996) identified that the emission of SO_2 is a major cause of acid rain. SO_2 contacted with aerosols in the air. The wet surface of the aerosol provided a hydrated area for SO_2 to become into solution (Boubel et al., 1994). In this study, the glass fiber filter provided a surface area for the adsorption of SO_2. Zero air passing through the humidifier provided water vapor to the inlet stream. Oxygen supplied from zero air reacted with sulfite ion forming sulfate ion on the filter. When TiO_2 powder was used without glass fiber filter as the supporting substrate, only a few ppb SO_2 differences were observed between the inlet stream and the outlet stream. Using a blank glass fiber filter only, similar SO_2 removal was observed compared to that of the TiO_2 filter. The IC result and the SO_2 concentration differences between the outlet stream and the inlet stream both supported the postulation that the adsorption of SO_2 had become SO_4^{2-}. In addition, the sulfate ion, SO_4^{2-}, is a frequently used indicator for the identification of acid rain (Oikawa et al., 1994; Tanaka et al., 1999) caused by the emission of SO_2.

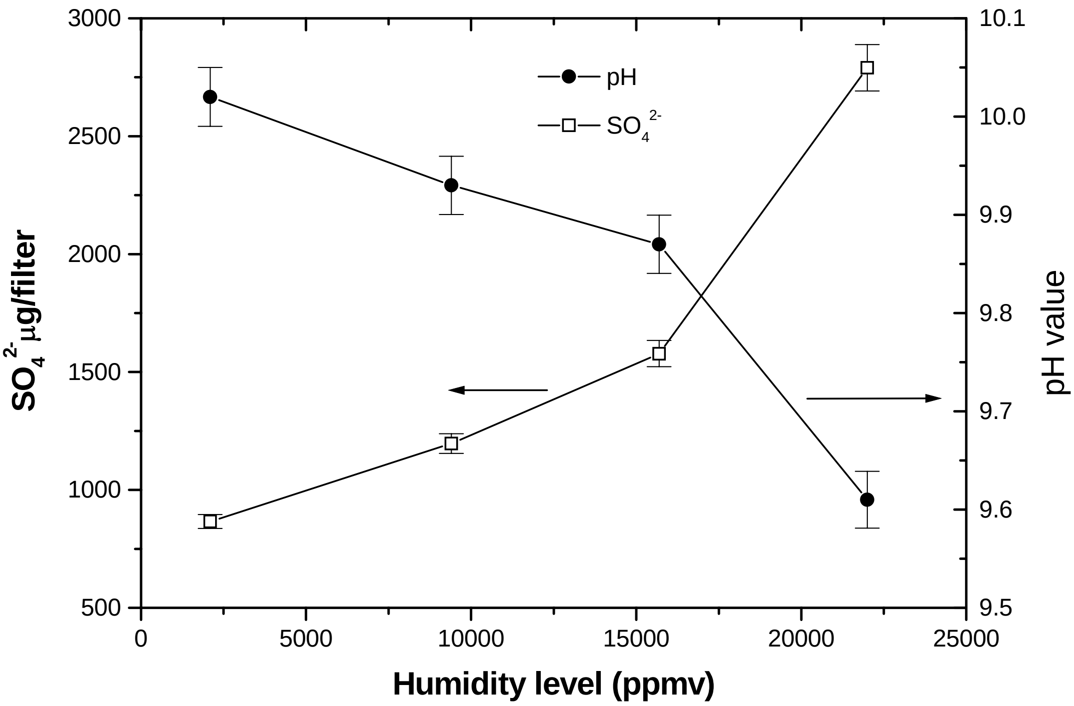

Figure 4.12 Sulfate ion (SO_4^{2-}) concentration under different relative humidity levels at an initial concentration of 200 ppb SO_2. Experimental conditions: Residence time 1.2 min.

4.6 Benzene, Toluene, Ethylbenzene and o-Xylene (BTEX)

4.6.1 Photodegradation of BTEX

Photolysis test were conducted by passing 20 ppb BTEX to the reactor with UV lamp turned on and without the presence of TiO_2. No removal of BTEX was observed by photolysis. Obee and Brown (1995) also showed that no removal of toluene was observed by photolysis. Blank test were also conducted by passing 20 ppb BTEX to the reactor without the presence of TiO_2 and UV lamp turned off. No BTEX removal was observed.

Prior to the experiment, the adsorption had reached equilibrium, as shown in the steady concentration from 0 min to 60 min. At 60 min, the UV lamp was turned on and the photodegradation of BTEX initiated. The concentration of BTEX dropped rapidly in the first 30 min and reached a photo-steady-state concentration at 120 min, as shown in Fig. 4.13. O-xylene has the lowest photo-steady-state concentration, followed by ethylbenzene, toluene and benzene. Similar results were obtained from other studies. The reaction rate of BTEX at a higher concentration (50 mg/m^3) also follows the same order, benzene having the lowest reaction rate followed by toluene, ethylbenzene and xylene (d'Hennezel and Ollis, 1997). The difference in the reaction rate of BTEX under the same residence time is possibly due to different amounts of BTEX adsorbed by the TiO_2 surface. Larson and Falconer (1997) conducted an adsorption test for benzene, toluene and p–xylene using P25 TiO_2. The results showed that p-xylene adsorbed on TiO_2 more than toluene, followed by benzene. It is reasonable to suggest that the amount of pollutant adsorbed on the catalyst surface affected the photodegradation rate of BTEX. Another possible reason is that the reaction rate between OH radicals and BTEX is different. Study (Atkinson, 1990) indicated that OH radicals react more rapidly with o-xylene, followed by ethylbenzene, toluene and benzene under atmospheric environment and the reaction rate in this study followed the same trend. Catalyst deactivation was reported from several studies (d'Hennezel and Ollis, 1997; Alberici and Jardim, 1997). In this study, no deactivation was found for BTEX as indicated by the color change of the TiO_2 filter. In order to confirm the absence of deactivation, the same filter was tested 5 times under the same conditions and the conversion of BTEX was within ±5% for each test. The absence of deactivation is possibly due to the low concentration of BTEX in this study. Intermediates may have accumulated on the TiO_2 filter and deactivate the photocatalytic process. However, the amount of intermediates is relatively small compared to the amount of TiO_2 on the filter. The reported deactivation usually applies a pollutant level of several hundreds ppm. The BTEX level in this study is ppb level, which is a thousand times lower than that reported with catalyst deactivation. This suggestion is in agreement with the data obtained by Alberici and Jardim (1997). They conducted a deactivation test using 505 ppm and 17 ppm toluene. The conversion decreased from about 90% to 20.9% when 505 ppm of toluene was applied. The conversion yield dropped to 50% with the use of 17 ppm of toluene. As in this study, only a ppb level of pollutant is conducted and the TiO_2 to pollutant ratio is much higher. It suggests that deactivation is unlikely occurred when trace level of pollutants are applied.

From the results of the GC/MS analysis, no gaseous phase intermediate was identified. No gaseous phase aldehydes were also found by the HPLC analysis. Studies (Sauer et al., 1995; Luo and Ollis, 1996) also showed that no gaseous phase intermediate was detected by an on-line GC/FID during the photodegradation of toluene. To determine the intermediates adsorbed on the TiO_2 surface, the TiO_2 filter after the photodegradation of BTEX was immersed in ethanol. The resultant solution was filtered and analyzed by CG/MS to determine any intermediates formed on the TiO_2 filter. Benzaldehyde and benzyl alcohol was qualitatively identified from the GC/MS analysis. The results observed in this study are similar to that reported by d' Hennezel et al. (1998). They used diethylether and ultrasonication to extract the remains of the TiO_2 and benzaldehyde, benzyl alcohol and benzoic acid were identified. Using temperature-programmed oxidation and desorption, Larson and Falcon (1997) identified benzaldehyde, benzyl alcohol and *m*-cresol as intermediates from the photodegradation of toluene using Degussa P25 as the photocatalyst. These results were further confirmed by Cao and co-workers (2000) using a FTIR technique and these intermediates poisoned the catalyst surface by blocking reaction sites. Intermediates generated from the photodegradation of benzene were phenol and hydroquinone (d'Hennezel et al., 1998). O-tolualdehyde and o-toluic acid were reported as intermediate generated from the photodegradation of o-xylene (Ameen and Raupp, 1999). Since the concentrations conducted in this study were only at ppb level, the resultant signal to noise ratio of the GC/MS analysis was high. Thus, only benzaldehyde and alcohol were identified as intermediate from the photodegradation of BTEX. From the intermediates identified in this study, the photodegradation mechanism is similar to those reported by d'Hennezel et al. (1998).

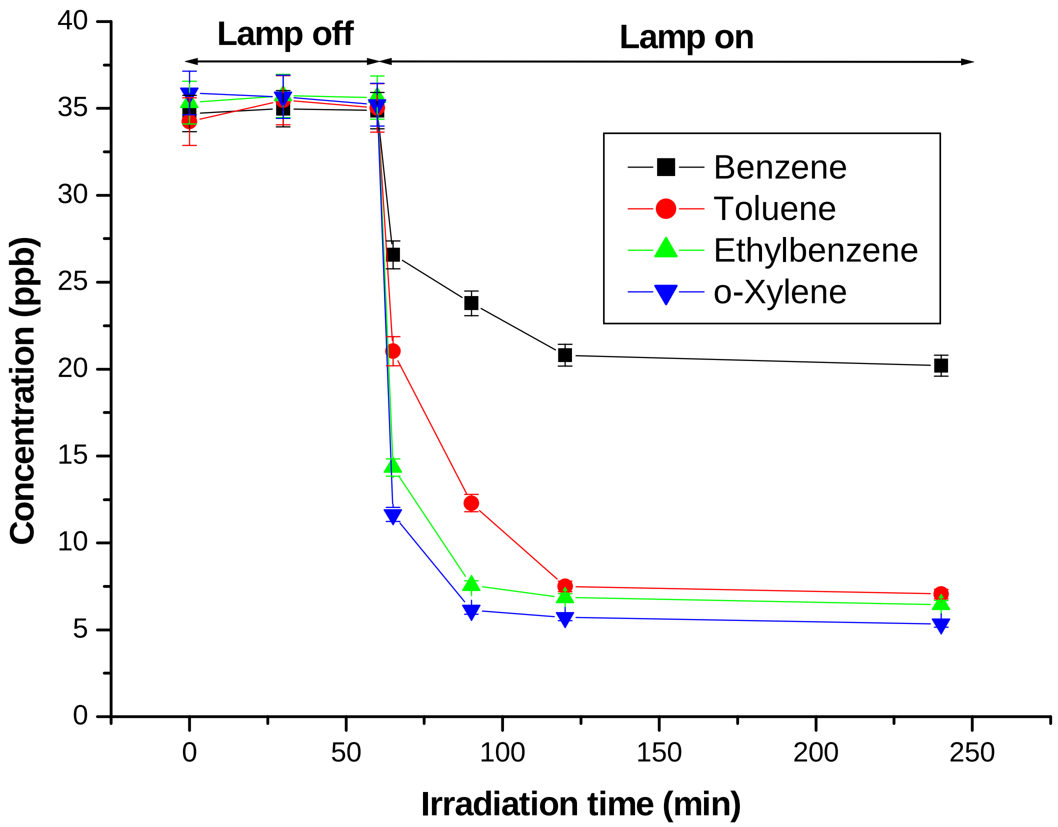

Figure 4.13 Photodegradation of 35 ppb BTEX. Experimental conditions: Residence time 11.4 min; humidity level 2100 ppmv.

4.6.2 Effects of initial concentrations

The effects of initial concentrations on BTEX conversion is shown in Fig. 4.14.

It can be observed that the conversion of BTEX increased with increasing BTEX concentrations. Since the experiment was conducted using ppb levels pollutant, the increase in pollutant concentration enhanced the adsorption of pollutant on the TiO_2 surface. The results obtained in this study are contrary from those reported by others. Zhang et al. (2003), Wang and Ray (2000), and Kim and Hong (2002) reported that the toluene conversion decreased with increasing concentration. Ameen and Raupp (1999) reported a decreasing reaction rate with increasing o-xylene concentration. Li et al. (2002) showed that the conversion of ethylbenzene decreased with increasing concentration. The above were studies conducted using an initial concentration of around one hundred ppm. The decreased in conversion with increasing pollutant concentration is due to the accumulation of intermediates on the TiO_2 surface. The increase in initial pollutant concentration has a positive impact on the accumulation of pollutant. As in this study, the pollutant applied was typical indoor ppb levels. The accumulation of intermediate was minimal and no deactivation was observed. Hence, the effect of higher pollutant adsorption on the TiO_2 surface is greater than the accumulation of intermediates. Therefore, the conversion of BTEX increased with increasing initial concentration. It is also noted that the conversion order (X>E>T>B) is the same under different initial concentrations.

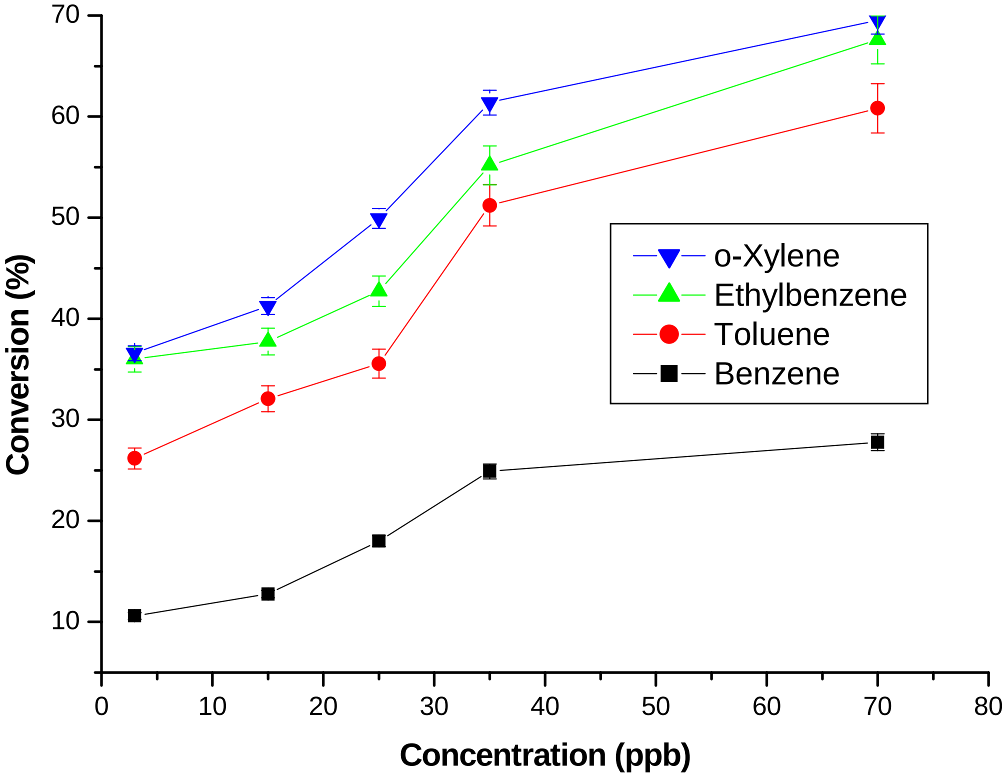

Figure 4.14 Photodegradation of BTEX under different initial concentrations. Experimental conditions: residence time 3.8 min; humidity levels 2100 ppmv.

4.6.3 Effects of residence time

Fig. 4.15 shows the photodegradation of 20 ppb BTEX at a humidity level of 2100 ppmv. Results showed that the conversion decreased with decreasing residence time. It can be assumed that a longer residence time, a higher rate of contact and length of contact time were achieved between the pollutants and the hydroxyl radicals, resulting in a higher conversion. Zhang et al. (2003) also showed that the conversion of toluene decreased with increasing flowrate. Hager et al. (2000) reported that the conversion of trichloroethylene and tetrachloroethylene decreased with increasing flowrate. It is noted that in this study, different compounds have different response to the variations of residence time. At a residence time of 3.7 min, the conversion difference between BTEX is not significant. The conversion difference between o-xylene and benzene, for example, is only 11.2%. However, as the residence time decreased, the conversion difference between BTEX increased. At a residence time of 0.6 min, the conversion difference between o-xylene and benzene increased to 28.2%. The effect of decreasing residence time is most significant for benzene, followed by toluene, ethylbenzene and o-xylene, which is exactly the same conversion pattern as shown in Fig. 4.13. Hence, a compound with a higher conversion is less affected by the variations of residence time, as in the case of o-xylene and ethylbenzene (within BTEX) and NO.

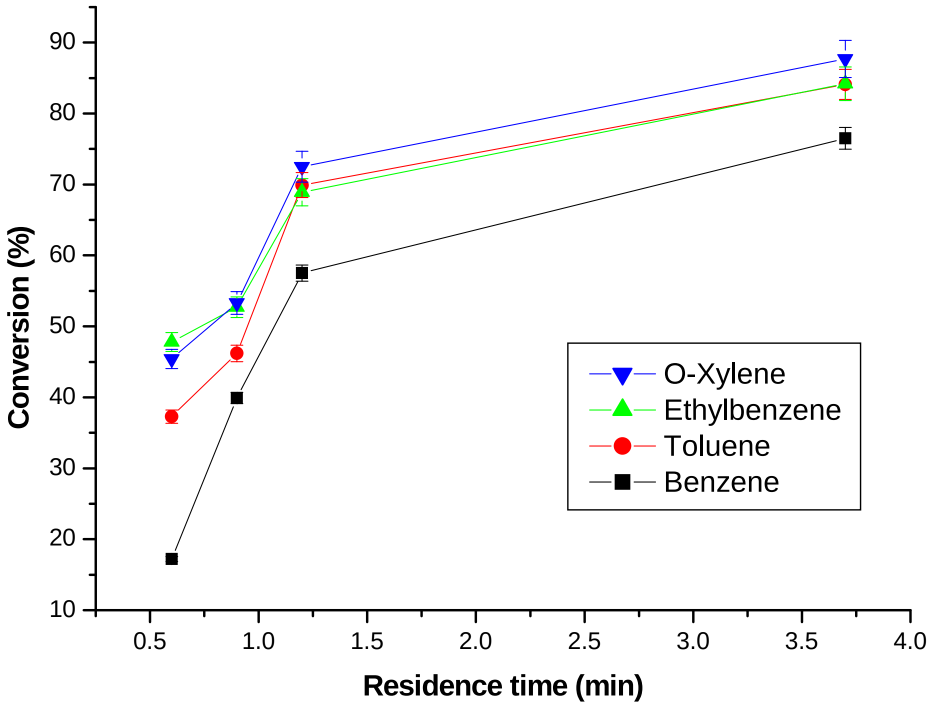

Figure 4.15 Photodegradation of BTEX under different residence time
Experimental conditions: humidity level 2100 ppmv; 20 ppb BTEX.

4.6.4 Effects of humidity levels

The impact on BTEX conversion at different humidity levels is shown in Fig. 4.16. The experiment was conducted with a BTEX concentration of 20 ppb at a residence time of 1.2 min. The conversion of BTEX decreased as the humidity levels increased. At a humidity of 2100 ppmv, the conversion of benzene, toluene, ethylbenzene and o-xylene is 57.5%, 69.9%, 68.9% and 72.5% respectively. As the humidity increased to 22000 ppmv, the conversion of BTEX dropped to 5.6%, 7.5%, 8.2% and 8.3% respectively. The experimental results clearly showed that the increase in humidity levels reduced the conversion of BTEX. This is probably due to the increase in water vapor competing with the adsorption site on the TiO_2 surface. However, Ibusuki and Takeuchi (1986) showed that the conversion of toluene increased with the increasing humidity levels. In addition, the conversions of benzene (d'Hennezel et al., 1998) and m-xylene (Peral and Ollis, 1992) were found to have increased with higher humidity levels. Their results suggested that the increase in water vapor increased the hydroxyl radicals formed on the TiO_2 surface due to water dissociation using TiO_2 (P25) as photocatalyst. The pollutant levels, however, applied in the above studies were all in the several hundreds ppm level. The effect of humidity on the conversion of a pollutant also depends on its concentration. Obee and Brown (1995) showed that the optimum conversion of toluene under different humidity levels depended on the initial toluene concentration. The results indicated that as the initial concentration of toluene decreased, the optimum humidity level also decreased. From the results of this study, it is not surprising that the conversion of BTEX decreased with increasing humidity and no optimum humidity level was found. At the ppb level, the competition for adsorption sites between BTEX and water vapor is a thousand times more than applying ppm level pollutants and only a small amount of water vapor is sufficient for the generation of OH radicals.

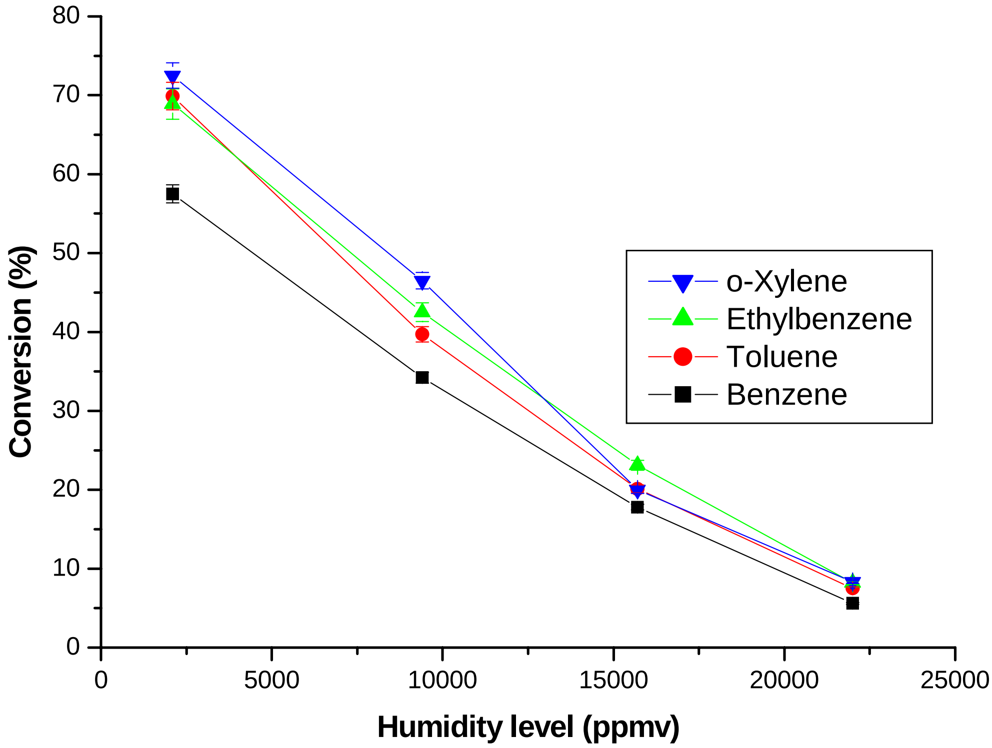

Figure 4.16 Photodegradation of BTEX under different humidity levels Experimental conditions: residence time 1.2 min; 20 ppb BTEX.

4.6.5 Photodegradation of BTEX by photocatalyst synthesized by sol-gel method

Table 4.6 shows the photodegradation of BTEX a residence time of 3.8 min. Photocatalyst T1 has a higher conversion of benzene and toluene of 10% and 6% compared to that of P25. No significant improved activity for ethylbenzene and o-xylene, however, was observed at humidity 2100 ppmv. Two reasons possibly account for this. Firstly, BTEX adsorbed a different amount on TiO_2. Larson and Falconer (1997) showed that p-xylene adsorbed on TiO_2 more than toluene, followed by benzene. The higher BET surface area of T1 provided a larger surface adsorption site, despite the effect of a combination of low level humidity plus the result of the competition between BTEX and water vapor. The conversion for benzene and toluene were thus improved. Secondly, the reaction rate of hydroxyl radicals of ethylbenzene and o-xylene is comparatively higher than benzene and toluene (Atkinson, 1990). The high conversion of ethylbenzene and o-xylene under the current experiment conditions might hinder the improved activity of T1.

The improved activity of T1 is more significant at a high level of humidity. The conversion of BTEX using photocatalyst T1 compared to P25 is even higher (Table 4.6). The conversion of BTEX is significantly reduced when the humidity level was 22000 ppmv owing to the competition water vapor for active sites. The extra BET surface of T1 provided more active sites for the adsorption of BTEX. It is noted that owing to the competition of water vapor for active sites, not only the conversions of benzene and toluene were improved but also those of ethylbenzene and o-xylene.

Experimental conditions	Photocatalyst	Conversion (%)			
		B	T	E	X
Humidity 2100 ppmv	T1	37.4	62.8	72.1	75.2
	T2	27.2	52.1	66.1	69.5
	P25	29.3	56.7	69.3	72.1
Humidity 22000 ppmv	T1	20.6	22.8	27.4	30.7
	T2	5.3	6.1	13.2	15.9
	P25	8.1	9.5	13.6	18.9

Table 4.6 Photodegradation of BTEX using photocatalyst T1, T2 and P25.

The effect of crystal size is not significant under the current experimental conditions. Although T2 has a smaller crystal size (10.2 nm) than that of P25 (18.8 nm), T2 has a lower NO and BTEX conversion than that of P25. The results presented in this study are contradicted with the results presented by Maria et al. (2001). This discrepancy is probably owing to the effect of water vapor and the different pollutant levels applied. These researchers conducted a toluene photodegradation at ppm levels with different crystal size photocatalyst. At ppb levels, the competition for adsorption sites between pollutants and water vapor is a thousand times when ppm levels are applied. The above results suggested that the BET surface area is more vital than the crystal size of the photocatalyst for the photodegradation of ppb level pollutants at high levels humidity.

4.7 Formaldehyde (HCHO)

4.7.1 Photodegradation of HCHO

Prior to the photodegradation of formaldehyde, a series of tests were conducted to evaluate the conversion of formaldehyde by photocatalysis and photolysis. Each test was conducted 4 times and the average value was reported. A residence time of 3.8 min and a humidity level at 2100 ppmv was used for all tests listed in Table 4.7.

A recovery test of the DNPH cartridge with the ozone scrubber was conducted to evaluate the sampling performance and the analytical procedures of the HPLC system. 50 ppb of formaldehyde was generated by diluting the formaldehyde from the standard gas with zero air. The sample was collected, eluted and analyzed according to the procedures described in chapter 3. As shown in Table 4.7, the recovery efficiency was 97%, which showed that the cartridge used for sampling and the analytical procedures of the HPLC system were in good conditions. A blank test was conducted by generating 50 ppb formaldehyde passing through the reactor with and without the presence of the TiO_2. Results in Table 4.7 shows that no formaldehyde was lost passing through the reactor.

A photolysis test was also conducted by generating the same amount of formaldehyde passing through the reactor without the presence of TiO_2 but with the UV lamp turned on. No photolysis was observed by comparing the formaldehyde concentration of the blank test. The photolysis result in this study is similar to that reported by Obee and Brown (1995). They decreased the UV intensity to eliminate the effect of formaldehyde photolysis on the reported formaldehyde oxidation rate. As in this study, the UV intensity applied was not sufficient to remove formaldehyde without the presence of the photocatalyst TiO_2. Also shown in the same table, the formaldehyde concentration at an irradiation time of 120 min is 5.9 ppb. A conversion of over 88% was achieved. The conversion is calculated similar to equation 4.7, but the initial concentration is the formaldehyde concentration generated at the inlet stream and the final concentration is the average formaldehyde concentration within an irradiation time of 120 min.

Experimental conditions	Initial HCHO conc. (ppb)	HCHO conc. (ppb) at 120 min
Pass through DNPH cartridge only (Recovery test)	50	48.5 ± 2.1
Pass through reactor without UV lamp on and TiO_2 (Blank test)	50	48.9 ± 1.8
Pass through reactor without UV lamp on but with TiO_2 (Blank test)	50	49.2 ± 1.9
Pass through reactor with UV lamp on only (Photolysis test)	50	49.0 ± 2.3
Pass through reactor with TiO_2 and UV lamp on (Photocatalysis test)	50	5.9 ± 0.3
Pass through DNPH cartridge with 200 ppb NO and 100 ppb NO_2 only (NO_x interference test)	50	48.7 ± 2.8

Table 4.7 Photodegradation and photolysis of formaldehyde. Experimental conditions: 50 ppb HCHO; humidity level 2100 ppmv; residence time 3.8 min.

4.7.2 Effects of initial concentrations

Fig. 4.17 shows the photodegradation of formaldehyde under different initial concentrations. No significant formaldehyde conversion difference was observed under different initial concentrations. Similar to the photodegradation of NO, Langmuir-Hinshelwood (L-H) rate expression is used to describe the gas-solid phase reaction for heterogeneous photocatalysis (Kim and Hong, 2002; Fox and Dulay, 1993; Serpone and Pelizzetti, 1989)

$$r = \frac{kKC}{1 + KC} \qquad (4.10)$$

where k is the rate constant, K is the adsorption constant and C is the formaldehyde concentration. By substituting the L-H rate expression into a mass balance equation of a plug flow reactor, the following expression is obtained (Alberici and Jardim; 1997; Zhang et al., 1994)

$$\frac{V}{Q} = \frac{1}{kK}\ln\left(\frac{C_o}{C}\right) + \frac{1}{k}(C_0 - C) \qquad (4.11)$$

where V is the volume of the reactor, Q is the flowrate through the reactor and C_o is the initial formaldehyde concentration. By rearranging equation 4.11, a linear form is obtained, as shown in equation 4.12:

$$\frac{V/Q}{(C_o - C)} = \frac{1}{k} + \frac{1}{kK}\frac{\ln(C_o - C)}{(C_o - C)} \qquad (4.12)$$

If L-H kinetics is valid for a plug flow reactor, then a plot of $(V/Q)/(C_o\text{-}C)$ versus $\ln(C_o/C)/(C_o\text{-}C)$ should be linear. Equation 4.11 was tested by using different C_o and C. As shown in Fig. 4.18, the experimental data is in good agreement with the integral rate law analysis. The values of k and K can be obtained from the intercept and slope of Fig. 4.18. The values of k and K are 84.75 ppb/min and 0.013 ppb^{-1}. Thus, the photocatalytic reaction occurred on the photocatalyst surface but not in the bulk fluid. Similar results were reported by Noguchi et al. (1998). They also showed that the oxidation rate followed the L-H model and increased with increasing initial formaldehyde concentrations.

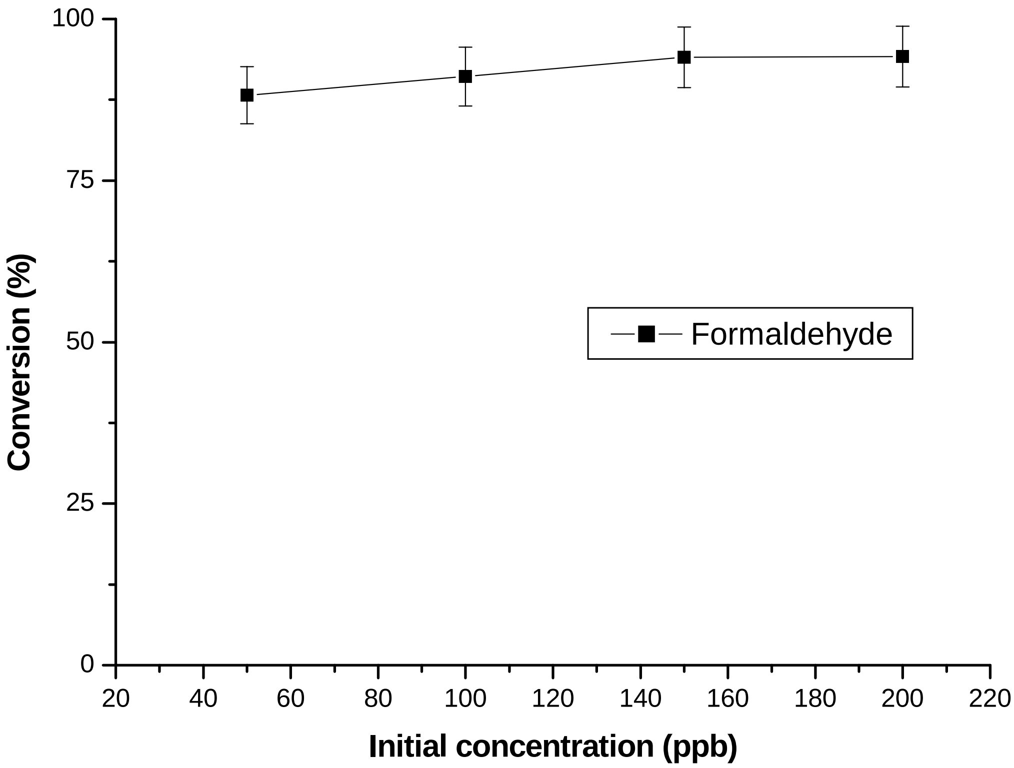

Figure 4.17 Photodegradation of formaldehyde under different initial concentrations. Experimental conditions: 50 ppb HCHO; humidity level 2100 ppmv; residence time 3.8 min.

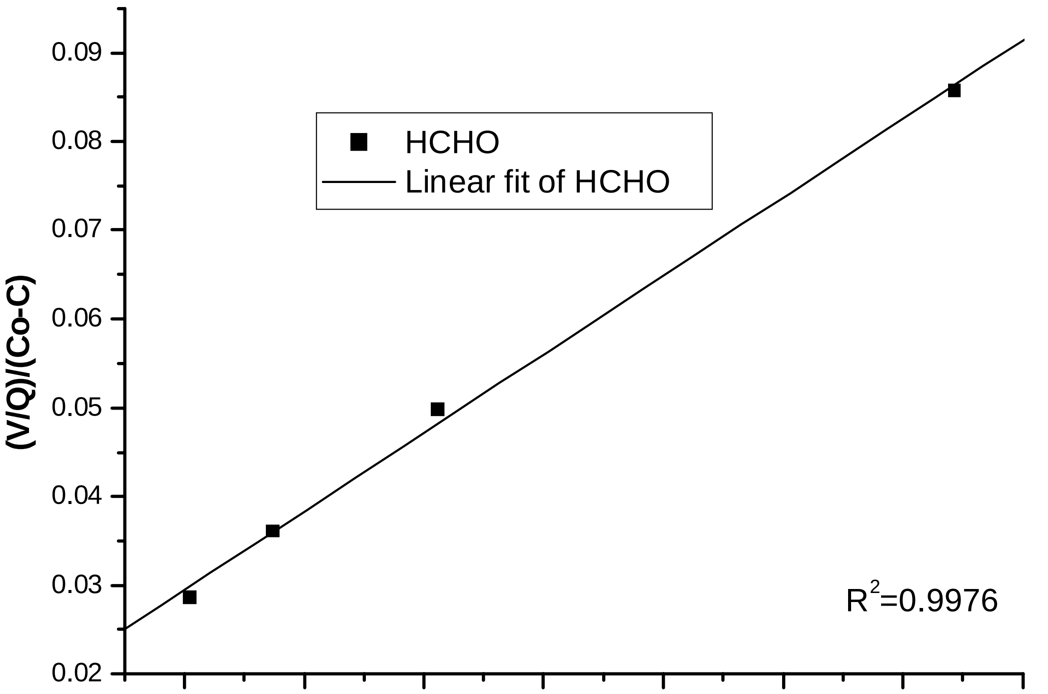

Figure 4.18 L-H plot of formaldehyde photodegradation. Experimental conditions: humidity level 2100 ppmv, residence time 3.8 min.

4.7.3 Effects of residence time

Fig. 4.19 shows the photodegradation of formaldehyde under different residence time at a humidity level of 2100 ppmv. The conversion decreased from 88.2% to 77.2% when the residence time decreased from 3.8 min to 0.9 min. At a longer residence time, a higher rate of contact and length of contact time were achieved between the hydroxyl radicals and formaldehyde, resulting in a higher conversion. Similar findings for NO (Devahasdin et al., 2003), Volatile Organic Compounds (VOCs) (Zhang et al., 2003) and 2-propanol (Hager and Bauer, 1999) were reported. The adverse effect of decreasing residence time on formaldehyde is lesser compared to BTEX. The conversion of toluene, for instance, decreased from 84.1% to 37.3% whereas the conversion of formaldehyde decreased from 88.2% to 77.2% when the residence time decreased from 3.9 min to 0.6 min. This is probably due to the difference in bonding energy of toluene and formaldehyde on the surface hydroxyl groups of the titania surface. Toluene adsorbed on the surface hydroxyl groups via OH···π electron type complex (Nagao and Suda, 1989), whereas formaldehyde via hydrogen bonding (Obee and Brown, 1995). The bonding energy of hydrogen bonding is higher than the OH···π electron type complex. The adsorption between formaldehyde and the surface of titania is higher compared to toluene. Thus, the conversion of formaldehyde was higher than toluene and similar results were reported by Obee and Brown (1995).

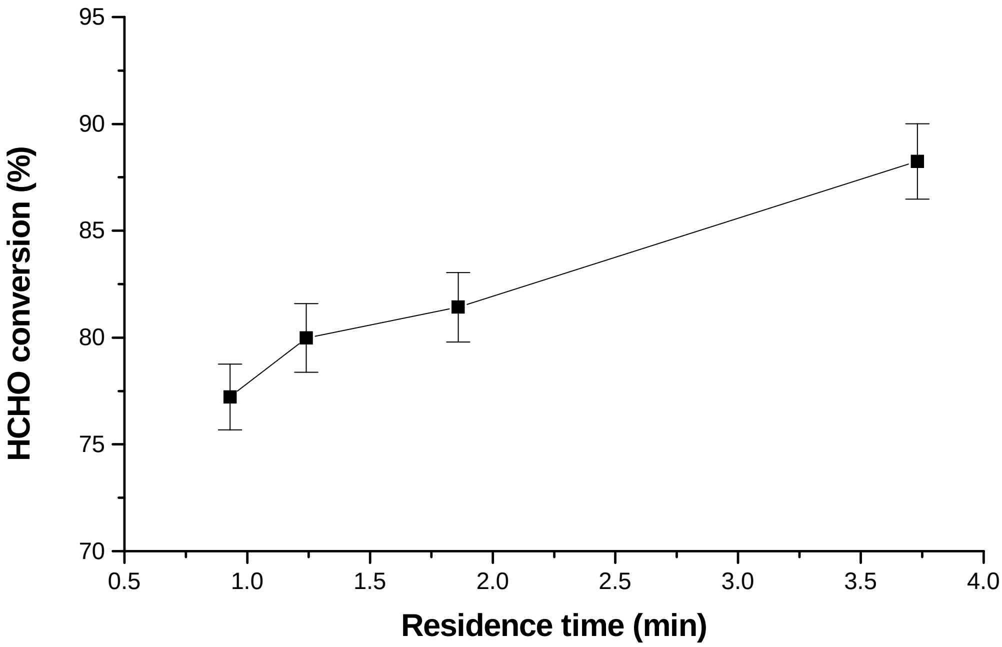

Figure 4.19 Impact on HCHO conversion under different residence time. Experimental conditions: 50 ppb HCHO; humidity level 2100 ppmv.

4.7.4 Effects of humidity levels

Fig. 4.20 shows the photodegradation of formaldehyde under different humidity levels at a residence time of 1.2 min. The formaldehyde conversion decreased from 80% to 54% when the humidity level increased from 2100 ppmv to 22000 ppmv. At a higher humidity level, water molecule competed with formaldehyde for adsorption sites on TiO_2. This phenomena is similar to those reported for NO and BTEX in the previous sections. The adverse effect of increasing humidity levels on formaldehyde conversion is also less significant compared to BTEX.

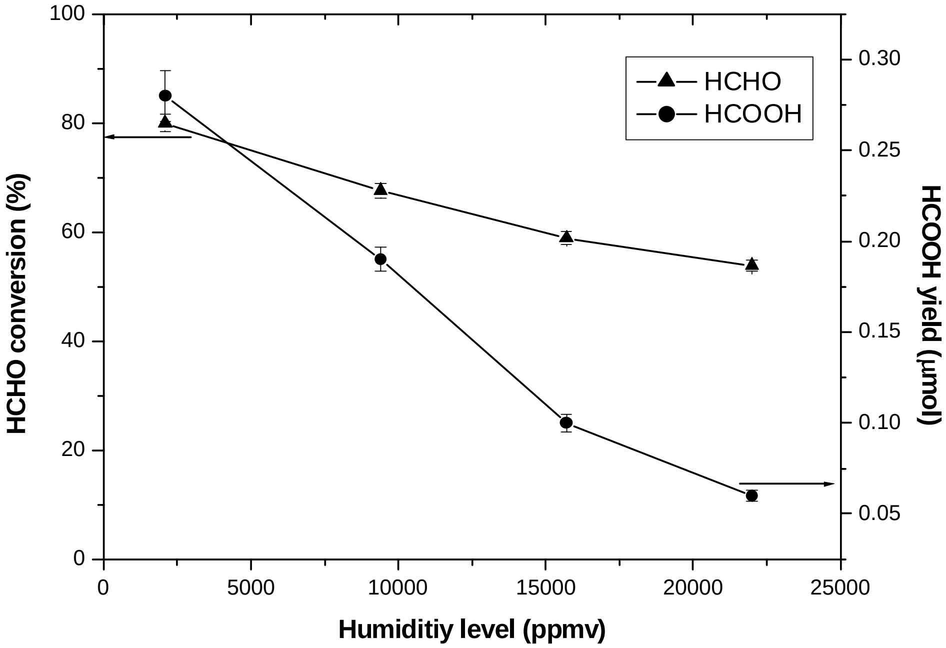

Figure 4.20 Impact on HCHO conversion and HCOOH yield under different humidity levels. Experimental conditions: 50 ppb HCHO; residence time 1.2 min.

The effect of humidity on the photodegradation rate may be quantitatively described by the following equation (Peral and Ollis, 1992):

$$r = \frac{r_o}{1 + K_H [H_2O]^{\beta}} \qquad (4.13)$$

where r_o is the reaction rate under the absence of water. By rearranging equation 4.13 into equation 4.14, the inverse of the reaction rate is plotted against the water vapor concentration, as shown in Fig. 4.21.

$$\frac{1}{r} = \frac{1}{r_o} + \frac{K_H}{r_o}[H_2O]^{\beta} \qquad (4.14)$$

From the results obtained in Fig. 4.21, the relationship between the reverse of the reaction rate and water vapor concentration can be described as $1/r = 1.56003+0.001302[H_2O]^{0.88917}$, and $\beta = 0.89$, $r_o = 0.641$ μmol/m^2 min, K_H =

8.346×10^{-4} ppm^{-1}.

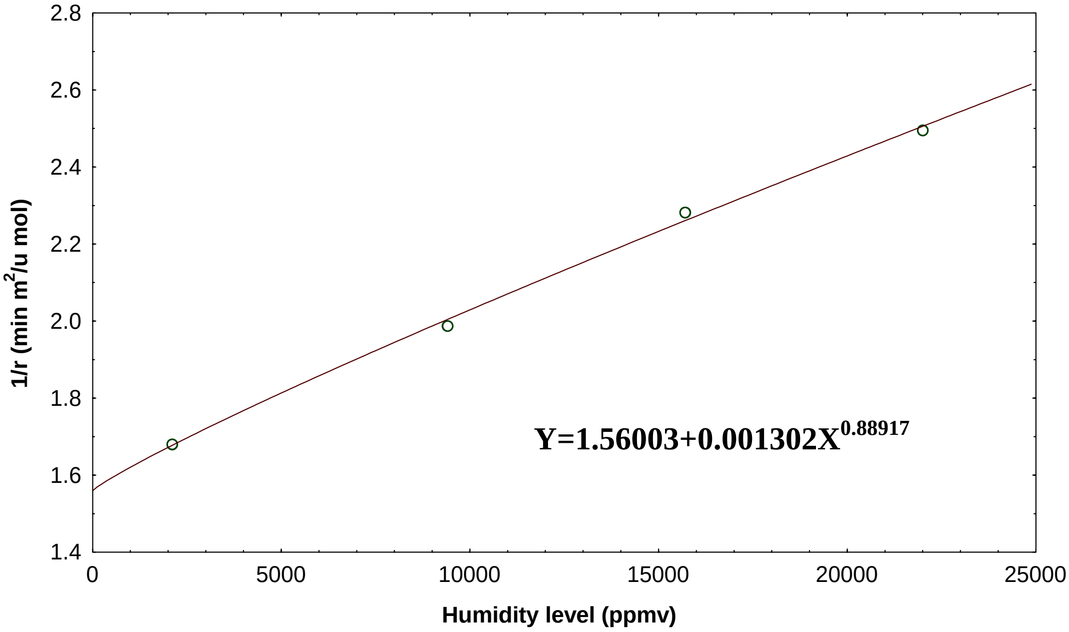

Figure 4.21 Inverse of reaction rate of formaldehyde photodegradation vs. humidity levels. Experimental conditions: residence time 1.2 min, 50 ppb HCHO.

Formic acid is the most commonly found intermediate from the conversion of formaldehyde by photolysis (equations 4.23-4.26) (Veyret et al., 1989), photocatalysis in aqueous phase (Shin et al., 1996) and gaseous phase (equations 4.1-4.4 and 4.27-4.29) (Peral and Ollis, 1992; Yang et al., 2000).

$$CH_2O + hv \rightarrow H + HCO\cdot \qquad (4.23)$$

$$\cdot CHO + HO_2\cdot \longrightarrow HOCH_2OO \qquad (4.24)$$

$$HOCH_2OO + HO_2\cdot \longrightarrow HOOCH_2OH + O_2 \qquad (4.25)$$

$$HOOCH_2OH \longrightarrow H_2O + HCOOH \qquad (4.26)$$

$$HCHO + OH\cdot \longrightarrow HCO\cdot + H_2O \qquad (4.27)$$

$$HCO\cdot + OH\cdot \longrightarrow HCOOH \qquad (4.28)$$

$$HCOOH + 2h^{+} \longrightarrow CO_2 + 2H^{+} \qquad (4.29)$$

In this study, formic acid was also detected under different humidity levels. As shown in Fig. 4.20, the yield of formic acid decreased with increasing humidity levels. This is probably due to the decrease in HCHO conversion with increasing humidity levels. Prior to the formation of CO_2, formaldehyde is first oxidized to formic acid, as shown in equation 4.29. Thus, the yield of formic acid is also an important parameter to indicate the photo-oxidation of formaldehyde.

4.8 Quantum yield

Quantum yield is an important parameter which shows the utilization of the irradiation of a photocatalyst. Quantum yield is calculated by the following equation:

$$Quantum\,Yield = \frac{\text{mol of reactant consumed or product formed}}{\text{mol of photons (or einstein) absorbed}} \qquad (4.30)$$

The numerator can be calculated from the amount of pollutant removed, and the denominator can be measured and calculated by the following equation:

$$I_a = I_o - I_t + I_f + I_b$$

where I_o is the incident photo flux, I_a is the intensity adsorbed in the film, I_t is the transmitted intensity, I_f is the forward-scattered intensity, and I_b is the backscattered intensity.

I_o can be measured directly using the UV power meter. However, the values of I_b, I_f, and I_t were not able to obtain from the current experimental setup.

In view of difficulties in obtaining the values of I_b, I_f, and I_t, "apparent quantum yield" was proposed instead of quantum yield to evaluate the utilization of irradiation. The calculation of apparent quantum yield is shown in the following equation:

$$Apparent\ Quantum\ Yield = \frac{\text{mol of reactant consumed or product formed}}{\text{mol of incident photons (or einstein)}} \tag{4.31}$$

The mole of incident photons can be measured by actinometry (Heller and Langan, 1981), based on the mole of Fe^{2+} formed, excitation wavelength and irradiation time.

Since the formation of Fe^{2+} from E-a-(2,5-dimethyl-3-furylethylidene) isopropylidene succinic anhydride (parent chemical) is sensitive to all wavelength of irradiation (even fluorescence light), the measurement of incident photons can only be achieved in a dark room.

In this study, the value of quantum yield is not obtained due to no dark room is available for measurement of actinometry. Nevertheless, this parameter is important to compare the utilization of irradiation between different photocatalyst such as P25 and photocatalyst syntheses by sol-gel method. Although results showed that a higher NO and BTEX conversions were obtained by photocatalyst syntheses by sol-gel method, no information on irradiation utilization is available. This particular information is very important for practical application, which assists the design of light irradiation geometry.

4.9 Summary

The feasibility of applying photocatalytic technology for indoor air purification was evaluated by typical indoor air pollutants namely NO, CO, SO_2, BTEX (most abundant VOCs) and HCHO with reference to their typical indoor air pollutant levels. Sensitive analyses were conducted for the aforementioned pollutants under different residence time, initial concentrations and humidity levels.

No conversion was observed for CO and SO_2, but more than 70% of the SO_2 was adsorbed on the glass fiber filter (TiO_2 coating substrate). The photodegradation of NO reached a photo-steady-state concentration in 5 min, whereas nearly 120 min was need for BTEX. Deactivation was observed for the photodegradation of NO but not for BTEX. The conversions of NO and HCHO did not change significantly under different initial concentrations, but the conversions of BTEX increased with increasing initial concentrations.

The conversion of NO, BTEX and HCHO decreased with decreasing residence time and with increasing humidity levels. The adverse effect of increasing humidity levels on pollutant conversion is much more significant than other parameters. By synthesizing the photocatalyst using sol-gel method, the increase in BET surface area of the photocatalyst increased the pollutant conversion especially at high humidity levels.

The value of quantum yield is a key parameter to determine the efficiency of a photocatalyst, though it is not determined in this study due to laboratory constrains.

Chapter 5 Removal of indoor air pollutants by photocatalyst loaded on activated carbon filter

5.1 Introduction

In the previous chapter, it is shown that the high humidity levels drastically and adversely affected all the conversion of all pollutants studied. Although the photocatalyst synthesized by sol-gel method improve the photocatalytic activity, the conversion is not very significant. In this chapter, it depicts the effect of using activated carbon filter as a coating substrate and the conversion is compared to that of using glass fiber filter.

5.2 Characterization of photocatalyst loaded on activated carbon filter

Fig. 5.1 (a) shows the micrograph of the activated carbon which has a porous structure. The activated carbon filter consists multiple layers of glass fiber layer and activated carbon with a glass fiber layer at the top and bottom surface, as shown in Fig. 5.1 (b). The glass fiber layer is so lean that the activated carbon is visible on its surface. Hence, the activated carbon filter presented a speckled appearance. After calcination, TiO_2 particles agglomerated and adhered on the activated carbon. On the utmost layer, the activated carbon and the glass fiber are coated with TiO_2. Fig. 5.1 (c) clearly shows that TiO_2 particles are in contact with the activated carbon. Fig. 5.1 (d) shows that the inner layer of the glass fiber and the activated carbon is also coated with TiO_2. The smaller size TiO_2 enable it to be penetrated and impinged inside the activated carbon filter. The BET surface area of the activated carbon (AC) powder extracted from the activated carbon filter was 1115 m^2/g. The activated carbon filter coated with TiO_2 is denoted as TiO_2/AC filter where as TiO_2 coated on glass fiber filter is denoted as TiO_2 filter.

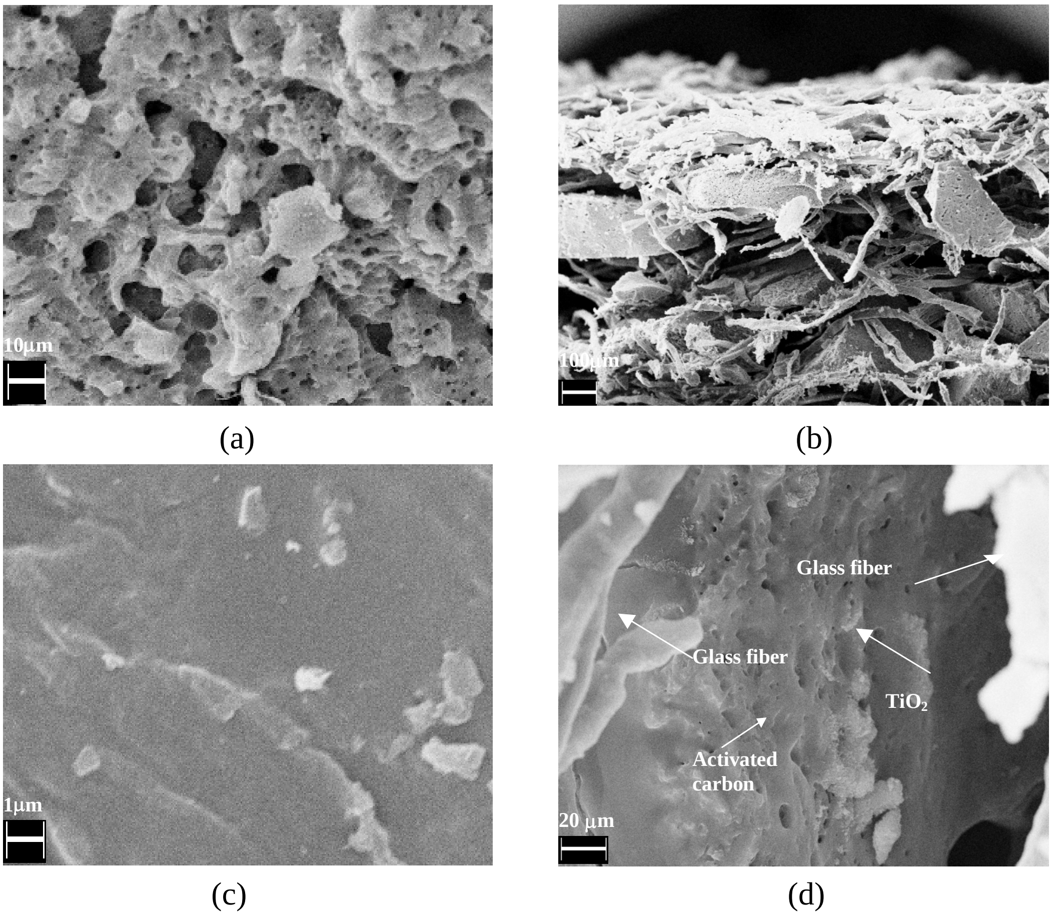

Fig 5.1 Scanning electron micrographs of (a) activated carbon, (b) glass fiber comprehend with activated carbon, (c) intimate contact of TiO_2 and activated carbon (d) inner layer of activated carbon coated with TiO_2.

5.3 *Nitrogen oxide (NO)*

5.3.1 Adsorption of NO

Fig. 5.2 shows the adsorption of 200 ppb NO at a humidity level of 2100 ppmv under different residence time. Each experiment set was conducted 4 times and the average value was reported. Three kinds of filter were tested, namely TiO_2 filter, AC filter and TiO_2/AC filter. Under continuous flow at different residence time, no adsorption of NO was found for the TiO_2 filter within the experimental error. The adsorption capacity of the AC filter and TiO_2/AC filter was identical, owing to no adsorption capacity having been found on TiO_2. In addition, the BET surface area of the AC is 24 times higher than the TiO_2 (P25) and the adsorption contributed by the TiO_2 is not significant. Matos et al. (1998) also showed that no additive adsorption capacity was found when TiO_2 (P25) was added to AC. The adsorption capacity of NO increased, with increasing residence time, for the AC filter and TiO_2/AC filter. The amount of NO adsorbed increased from 9% to 35% when the residence time increased from 0.6 min to 3.7 min. With other parameters such as weight of carbon and inlet pollutant concentration fixed, the increased in residence time (decreased in volumetric flowrate) reduced the amount of pollutant exited the outlet stream (Wood, 2002).

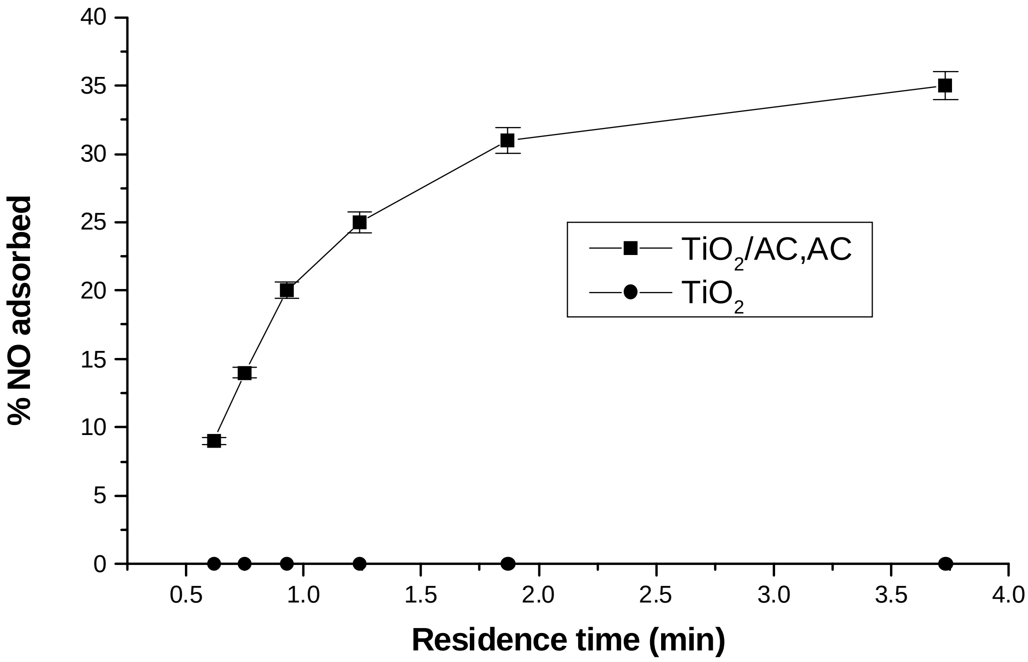

Figure 5.2 Amount of NO adsorbed in the dark under different residence times. Experimental conditions: Humidity level 2100 ppmv, 200 ppb NO.

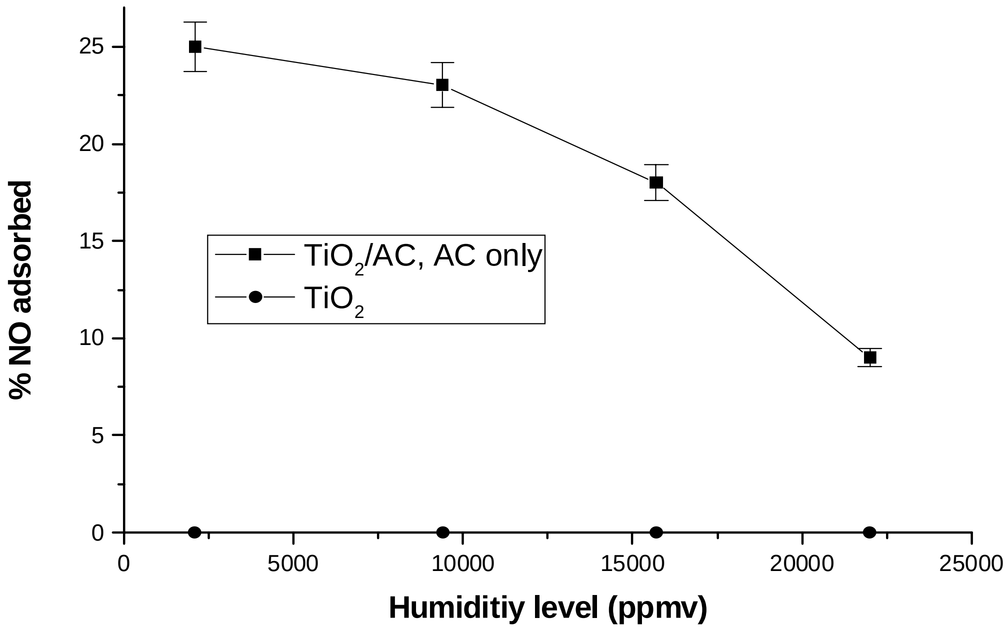

Figure 5.3 Amount of NO adsorbed in the dark under different humidity levels. Experimental conditions: Residence time 1.2 min, 200 ppb NO.

Fig. 5.3 shows the adsorption of 200 ppb at a residence time of 1.2 min under different humidity levels. The NO adsorption capacity decreased with increasing humidity levels. When the humidity level increased beyond 16000 ppmv, the NO adsorption capacity significantly reduced. Richter et al. (1985) also reported that high levels of relative humidity inhibited the adsorption of NO on activated carbon.

Blank tests were also conducted for the AC filter. The concentrations of NO and with the presence of illumination were monitored using an AC filter. No change in NO concentration was observed between the presence and absence of UV illumination. The result showed that only adsorption occurred on AC filter but no photolysis or photocatalysis was observed.

It is also reported that the adsorption of pollutants on activated carbon increased with increasing temperature (Cheremisinoff et al., 1980; Khan and Ghoshal, 2000). All the experiments were conducted at a temperature of 25 ± 1°C. This small temperature variation on the pollutant adsorption capacities is insignificant compared to the effect of residence time and humidity levels. Matos et al. (1998) also reported that the adsorption is not affected when the temperature increased by 1°C.

5.3.2 Removal of NO by AC, TiO_2 and TiO_2/AC filter

Fig. 5.4 shows the removal of 200 ppb NO under different residence time at a humidity level of 2100 ppmv. The term “conversion” used in the previous sections has the same meaning of the term “removal” used in this section. The use of “removal” is used to describe the pollutant adsorbed by AC. It is inadequate to use “conversion” in figures with pollutant removed by AC, TiO_2 and TiO_2/AC filter since activated carbon did not convert but only adsorb pollutant. Using TiO_2/AC, the NO removal is higher compared with using TiO_2. The amount of NO adsorbed on AC decreased from 35% to 9% when the residence time decreased from 3.7 min to 0.6 min. However, the NO_x removal between using TiO_2/AC and TiO_2 is not as significant as BTEX (see the following section). Under low humidity in which the competition effect between water vapor and NO is not significant, the high NO removal rate under the experimental conditions might hinder the effect of AC.

The generation of NO_2 increased with decreasing residence time. For instance, the generation of NO_2 increased from 1.6% to 9.2% when the residence time decreased from 3.7 min to 0.6 min. The effect of TiO_2/AC on the generation of NO_2 also increased with decreasing residence time. NO_2 can be considered as an intermediate as shown in the following equations (Komazaki et al., 1999; Matsuda et al., 2001).

$$NO + HO_2\cdot \rightarrow NO_2 + OH\cdot \qquad (5.1)$$

$$NO_2 + OH\cdot \rightarrow HNO_3 \qquad (5.2)$$

It is presumed that the NO_2 generated from the photodegradation of NO is assembled on the AC by its large adsorption capacity. The adsorbed NO_2 is further photodegradated to HNO_3, which reduced the amount of NO_2 exiting the system. The results clearly showed that the combination of TiO_2 and AC not only increased the target pollutants (NO) removal but also reduced the amount of the intermediate (NO_2). It is also reported (Torimoto et al., 1996) that the use of TiO_2 loaded with zeolite also reduced the amount of intermediate for the photodegradation of propyzamide in aqueous phase. Using TiO_2 or AC alone, the NO removal rate was low. The combination of TiO_2 and AC has an enhancement effect on NO removal.

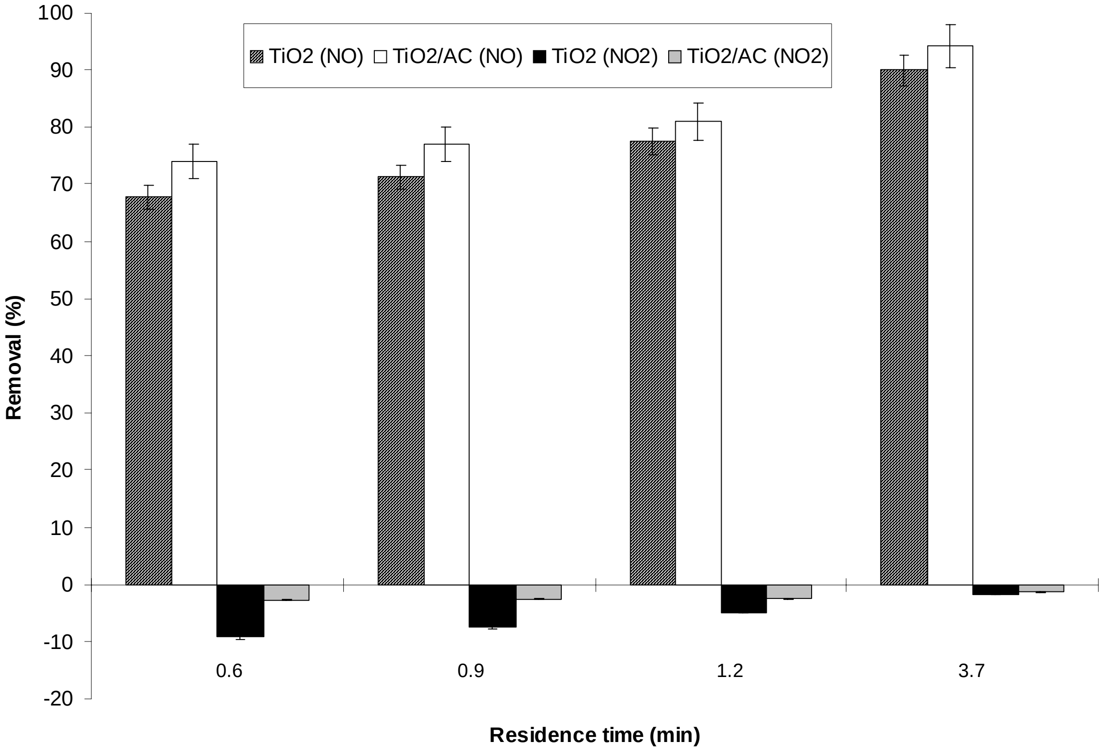

Figure 5.4 NO and NO_2 conversion under different residence time. Experimental conditions: Humidity level 2100 ppmv, 200 ppb NO.

Fig. 5.5 shows the NO removal at a residence time of 1.2 min under different humidity levels. A higher NO removal was also achieved when TiO_2 is immobilized on an AC filter. The use of TiO_2/AC is less affected by the increasing humidity levels. As can be seen clearly in the same figure that the use of TiO_2/AC decreased NO_2

generation. The NO_2 generation increased with increasing humidity levels owing to the water competition effect. By immobilizing TiO_2 on the AC filter, the NO_2 generation from the photodegradation of NO is adsorbed and thereby further photodegradated to HNO_3 according to equation (5.2). Without the presence of AC, the NO_2 generated could not be adsorbed on TiO_2 and exiting the system. Another possible reason for the higher NO removal rate using TiO_2/AC filter is that the activated carbon able to absorb and concentrate the water vapor (Wood, 2002), leaving the TiO_2 more adsorption sites for the adsorption of NO in the air.

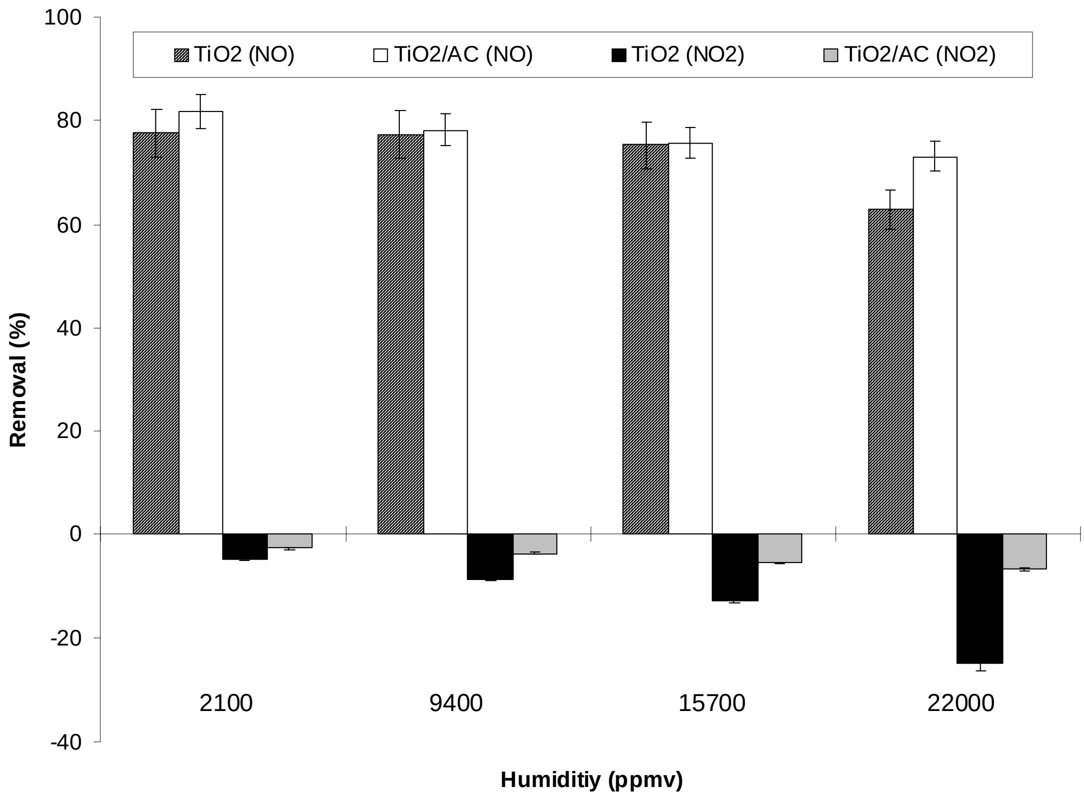

Figure 5.5 NO and NO_2 conversion under different humidity levels. Experimental conditions: Residence time 1.2 min, 200 ppb NO.

5.3.3 Long term activity and deactivation

Previously we reported that no deactivation of BTEX occurred when TiO_2 is immobilized on a glass fiber filter. Using an AC filter as the coating substrate, no deactivation was also observed for BTEX. The same TiO_2/AC was tested 5 times under the same conditions and the BTEX removals were within ± 5% for each test.

Deactivation was found for NO when TiO_2 is immobilized on a glass fiber filter. From the practical point of view, it is important to have a long life filter and thus avoid the frequency of replacements. As shown in Fig. 5.6, the photo-steady-state concentrations of NO and NO_2 using TiO_2 and TiO_2/AC at a residence time of 1.2 min and a humidity level of 22000 ppmv. The use of the AC filter demonstrated clearly the suppression of NO_2 exiting the system. Deactivation was observed using TiO_2 only and the NO_2 concentration increased from 14.2 ppb to 72.5 ppb, as shown in Fig. 5.6 from 5 min to 1320 min. Using TiO_2/AC, no increase in NO_2 concentration was observed. The large adsorption capacity of AC successively decreased NO_2 exited to the system and increased the life time of the filter.

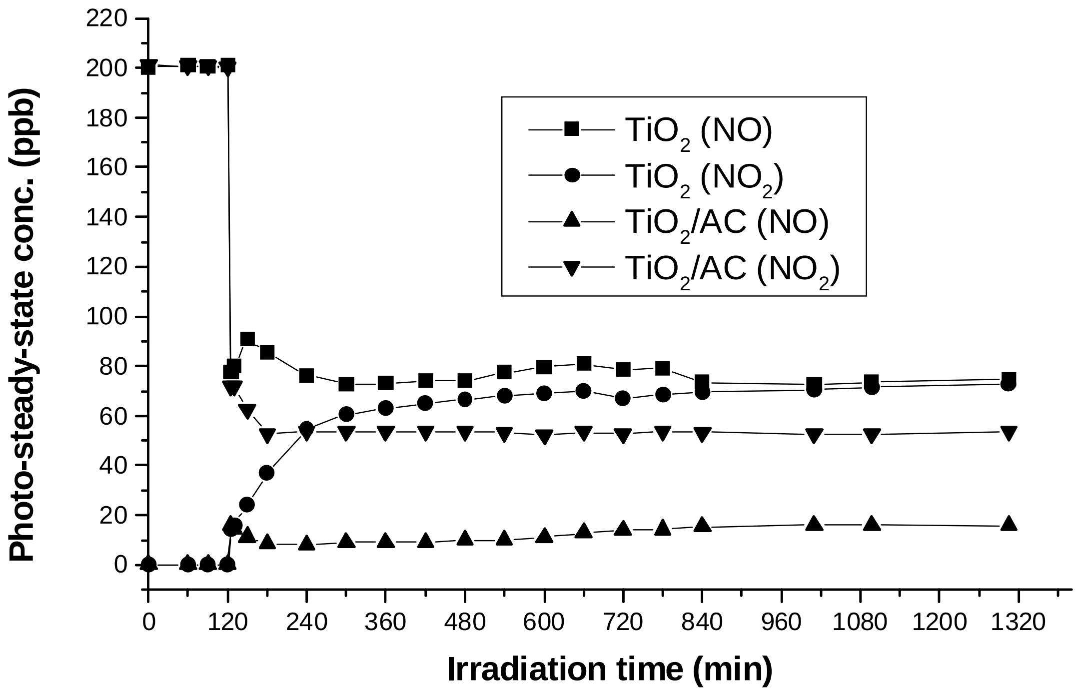

Figure 5.6 Long term activity of TiO_2 and TiO_2/AC. Experimental conditions: Residence time 1.2 min, humidity level 22000 ppmv, 200 ppb NO.

5.4 Benzene, Toluene, Ethylbenzene and o-Xylene (BTEX)

5.4.1 Adsorption of BTEX

Fig. 5.7 shows the adsorption of 20 ppb BTEX at a humidity level of 2100 ppmv under different residence time. The adsorption capacity of the AC filter was identical to that of TiO_2/AC filter. No adsorption of BTEX was found for TiO_2 within the experimental error. The four compounds have a very similar adsorption capacity, with only 1% to 2% difference. It is also reported (Urano et al., 1982) that the amount of benzene, toluene and o-xylene adsorbed on AC is similar.

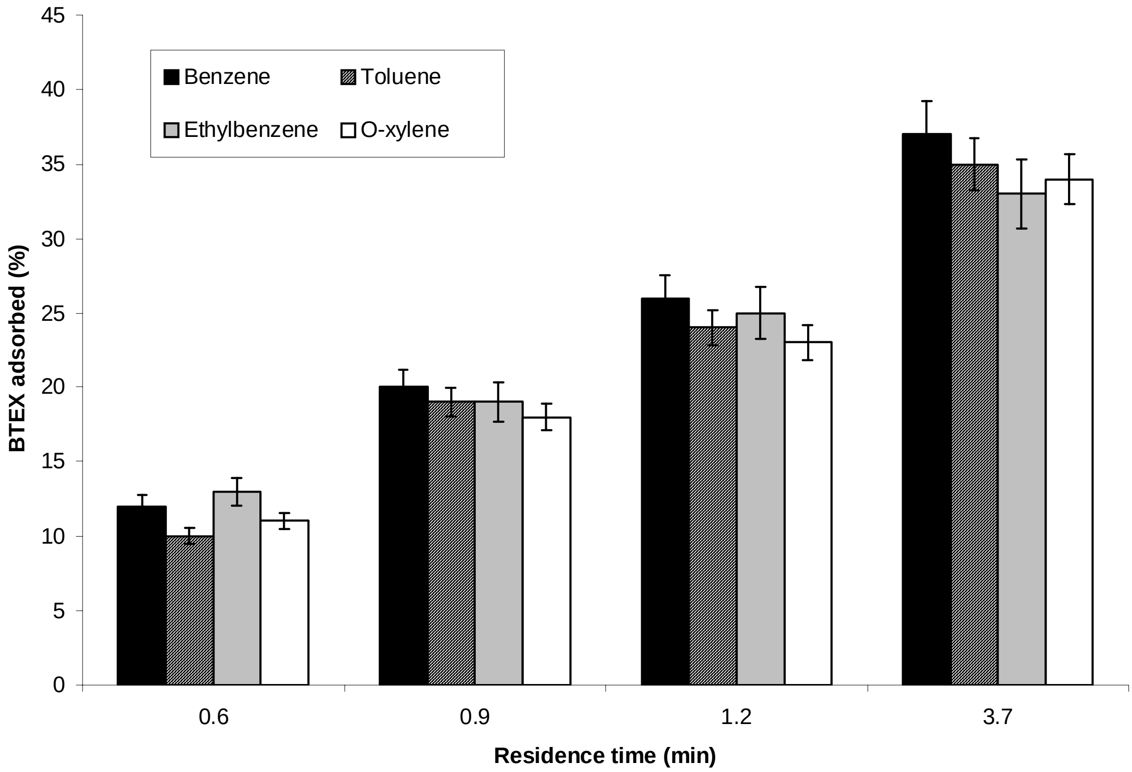

Figure 5.7 Amount of BTEX adsorbed in the dark under different residence time. Experimental conditions: Humidity level 2100 ppmv, 20 ppb BTEX.

As seen in Fig. 5.8, the adsorption capacity of BTEX also shows a similar result. Studies found that the presence of water vapor significantly reduced the pollutant adsorption capacity on AC. At a relative humidity of 20300 ppmv, capillary condensation of water vapor occurred inside the AC and blocked the adsorption sites for the pollutant (Cheremisinoff and Ellerbusch, 1980; Cal et al., 1996). In this study, the adsorption capacity of NO and BTEX also significantly reduced at a similar humidity level. The above results suggested that the adsorption of pollutants primarily occurs on the activated carbon. Similar to the photodegradation of NO, blank test was also conducted for BTEX. No photolysis or photocatalysis was observed using AC filter only. The variation of temperature did not affect the amount of BTEX adsorbed on AC filter.

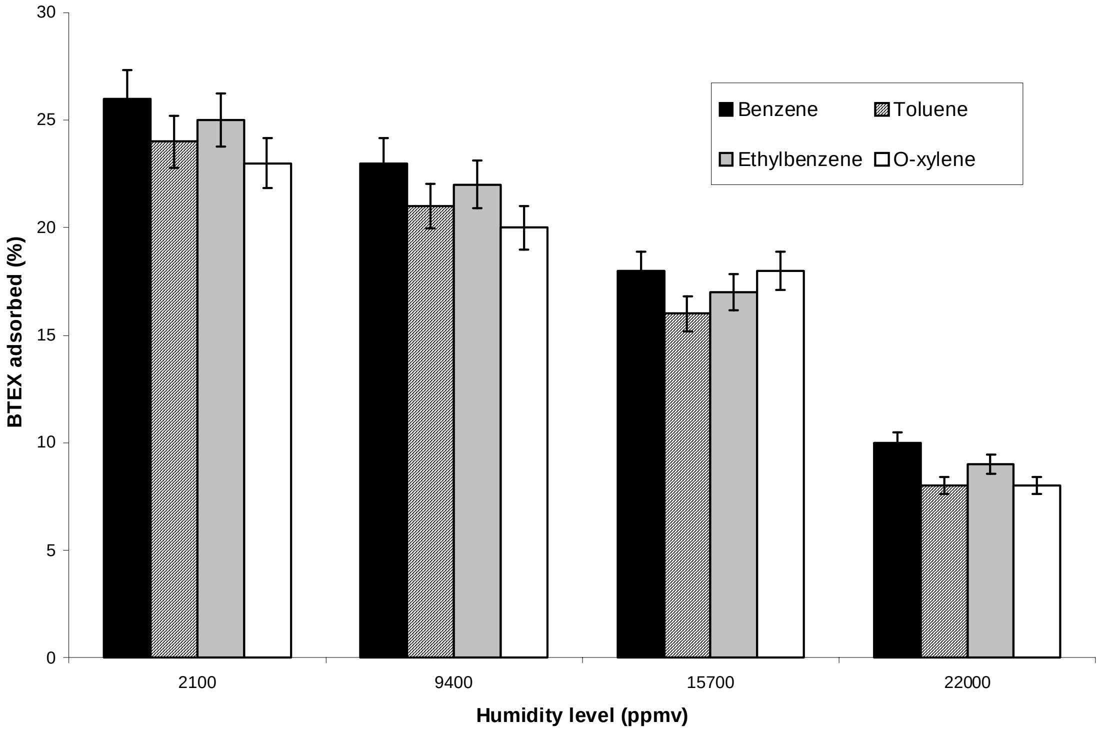

Figure 5.8 Amount of BTEX adsorbed in the dark under different humidity levels. Experimental conditions: Residence time 1.2 min, 20 ppb BTEX.

5.4.2 Removal of BTEX by AC, TiO_2 and TiO_2/AC filter

The removals of benzene, toluene, ethylbenzene and o-xylene (BTEX) at a humidity level of 2100 ppmv under different residence time are shown in Fig 5.9 to Fig. 5.12, respectively. The removals of BTEX using TiO_2 and TiO_2/AC increased with increasing residence time. At a longer residence time, a longer contact time between the pollutants and the hydroxyl radicals was achieved. At a residence time of 3.7 min, the removal rate between TiO_2 and TiO_2/AC is not significant. This is probably due to the fact that the pollutant diffusion rate from the gaseous phase to TiO_2 is similar to the pollutant diffusion rate from AC to TiO_2 under such a long residence time. In addition, under a low humidity environment where the competition effect between the water vapor and the pollutants for active adsorption sites is not significant, the pollutants are easily adsorbed on TiO_2 and photodegradated. As the residence time decreased, however, the removals of BTEX between TiO_2 and TiO_2/AC increased significantly. Although the amount of BTEX adsorbed on the AC decreased from 35% (on average) to 10% (on average) when the residence time decreased from 3.7 min to 0.6 min, a substantial amount of BTEX can still be adsorbed on the AC. The BTEX adsorbed on AC is then diffused to the nearby TiO_2 for photodegradation. It suggests that at a lower residence time, the collision rate of the pollutants from the gaseous phase decreased more significantly than the pollutants supplied from the AC. Studies (Takeda et al., 1995; Torimoto et al., 1996) also showed that the addition of AC concentrated the pollutants around TiO_2 and increased the photodegradation rate. It is also noted that at the same residence time, the removal of o-xylene is higher than ethylbenzene, followed by toluene and benzene. The reasons were explained in chapter 4.

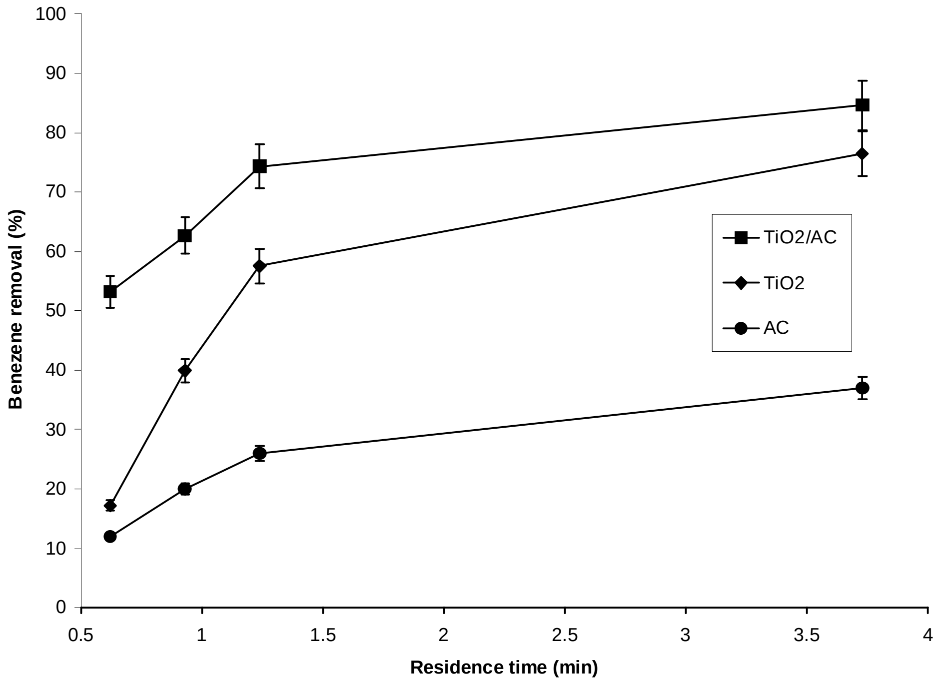

Figure 5.9 Benzene removal under different residence time. Experimental conditions: humidity level 2100 ppmv, 20 ppb BTEX.

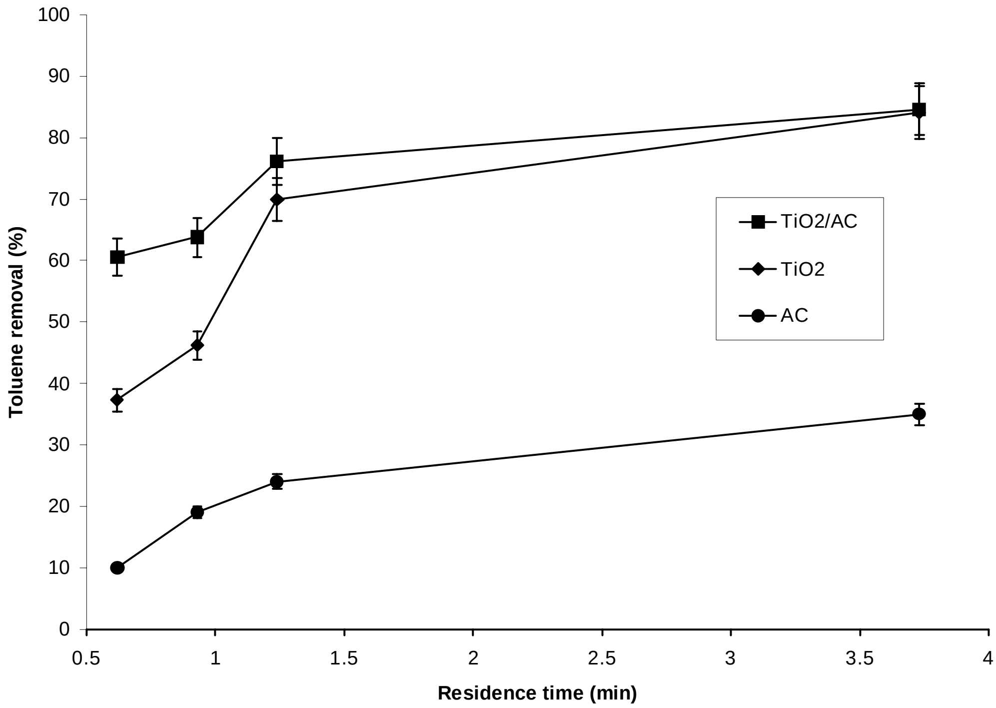

Figure 5.10 Toluene removal under different residence time. Experimental conditions: humidity level 2100 ppmv, 20 ppb BTEX.

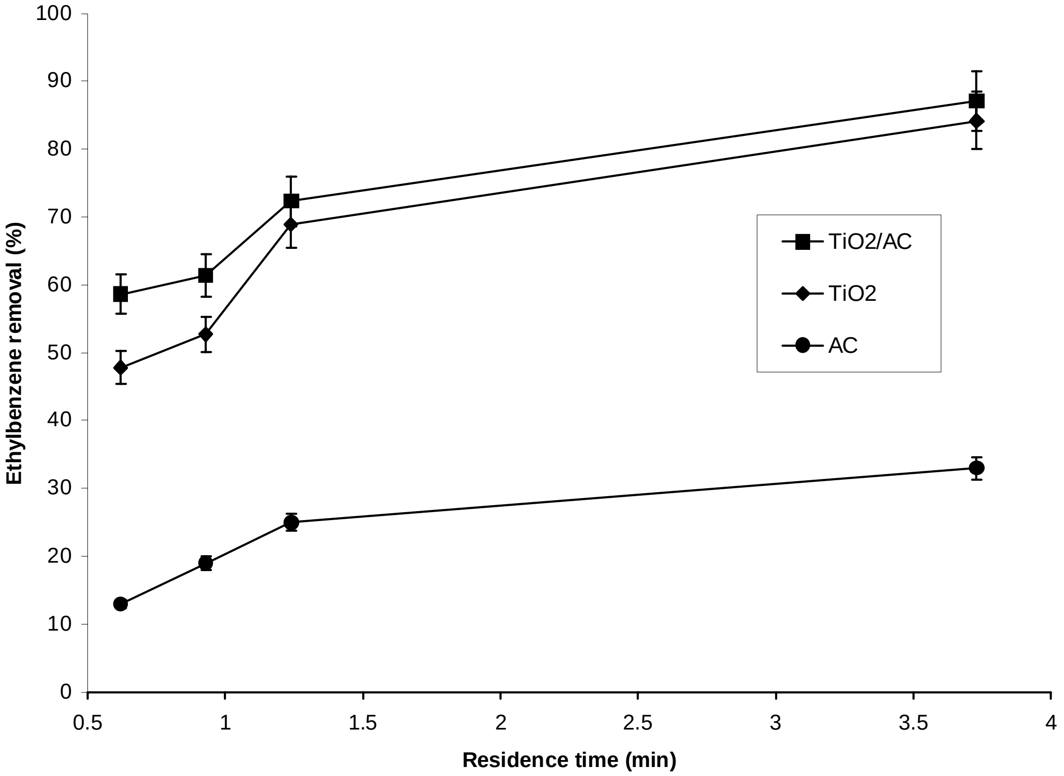

Figure 5.11 Ethylbenzene removal under different residence time. Experimental conditions: humidity level 2100 ppmv, 20 ppb BTEX.

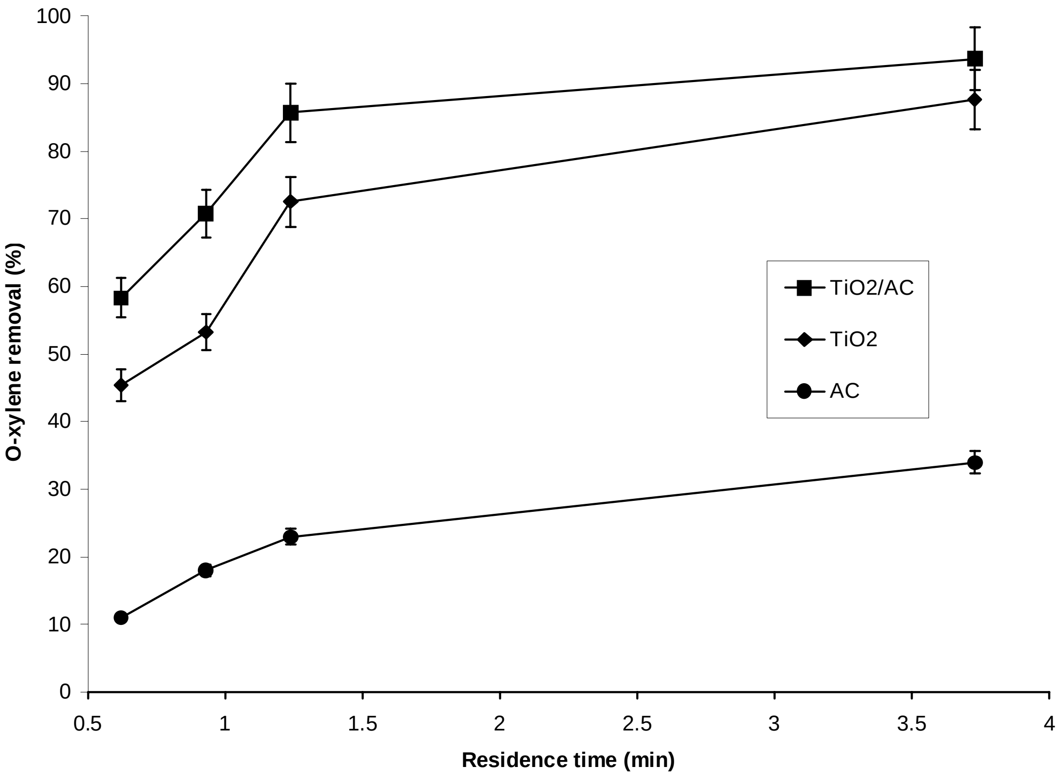

Figure 5.12 o-Xylene removal under different residence time. Experimental conditions: humidity level 2100 ppmv, 20 ppb BTEX.

The removals of benzene, toluene, ethylbenzene and o-xylene (BTEX) at a residence time of 1.2 min under different humidity levels are shown in Fig 5.13 to Fig. 5.16, respectively. The removals of BTEX decreased significantly with increasing humidity levels owing to the competition effect between benzene and water vapor as previously reported in chapter 4. When TiO_2 was immobilized on the AC filter, the removal of BTEX only decreased by 14%, 13%, 9% and 18%, respectively when the humidity level was increased from 2100 ppmv to 22000 ppmv. The removals of BTEX decreased by more than 50% when TiO_2 was immobilized on the glass fiber filter when the humidity level was increased from 2100 ppmv to 22000 ppmv. The results clearly show that the combination of TiO_2 and AC increased the BTEX removals significantly. This is probably due to the amount of BTEX adsorbed on the AC under different humidity levels. Although at high humidity levels water competed with benzene for adsorption sites on TiO_2 and AC, the large adsorption capacity of AC still able to adsorb pollutants (Fig 5.3 and 5.7). At a humidity level of 22000 ppmv, 7.5% (on average) of BTEX was adsorbed on the AC. By immobilizing TiO_2 on AC filter, a portion of the TiO_2 is in contact with the AC which concentrated pollutants by adsorption. It is presumably that the difference in pollutant concentration between the TiO_2 adsorbed with water and the TiO_2 in contact with the AC contributes to the diffusion of pollutants from the AC to the TiO_2 for photodegradation. In essence, the

AC acted as a local pollutant concentrator and supplier to the TiO_2 for photodegradation. Once the pollutant diffused from the AC to the TiO_2, AC adsorbed pollutants again from the gaseous stream and continued to diffuse to TiO_2. This pollutant transfer cycle from gaseous phase to AC to TiO_2 is the key factor for the improved pollutant removal. However, study (Ibusuki and Takeuchi, 1994) showed that the use of TiO_2 and AC did not greatly increased the photodegradation rate despite the AC concentrated the pollutants. This discrepancy is probably due to the method of TiO_2 immobilization on AC and experimental conditions being different. The work of those researchers is based on a mechanical mix of TiO_2 powder with AC powder, using ppm level NO as target pollutant. In this study, TiO_2 is immobilized on an AC filter and intimate contact is observed from the SEM micrographs. It is probably that the intimate contact between TiO_2 and AC is the key factor for pollutant diffusion and thus enhanced the photodegradation. It is also noted that the pollutant concentrations are lower in this study. At a ppb level concentration, the effect of adsorption and water vapor is more vital than ppm level concentration. Thus, the problem of competition for adsorption sites between water vapor and pollutants is successfully resolved by adsorbing pollutants on AC. From the above results, an enhancement effect of TiO_2 and AC is observed even under high humidity levels. The removal of TiO_2/AC is much higher than using TiO_2 or AC only. Previously we reported no aldehydes were detected for TiO_2 immobilized on a glass fiber filter. Aldehydes were also not detected using TiO_2/AC.

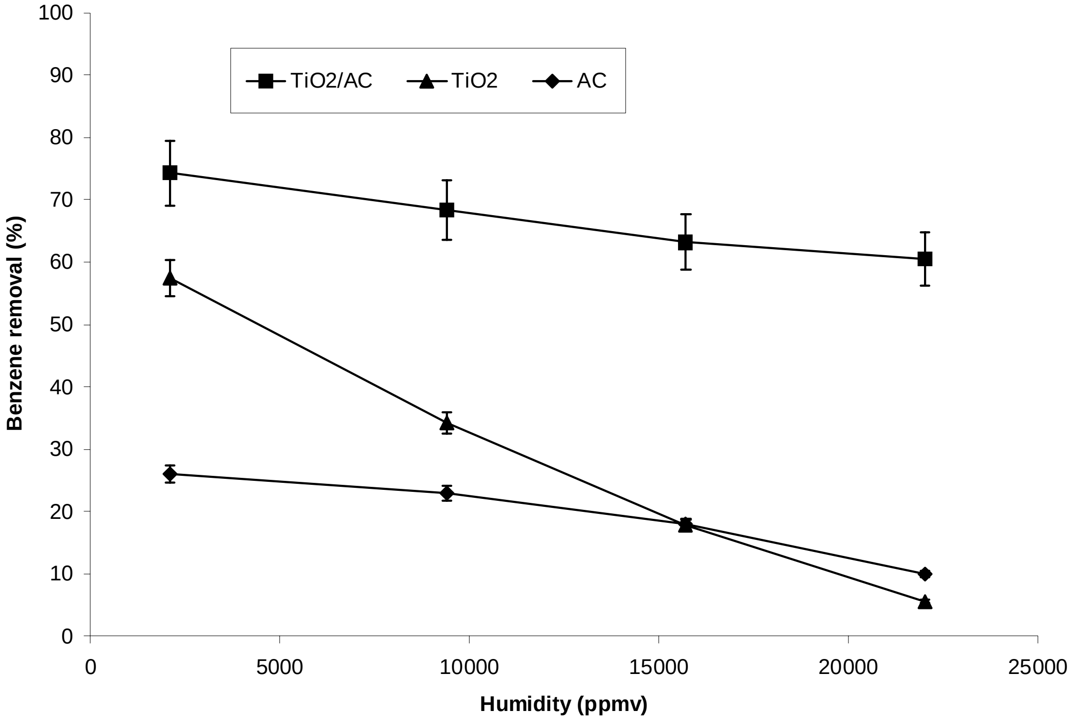

Figure 5.13 Benzene conversion under different humidity levels. Experimental conditions: residence time 1.2 min, 20 ppb BTEX.

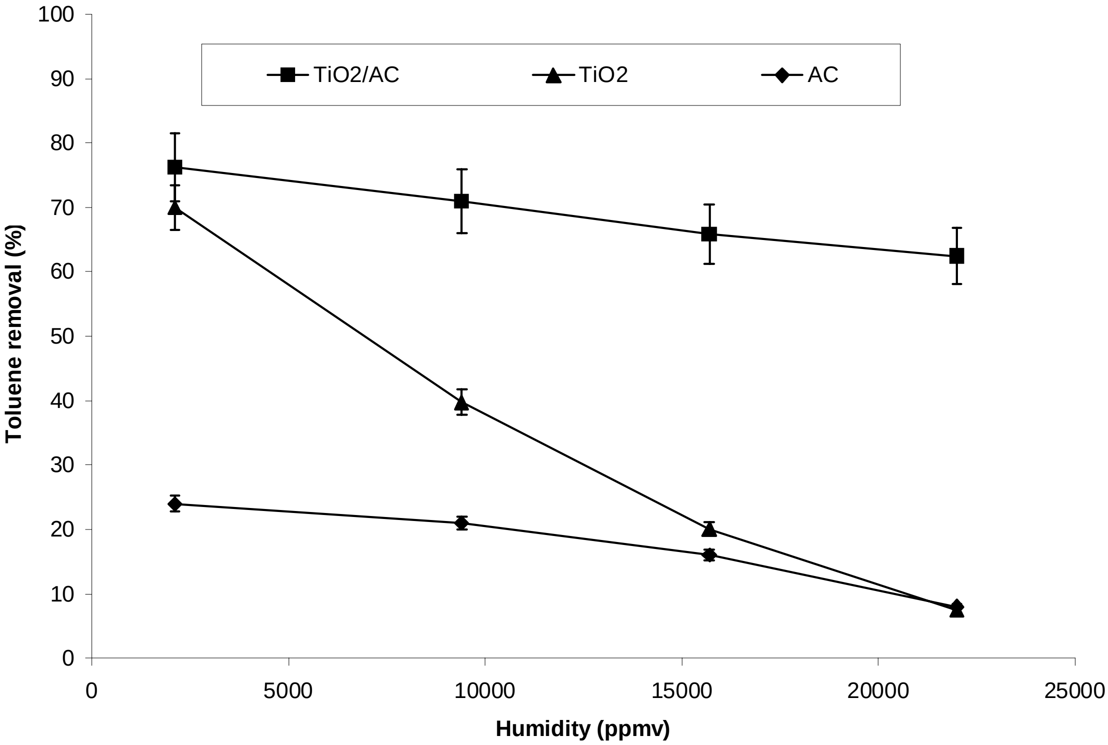

Figure 5.14 Toluene conversion under different humidity levels. Experimental conditions: residence time 1.2 min, 20 ppb BTEX.

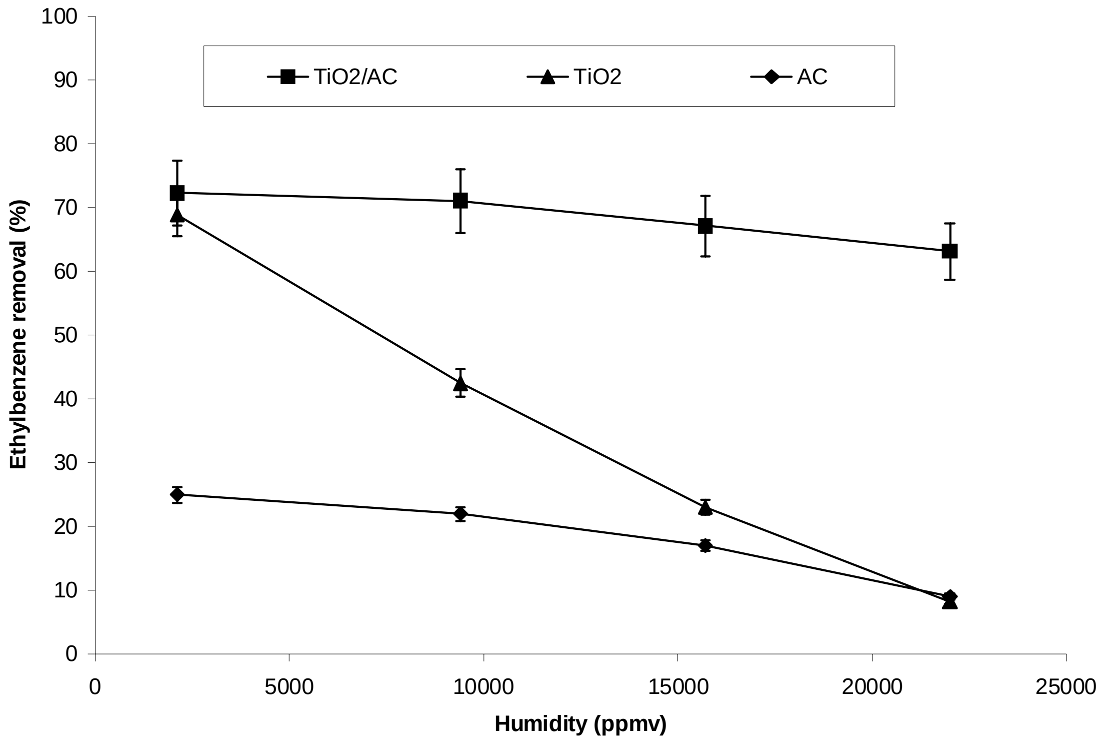

Figure 5.15 Ethylbenzene conversion under different humidity levels. Experimental conditions: residence time 1.2 min, 20 ppb BTEX.

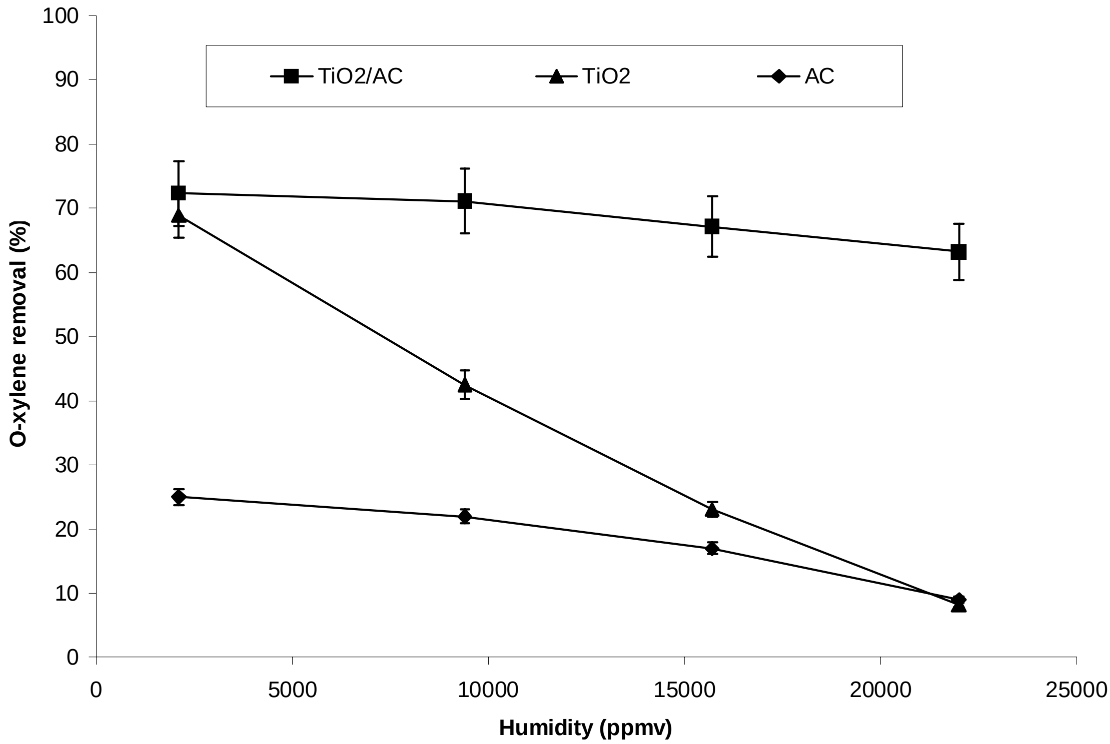

Figure 5.16 o-Xylene conversion under different humidity levels. Experimental conditions: residence time 1.2 min, 20 ppb BTEX.

5.5 Summary

In the previous chapter, it is reported that at high humidity levels, the conversion of pollutants by photocatalysis was drastically decreased. Although the increase in BET surface area of the photocatalyst increased the conversion, the degree is not very significant. By immobilizing TiO_2 on activated carbon filter rather than glass fiber filter, the pollutant removal was significantly increased. At a humidity level of 22000 ppmv, only less than 10% of NO and BTEX are removed using AC only, whereas 40% and less than 10% of NO and BTEX respectively, are removed by TiO_2 only. When TiO_2 is immobilized on activated carbon filter, the removal of NO increased to 66% and more than 60% for BTEX. The increased removal of using TiO_2/AC is owing to the large adsorption capacity of AC. Pollutants adsorbed on AC are diffused to the TiO_2 for photodegradation. The pollutant concentrations in AC are then reduced and adsorbed pollutants from the gaseous phase again and diffused to TiO_2. This adsorption and photodegradation cycle is suggested for the improved removal of TiO_2/AC. NO_2, as an intermediate from the photodegradation of NO, was also suppressed significantly by the use of TiO_2/AC. No deactivation was found for the photodegradation of BTEX. When using TiO_2/AC under prolonged testing, no deactivation was found for the NO which was found when using TiO_2 only.

Chapter 6 Removal of multiple indoor air pollutants by photocatalyst loaded on glass fiber filter and activated carbon filter

6.1 Introduction

It is shown in the previous chapter that the use of activated carbon significantly increased the conversion of pollutants especially at low residence time and high humidity levels. To further evaluate the feasibility of applying photocatalytic technology for indoor air purification, multiple pollutants were simultaneously generated to identify their reciprocal effects. Photocatalytic degradation of multiple pollutants was both conducted on photocatalyst loaded on glass fiber filter and activated carbon filter.

6.2 Concurrent photodegradation of NO and BTEX by TiO_2 filter

6.2.1 Effects of residence time

Variations of residence time were tested to evaluate the photodegradation activity of BTEX and NO. Fig. 6.1 shows the photodegradation of 20 ppb BTEX with the presence of 200 ppb NO at a humidity level of 2100 ppmv. Results showed that the conversion decreased with decreasing residence time. It can be assumed that a longer residence time, a higher rate of contact and length of contact time were achieved between the pollutants and the hydroxyl radicals, resulting in a higher conversion. The adverse effect of residence time is similar to the presence of single pollutant only, as reported in chapter 4.

As shown in Fig 6.1, the conversion of BTEX with the presence of NO is higher than BTEX solely under different residence time. The enhancement of BTEX conversion is due to the generation of hydroxyl radicals (OH·) during the photodegradation of NO, as shown in equation 6.1 and 6.2 (Komazaki et al., 1999).

$$NO + HO_2 \cdot \rightarrow NO_2 + OH \cdot \quad (6.1)$$

Or the NO_2 generated reacts with NO form 2 hydroxyl radicals and 2 NO molecules as follows:

$$NO_2 + NO + H_2O \rightarrow 2HONO \rightarrow 2OH \cdot + 2NO \quad (6.2)$$

The addition of NO resulted the highest enhancement effect for benzene and toluene. This is probably due to the reaction rate of OH radicals of ethylbenzene and o-xylene being comparatively higher than benzene and toluene (Atkinson, 1990). The enhancement effect of NO may be hindered by the high conversion of ethylbenzene and o-xylene. Also noted is, the decrease in enhancement effect paralleled the decreasing residence time. At a shorter residence time, BTEX have a lower colliding frequency with the hydroxyl radicals generated from the photodegradation of NO. The enhancement effect is reduced with decreasing residence time.

Fig. 6.2 shows the photodegradation of NO with the presence and absence of BTEX. Under the presence of BTEX, the NO conversion is lower and generated a lower secondary pollutant NO_2. The overall NO_x conversion is also lower with the presence of BTEX under different residence time. The lower NO_2 generation can be explained by the lower conversion of NO, as shown in equation 6.1. Similar to the photodegradation of BTEX, NO conversion, with or without BTEX, decreased with decreasing residence time.

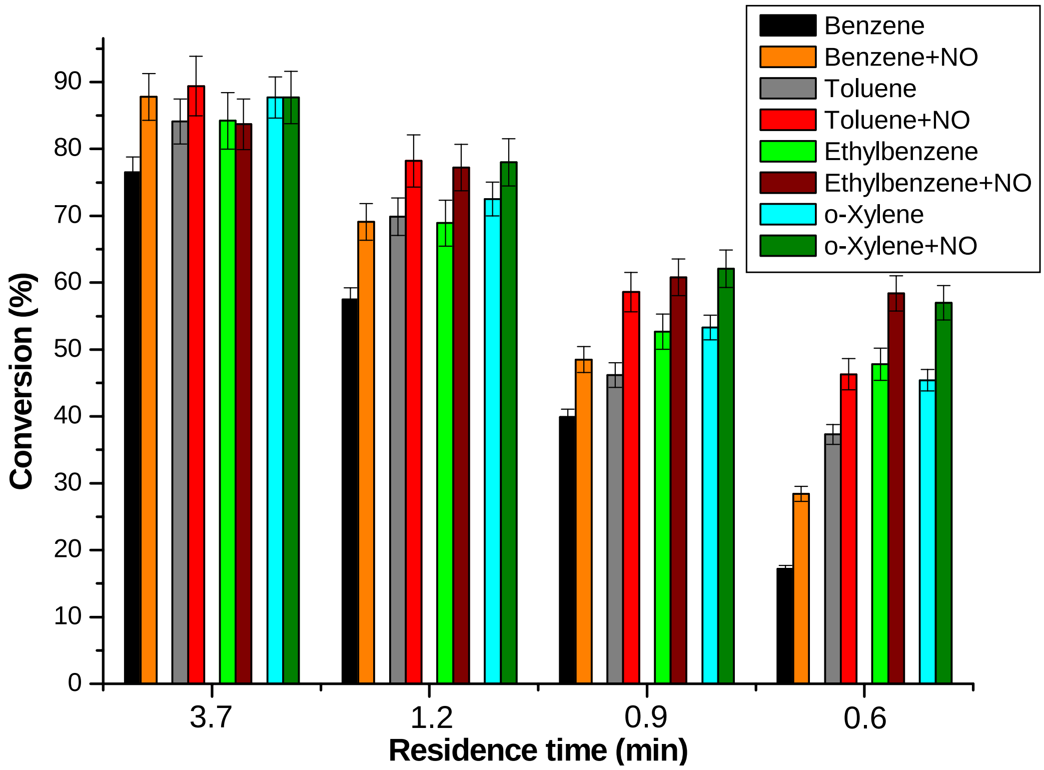

Figure 6.1 Variation of BTEX conversion under the presence of NO at different residence time. Experimental conditions: 20 ppb BTEX & 200 ppb NO; humidity level 2100 ppmv.

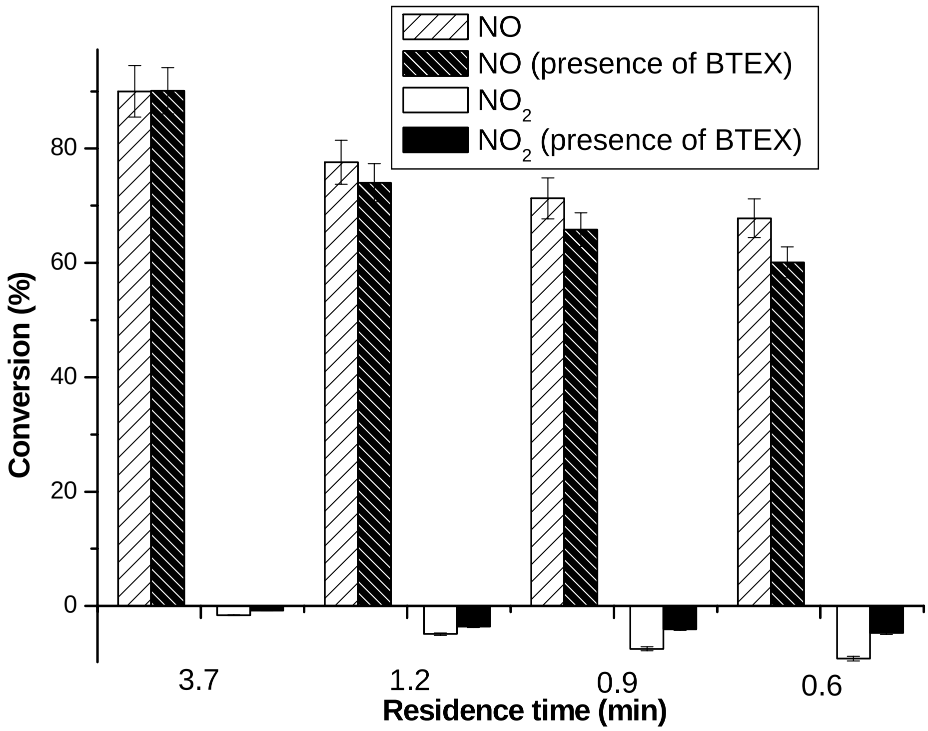

Figure 6.2 Variation of NO_x conversion under the presence of BTEX at different residence time. Experimental conditions: 20 ppb BTEX & 200 ppb NO; humidity level 2100 ppmv.

6.2.2 Effects of humidity levels

The impact on conversion at different humidity levels is shown in Fig. 6.3 and Fig. 6.4. The experiment was conducted with a NO concentration of 200 ppb and a BTEX concentration of 20 ppb at a residence time of 1.2 min. The promotion effect of NO on BTEX conversion is dependent on the levels of humidity. The promotion effect of NO only occurred at humidity levels of 2100 ppmv and 22000 ppmv, and NO inhibited BTEX conversion at humidity level between 9400 ppmv to 15700 ppmv. At low humidity, the competition of adsorption between BTEX and water vapor is relatively small, which enabled the hydroxyl radicals generated from the photodegradation of NO to have contact with BTEX and enhance the conversion. As the humidity increased, more water vapor is adsorbed on the TiO_2 surfaces. This increased competition for adsorption sites (Lichtin and Sadeghi, 1998). The presence of NO was also in competition with BTEX for an adsorption site. If BTEX is not able to react with the hydroxyl radicals generated from the photodegradation of NO and competition with water vapor and NO for adsorption sites, the conversion of BTEX with the presence of NO is lower than solely with BTEX. At humidity level of 22000 ppmv, the hydroxyl radicals generated by NO photodegradation is higher due to more dissociated water vapor. The increase in water vapor catalyzed equation 6.2 to a larger extends than equation 6.1. Presumably, the effect of the increase in hydroxyl radicals is larger than the competitive adsorption effect of water vapor, and thus increased the BTEX conversion.

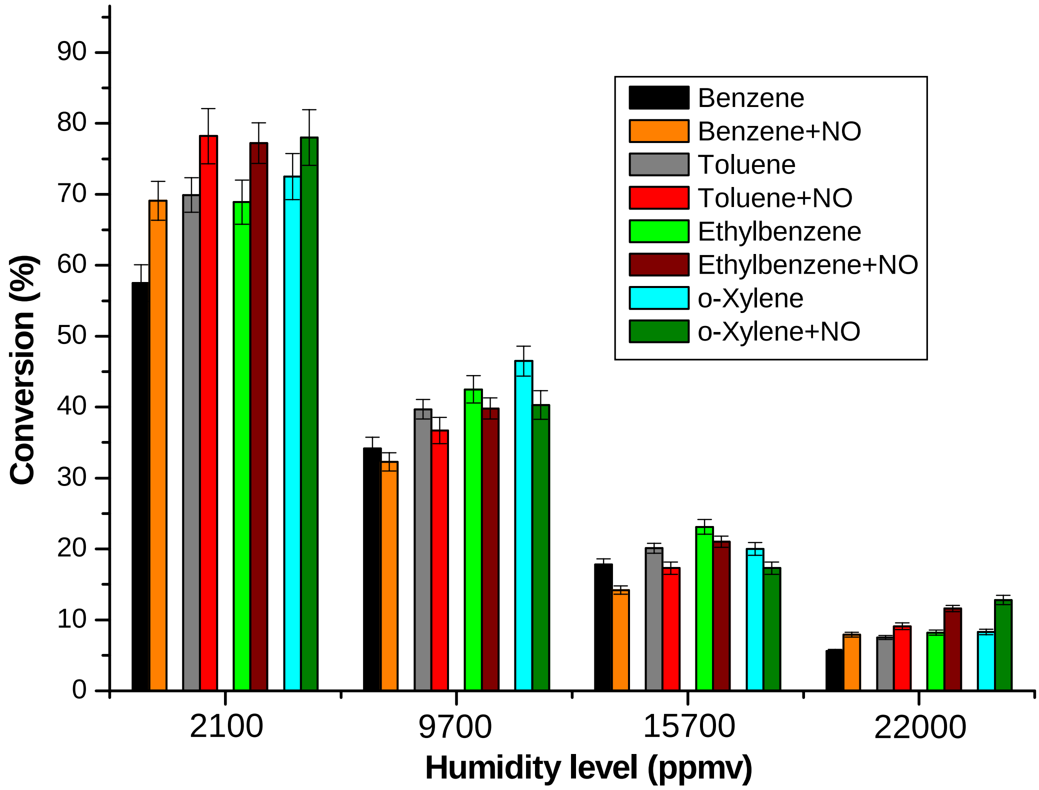

Figure 6.3 Variation of BTEX conversion under the presence of NO at different humidity levels. Experimental conditions: 20 ppb BTEX & 200 ppb NO; residence time 1.2 min.

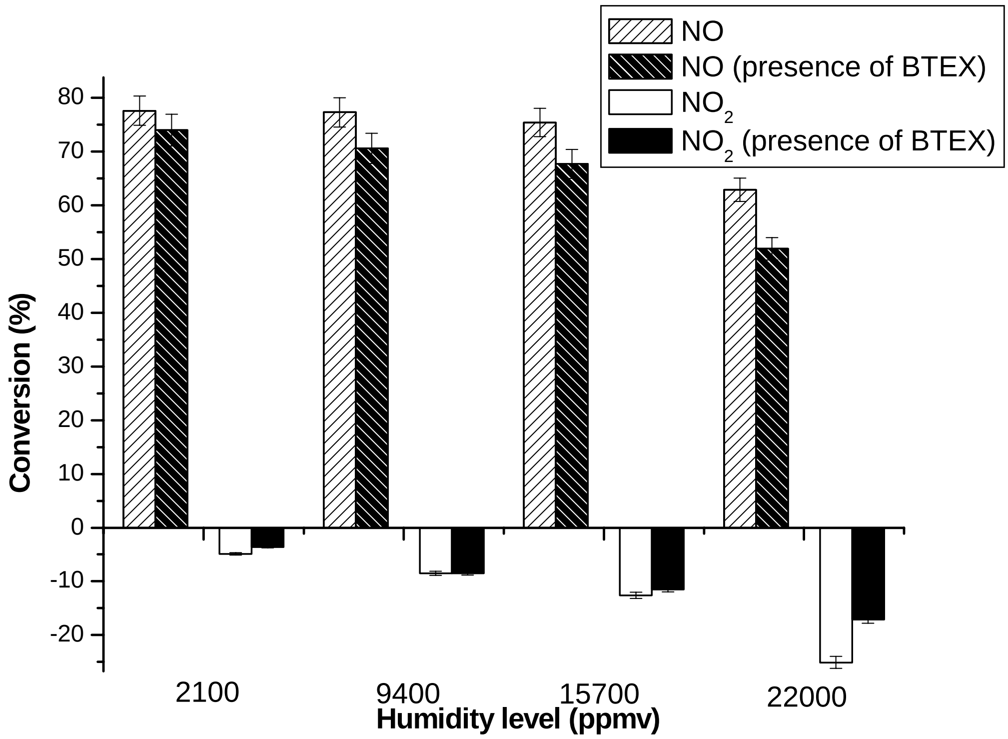

Figure 6.4 Variation of NO_x conversion under the presence of BTEX at different humidity levels. Experimental conditions: 20 ppb BTEX & 200 ppb NO; residence time 1.2 min.

6.2.3 *Effects of initial concentrations*

The impact of the photo-steady-state NO_x concentration and BTEX conversion under different initial NO concentrations are shown in Table 6.1. From the results, it can be seen that the photo-steady-state NO_x concentration increased as NO concentration with either the presence or the absence of BTEX also increased. As the amount of photocatalyst remained unaltered for different initial NO concentrations, it is reasonable to suggest that the outlet NO_x concentration increased as the amount of photocatalyst per pollutant decreased. The effect of BTEX can be seen clearly by comparing the photo-steady-state concentration of NO and NO_2. The presence of BTEX increased the NO concentration while decreasing the NO_2 concentration at different initial NO concentrations. This further reinforces the proposition that the reduction of NO conversion and NO_2 generation is due to the competition effect of NO and BTEX presented earlier.

	Photo-steady-state concentration (ppb)				Conversion (%)			
Initial NO (ppb)	NO	NO with BTEX	NO_2	NO_2 with BTEX	B	T	E	X
0	0	0	0	0	24.02	67.31	83.66	85.95
100	6	9.8	2.1	1.3	41.98	78.79	84.30	84.78
200	13	26.6	3.2	1.6	42.37	77.79	82.77	84.57
500	46.5	50.7	16.5	2.9	48.01	82.00	85.03	85.47
700	67.4	70.4	19.4	4.5	50.81	83.85	85.44	86.04
900	74.8	95	28.5	10.9	52.10	85.80	86.30	86.40

Table 6.1 Variation of BTEX and NO_x at different NO initial concentrations.

The promotion effect of BTEX by the photodegradation of NO is not significant under different initial NO concentrations. At a higher initial NO concentration, the conversion of BTEX is higher, however the increment is insignificant. For instance, the conversion of benzene only increased by 10% when the NO concentration was increased from 100 ppb to 900 ppb. The promotion effect of NO is lessened for toluene, followed by ethylbenzene and o-xylene. Compared to the absence of NO, the presence of NO has significantly increased the conversion of benzene and toluene by 20%. The insignificance of the NO promotion effect at high concentrations is probably due to the ratio of NO to BTEX being too high. The results of this study showed that 3 times the concentration of NO to BTEX is sufficient for the promotion effect. Table 6.2 shows the impact on the photodegradation of NO under different initial BTEX concentrations. The presence of BTEX, even as low as 3 ppb, increased the NO photo-steady-state concentration and decreased NO_2 concentration. However, the NO concentration variation from 3 ppb BTEX to 70 ppb BTEX is insignificant whereas the NO_2 concentration decreased with increasing BTEX concentration. The result is presumably due to the reaction between BTEX, OH radical and NO_2 under the presence of O_2. Atkinson showed that aromatic compounds react with OH radicals by two pathways; hydrogen atom abstraction (minor pathway) or the adduction of OH radicals to the aromatic ring (major pathway), as shown in equation 6.3 and equation 6.4 (Atkinson, 1990).

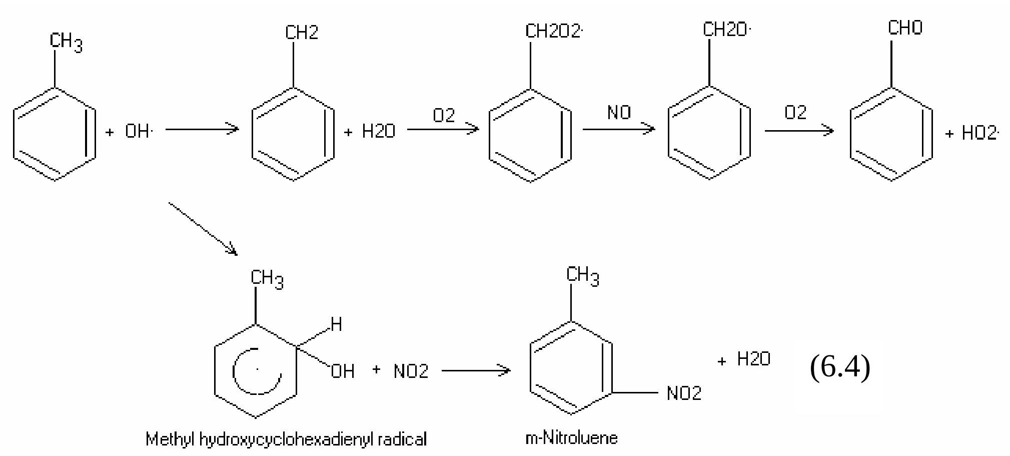

(6.3)

(6.4)

Our results also supported this postulation. Toluene, for instance, reacts with O_2 and NO and forms benzaldehyde and HO_2 radicals. From the result of this study, no decrease of NO concentration was found when increasing the BTEX concentration. The NO concentration varied only 3 ppb from 3 ppb to 70 ppb BTEX concentration. In addition, no benzaldehyde concentration was found from the HPLC analysis. Thus, equation 6.3 is also a minor pathway for heterogeneous photocatalysis for BTEX. The decrease in NO_2 concentration is presumably due to the reaction of methyl hydroxycyclohexadienyl (MHCHD) radicals with NO_2. The increase in BTEX concentration provides more aromatic compounds to form MHCHD, and thus the concentration of NO_2 was reduced to form m-nitrotoluene. Atkinson and Aschmann (1994) also showed that o-xylene reacted with NO_2 forming 2,3-butanedione. However, no peaks of the above products were detected by GC-MS. It is probably that the products formed are adsorbed on the filter. In addition, 40% of the products formed from the OH radical reaction with toluene is unknown and similar findings were reported for benzene (Atkinson et al., 1989), m-xylene and o-xylene (Grey et al., 1987).

The enhancement effect on the photodegradation of aromatic compounds was also reported (d'Hennezel and Ollis, 1997). The addition of trichloroethylene promoted the photodegradation of toluene, ethylbenzene and m-xylene but not benzene. The promotion effect of trichloroethylene is due to the chlorine radicals generated from the photodegradation. Also appeared that the chlorine radicals reacted with the substituted aromatics through hydrogen abstraction from the alkyl groups. Conversely, this study showed that the hydrogen abstraction path is minor and the adduction of OH radicals to the aromatic compound is the major pathway. The promotion of benzene was the highest compared to toluene, ethylbenzene and o-xylene.

Initial BTEX (ppb)	Photo-steady-state concentration (ppb)		Conversion (%)							
			Present of NO				Absent of NO			
	NO	NO_2	B	T	E	X	B	T	E	X
0.00	36.9	13.3	0.00	0.00	0.00	0.00	0.00	0.00	0.00	0.00
3.00	50.1	11.0	15.01	39.01	50.12	56.23	10.61	26.19	36.00	36.60
15.00	48.2	9.1	18.15	55.90	63.26	65.52	12.78	32.07	37.73	41.25
25.00	49.7	8.1	26.31	60.17	68.16	69.17	18.02	35.55	42.72	49.93
35.00	47.1	7.0	29.26	62.98	69.31	72.11	24.90	51.23	55.18	61.38
70.00	48.3	5.3	31.42	65.23	73.67	74.82	27.78	60.83	67.58	69.54

Table 6.2 Variation of BTEX and NO_x at different BTEX initial concentrations.

6.3 Concurrent photodegradation of NO and BTEX by TiO_2 filter and TiO_2/AC filter

6.3.1 Binary adsorption of NO and BTEX

Fig. 6.5 shows the adsorption of NO with and without the presence of BTEX at a humidity level of 2100 ppmv under different residence time. Each experiment set was conducted 4 times and the average value was reported. Previous sections showed that no difference in the amount of NO and BTEX adsorbed between TiO_2/AC and AC filter. Thus, only TiO_2/AC was studied for the adsorption test. No adsorption was found for NO and BTEX for TiO_2 filter with the experimental error. The amount adsorbed was determined by the pollutant concentration difference between the inlet stream and the outlet stream. The amount of NO adsorbed increased with increasing residence time despite the presence of BTEX. With the presence of BTEX, the amount of NO adsorbed was reduced by 5%. This agrees with the findings, of which, study (Cheremisinoff and Ellerbusch, 1980) showed that the existence of other pollutants decreased the adsorption capacity of a pollutant. Fig. 6.6 shows the influence of NO on the adsorption of BTEX with the same experimental conditions of Fig. 6.5. No significant difference in the amount of BTEX adsorbed on TiO_2/AC was observed. Study (Urano et al., 1982) also reported that the amount of benzene, toluene and o-xylene adsorbed on AC is similar. As in the case of NO, the presence of NO approximately reduced 5% of the adsorption capacity of BTEX.

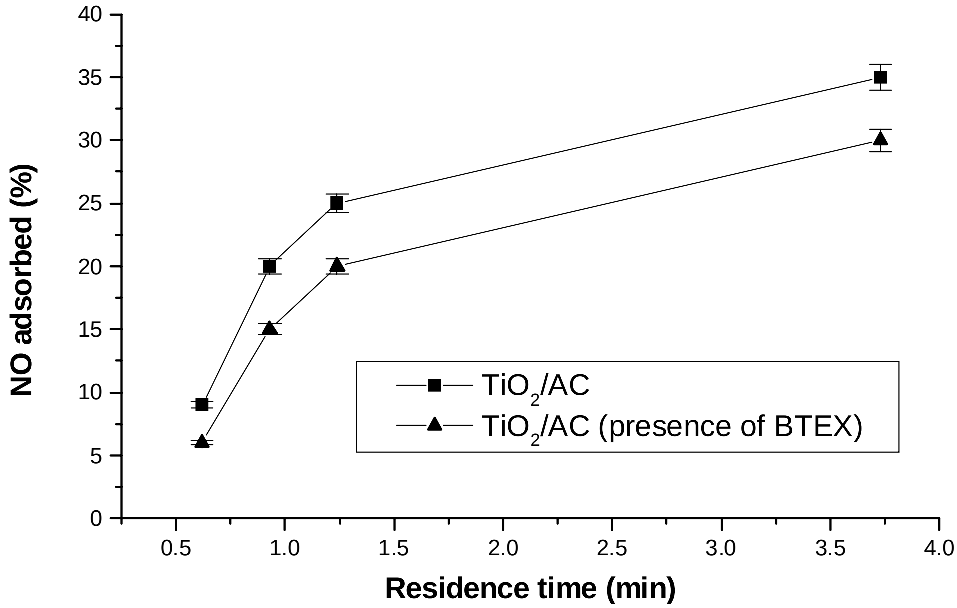

Figure 6.5 Amount of NO adsorbed with and without the presence of BTEX under different residence time. Experimental conditions: 200 ppb NO; 20 ppb BTEX; humidity level 2100 ppmv.

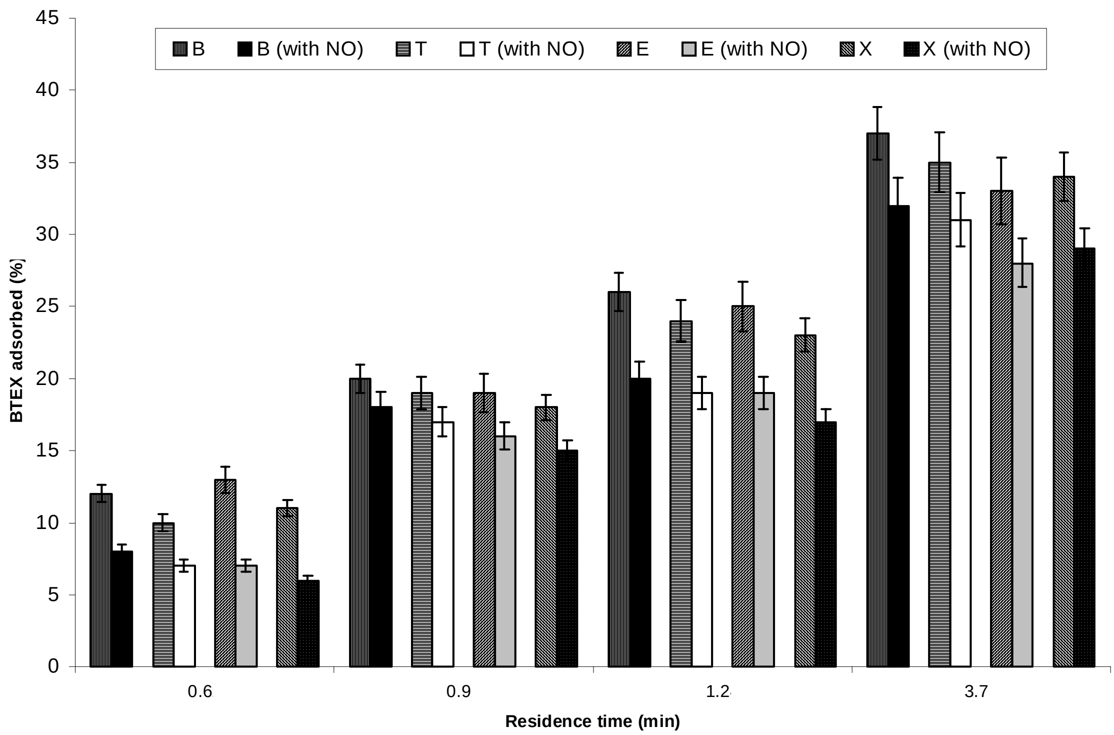

Figure 6.6 Amount of BTEX adsorbed with and without the presence of NO under different residence time. Experimental conditions: 200 ppb NO; 20 ppb BTEX; humidity level 2100 ppmv.

Fig. 6.7 shows the adsorption of NO with and without the presence of BTEX at a residence time of 1.2 min under different humidity levels. The presence of water vapor inhibited the adsorption of NO. The inhibition effect is more significant when the humidity level increased beyond 15000 ppmv. Studies (Cheremisinoff and Ellerbusch, 1980; Khan and Ghoshal, 2000) also showed that the inhibition effect of water vapor becomes significant when the humidity level increases beyond 20300 ppmv. Although the presence of BTEX inhibited the adsorption of NO on AC, the inhibition effect is not significant compared to the presence of water vapor. Fig. 6.8 shows the adsorption of BTEX with and without the presence of NO with the same experimental conditions of Fig. 6.7. The increase in humidity level inhibited the adsorption of BTEX. The presence of NO inhibited the adsorption of BTEX despite the levels of humidity

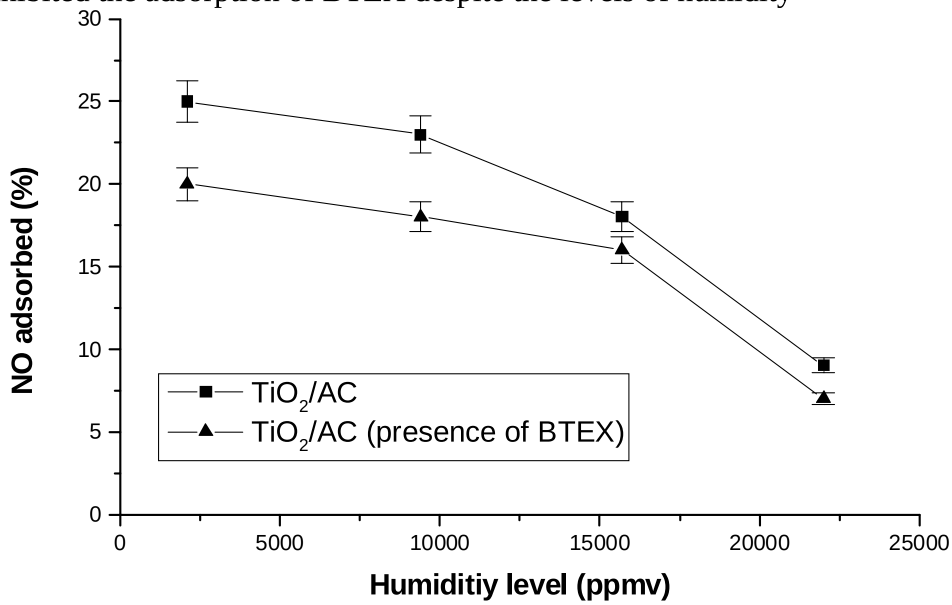

Figure 6.7 Amount of NO adsorbed with and without the presence of BTEX under different humidity levels. Experimental conditions: 200 ppb NO; 20 ppb BTEX; residence time 1.2 min.

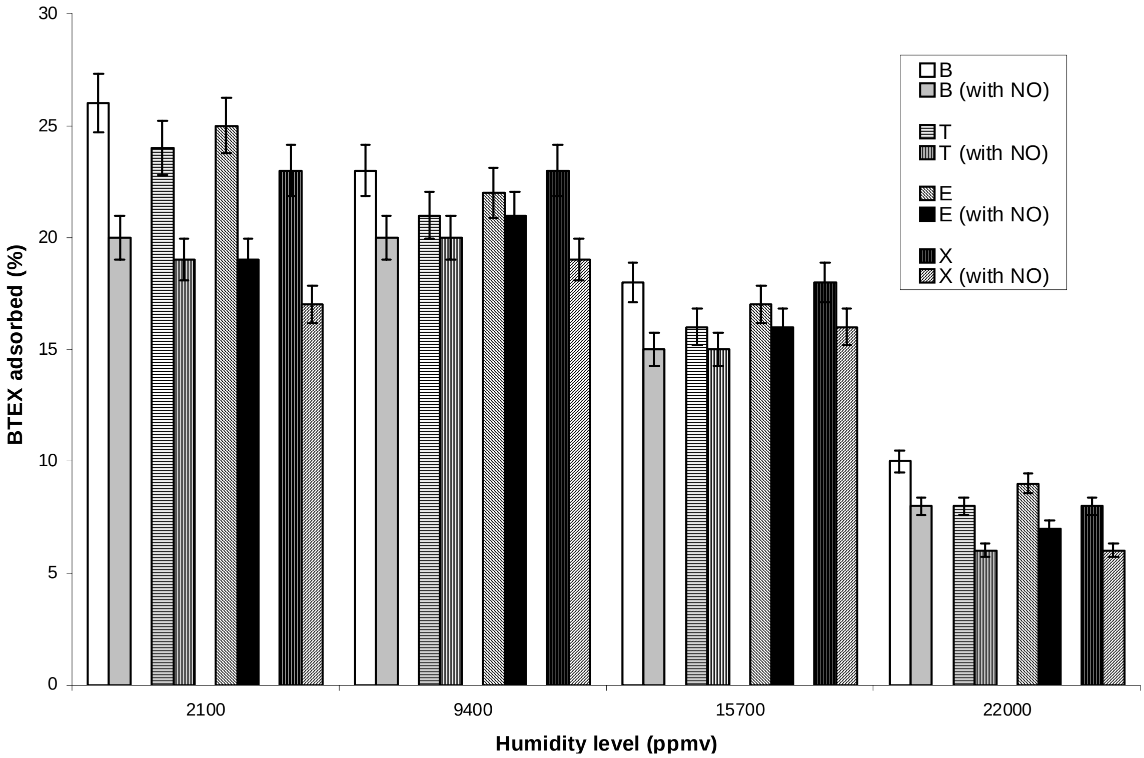

Figure 6.8 Amount of BTEX adsorbed with and without the presence of NO under different humidity levels. Experimental conditions: 200 ppb NO; 20 ppb BTEX; residence time 1.2 min.

6.3.2 Effects of residence time

Fig. 6.9 shows the effect of the presence of BTEX on the photodegradation of NO using TiO_2 and TiO_2/AC at a humidity level of 2100 ppmv under different residence time. The presence of BTEX inhibited the photodegradation of NO owing to the competition of adsorption sites on TiO_2. Similar effect was observed on TiO_2/AC. The conversion of NO decreased with decreasing residence time. At a lower residence time, the collision rate between NO and TiO_2 also decreased. For TiO_2/AC, the decrease in NO reduction is also contributed to the decrease in NO adsorbed on AC. Under a low humidity level where the competition effect between the pollutant and water vapor is not significant, the difference in NO conversion is not significant using TiO_2 and TiO_2/AC. Fig. 6.10 shows the generation of NO_2 from the photodegradation of NO with the same experimental conditions as shown in Fig. 6.9. The effects of using TiO_2/AC in reducing the NO_2 generation become more significant with decreasing residence time and the presence of BTEX. When the residence time decreased, the impact frequency between the pollutant and the TiO_2 surface also reduced. The use of AC caused the pollutant to be adsorbed and diffused to the TiO_2 for photodegradation. The adsorption of pollutants on AC is presumably less affected by the decrease in residence time compared to that of TiO_2 since the adsorption capacity of AC is much higher than TiO_2. In addition, owing to the large adsorption capacity of AC compared to TiO_2, the presence of BTEX did not significantly affected the generation of NO_2. Since no adsorption was found for NO and BTEX on TiO_2 filter, the photodegradation rate of NO_2 is manly depended on the collision rate between TiO_2 and NO_2. Thus, at a decreasing residence time, the generation of NO_2 using TiO_2 filter is more significant than using TiO_2/AC.

Table 6.3 shows the conversions of BTEX with and without the presence of NO using TiO_2 and TiO_2/AC at a humidity level of 2100 ppmv under different residence time. The conversions of BTEX decreased with decreasing residence time, which is similar to the photodegradation of NO. However, the decrease in conversions of BTEX using TiO_2/AC is significantly lower compared to that using TiO_2. In addition, the difference in BTEX conversions is higher than NO conversion using TiO_2/AC compared to TiO_2. This is probably owing to the high conversion of NO under low humidity levels which may hinder the effect of AC.

Residence time (min)	TiO_2 (BTEX only)				TiO_2/AC (BTEX only)				TiO_2 (NO + BTEX)				TiO_2/AC (NO + BTEX)			
	B	T	E	X	B	T	E	X	B	T	E	X	B	T	E	X
3.7	76.5	84.1	84.2	87.7	84.6	87.8	87.1	93.7	87.8	89.4	83.7	87.7	88.7	89.8	85.2	86.9
1.2	57.5	69.9	68.9	72.5	74.3	76.2	72.3	85.7	69.1	78.2	77.2	78.0	76.2	83.5	81.0	83.3
0.9	39.9	46.2	52.7	53.3	62.7	63.8	61.4	70.8	48.5	58.6	60.8	62.1	68.9	70.2	67.9	75.4
0.6	17.2	37.3	47.8	45.4	53.2	60.6	58.6	58.3	28.4	46.3	58.4	57.0	57.8	64.7	63.3	64.2

Table 6.3 BTEX conversions with and without the presence of NO using TiO_2 and TiO_2/AC under different residence time. B: benzene; T: toluene; E: ethylbenzene; X: o-xylene; Experimental conditions: 200 ppb NO; 20 ppb BTEX; humidity level 2100 ppmv.

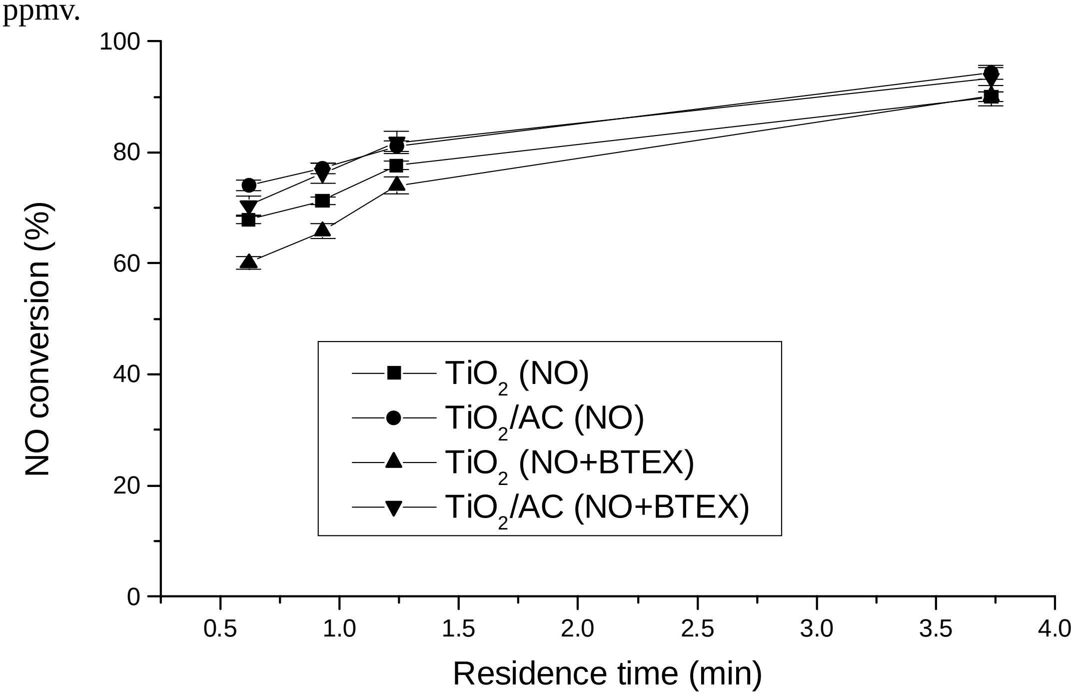

Figure 6.9 NO conversion using TiO_2 and TiO_2/AC with and without the presence of BTEX under different residence time. Experimental conditions: 200 ppb NO; 20 ppb BTEX; humidity level 2100 ppmv.

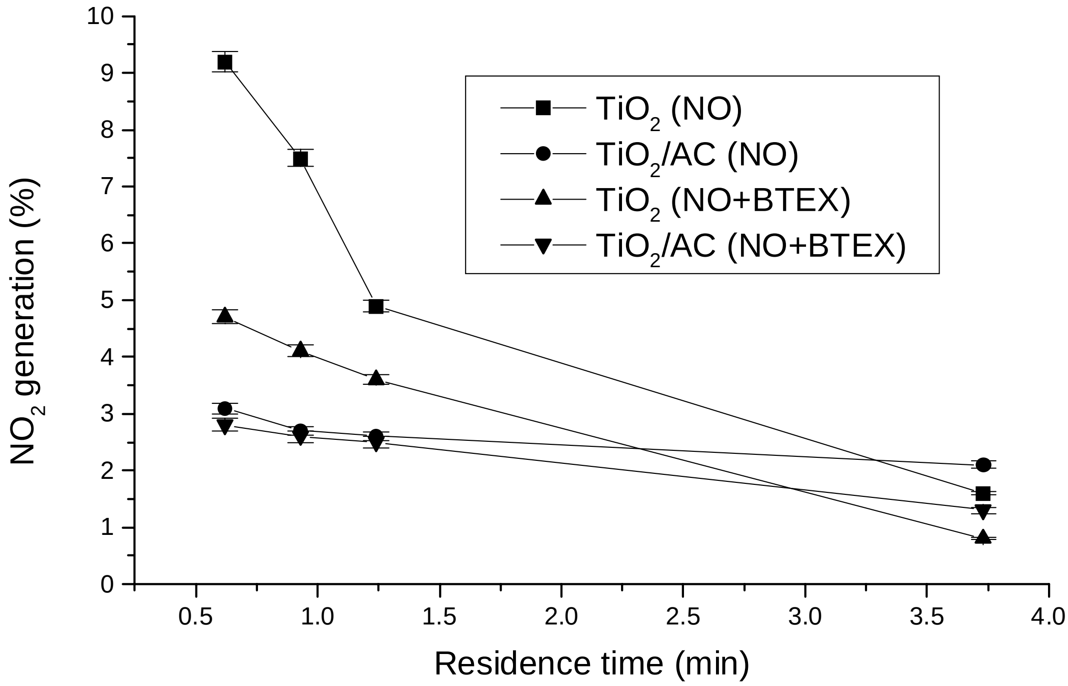

Figure 6.10 NO_2 generation using TiO_2 and TiO_2/AC with and without the presence of BTEX under different residence time. Experimental conditions: 200 ppb NO; 20 ppb BTEX; humidity level 2100 ppmv.

6.3.3 Effects of humidity levels

In order to investigate the effect of BTEX on the photodegradation of NO in detail, a binary photodegradation of NO and BTEX was performed under different levels of humidity at a residence time of 1.2 min since humidity is a vital parameter for photodegradation of pollutant at ppb level. As shown in Fig. 6.11, the photodegradation of NO decreased with increasing levels of humidity despite the presence of BTEX and the use of TiO_2 and TiO_2/AC. The decrease in photocatalytic activity is owing to the competition of adsorption sites on TiO_2 between pollutants and water vapor. However, when TiO_2 was immobilized on

AC, the decrease in NO conversion was significantly reduced. In addition, the inhibition effect of BTEX on the photodegradation of NO was also reduced using TiO_2/AC. This is probably due to the amount of NO adsorbed on AC (Fig. 6.6 and Fig 6.7) despite the high levels of humidity and the presence of BTEX. The amount of NO adsorbed on AC was then diffused to the TiO_2 for photodegradation. Similar findings were obtained by Torimoto et al. (1997) using TiO_2 with AC to increase the photodegradation rate of dichloromethane. These authors showed that the amount of dichloromethane adsorbed predominantly on AC rather than on TiO_2. The adsorbed dichloromethane then diffused from AC to TiO_2 for photodegradation.

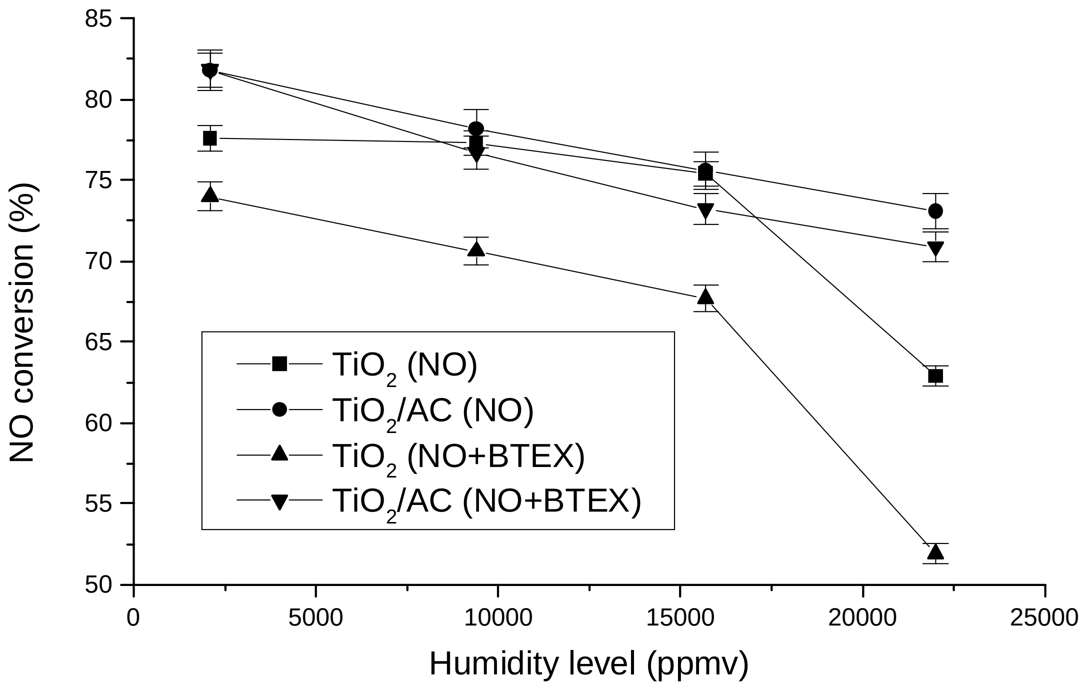

Figure 6.11 NO conversion using TiO_2 and TiO_2/AC with and without the presence of BTEX under different humidity levels. Experimental conditions: 200 ppb NO; 20 ppb BTEX; residence time 1.2 min.

Humidity level (ppmv)	TiO_2 (BTEX only)				TiO_2/AC (BTEX only)				TiO_2 (NO + BTEX)				TiO_2/AC (NO + BTEX)			
	B	T	E	X	B	T	E	X	B	T	E	X	B	T	E	X
2100	57.5	69.9	68.9	72.5	74.3	76.2	72.3	85.7	69.1	78.2	77.2	78.0	76.2	83.5	81.0	83.3
9400	34.2	39.7	42.5	46.5	68.4	70.9	71.1	71.2	32.3	36.7	39.8	40.3	70.6	73.9	75.6	78.0
15700	17.8	20.1	23.1	20.0	63.2	65.8	67.1	66.8	14.2	17.3	21.0	17.3	68.8	67.2	72.2	74.3
22000	5.6	7.5	8.2	8.3	60.5	62.5	63.2	57.9	7.9	9.1	11.6	12.8	67.7	68.9	69.2	67.8

Table 6.4 BTEX conversions using TiO_2 and TiO_2/AC with and without the presence of NO under different levels of humidity. B: benzene; T: toluene; E: ethylbenzene; X: o-xylene; Experimental conditions: 200 ppb NO; 20 ppb BTEX; residence time 1.2min.

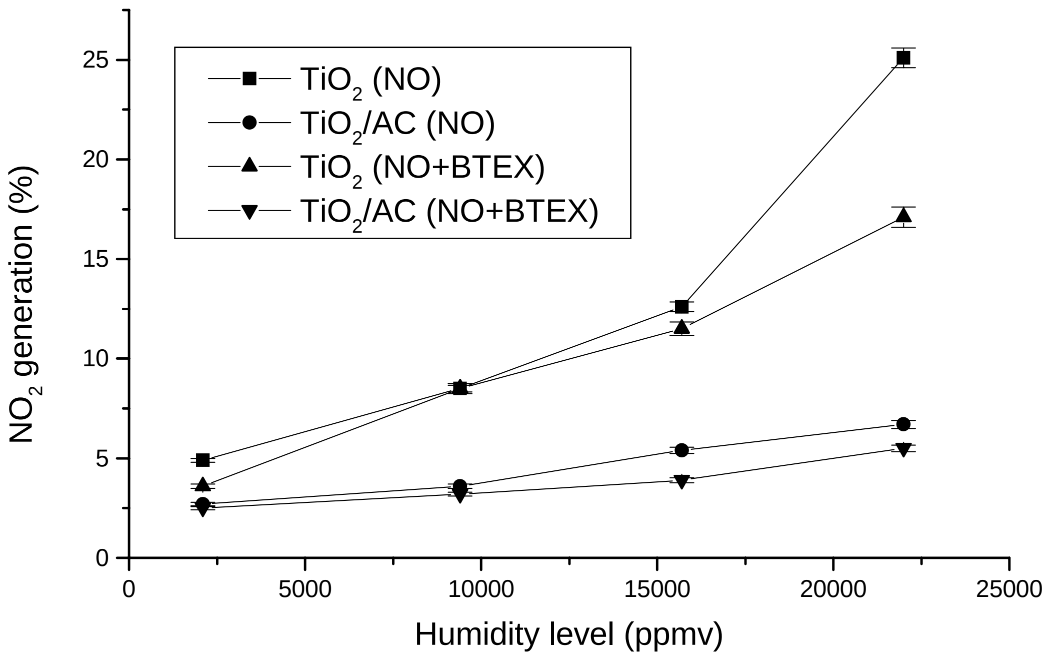

Figure 6.12 NO_2 generation using TiO_2 and TiO_2/AC with and without the presence of BTEX under different humidity levels. Experimental conditions: 200 ppb NO; 20 ppb BTEX; residence time 1.2 min.

Fig. 6.12 shows the generation of NO_2 from the photodegradation of NO with the same experimental conditions as shown in Fig. 6.11. The generation of NO_2 was largely suppressed by the use of TiO_2/AC despite the presence of BTEX. For instance, nearly 25% of NO_2 was generated using TiO_2 whereas only less than 5% of NO_2 was generated using TiO_2/AC at a humidity level of 22000 ppmv with the presence of BTEX. The immobilization of TiO_2 on AC not only reduced the target pollutant NO but also the intermediate NO_2. Study (Torimoto et al., 1996) also showed that the use of TiO_2 with activated carbon reduced the amount of intermediate from the photodegradation of propyzamide.

Table 6.4 shows the conversions of BTEX with and without the presence of NO using TiO_2 and TiO_2/AC at a residence time of 1.2 min under different levels of humidity. The effect of TiO_2/AC in BTEX conversions is even more significant compared to the effect of difference in residence time as shown in Table 6.3. Under high humidity levels, water vapor competed with the pollutants for adsorption sites. Although the amount of BTEX adsorbed on AC decreased with increasing humidity (Fig. 6.8), the adsorbed BTEX on AC was still able to diffuse to the TiO_2 for photodegradation. Under high humidity level, the presence of NO did not affect the conversion of BTEX significantly.

6.4 Concurrent photodegradation of NO and CO by TiO_2 filter

The concentration of CO conducted in this study is 2 ppm, which is a typical indoor CO level (Akland et al., 1985). Table 6.5 shows the concurrent photodegradation of NO and CO. As shown in the table, no conversion of CO was found under different levels of humidity and residence time. This is probably due to the amount adsorbed on the TiO_2 is rather low. Takahama et al. (1997) showed that the Pt-deposited photocatalyst TiO_2 achieved 80% CO conversion at 50 ppmv whereas no conversion was reported using bare TiO_2. The function of Pt is to increase the adsorption of CO on the TiO_2 surface. In this study, only an indoor CO level of 2 ppm was applied thus that reason no CO conversion was observed. As shown in Table 6.5, no promotion effect was observed when NO was co-injected with CO. Presumably, the amount of CO adsorbed on the photocatalyst is too small to be promoted by the hydroxyl radicals generated by the photodegradation of NO. Conversely, no competition effect of CO on NO is observed under different levels of humidity and residence time. Under typical indoor levels, no reaction and competition effect of CO was found.

Experimental conditions	Initial concentration		Conversion (%)	
	CO (ppm)	NO (ppb)	CO	NO
Humidity 2100 ppmv; R.T. 11.4 min	2	0	0	0
Humidity 22000 ppmv; R.T. 3.8 min	2	0	0	0
Humidity 2100 ppmv; R.T. 11.4 min	2	200	0	95.50
Humidity 22000 ppmv; R.T. 3.8 min	2	200	0	64.98

Table 6.5 Photodegradation of NO co-injected with CO.

6.5 Concurrent photodegradation of NO and NO_2 by TiO_2 filter

Table 6.6 shows the photodegradation of NO, NO_2, and NO co-injected with NO_2 at a residence time of 11.4 min and 2100 ppmv humidity. It clearly shows that

NO promoted the photodegradation of NO_2 while the presence of NO_2 inhibited the conversion of NO. For instance, the conversion of NO_2 at 45 ppb increased from 59.8% to 77.8% under the presence of 200 ppb NO. At 90 ppb NO_2, the increased NO_2 conversion was smaller when compared to that of 45 ppb NO_2. The NO_2 conversion only increased from 73.8% to 85.4%. As the same amount of NO was used for both experiments, smaller NO_2 concentration will has a higher promotion effect as the hydroxyl radicals generated from the photodegradation of NO is higher per NO_2. The promotion effect of NO was also reported previously. It is also noted that the conversion of NO decreased with an increase in the amount of NO_2 co-existing in the system. The conversion of NO decreased from 93.6% to 90% and to 85.6% when 45 ppb NO_2 and 90 ppb NO_2 was co-injected respectively. When the total amount of active sites on the photocatalyst remained the same, the total amount of pollutants per active sites decreased. The competition effect between NO and NO_2 was also reported at a concentration of 10 ppm NO (Matsuda et al., 2001).

Initial concentration		Conversion (%)	
NO (ppb)	NO_2 (ppb)	NO	NO_2
0	45	0	59.8
0	90	0	73.8
200	0	93.6	0
200	45	90.0	77.8
200	90	85.6	85.4

Table 6.6 Photodegradation of NO co-injected with NO_2.

6.6 *Concurrent photodegradation of NO and SO_2 by TiO_2 filter*

6.6.1 Effects of humidity levels

Fig. 6.13 shows the photodegradation of NO with and without the presence of SO_2 under different humidity levels at a residence time of 1.2 min. The initial concentrations of NO and SO_2 were 200 ppb. The presence of SO_2 inhibited the conversion of NO despite the levels of humidity. The photodegradation of NO is adversely affected by increasing humidity levels. Fig. 6.14 shows the generation of NO_2 from the photodegradation of NO. The experimental conditions are identical to Fig. 6.13. The presence of SO_2 not only inhibited the conversion of NO but also increased the generation of NO_2. With the presence of SO_2, the NO_2 generation increased by 10%.

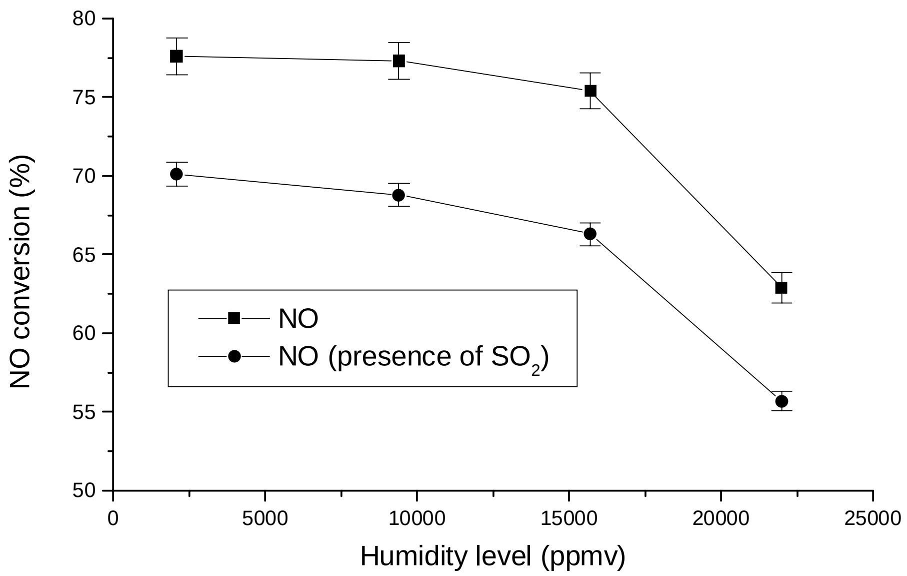

Figure 6.13 Conversion of NO with and without the presence of SO_2 at an initial concentration of 200 ppb NO & SO_2. Experimental conditions: Residence time 1.2 min; humidity level 2100 ppmv.

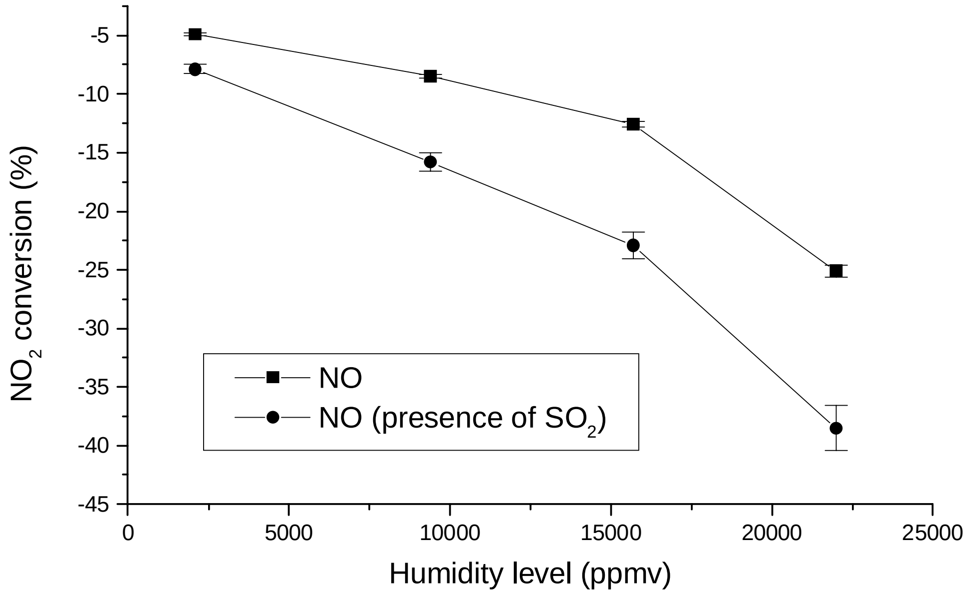

Figure 6.14 Conversion of NO_2 with and without the presence of SO_2 at an initial concentration of 200 ppb NO & SO_2. Experimental conditions: Residence time 1.2 min; humidity level 2100 ppmv.

The binary photodegradation of NO and CO results showed that no photodegradation of CO was found under different residence time and levels of humidity. The existence of CO does not promote or inhibit the photodegradation of NO. Although no photodegradation of SO_2 was found in this study, the existence of SO_2 reduced the conversion of NO and increased the generation of NO_2. The difference between the effects of SO_2 and CO is probably due to the product formed on the filter.

The increase in NO_2 content is probably due to the presence of sulfate ion. NO is photodegradated to NO_2 and then converted to HNO_3 as is illustrated in the following equations (Komazaki et al., 1999; Matsuda et al., 2001):

$$NO + HO_2\cdot \rightarrow NO_2 + OH\cdot \quad (6.1)$$

$$NO_2 + OH\cdot \rightarrow HNO_3 \qquad (6.5)$$

The nitric acid formed on the TiO_2 decreased the photoactivity and thus deactivation occurred (Hashimoto et al., 2001). Nitrate ion was used to identify the formation of nitric acid on the TiO_2 (Ibusuki and Takeuchi, 1994). According to equations (6.1) and (6.5), NO_2 concentration is controlled by NO conversion rate. The presence of SO_2 inhibited the photodegradation of NO, and thus a lower NO_2 concentration is anticipated. The NO_2 concentration, however, increased despite a lower NO conversion. This is probably due to the generation of sulfate ion presents before the start of the UV irradiation. The formation of HNO_3 from NO_2 at the initial stage of the NO photodegradation is inhibited. The sulfate ion blocked the adsorption sites of TiO_2 for converting NO_2 to HNO_3, leading to the increase of NO_2 exited to the outlet stream. The presence of SO_2 showed a clear inhibition effect not only on the target pollutant NO but also on the intermediate NO_2. The overall NO_x conversion decreased with the presence of SO_2.

Table 6.7 shows the concentrations of the sulfate ion and the nitrate ion from the photodegrdation of NO, SO_2 and NO with SO_2. Sulfate ion and nitrate ion presented even though only NO and SO_2 was generated, respectively. This is due to the blank concentration of the sulfate and nitrate ion presented on the TiO_2 filter. When 200 ppb of NO is photodegradated, 404 μg/filter of nitrate ion was found. The nitrate ion was generated from the photodegradation of NO according to equation (6.1) and (6.5). However, when SO_2 was co-injected with NO, the formation of nitrate ion decreased which is an indication of a decrease in HNO_3 formation. The presence of sulfate ion competed with nitrate ion for adsorption sites on TiO_2. Thus, the generation of NO_2 increased in the outlet stream. Study also showed that the presence of SO_4^{2-} ion decreased the photo-decomposition of Astrazone Orange. The presence of adsorbed ion competed with the Astrazone Orange for adsorption sites on the TiO_2 surface (Sokmen and Ozkan, 2002). The results of the sulfate ion and nitrate ion from IC analysis in this study indicated that the inhibition effect of SO_2 on the NO_x photodegradation is due to the presence of SO_4^{2-} ion. In the results shown in Table 4.5, we showed that no photodegradation of SO_2 occurred. Hence, the inhibition effect of SO_4^{2-} ion is due to the competition of adsorption sites between NO on the TiO_2 surface but not due to the competition of photo-active spices such as hydroxyl radicals.

Experimental conditions	SO_4^{2-} ions (μg/sheet)	NO_3^- ions (μg/sheet)
NO only	39	404
SO_2 only	417	49
NO and SO_2	448	162

Table 6.7 Sulfate ion (SO_4^{2-}) and nitrate ion (NO_3^-) from the photodegradation of SO_2 and NO; humidity level 2100 ppmv; residence time 1.2 min.

6.7 Concurrent photodegradation of NO and SO_2 by TiO_2 filter and TiO_2/AC filter

6.7.1 Adsorption of SO_2 by TiO_2/AC filter

Prior to the investigation of binary photodegradation of NO with SO_2, it is necessary to examine the photodegradation of SO_2 by TiO_2 filter and TiO_2/AC filter. Previously we reported that no photodegradation of SO_2 was observed by using TiO_2 powder only. Fig. 6.15 shows the SO_2 removal by TiO_2 and TiO_2/AC. The removal of SO_2 increased with increasing humidity using TiO_2 filter, whereas a decreasing trend was observed for TiO_2/AC. At a humidity level of 22000 ppmv, the TiO_2 filter adsorbed 14% SO_2 more than TiO_2/AC filter. The glass fiber filter, used as the supporting substrate, adsorbed more than 75% of SO_2. However, no adsorption was observed for TiO_2 powder only (without the use of glass fiber filter as supporting substrate) within the experimental error. The SO_2 removal increased from 77% to 80% when the humidity level increased from 2100 ppmv to 22000 ppmv. The adsorption of SO_2 on the glass fiber filter is owing to the formation of sulfate ion. The concentration of the sulfate ion increased with increasing humidity. An opposite trend was observed when using TiO_2/AC filter. The SO_2 removal decreased from 71% to 68% when the humidity level increased from 2100 ppmv to 22000 ppmv. This is probably due to the competition between the SO_2 and water vapor for adsorption sites on activated carbon. Studies showed that the presence of water vapor inhibited the adsorption of NO (Richter et al., 1985), benzene (Cal et al., 1996) and VOCs (Khan and Ghoshal, 2000) on activated carbon.

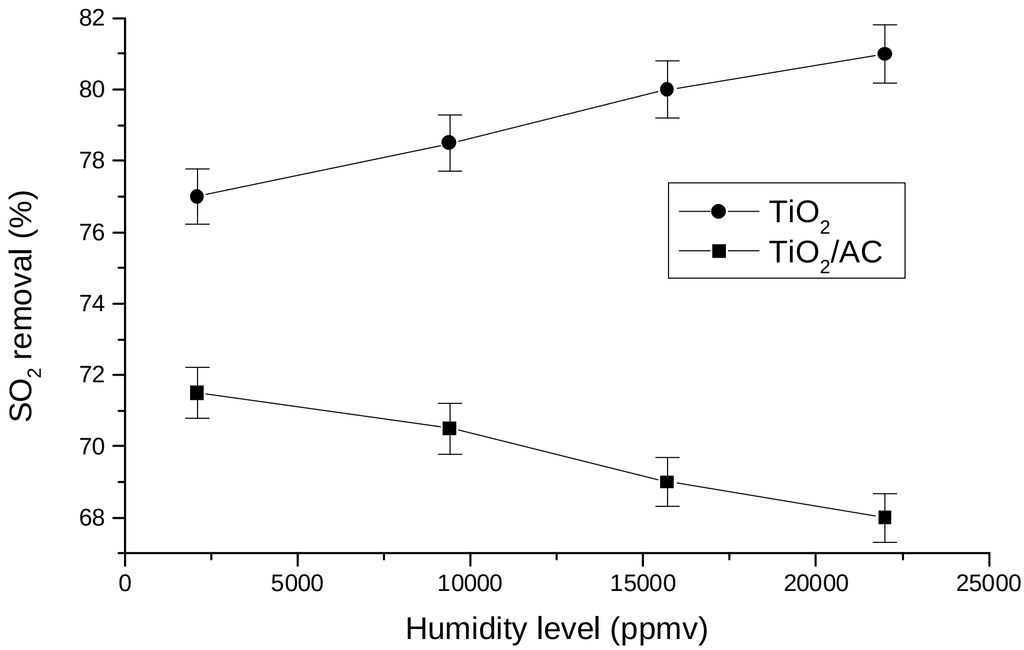

Figure 6.15 SO_2 removal using TiO_2 and TiO_2/AC under different humidity levels. Experimental conditions: 200 ppb SO_2; residence time 1.2 min.

6.7.2 Effects of humidity

Fig. 6.16 shows the binary photodegradation of NO with the presence of SO_2 using TiO_2 and TiO_2/AC filter under different humidity levels at a residence time of 1.2 min. Similar to the presence of BTEX, the presence of SO_2 inhibited the conversion of NO. Under the presence of SO_2, the conversion of NO decreased to 55.7% when using TiO_2 filter, whereas 65.1% of NO conversion was achieved using TiO_2/AC filter. The inhibition effect of SO_2 is owing to the formation of sulfate ion on the TiO_2 and competed with NO for the adsorption sites. SO_2 adsorbed on activated carbon and formed sulfuric acid (Lizzio and DeBarr, 1997, Raymundo-Pinero et al., 2001). With the presence of water vapor, the sulfuric acid disassociated into sulfate ion. This sulfate ion, similar to the pollutant diffusion from the activated carbon to the TiO_2, diffused to the TiO_2 surface and competed with the pollutants for adsorption sites on the TiO_2. Nevertheless, the activated carbon also concentrated the pollutant from the inlet stream to the TiO_2 for photodegradation. Another possible reason is that the amount of SO_2 removed by TiO_2 is higher than TiO_2/AC (see Fig.6.15). Using TiO_2/AC, the conversion of NO is 10% higher than using TiO_2.

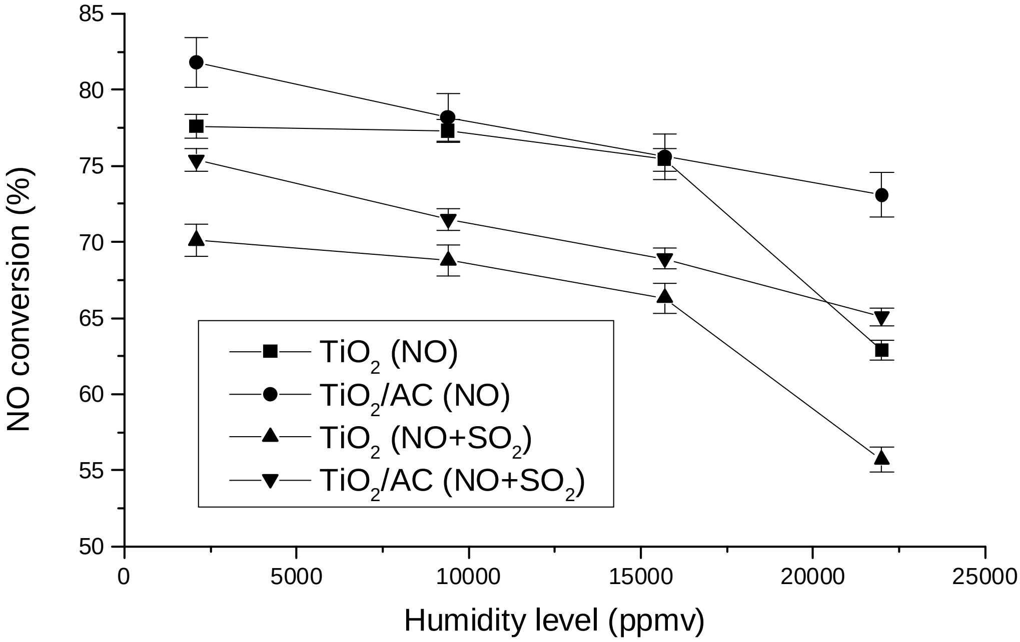

Figure 6.16 NO conversion using TiO_2 and TiO_2/AC with and without the presence of SO_2 under different humidity levels. Experimental conditions: 200 ppb NO; 200 ppb SO_2; residence time 1.2 min.

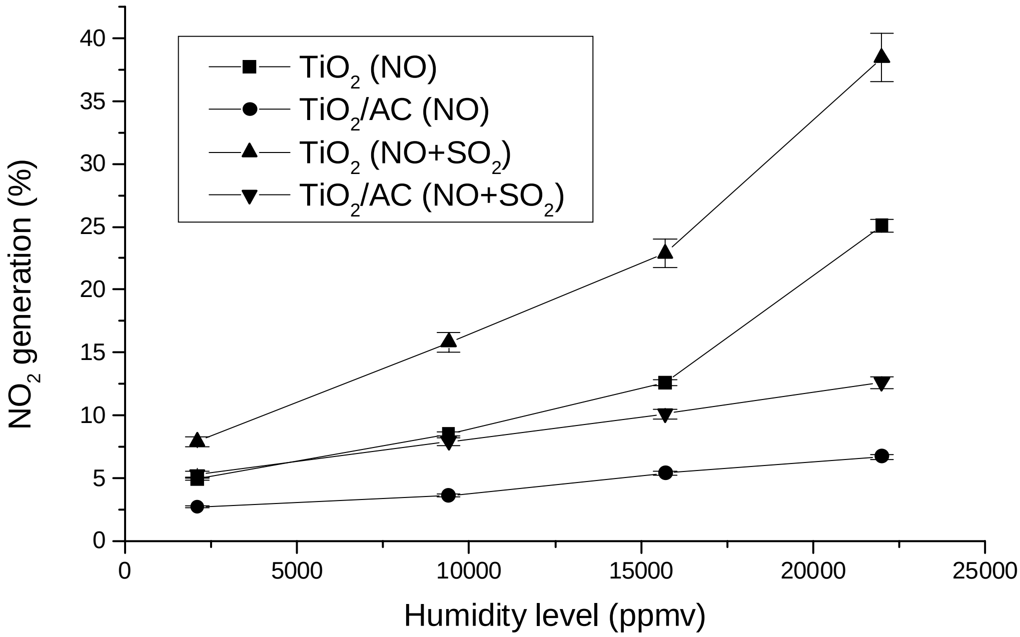

Figure 6.17 NO_2 generation using TiO_2 and TiO_2/AC with and without the presence of SO_2 under different humidity levels. Experimental conditions: 200 ppb NO; 200 ppb SO_2; residence time 1.2 min.

Fig. 6.17 shows the NO_2 generation with the same experimental conditions as shown in Fig. 6.16. The effect of TiO_2 immobilized on activated carbon is significant in suppressing the generation of NO_2. With the presence of SO_2, over 35% and only around 10% of NO_2 was generated using TiO_2 filter and TiO_2/AC filter, respectively. It is worth noting that at a low humidity level (2100 ppmv), the effect in reducing NO_2 generation using TiO_2 filter and TiO_2/AC filter is not significant. Under low humidity levels, the competition effect between the pollutants and the water vapor is not significant. Using TiO_2 merely with the presence of SO_2, only 7.9% of NO_2 was generated, whereas 5.3% of NO_2 was generated using TiO_2/AC. When the humidity level increased to 22000 ppmv, the adsorption sites on the TiO_2 were blocked by the water vapor and the sulfate ion formed from the adsorption of SO_2. The NO_2 generated from the photodegradation of NO leaving to the outlet stream without further photodegradated to HNO_3 owing to the adsorption site occupied by the water vapor and sulfate ion. Using activated carbon, the NO_2 generated adsorbed on it and thereby diffused to TiO_2 for photodegradation.

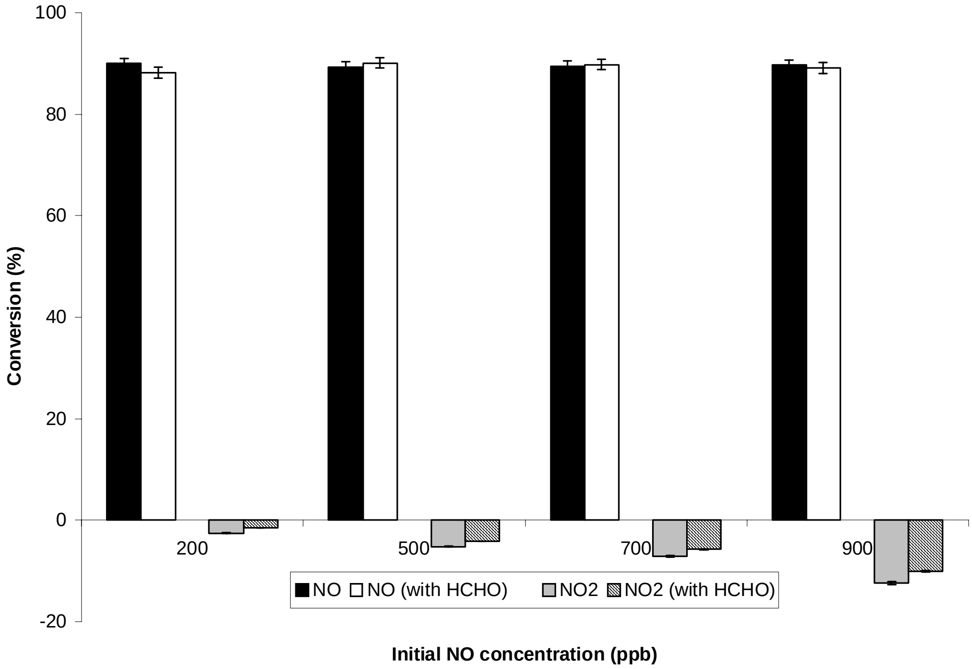

Figure 6.18 Impact on NO_x conversions with and without the presence of HCHO under different initial NO concentrations. Experimental conditions: 50 ppb HCHO; residence time 3.8 min; humidity level 2100 ppmv.

6.8 Concurrent photodegradation of NO and HCHO by TiO_2 filter

6.8.1 Effects of initial concentrations

The impact on the photodegradation of NO_x (NO and NO_2) under the presence of formaldehyde at a humidity level of 2100 ppmv and at a residence time of 3.8 min is shown in Fig. 6.18. It can be observed that the conversion of NO is similar despite the difference in initial NO concentrations. However, the NO_2 concentration with the presence of formaldehyde is lower than the absence of formaldehyde.

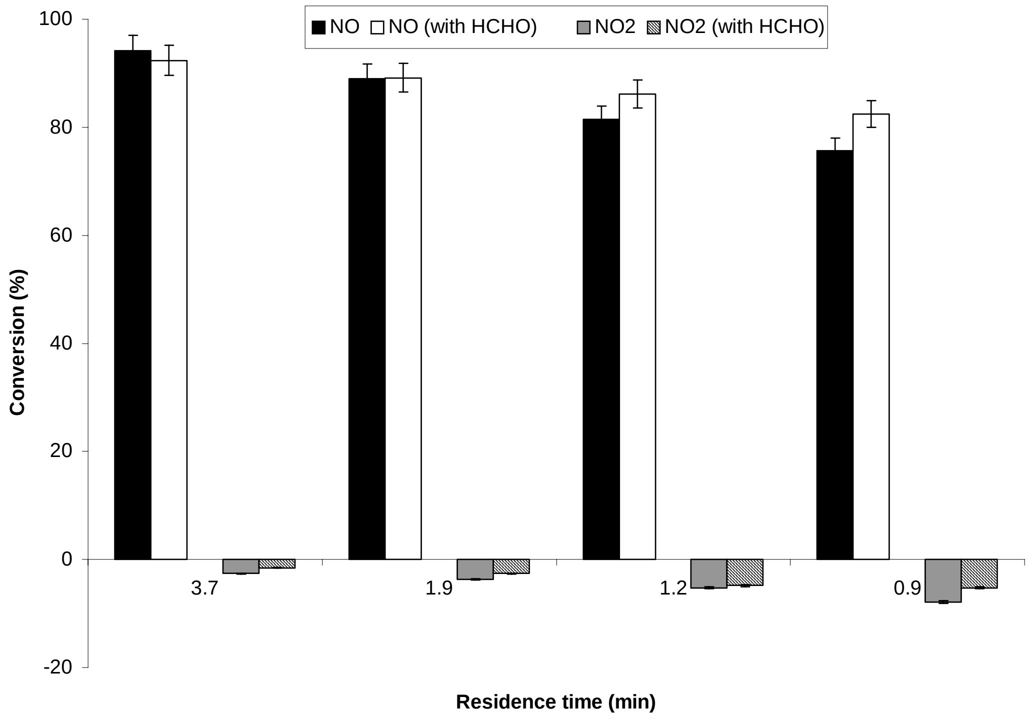

Figure 6.19 Impact on NO_x conversions with and without the presence of HCHO under different residence time. Experimental conditions: 50 ppb HCHO; 200 ppb NO; humidity level 2100 ppmv.

6.8.2 Effects of residence time

Fig. 6.19 shows the NO conversion and NO_2 generation with and without the presence of formaldehyde at a humidity level of 2100 ppmv under different residence time. Apart from the NO conversion at 3.8 min, the presence of formaldehyde promoted the conversion of NO. Also noted is the presence of formaldehyde reduced the generation of NO_2 despite the variations of residence time.

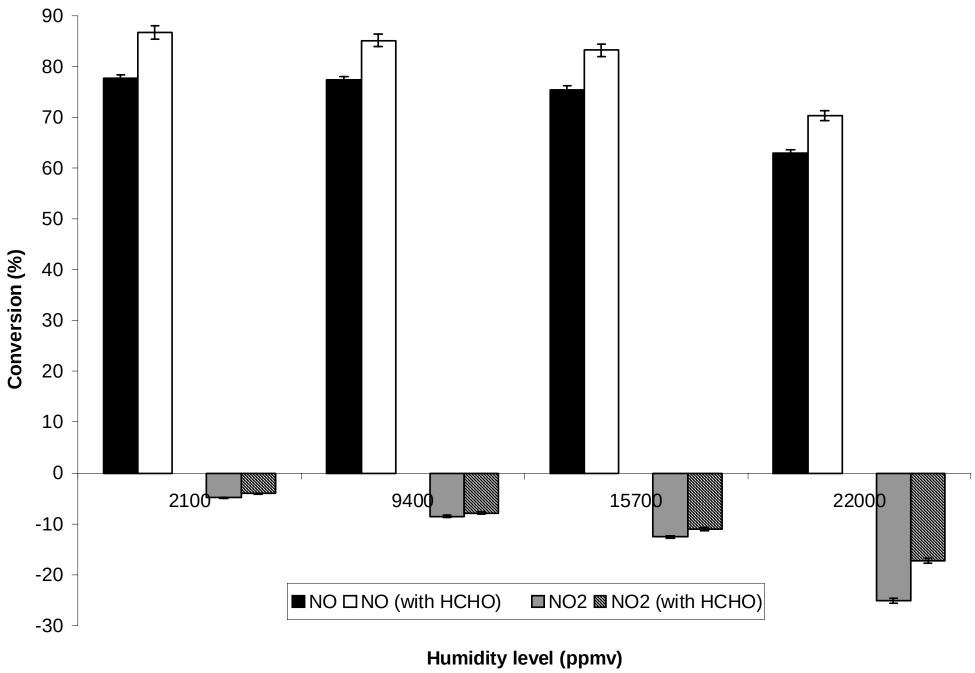

Figure 6.20 Impact on NO_x conversions with and without the presence of HCHO under different humidity levels. Experimental conditions: 50 ppb HCHO; 200 ppb NO; residence time 1.2 min.

6.8.3 Effects of humidity levels

Fig. 6.20 shows the impact on the presence of formaldehyde on the NO_x conversion under different humidity levels at a residence time of 1.2 min. It can be observed that the promotion effect of NO conversion and the inhibition effect on NO_2 generation is more significant with increasing humidity levels. In Fig. 6.18, the promotion effect of formaldehyde not being significant is probably due to the higher conversion of NO under the experimental conditions. Under low humidity levels where the competition effect between water vapor and NO for adsorption sites on TiO_2 is not significant and a long residence time was provided, more than 90% of NO conversion was achieved despite the variations of initial NO concentrations. The high NO conversion hindered the promotion effect of formaldehyde. In addition, only a small amount of NO_2 was generated which made it difficult to observe the effect of NO_2 during the photodegradation of formaldehyde. In Fig. 6.19, the decreased in NO conversion with decreasing residence time manifested the promotion effect of formaldehyde. At a residence time of 0.9 min, the NO conversion with the presence of formaldehyde is 10% higher than NO only. In Fig. 6.20, the NO conversion at a humidity level of 22000 ppmv significantly decreased due to the competition of adsorption sites on TiO_2 between water vapor and NO. NO_2, as an intermediate generated from the photodegradation of NO, was also significantly higher at 22000 ppmv humidity level. The higher in NO_2 generation allowed it to react with formaldehyde during photodegradation.

The promotion effect of formaldehyde on NO conversion and reduction of NO_2 exiting the system is probably due to the radicals formed from the formaldehyde photodegradation. As shown in equation 6.14, a HCO radical was formed from the photodegradation of HCHO (Yang et al., 2000). HCO radical may react with oxygen forming HO_2 radicals since zero air used in this study contained abundant of oxygen. $HCO \cdot + O_2 \longrightarrow HO_2 \cdot + CO$ (6.14)

The peroxy radical generated from the photodegradation of HCHO is probably the reason that a higher NO conversion was observed, according to the reaction showed in equation 14.

HCO radical might also react with NO_2, according to equation 6.15 (Smith et al., 2002).

$$NO_2 + HCO \cdot \longrightarrow HONO + CO \qquad (6.15)$$

Since the photodegradation of formaldehyde simultaneously occurred with NO, the NO_2 generated might react with HCO radicals forming HONO. Similar reactions were also reported from the photolysis studies (Butkovskaya and Setser, 1998) between formaldehyde and NO_x.

Atkinson (1990) also reported that alkyl peroxy radicals ($HOCH_2O_2$) from equation 4.25 reacted with nitrogen dioxide (NO_2) forming peroxyalkyl nitrate ($HOCH_2O_2NO_2$), as shown in equation 6.16.

$$HOCH_2OO + NO_2 \longrightarrow HOCH_2OONO_2 \qquad (6.16)$$

The exact reaction pathway during the concurrent photodegradation of formaldehyde and NO_2 is not ascertained. Nevertheless, from the concentrations of formaldehyde and NO_2 observed in the experiments conducted, reactions between formaldehyde and NO_2 are highly plausible. Thus, the presence of formaldehyde provided an alternative reaction for NO_2, thereby reducing the NO_2 concentration.

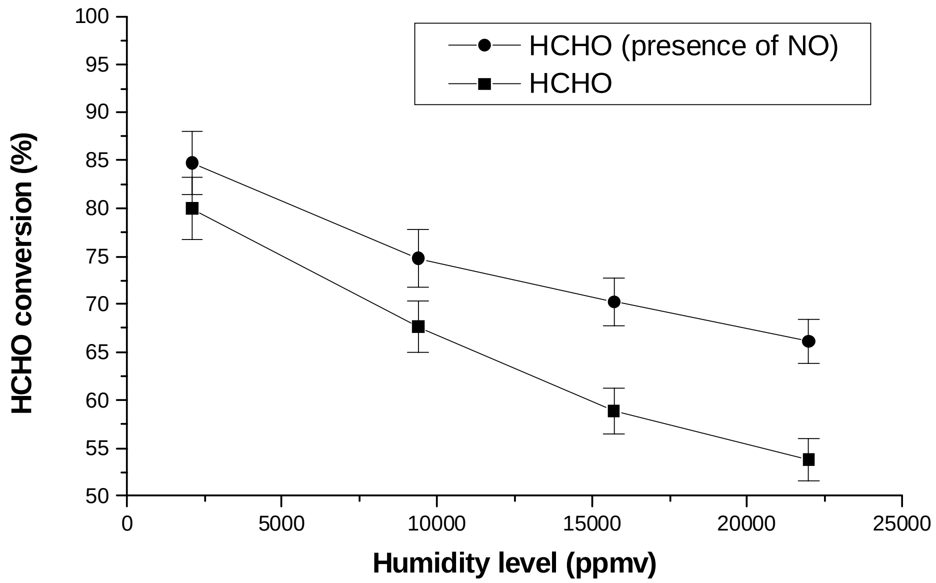

Figure 6.21 Impact on HCHO conversion with and without the presence of NO under different humidity levels. Experimental conditions: 50 ppb HCHO; 200 ppb NO; residence time 1.2 min.

6.9 Concurrent photodegradation of HCHO and NO by TiO_2 filter

Fig. 6.21 shows the photodegradation of formaldehyde with and without the presence of 200 ppb NO at a residence time of 1.2 min under different humidity levels. The promotion effect of NO on formaldehyde conversion was observed despite the variations of humidity levels. The promotion effect of NO increased with increasing humidity levels. The high conversion of formaldehyde at a low humidity level might hinder the promotion effect of NO. At high humidity levels, water competed with formaldehyde for adsorption sites on TiO_2 and thus reduced the conversion. The promotion effect of NO is more significant when the formaldehyde conversion is low. The promotion effect of NO is due to the hydroxyl radicals generated from the photodegradation of NO, as shown in equation 6.1.

Table 6.8 shows the formic acid yield from the photodegradation of formaldehyde with and without the presence of 200 ppb NO under different humidity levels. The concentration of formic acid with the presence of NO was higher than without the presence of NO despite the humidity levels. As shown in Fig. 6.21, the presence of NO promoted the conversion of formaldehyde. Thus, a higher formic acid yield was observed due to a higher formaldehyde conversion. This is in agreement that under the presence of NO, a higher formaldehyde conversion was observed.

Humidity level (ppmv)	Formic acid yield (μmol)	Formic acid concentration with the presence of 200 ppb NO (μmol)
2100	0.28	0.37
9600	0.13	0.22
15700	0.10	0.15
22000	0.06	0.09

Table 6.8 HCOOH yield with and without the presence of NO under different humidity levels. Experimental conditions: 50 ppb HCHO; 200 ppb NO; residence time 1.2 min.

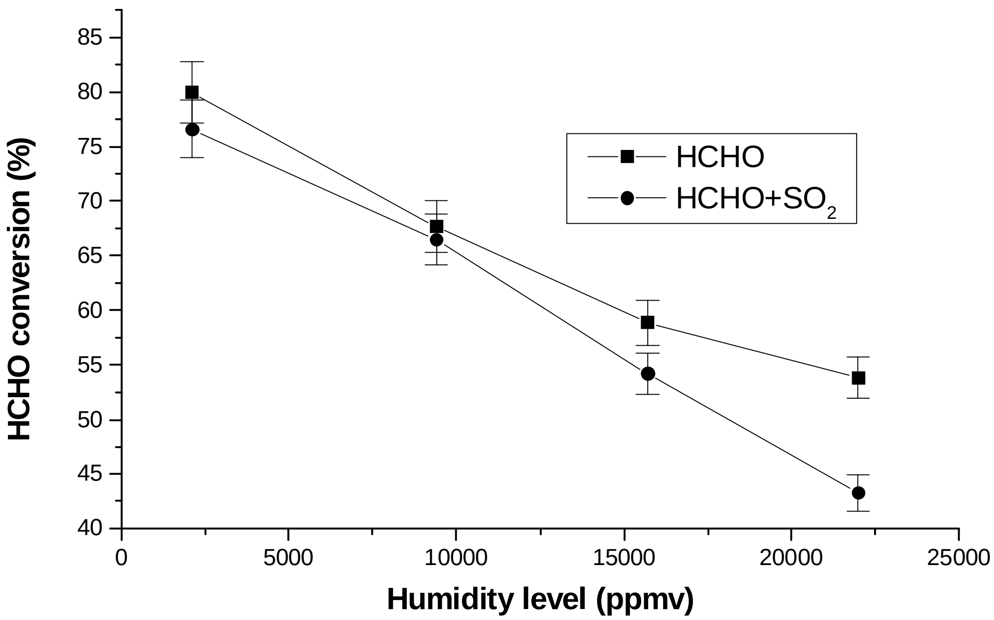

Figure 6.22 Impact on HCHO conversion with and without the presence of SO_2 under different humidity levels. Experimental conditions: 50 ppb HCHO; 200 ppb SO_2; residence time 1.2 min.

6.10 Concurrent photodegradation of HCHO and SO_2 by TiO_2 filter

Fig. 6.22 shows the conversion of 50 ppb formaldehyde with and without the presence of 200 ppb SO_2 at a residence time of 1.2 min under different humidity levels. The conversion of formaldehyde, despite the presence of SO_2, decreased with increasing humidity levels. In addition to the inhibitory effect of increasing humidity levels on the conversion of formaldehyde, the presence of SO_2 further decreased the conversion by 10% at a humidity level of 22000 ppmv. This is owing to the formation of sulfate ion under the presence of SO_2. Sulfate ion was readily formed after the introduction of SO_2 gas into the reactor.

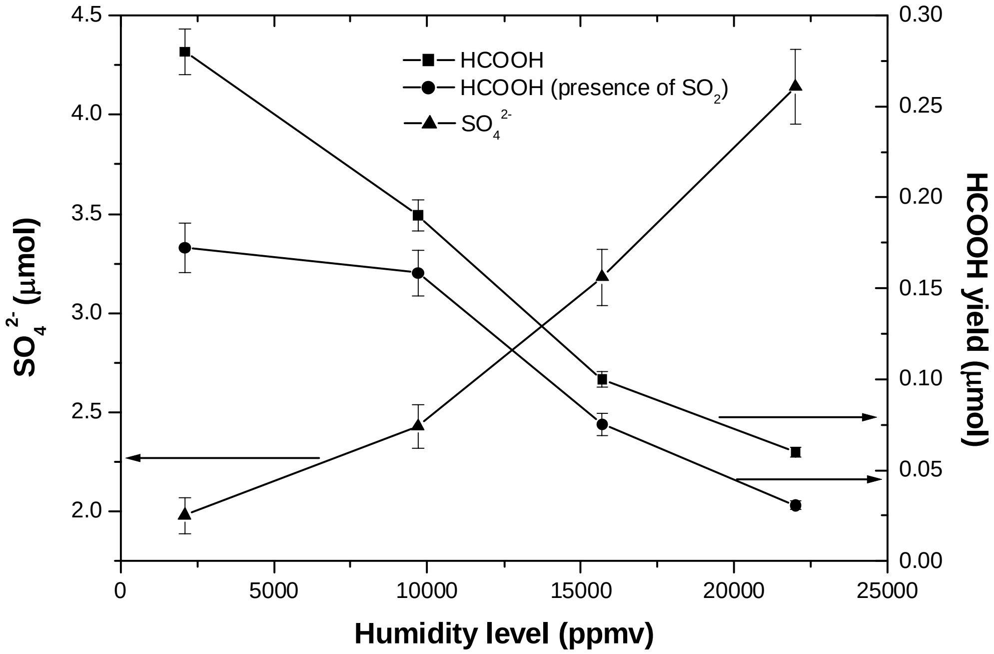

Figure 6.23 Impact on HCOOH yield with and without the presence of SO_2 under different humidity levels. Experimental conditions: 50 ppb HCHO; 200 ppb SO_2; residence time 1.2 min.

c

n

1.98 to 4.14 μmol when the humidity level increased from 2100 to 22000 ppmv, whereas the formic acid yield under the presence of SO_2 decreased from 0.17 to 0.03 μmol. The formic acid yield under the presence of SO_2 is also lower than without the presence of SO_2. Thus, it can be clearly observed that the formation of sulfate ion inhibited the yield of formic acid and a lower formaldehyde conversion is observed. When SO_2 and formaldehyde were introduced to the reactor, sulfate ion formed and adsorbed on the TiO_2 surface immediately. The formation and deposition of the sulfate ion, prior to the photodegradation of formaldehyde, render the TiO_2 surface inaccessible to photodegradate formaldehyde. Studies also showed that the presence of sulfate ion inhibited the photodegradation of ethanol (Abdullah et al., 1990), ethylene (Yamazaki et al., 2001), dichloroethane (Chen et al., 1997) and organic dye (Sokmen and Ozkan, 2002). The above authors elucidated that the sulfate ion competed with pollutants for adsorption sites on the TiO_2 surface. Thus, the presence of sulfate ion inhibited the conversions of pollutants simultaneously present, despite in the gaseous gas or aqueous phase.

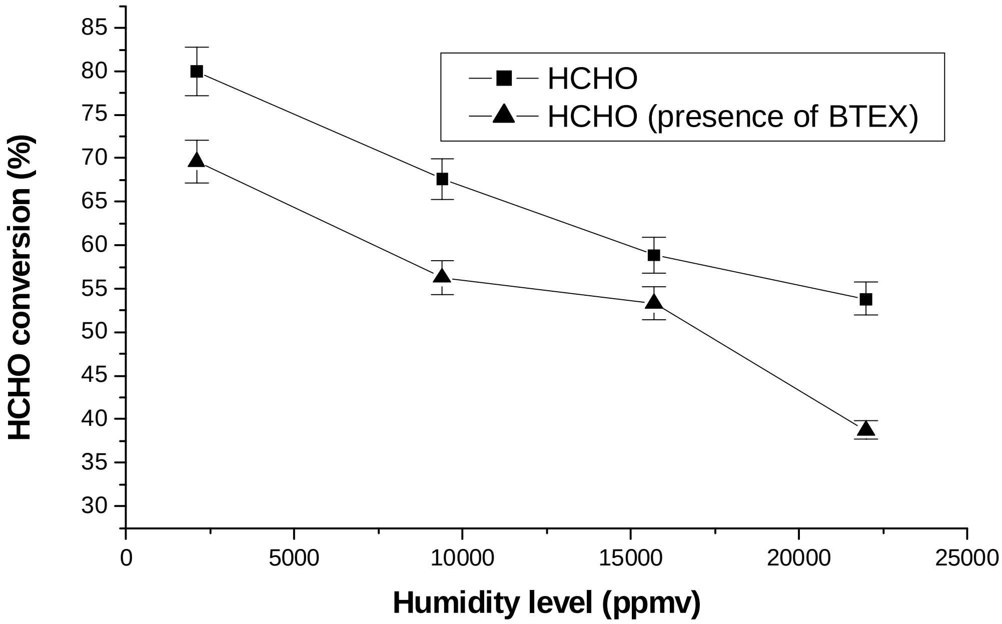

Figure 6.24 Impact on HCHO conversion with and without the presence of BTEX under different humidity levels. Experimental conditions: 50 ppb HCHO; 20 ppb BTEX; residence time 1.2 min.

6.11 Concurrent photodegradation of HCHO and BTEX by TiO_2 filter

Fig. 6.24 shows the conversion of 50 ppb formaldehyde with and without the presence of 20 ppb BTEX at a residence time of 1.2 min under different humidity levels. Similar to the inhibitory effect of SO_2, the presence of BTEX inhibited the conversion of formaldehyde despite the variation of humidity levels. The presence of BTEX decreased the conversion of formaldehyde by around 10% at different humidity levels. Previous study also showed that the presence of BTEX also inhibited the conversion of NO. The presence of BTEX competed with formaldehyde for adsorption sites on TiO_2 and inhibited the conversion of formaldehyde. Luo and Ollis (1996) also showed that the conversion of trichloroethylene was decreased with the introduction of toluene in the feed stream.

From the results of the GC/MS analysis, no gaseous phase intermediate was identified. No gaseous phase aldehydes were also found by the HPLC analysis. Studies (Luo and Ollis, 1996; Sauer et al., 1995) also showed that no gaseous phase intermediate was detected by an on-line GC/FID during the photodegradation of toluene. To further elucidate the inhibitory effect of BTEX on formaldehyde conversion, the TiO_2 filter after the concurrent photodegradation of BTEX and formaldehyde was immersed in ethanol. The resultant solution was filtered and analyzed by CG/MS to determine any intermediates formed on the TiO_2 filter. Benzaldehyde and benzyl alcohol was qualitatively identified from the GC/MS analysis. The results observed in this study are similar to that reported by d' Hennezel et al. (1998). They used diethylether and ultrasonication to extract the remains of the TiO_2 and benzaldehyde, benzyl alcohol and benzoic acid were identified. Using temperature-programmed oxidation and desorption, Larson and Falcon (1997) identified benzaldehyde, benzyl alcohol and *m*-cresol as intermediates from the photodegradation of toluene using Degussa P25 as the photocatalyst. These results were further confirmed by Cao and co-workers (2000) by FTIR and these intermediates poisoned the catalyst surface by blocking reaction sites. Hence, during the concurrent photodegradation of BTEX and formaldehyde, the intermediates generated from the photodegradation of BTEX blocked the active surface sites of TiO_2, thereby decreasing the conversion of formaldehyde. Intermediates generated from the photodegradation of benzene were phenol and hydroquinone (d'Hennezel et al., 1998). O-tolualdehyde and o-toluic acid were reported as intermediate generated from the photodegradation of o-xylene (Ameen and Raupp, 1999). Since the concentrations conducted in this study were only at ppb level, the resultant signal to noise ratio of the GC/MS analysis was high. Thus, only benzaldehyde and alcohol were identified as intermediate from the photodegradation of BTEX.

Fig. 6.25 shows the yield of formic acid with and without the presence of BTEX. The experimental conditions were identical to those in Fig. 6.24. Under the presence of BTEX, the yield of formic acid is lower compared to the absence of BTEX. At a humidity level of 2100 ppmv, the conversion of BTEX is much higher than at 22000 ppmv and probably a larger amount of intermediates were formed. Hence, at a humidity level of 2100 ppmv, the inhibition effect on the yield of formic acid is higher compared to other humidity levels.

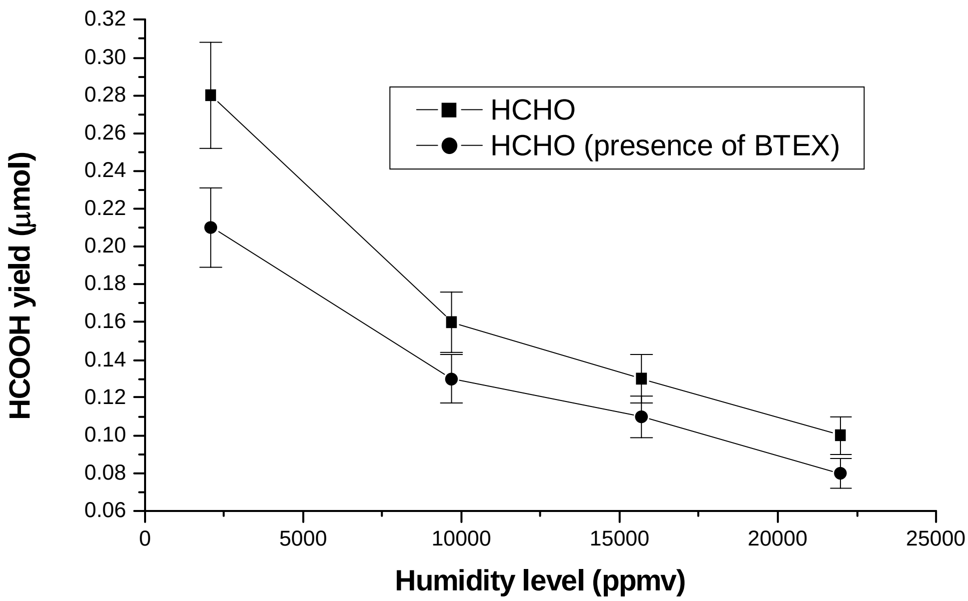

Figure 6.25 Impact on HCOOH yield with and without the presence of BTEX under different humidity levels. Experimental conditions: 50 ppb HCHO; 20 ppb BTEX; residence time 1.2 min.

6.12 Summary

The feasibility of applying photocatalysis for indoor air purification was further evaluated by removing multiple pollutants simultaneously. The reactions matrix between different pollutants is shown in Table 6.9.

	NO	CO	NO_2	SO_2	BTEX	HCHO
NO		Nil	P	Nil	P	P
CO	Nil		Nil	Nil	Nil	Nil
NO_2	I	Nil		N.A.	N.A.	N.A.
SO_2	I	Nil	N.A.		I	I
BTEX	I	Nil	N.A.	Nil		I
HCHO	P	Nil	N.A.	Nil	P	

Table 6.9 Summary of reactions between different pollutants.
Nil: no reaction; N.A.: not available
P: Promotion I: Inhibition

Since no photodegradation of CO was observed, the presence of CO did not have any effect on the conversion of other pollutants. The presence of NO promoted the conversion of BTEX, NO_2 and HCHO, which is due to the generation of hydroxyl radical from the photodegradation of NO. The presence of BTEX inhibited the conversion of NO and HCHO. Benzaldehyde and benzyl alcohol was qualitatively identified as the intermediates generated from the photodegradation of BTEX, which blocked the active sites of TiO_2. The formation of sulfate ion under the presence of SO_2 also inhibited the conversion of NO, BTEX and HCHO. The presence of HCHO promoted the conversion of NO and BTEX, which is probably due to the generation of HCO radical from the photodegradation of HCHO.

By immobilizing TiO_2 on the activated carbon filter, the inhibition effect of SO_2 and BTEX was significantly reduced. Under high humidity levels, the inhibition effect of water vapor is more significant compared to the presence of other pollutants.

Chapter 7 Removal of indoor air pollutant by photocatalyst TiO_2 installed in a commercial air cleaner

7.1 Introduction

After achieving successful results of the TiO_2 load on the activated carbon for photodegradation of multiple indoor air pollutants at high humidity levels in the laboratory scale reactor, it is essential to verify if the same results can be achieved for practical application. This is important because it provides useful data for manufacturer to have a better understanding of photocatalysis in real application. A commercial air cleaner was inquired and the TiO_2 filter and TiO_2/AC filter was installed in it and tested in an environmental chamber. The pollutant removal efficiency of the air cleaner itself was also tested. Similar results were achieved using the commercial air cleaner as compared to the laboratory scale reactor. To further evaluate the TiO_2/AC by practical application, on site testing was also conducted by installing the TiO_2/AC filter in an air duct inside an office building

7.2 Indoor air pollutants removal by commercial air cleaner installed with TiO_2 filter & TiO_2/AC filter

7.2.1 Leakage test of the environmental chamber

Prior to the evaluation of the air cleaner, a blank test was conducted for NO and toluene. An initial 200 ppb NO concentration was achieved by controlling the amount of 50 ppm NO injected from the standard gas. 30 min was allowed for mixing and the initial concentration was collected and analyzed. In all experiments, the initial NO and toluene concentration was controlled to be 200 ± 5 ppb and 2.15± 0.05 ppm, respectively. At time intervals 30 min, 60 min and 120 min, samples were collected. As shown in Fig. 7.1, the initial NO concentration was similar to the NO concentration at 120 min. Similar result was obtained for toluene, as shown in Fig. 7.2. Thus, the environmental chamber was suitable for the testing of air cleaner without pollutant removal due to chamber leakage. Photolysis study was also conducted for UVA and UVC lamp. No removal of NO was observed using UVA lamp, whereas 20 ppb of NO removal was observed using UVC lamp.

Apart from the experiments with the indication of AC+HEPA setting, all the experiments were conducted without the original AC filter from the air cleaner. The HEPA filter was remained to maintain a constant flow for all experiments.

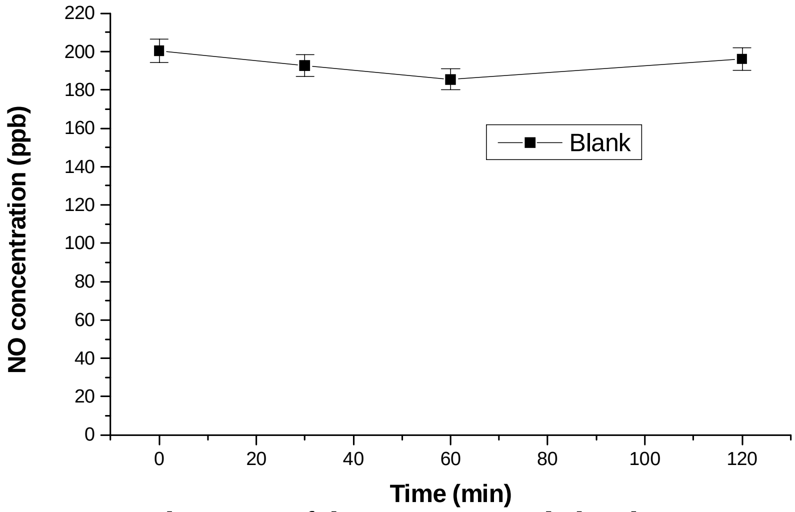

Figure 7.1 Leakage test of the environmental chamber using NO.

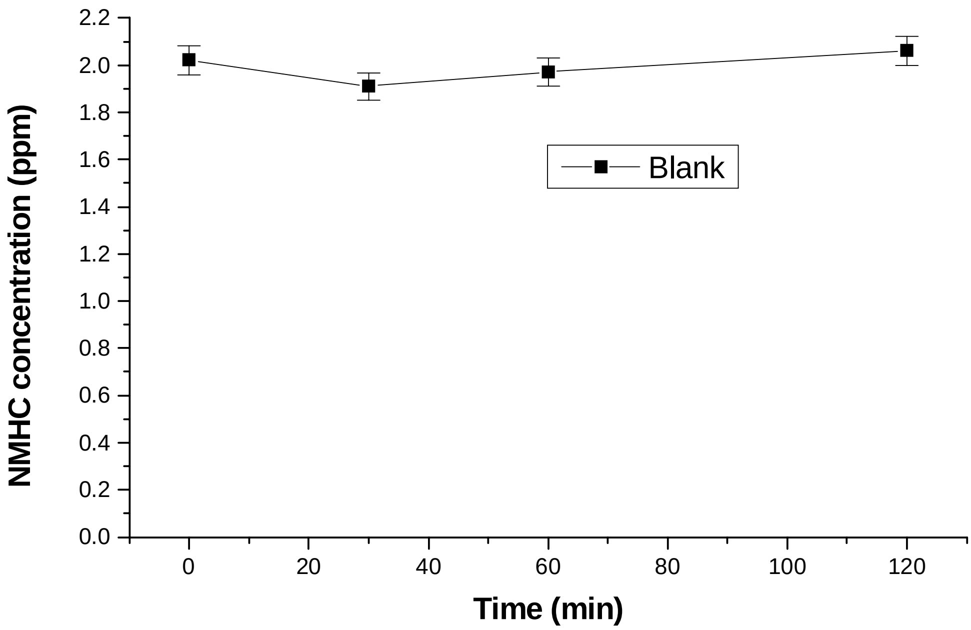

Figure 7.2 Leakage test of the environmental chamber using toluene.

7.2.2 NO removal by the air cleaner without TiO_2 and TiO_2/AC filter

The original setting (AC+HEPA) of the air cleaner was evaluated to identify the removal of NO. This evaluation is vital as to truly investigate the removal efficiency of TiO_2 filter and TiO_2/AC filter mounted on the air cleaner despite the removal efficiency of the AC+HEPA. Fig. 7.3 shows three settings of the air cleaner namely AC+HEPA, AC+HEPA+UVA and AC+HEPA+UVC. The NO concentration decreased from 200 ppb to 175 ppb at 60 min using AC+HEPA. However, the NO concentration increased back to around the initial concentration at 120 min. Presumably, the initial decrease of the NO concentration is due to the NO adsorption capacity of the activated carbon filter (Teng and Suuberg; 1993). The increase in NO concentration is probably due to the release of NO from the AC filter. Desorption of pollutant was also reported from AC filter (Schleibinger and Ruden; 1999). Similar result was observed for AC+HEPA+UVA setting. The NO concentration decreased at 60 min but increased to the initial concentration at 120 min. The use of UVA lamp was not able to remove NO, as reported in other studies (Devahasdin et al., 2003). Using UVC lamp instead of UVA lamp, however, a decrease of 25 ppb NO was observed at 120 min. Since the wavelength of the UVC lamp ranged from 200 nm to 300 nm, it included the commencement (Flory and Johnston, 1935) of the NO adsorption band and thus a reduction in NO concentration was observed.

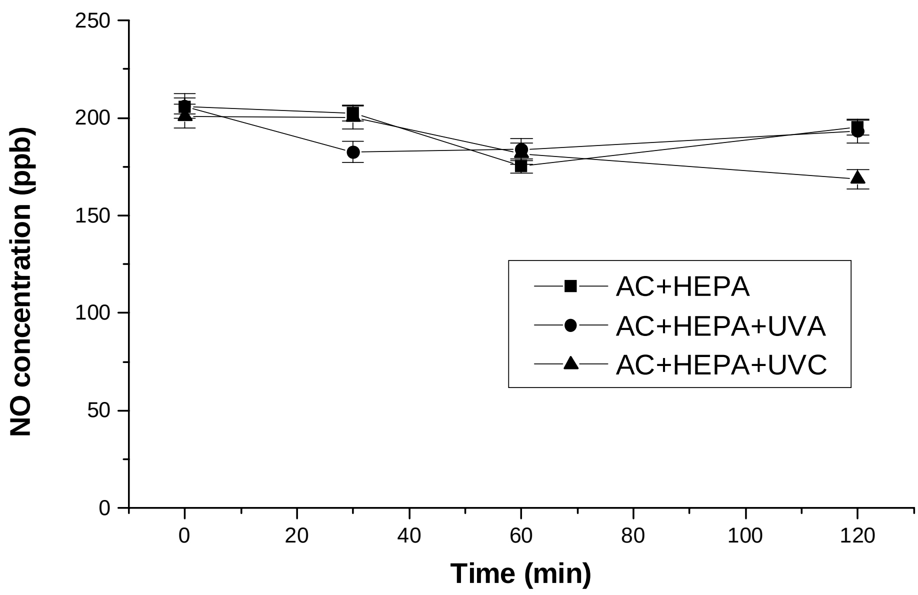

Figure 7.3 NO removal using the air cleaner settings.

7.2.3 NO removal of the air cleaner with TiO_2 filter using UVA and UVC lamp

Fig. 7.4 shows the photodegradation of NO using UVA lamp and UVC lamp. The time profile of NO photodegradation is identical using UVA lamp and UVC lamp. However, a higher NO removal was observed for UVC lamp. The NO concentration at 120 min using UVA lamp is 34.6 ppb, which is 12.6 ppb higher than using UVC lamp. This is probably due to a higher UV intensity was applied using UVC lamp. The measured UV intensity of UVC lamp (2.76 mW/cm^2) was nearly double than that using UVA lamp (1.49 mW/cm^2). Thus, at a higher UV intensity, more hydroxyl radicals were generated (Li et al., 1998; Kim and Hong, 2002) to react with NO and a higher NO removal was achieved. In addition, study (Matthews and McEvoy, 1992) also showed that TiO_2 particles adsorbed light more strongly for shorter wavelength than longer wavelength and reduced time participating in energy wasting recombination reactions.

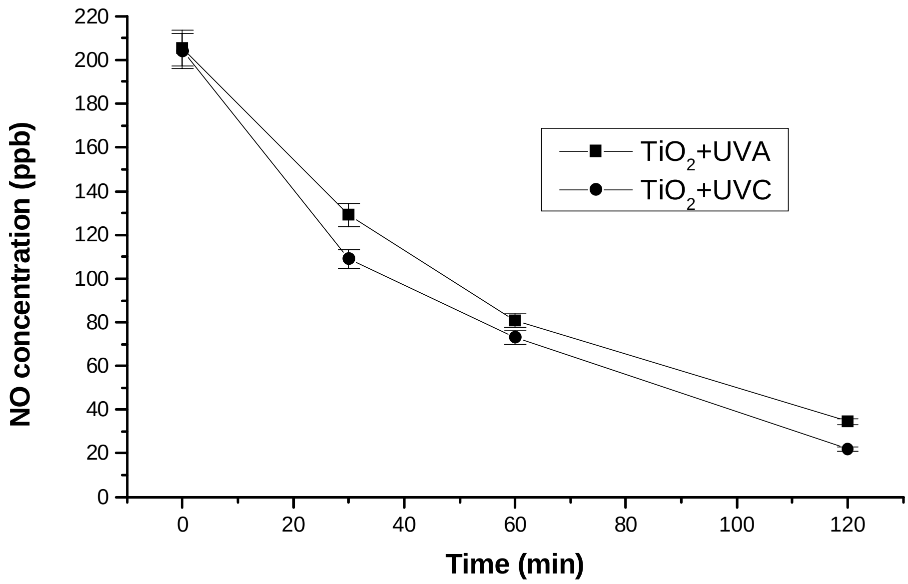

Figure 7.4 NO removal using TiO_2 filter with UVA lamp and UVC lamp.

7.2.4 NO removal of the air cleaner with TiO_2 filter and TiO_2/AC filter

Fig. 7.5 shows the photodegradation of NO using TiO_2 filter and TiO_2/AC filter. The NO concentration at 120 min was 34.6 ppb and 6.3 ppb using TiO_2 filter and TiO_2/AC filter, respectively. Also shown in the same figure, the NO concentration reached a steady state at 60 min whereas the NO concentration using TiO_2 filter was still decreasing. Under such a small residence time and low NO concentration, the probability of NO contact with the hydroxyl radicals is rather low (Shiraishi et al., 2003). The use of activated carbon is to increase the adsorption of NO. The adsorbed NO is then transferred to TiO_2 for photodegradation. Study using TiO_2/AC filter in the photoreactor also showed that the effect of using activated carbon filter as supporting substrate is more significant at a lower residence time. At a high residence time, the pollutant diffusion rate from the gaseous phase to TiO_2 is similar to the pollutant diffusion rate from the activated carbon filter to TiO_2. However, when such a high residence time is not applicable such as the air cleaner, the enhancement effect of using the activated carbon as the supporting substrate for TiO_2 is more significant than in the photoreactor.

Another possible reason for the higher NO removal using TiO_2/AC filter is the high relative humidity level used in this study. Water vapor competed with NO for adsorption sites on TiO_2 which reduced the NO removal rate. Studies also showed that the oxidation rate decreased with increasing humidity levels for toluene (Cao et al., 1999) acetone (Kim and Hong, 2002), and 1-Butene (Cao et al., 2000). The above authors elucidated that water molecules competed with pollutants for adsorption sites on TiO_2 surfaces. Study also showed that the TiO_2 surface is full of hydroxyl groups which adsorbed water via hydrogen bond. Benzene and toluene, for instance, adsorbed stronger on dehydroxylated surface than hydroxyl surface (Nagao and Suda, 1999). Although at high humidity levels, water competed with NO for adsorption sites on TiO_2 and activated carbon, the large adsorption capacity of the activated carbon still able to adsorb NO because its surface area is 24 times larger than TiO_2. The adsorbed NO was then diffused to the TiO_2 for photodegradation. Using TiO_2 only for indoor air purification at ppb level pollutant concentration, NO competed with water for adsorption sites and the probability of contacting the hydroxyl radials is low. Thus, the application of TiO_2/AC filter showed a promising and efficient method for indoor air purification.

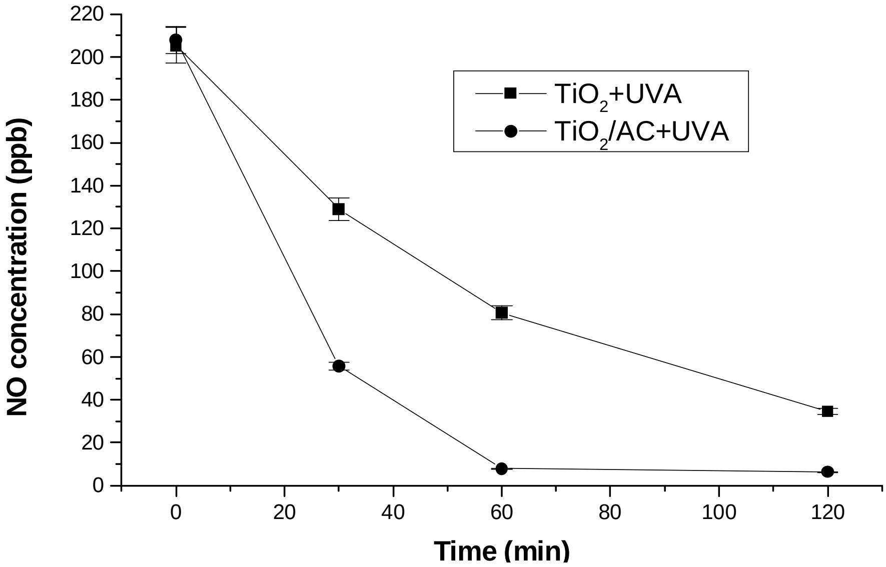

Figure 7.5 NO removal using TiO_2 filter and TiO_2/AC filter.

7.2.5 Intermediate generated from the photodegradation of NO

Studies (Hashimoto et al., 2001; Nakamura et al., 2000; Dalton et al., 2002) showed that NO_2 is the intermediate generated from the photodegradation of NO, as shown in equation (7.1) and (7.2):

$$NO + HO_2\cdot \rightarrow NO_2 + OH\cdot \qquad (7.1)$$

$$NO_2 + OH\cdot \rightarrow HNO_3 \qquad (7.2)$$

In this study, NO_2 was also observed as the intermediate from the photodegradation of NO. As shown in Fig. 7.6, around 6 ppb of NO_2 was observed as the background concentration inside the environmental chamber. The NO_2 concentration decreased from 7.9 ppb to 3.6 ppb at 120 min for the AC+HEPA setting. The decrease in NO_2 concentration is probably due to the adsorption of NO_2 on the AC filter (Rubel and Stencel, 1996). However, using TiO_2 filter with UVA lamp, the NO_2 concentration increased from 7 ppb to 26 ppb. Using TiO_2/AC filter, the NO_2 concentration increased slightly from 7.1 ppb to 9.2 ppb at 30 min. The NO_2 concentration then decreased to 3.2 ppb at 120 min. The large discrepancy of NO_2 concentration generated is due to the difference in using TiO_2 and TiO_2/AC. According to equations 7.1 and 7.2, NO_2 generated from the photodegradation of NO would further photo-oxidized to HNO_3. The residence time of the air cleaner provided was too low and NO_2 exited the air cleaner without further photodegradation. Using TiO_2/AC filter, however, the activated carbon provided another adsorption site for NO_2. Similar to NO, NO_2 adsorbed on AC is then diffused to TiO_2 and photo-oxidized to HNO_3. Study (Torimoto et al., 1996) also showed that the combination of TiO_2 with adsorbent not only increased the propyzamide removal rate but also reduced the amount of intermediate exited the system.

To accurately and truly evaluate the removal efficiency of NO using TiO_2 and TiO_2/AC filter mounted in the air cleaner, the following equation is used.

$$NO_x \text{ removal efficiency} = \frac{\text{Initial } NO_x \text{ conc. - final } NO_x \text{ conc.}}{\text{Initial } NO_x \text{ conc.}} \times 100\% \qquad (7.3)$$

where initial NO_x concentration is the initial NO and NO_2 concentration inside the environmental chamber and the final NO_x concentration is the NO and NO_2 concentration inside the environmental chamber at 120 min. The use of NO_x rather than merely NO for the pollutant removal efficiency evaluation because NO_2 generated from the photodegradation of NO is also a common indoor air pollutant (Jones, 1999). By applying equation 7.3, the NO_x removal efficiency using TiO_2 filter and TiO_2/AC filter is 70.5% and 95.4%, respectively. Thus, the use of TiO_2/AC filter not only increased the NO (target pollutant) removal rate but also reduced the generation of NO_2 (intermediate).

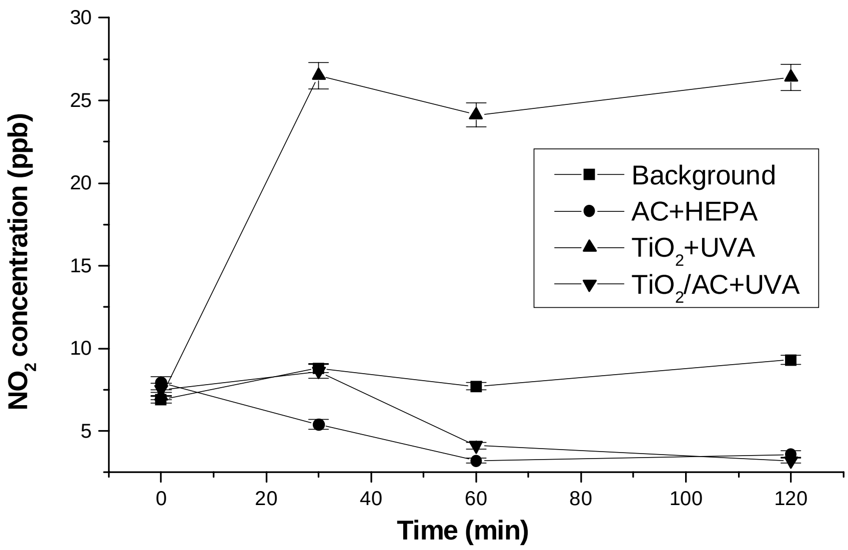

Figure 7.6 Intermediate generated from the photodegradation of NO under different experimental conditions.

7.2.6 Toluene removal of the air cleaner with TiO_2 filter and TiO_2/AC filter

Fig. 7.7 shows the photodegradation of toluene using the AC+HEPA, TiO_2 filter and TiO_2/AC filter with the UVA lamp. The use of AC+HEPA setting of the air cleaner decreased the NMHC concentration from 2.12 ppm to 1.48 ppm. This is probably due to adsorption of toluene on the activated carbon filter, as reported in other studies (Urano et al., 1982; VanOsdell et al., 1996). However, the toluene removal is lower compared to TiO_2+UVA and TiO_2/AC+UVA. At a relative humidity higher than 60%, capillary condensation of water vapor occurred within the pores of activated carbon and making them unavailable for organic vapor adsorption (Cal et al., 1996; Khan and Ghoshal, 2000). Since the experiment was conducted at a relative humidity of 70%, the competition of adsorption sites on activated carbon between water vapor and toluene reduced its removal efficiency. Similar to the photodegradation of NO, the use of TiO_2/AC filter achieved a lower NMHC concentration. The NMHC concentration was 1.06 and 0.23 ppm using the TiO_2 filter and TiO_2/AC filter, respectively. The toluene removal efficiency difference between the TiO_2 filter and the TiO_2/AC filter was larger than NO removal efficiency. As shown in Table 7.1, the difference in NMHC removal efficiency is 49.5% whereas only 13.8% in NO removal efficiency is observed. Similar results were reported previously using the laboratory scale reactor. The high NO removal efficiency by the TiO_2 filter might hinder the enhancement effect of the TiO_2/AC filter. Using a less photoreactive compound such as toluene, the enhancement effect of the TiO_2/AC filter is more significant, as shown in this study. However, under the presence of other pollutants, such as hydrocarbons, the removal rate of NO is reduced due to competition of adsorption sites on TiO_2. Thus, the difference in NO removal efficiency between using TiO_2 filter and TiO_2/AC filter will be higher if other pollutants are presence.

Pollutant	TiO_2 filter removal efficiency (%)	TiO_2/AC filter removal efficiency (%)
NO (ppb)	83.2	97.0
NO_x (ppb)	70.5	95.4
NMHC (ppm)	50.0	89.5

Table 7.1 NO, NO_x and NMHC removal efficiency using TiO_2 filter and TiO_2/AC filter.

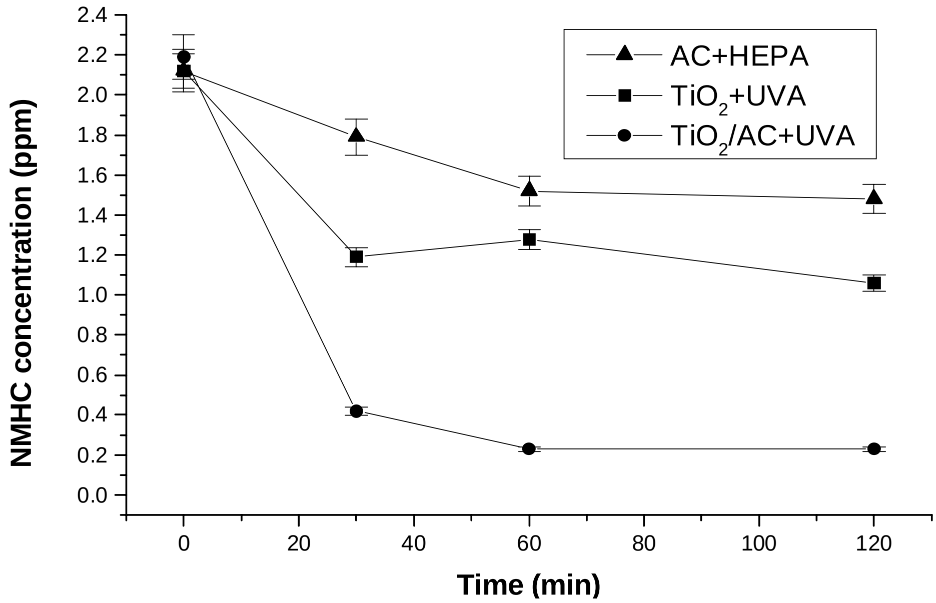

Figure 7.7 Toluene removal by the air cleaner with AC+HEPA, TiO_2 filter and TiO_2/AC filter.

7.3 *Indoor air pollutants removal via air duct installed with TiO_2/AC filter*

7.3.1 *Background concentrations inside the office*

The background concentration of the target pollutants are shown in Table 7.2. The sampling was conducted for 3 days with 1 morning and 1 afternoon session. During the sampling, the activity inside the office was not affected. Since the pollutant concentrations did not vary tremendously between locations (Fig. 3.19), only the average concentrations of the sampling locations are shown. In general, the pollutant concentration in this office is low.

Date	Session	Average NO (ppb)	Average NO_2 (ppb)	Average NMHC (ppm)	Average air borne bacteria (cfu/m^3)
1	Morning	68.8	2.4	0.69	248
1	Afternoon	75.2	3.1	0.53	183
2	Morning	78.6	2.5	0.67	210
2	Afternoon	53.7	3.9	0.60	327
3	Morning	124.5	3.4	1.10	247
3	Afternoon	58.3	3.5	1.10	201
Average		***76.5***	***3.1***	***0.78***	***236***

Table 7.2 Background pollutant concentrations inside the office.

7.3.2 *Pollutant concentrations after installing TiO_2/AC filter inside the air duct*

Table 7.3 shows the pollutant concentrations after installing the TiO_2/AC filter. All pollutants concentration decreased after installing the TiO_2/AC filter. As shown in Table 7.4, the amount of NO only reduced by 3.4% and the result is not significant. The percentage of reduction is calculated by the following formula:

$$\% \text{ Reduced} = \frac{\text{Background concentration - Concentration after installing APS}}{\text{Background concentration}} x100\%$$

This is probably due to the scale of the TiO_2/AC filter is not sufficient to handle the large amount of pollutant to be treated at a given period of time. Inside the office, there are 4 air handling units but only 1 TiO_2/AC filter was installed due to on-site installation problem. Nevertheless, a decrease of all the target pollutant concentration was observed after the installation of the TiO_2/AC filter. It is anticipated that the pollutant removal efficiency will be increased if all the 4 air handling units are installed with the TiO_2/AC filter.

Date	Session	Average NO (ppb)	Average NO_2 (ppb)	Average NMHC (ppm)	Average air borne bacteria (cfu/m^3)
1	Morning	60.9	1.8	0.72	226
1	Afternoon	37.4	0.2	0.63	181
2	Morning	76.3	2.2	0.47	239
2	Afternoon	123.7	3.0	0.40	179
3	Morning	88.1	2.6	0.70	122
3	Afternoon	57.1	3.1	1.10	167
Average		***73.9***	***2.2***	***0.67***	***186***

Table 7.3 Pollutant concentrations inside the office after installing the TiO_2/AC filter.

	Average NO (ppb)	Average NO_2 (ppb)	Average NMHC (ppm)	Average air borne bacteria (cfu/m^3)
Before installation of TiO_2/AC filter	76.5	3.1	0.78	236
After installation of TiO_2/AC filter	73.9	2.2	0.67	186
% Reduced	***3.4%***	***29.0%***	***14.1%***	***21.2%***

Table 7.4 Pollutant concentrations inside the office after installing the TiO_2/AC filter.

Another possible reason for the low removal pollutant efficiency observed inside the office compared to the air cleaner and the large circulation air duct is the dust loading. Although pre-filter was installed in the fresh air intake of the building, dust generating activity such as smoking was observed inside the office. Once the dust is imposed on the TiO_2/AC filter, it impaired the illumination of the UV lamp on the TiO_2 surface.

7.4 Summary

A commercial air cleaner installed with a TiO_2 filter and a TiO_2/AC filter was evaluated inside an environmental chamber. Leak test showed that no pollutant removal was due to chamber leakage. The original setting (AC+HEPA) of the air cleaner showed no NO and little toluene removal. The use of TiO_2 filter removed 83.2% of NO but generated 12.9% of NO_2. Using TiO_2/AC filter, the NO removal efficiency increased to 97% and the generation of NO_2 decreased to

1.6%. The use of TiO_2/AC filter not only increased the target pollutant removal efficiency but also reduced the amount of intermediate exiting the system. The removal efficiency of the TiO_2/AC filter compared to the TiO_2 filter is even higher when the target pollutant is less photoreactive, such as toluene, used in this study. Thus, under a low residence time, low pollutant concentration and high levels of relative humidity, the use of TiO_2/AC filter showed a promising and efficient method for indoor air purification. This study also showed that the enhancement effect of the TiO_2/AC filter shown in the laboratory scale using the photoreactor is also verified by installing it into an air cleaner available in the commercial market.

The installation of the TiO_2/AC filter inside the air duct of an office has successfully reduced the pollutants concentration. The conversion, however, is not as significant as the air cleaner. This is probably due to a higher dust loading was observed inside the office. The deposition of dust by the return air impaired the illumination of UV light on the TiO_2 surface. Owing to the on-site air duct problem, only 1 TiO_2/AC filter was installed for 4 air handing unit. The pollutant removal efficiency will be higher if more TiO_2/AC filter is installed inside the air duct.

Chapter 8 Conclusion

The use of photocatalysis for indoor air purification was evaluated by using typical indoor air pollutants namely nitrogen monoxide (NO), nitrogen dioxide (NO_2), carbon monoxide (CO), sulfur dioxide (SO_2), benzene, toluene, ethylbenzene and o-xylene (BTEX, most abundant VOCs), and formaldehyde (HCHO) with reference to their typical indoor concentration. The selected target pollutants are most commonly found in indoor environment.

Sensitive analyses for the above pollutants were conducted under different initial pollutant concentrations, residence time and humidity levels. NO, NO_2, BTEX and HCHO were photo-oxidized but no reaction was observed for CO and SO_2. However, sulfate ion was detected under the presence of SO_2. The effect of initial concentrations on NO and HCHO was not significant, whereas the conversions of BTEX increased with increasing initial BTEX concentrations. The pollutants conversion decreased with decreasing residence time and with increasing humidity levels. The increasing humidity levels affected the conversion most significantly and adversely compared to the effect of initial pollutant concentrations and residence time. Amount all the target pollutants, the conversions of BTEX are the lowest and its most significantly affected by the humidity levels. Deactivation was only observed from the photodegradation of NO.

The reciprocal effects between different pollutants were evaluated by the photodegradation of multiple pollutants simultaneously. Since no reaction was found for CO, it has no interaction with other pollutants during photodegradation. The formation of sulfate ion under the presence of SO_2 inhibited the conversions of NO, BTEX and HCHO. NO_2, as an intermediate generated from the photodegradation of NO, also increased under the presence of SO_2. The presence of sulfate ion competed with other pollutants for adsorption site and thereby decreased its conversion. Similarly, the presence of BTEX inhibited the conversion of NO, NO_2 and HCHO. Intermediate such as benzaldehyde and benzyl alcohol was detected from the photodegradation of BTEX. These intermediates block the active sites of the photocatalyst and reduced the conversion of other pollutants simultaneously presence. On the contrary, the presence of NO promoted the conversions of BTEX and HCHO. The promotion effect of NO was achieved by the OH radicals generated from the photodegradation of NO. Similar to the photodegradation of NO, the presence of HCHO also promoted the conversion of NO and BTEX.

In order to rectify the high humidity levels problem, TiO_2 was synthesized by sol-gel method to modify its physical and chemical properties. Photocatalyst with a higher BET surface area was found to have a higher conversion under different levels of humidity. The increase in conversion is most significant at high humidity levels.

Although the increase in BET surface area of the photocatalyst is a feasible method, the conversion is not high enough for practical application. TiO_2 was then loaded on activated carbon filter (TiO_2/AC filter) to increase the adsorption of the pollutant. The increase in pollutant conversion, especially at high humidity levels and the presence of inhibitory pollutants such as BTEX and SO_2, is most significant. Using TiO_2/AC filter compared to TiO_2 filter under the presence of SO_2, the conversion of NO increased by 10% and the generation of NO_2 decreased by more than 20%. A 50% increase of benzene removal was observed using TiO_2/AC filter compared to using TiO_2 filter only. Deactivation was also eliminated using TiO_2/AC filter during the photodegradation of NO.

In order to test the TiO_2/AC filter for practical use, the TiO_2/AC filter was installed in a commercial air cleaner and tested inside an environmental chamber. The use of TiO_2 filter removed 83.2% of NO but generated 12.9% of NO_2. Using TiO_2/AC, the NO removal efficiency increased to 97% and the generation of NO_2 decreased to 1.6%. The use of TiO_2/AC filter not only increased the target pollutant removal efficiency but also reduced the amount of intermediate exiting the system. The removal efficiency of the TiO_2/AC filter compared to the TiO_2 filter is even higher when the target pollutant is less photoreactive, such as toluene, used in this study. It is worthwhile to note that the enhancement effect of the TiO_2/AC filter shown in the laboratory scale using the photoreactor is also verified by installing it into an air cleaner available in the commercial market.

The installation of the TiO_2/AC filter inside the air duct of an office has successfully reduced the pollutants concentration. The conversion, however, is not as high as the air cleaner. This is probably due to a higher dust loading was observed inside the office. The deposition of dust by the return air impaired the illumination of UV light on the TiO_2 surface. Owing to the on-site air duct problem, only 1 TiO_2/AC filter was installed for 4 air handing unit. The pollutant removal efficiency will be higher if more TiO_2/AC filters are installed inside the air ducts.

To alleviate the dust deposition problem, a novel liquid phase deposition (LPD) method was used to coat TiO_2 on stainless steel surface. The TiO_2 thin film was calcinated at different temperatures. When calcination temperature was below 400^oC, there was no photocatalytic activity observed because the TiO_2 thin film was composed of amorphous TiO_2 or the amount of anatase TiO_2 in the film was too low. With increasing calcination temperature, the photocatalytic activity increased due to the enhancement of crystallization of anatase and the increase of Fe^{3+} concentration in the thin film. At 500^{o}C, the film showed the highest photocatalytic activity. This was ascribed to the fact that an optimal Fe^{3+} concentration was obtained in the film, which reduced the recombination of photogenerated free carriers. At 700^{o}C, the photocatalytic activity of the film decreased. This was due to the fact that the increase of Fe^{3+} content in the film due to the diffusion of Fe^{3+} ions from the surface of stainless steel, which exceeded an optimal Fe^{3+} dopant concentration, and Fe^{3+} ions steadily became recombination centers of photo-generated electrons and holes. At 900^{o}C, the TiO_2 thin film showed the lowest photocatalytic activity. This is attributed to the results of the further increase of Fe^{3+} concentration, the phase transformation from the anatase to rutile and the sintering and growth of TiO_2 crystallites. The stainless steel coated with TiO_2 will be made in a monolith with it longitudinal direction parallel to the flow direction to reduce the dust deposition.

The use of TiO_2/AC filter is feasible to apply for practical application such as air cleaner. It is especially suitable to be used in Hong Kong where high humidity levels are always encountered. More work is still needed to achieve a higher performance for installation in the air duct. Photocatalyst fabricated in a monolith form may be able to reduce the dust deposition problem on the photocatalyst.

References:

1. Abdullah, M., Low, G.K.C., Matthews, R.W., 1990. Effects of common inorganic anions on rates of photocatalytic oxidation of organic-carbon over illuminated titanium-dioxide. *Journal of Physical Chemistry* 94, 6820-6825.
2. Akland, G.G., Hartwell, T.D., Johnson, T.R., Whitmore, R.W., 1985. Measuring human exposure to carbon monoxide in Washington, D.C., and Denver, Colorado, during the winter of 1982-1983. *Environmental Science and Technology* 19, 911-918.
3. Alberici, R.M., Jardim, W.F., 1997. Photocatalytic destruction of VOCs in the gas-phase using titanium dioxide. *Applied Catalysis B: Environmental* 14, 55-68.
4. Albert, W.M., 1994. Indoor air pollution: NO, NO_2, CO and CO_2. *Journal of Allergy Clinic Immunology* 94, 289-295.
5. Al-Ekabi, H., Serpone, N., 1988. Kinetics studies in heterogeneous photocatalysis. I Photocatalytic degradation of chlorinated phenols in aerated aqueous solutions over titania supported on a glass matrix. *Journal of Physical Chemistry* 92, 5726-5731.
6. Al-Rehaili, A.M., 2002. Outdoor-indoor air quality in Riyadh: SO_2, NH_3, and HCHO. *Environmental Monitoring and Assessment* 79, 287-300.
7. Ameen, M.M., Raupp, G.B., 1999. Reversible Catalyst Deactivation in the photocatalytic Oxidation of Dilute o-xylene in Air. *Journal of Catalysis* 184, 112-122.
8. Anderson L.G., Lanning, J.A., Barrell, R., Miyagishima, J., Jones, R.H., Wolfe, P., 1996. Sources and sinks of formaldehyde and acetaldehyde:

An analysis of Denver's ambient concentration data. *Atmospheric Environment* 30, 2113-2123.

9. Anderson, I., Lundquist, G.R., Molhave, L., 1975. Indoor air pollution due to chipboard used as a construction material. *Atmospheric Environment* 9, 1121-1127.

10. Anpo, M., Chiba, K., Tomonari, M., Coluccia, S., Che, M., Fox, M.A. 1991. Photocatalysis on Native and Platinum-Loaded TiO_2 and ZnO Catalysts-Origin of Different Reactivities on Wet and Dry Metal-Oxides. *Bulletin of the Chemical Society of Japan* 64, 543-551.

11. Ao, C.H., Lee, S.C., 2003. Enhancement effect of TiO_2 immobilized on activated carbon filter for the photodegradation of pollutants at typical indoor air level. *Applied Catalysis B: Environmental* 43, 191-205.

12. Ao, C.H., Lee, S.C., 2004. Combination effect of activated carbon with TiO_2 for the photodegradation of binary pollutants at typical indoor air level. *Journal of Photochemistry and Photobiology A: Chemistry* 161, 131-140.

13. Ao, C.H., Lee, S.C., Mak, C.L., Chan, L.Y., 2003. Photodegradation of volatile organic compounds (VOCs) and NO for indoor air purification using TiO_2: promotion versus inhibition effect of NO. *Applied Catalysis B: Environmental* 42, 119-129.

14. Ao, C.H., Lee, S.C., Yu, J.C., 2003. Photocatalyst TiO_2 supported on glass fiber for indoor air purification: effect of NO on the photodegradation of CO and NO_2. *Journal of Photochemistry and Photobiology A: Chemistry* 156, 171-177.

15. Arana, J., Diaz, O.G., Saracho, M.M., Rodriguez, J.M.D., Melian, J.A.H., Pena, J.P., 2001. Photocatalytic degradation of formic acid using Fe/TiO_2 catalysts: the role of Fe^{3+}/Fe^{2+} ions in the degradation mechanism. *Applied Catalysis B-Environmental* 32, 49-61.

16. Arana. I, Dona-Rodriguez, J.M., Rendon, E.T., Cabo, C.G.I., Gonzalez-Diaz, O., Herrera-Melian, J.A., Perez-Pena, J., Colon, G., Navio, J.A., 2003. TiO_2 activation by using activated carbon as a support - Part II. Photoreactivity and FTIR study. *Applied Catalysis B-Environmental* 44, 153-160.

17. Arnts, R.R., Tejada, S.B., 1989. 2,4-dinitrophenylhydrazine-coated silica-gel cartridge method for determination of formaldehyde in air - identification of an ozone interference. *Environmental Science and Technology* 23, 1428-1430.

18. Atkinson, R., 1990. Gas-Phase Tropospheric Chemistry of Organic-Compounds - A Review. *Atmospheric Environment Part A-General Topics* 24, 1-41.

19. Atkinson, R., Aschmann, S.M., 1994. Products of the Gas-Phase Reactions of Aromatic-Hydrocarbons - Effect of NO_2 Concentration. *International Journal of Chemical Kinetics* 26, 929-944.

20. Atkinson, R., Aschmann, S.M., Arey, J., Carter, W.P.L., 1989. Formation of Ring-Retaining Products from the OH Radical-Initiated Reactions of Benzene and Toluene. *International Journal of Chemical Kinetics* 21, 801-827.

21. Baker, M.D., Henretig, F.M., Ludwig, S., 1988. Carboxyhemoglobin Levels in Children with Nonspecific Flu-Like Symptoms. *Journal of Pediatrics* 113, 501-504.

22. Balasubramanian, G., Dionysiou, D.D., Suidan, M.T., Subramanian, Y., Baudin, I., Laine, J.M.., 2003. Titania powder modified sol-gel process for photocatalytic applications. *Journal of Materials Science* 38, 823-831.

23. Bardana, E.J., 1997. Sick building syndrome - a wolf in sheep's clothing. *Annals of Allergy Asthma & Immunology* 79, 283-293.

24. Blake, D.M., 2001-1994. Bibliography of Work on Photocatalytic Removal of Hazardous Compounds from Water and Air, National Renewable Energy Laboratory, Golden, U.S. (www.nrel.gov/biomass/renew_efficient.html).

25. Blake, N.R., Griffin, G.L., 1988. Selectivity Control during the Photoassisted Oxidation of 1-Butanol on Titanium-Dioxide. *Journal of Physical Chemistry* 92, 5697-5701.

26. Blanco, J., Avila, P., Bahamonde, A., Alvarez, E., Sanchez, B., Romero, M., 1996. Photocatalytic destruction of toluene and xylene at gas phase on a titania based monolithic catalyst. *Catalysis Today* 29, 437-442.

27. Boer, K.W. Survey of Semiconductor Physics. Van Nostrand Reinhold, New York, p 249.

28. Boubel, R.W., Fox, D.L., Turner, D.B., Stern, A.C., Fundamentals of Air Pollution, Academic Press, London, 1994, p. 150

29. Brauer, M., Rasmussen, T.R., Kargarrd, S.K., Spengler, J.D., 1993. Nitrous acid formation in an experimental exposure chamber. *Indoor Air* 3, 94-105.

30. Breysse, P.A., 1984. Formaldehyde levels and accompanying symptoms associated with individuals residing in over 1000 conventional and mobile homes in the state of Washington. *Indoor Air* 3, 403-408.

31. Brinker, C.J., Scherer, G.W., 1990. Sol-Gel Science: The Physics and Chemistry of Sol-Gel Processing. Academic press, London, p.2.

32. Burns, R.A., Crittenden, J.C., Hand, D.W., Selzer, V.H., Sutter, L.L., Salman, S.R., 1999. Effect of inorganic ions in heterogeneous photocatalysis of TCE. *Journal of Environmental Engineering-ASCE* 125, 77-85.

33. Burr, M.L., 1997. Health effects of indoor combustion products. *Journal of the Royal Society of Health* 117, 348-350.

34. Burr, M.L., St-Leger, A.S., Yarnell, J.W.G., 1981. Wheezing, dampness, and coal fires. *Community Medicine* 3, 205-209.

35. Burton, B.T., 1997. Volatile organic compounds. In: Bardana, E.J., Montanaro, A. (Eds.), Indoor Air Pollution and Health. Marcel Dekker, New York, pp. 127-153.

36. Butkovskaya, N.I., Setser, D.W., 1998. Infrared chemiluminescence study of the reactions of hydroxyl radicals with formaldehyde and formyl radicals with H, OH, NO, and NO_2. *Journal of Physical Chemistry A* 102, 9715-9728.

37. Cal, M.P., Rood, M.J., Larson, S.M., 1996. Removal of VOCs from humidified gas streams using activated carbon cloth. *Gas Separation & Purification* 10, 117-121.

38. Canela, M.C., Alberici, R.M., Jardim, W.F., 1998. Gas-phase destruction of H_2S using TiO_2/UV-VIS. *Journal of Photochemistry and Photobiology A: Chemistry* 112, 73-80.

39. Cao, L., Gao, Z., Suib, S.L., Obee, T.N., Hay, S.O., and Freihauty, J.D., 2000. Photocatalytic oxidation of toluene on nanoscale TiO_2 catalysts: studies of deactivation and regeneration. *Journal of Catalysis* 196, 253-261.

40. Cao, L., Huang, A., Spiess, F.J., Suib S.L., 1999. Gas-Phase Oxidation of 1-Butene Using Nanoscale TiO_2 Photocatalysts. *Journal of Catalysis* 188, 48-57.

41. Carlier, P., Hannachi, H., Mouvier, G., 1986. The Chemistry of Carbonyl-Compounds in the Atmosphere - A Review. *Atmospheric Environment* 20, 2079-2099.

42. Carrer, P., Maroni, M., Alcini, D., Cavallo, D., Fustinoni, S., Lovato, L., Visigalli, F., 2000. Assessment through environmental and biological measurements of total daily exposure to volatile organic compounds of office workers in Milan, Italy. *Indoor Air* 10, 258-268.

43. Chan, C.C., Yanagisawa, Y., Spengler, J.D. 1990. Personal and Indoor Outdoor Nitrogen-Dioxide Exposure Assessments of 23 Homes in Taiwan. *Toxicology and Industrial Health* 6, 173-182.

44. Chao, C.H.Y., 2001. Comparison between indoor and outdoor air contaminant levels in residential buildings from passive sampler study. *Building and Environment* 36, 999-1007.

45. Chao, C.Y., Chan, G.Y., 2001. Quantification of indoor VOCs in twenty mechanically ventilated buildings in Hong Kong. *Atmospheric Environment* 35, 5895-5913.

46. Chen, H.Y., Zahraa, O., Bouchy, M., 1997. Inhibition of the adsorption and photocatalytic degradation of an organic contaminant in an aqueous suspension of TiO_2 by inorganic ions. *Journal of Photochemistry and Photobiology A: Chemistry* 108, 37-44.

47. Cheremisinoff, P.N., Ellerbusch, F. (Ed.), Carbon adsorption handbook, Ann Arbor Science Publishers, Michigan, 1980.

48. Cho, K.C., Hwang, K.C., Sano, T., Takeuchi, K., Matsuzawa, S., 2004. Photocatalytic performance of Pt-loaded TiO_2 in the decomposition of gaseous ozone. *Journal of Photochemistry and Photobiology A: Chemistry* 161, 155-161.

49. Cohen, R. C.; Murphy, J. G., 2003. Photochemistry of NO_2 in Earth's Stratosphere: Constraints from Observations. *Chemical Reviews* 103, 4985-4998.

50. Colon, G., Hidalgo, M.C., Navio, J.A., 2003. Photocatalytic behavior of sulphated TiO_2 for phenol degradation. *Applied Catalysis B-Environmental* 45, 39-50.

51. Cooper, J.A., 1980. Environmental impact of residential wood combustion emissions and its implications. *Journal of the Air Pollution Control Association* 30, 855-861.

52. Coultas, D.B., Lambet, W.E., 1991. Carbon monoxide. In: Sanet, J.M., Spengler, J.D. (Eds.), Indoor Air Pollution: A Health Perspective. Johns Hopkins University Press, Baltimore, MD, pp. 187-208.

53. Cunningham, J., Hodnett, B.K., 1981. Kinetic-Studies of Secondary Alcohol Photooxidation on ZnO and TiO_2 at 348-K Studied by Gas-Chromatographic Analysis. *Journal of the Chemical Society-Faraday Transactions I* 77, 2777-2801.

54. Cunningham, J., Srijaranai, S., 1991. Sensitized photo-oxidations of dissolved alcohols in homogenous and heterogeneous systems Part 2. TiO_2-sensitized photodehydrogenations of benzyl alcohol. *Journal of Photochemistry and Photobiology A: Chemistry* 58, 361-371.

55. Daisey, J.M., Hodgson A.T., Fisk, W.J., Mendell, M.J., Tenbrinke, J., 1994. Volatile Organic-Compounds in 12 California Office Buildings - Classes, Concentrations and Sources. *Atmospheric Environment* 28, 3557-3562.

56. Dalton J.S., Janes, P.A., Jones, N.G., Nicholson, J.A., Hallam, K.R., Allen, G.C., 2002. Photocatalytic oxidation of NO_x gases using TiO_2: a surface spectroscopic approach. *Environmental Pollution* 120, 415-422.

57. Deki, S., Aoi, Y., Hiroi, O., Kajinami, A., 1996. Titanium (IV) Oxide Thin Films Prepared from Aqueous Solution. *Chemistry Letters* 433-434.

58. Deki, S., Aoi, Y., Kajinami, A., 1997. A novel wet process for the preparation of vanadium dioxide thin film. *Journal of Materials Science* 32, 4269-4273.

59. Deki, S., Aoi, Y., Okibe, J., Yanagimoto, H., Kajinami, A., Mizuhata, M., 1997a. Preparation and characterization of iron oxyhydroxide and iron oxide thin films by liquid-phase deposition. *Journal of Materials Chemistry* 7, 1769-1772.

60. Deki, S., Aoi, Y., Yanagimoto, H., Ishii, K., Akamatsu, K., Mizuhata, M.,Kajinami, A., 1996a. Preparation and characterization of Au-dispersed TiO_2 films by a liquid-phase deposition method. *Journal of Materials Science* 6, 1879-1882.

61. Deki, S., Iizuka S., K., Akamatsu, Mizuhata, M., Kajinami, A., 2001. Novel fabrication method for $Si_{1-x}Ti_xO_2$ thin films with graded composition profiles by liquid phase deposition. *Journal of Materials Chemistry* 11, 984-986.

62. Devahasdin, S., Fan, C., Li, K., Chen, D.H., 2003. TiO_2 photocatalytic oxidation of nitric oxide: transient behavior and reaction kinetics. *Journal of Photochemistry and Photobiology A: Chemistry* 156, 161-170.

63. d'Hennezel, O., Ollis, D.F., 1997. Trichloroethylene-promoted photocatalytic oxidation of air contaminants. *Journal of Catalysis* 167, 118-126.

64. d'Hennezel, O., Pichat, P., Ollis, D.F., 1998. Benzene and toluene gas-phase photocatalytic degradation over H_2O and HCL pretreated TiO_2: by-products and mechanisms. *Journal of Photochemistry and Photobiology A: Chemistry* 118, 197-204.

65. Dibble, J.A., Raupp, G.B., 1992. Fluidized-bed photocatalytic oxidation of trichloroethylene in contaminated airstreams. *Environmental Science and Technology* 26, 492-495.

66. Duan, X., Su, D., Zhu, Z., Chen, X., Shi, P., 2002. Photocatalytic decomposition of toluene by TiO_2 film as photocatalyst. *Journal of Environmental Science & Health Part A-Toxic/Hazardous Substances & Environmental Engineering* 37, 679-692.

67. Durgakumari, V., Subrahmanyam, M., Rao, K.V.S., Ratnamala, A., Noorjahan, M., Tanaka, K., 2002. An easy and efficient use of TiO_2 supported HZSM-5 and TiO_2+HZSM5 zeolite combinate in the photodegradation of aqueous phenol and p-chlorophenol. *Applied Catalysis A-General* 234, 155-165.

68. Eberlein-Konig, B., Przybilla, B., Kuhnl, P., Pechak, J., Gebefugi, I., Klenschmidt, J., Ring, J., 1998. Influence of airborne nitrogen dioxide or formaldehyde on parameters of skin function and cellular activation in patients with atopic eczema and control subjects. *Journal of Allergy and Clinical Immunology* 101, 141-143.

69. Einaga, H., Futamura, S., Ibusuki, T., 1999. Photocatalytic decomposition of benzene over TiO_2 in a humidified airstream. *Physical Chemistry Chemical Physics* 1, 4903-4908.

70. Einaga, H., Futamura, S., Ibusuki, T., 2002. Heterogeneous photocatalytic oxidation of benzene, toluene, cyclohexene and cyclohexane in humidified air: comparison of decomposition behavior on photoirradiated TiO_2 catalyst. *Applied Catalysis B: Environmental* 38, 215-225.

71. Einaga, H., Harada, M., Futamura, S., Ibusuki, T., 2003. Generation of active sites for CO photooxidation on TiO_2 by platinum deposition. *Journal of Physical Chemistry B* 107, 9290-9297.

72. Farias, R.F., 2001. Synthesis of TiO_2 (Anatase) by Sol–Gel Process Performed in Metal Chlorides Saturated Aqueous Solutions. *Journal of Colloid and Interface Science* 239, 584-586.

73. Fernand-Caldas, E., Fox, R.W., 1992. Environmental-Control of Indoor Air-Pollution. *Medical Clinics of North America* 76, 935-952.

74. Flory, P.J., Johnston, H.L., 1935. The photodecomposition of nitric oxide. *Journal of the American Chemical Society* 57, 2641-2651.

75. Fox, M.A., Dulay, M.T., 1993. Heterogeneous photocatalysis. *Chemical Reviews* 93, 341-357.

76. Frank, S.N., Bard, A.J., 1977. Heterogeneous photocatalytic oxidation of cyanide ion in aqueous solution at TiO_2 powder. *Journal of American Chemical Society* 99, 303-304.

77. Fu, S.U., Calvert, J.G., Shaw, J.H., 1979. Spectroscopic and kinetic studies of a new metastable species in the photo-oxidation of gaseous formaldehyde. *Chemical Physics Letters* 65, 221-225.

78. Fu, X., Zeltner, W.A., Anderson, M.A., 1995. The gas-phase photocatalytic mineralization of benzene on porous titania-based catalysts. *Applied Catalysis B: Environmental* 6, 209-224.

79. Fujihara K, Izumi S, Ohno T, Matsumura M., 2000. Time-resolved photoluminescence of particulate TiO2 photocatalysts suspended in aqueous solutions. *Journal of Photochemistry and Photobiology A: Chemistry Reviews* 132, 99-104.

80. Fujishima, A., Honda, K., 1972. Electrochemical Photolysis of Water at a Semiconductor Electrode. *Nature* 238, 37.

81. Fujishima, A., Rao, T.N., Tryk, D.A., 2000. Titanium dioxide photocatalysis. *Journal of Photochemistry and Photobiology C: Photochemistry Reviews* 1, 1-21.

82. Gabele, P.A., 1990. Characterization of Emissions from a Variable Gasoline Methanol Fueled Car. *Journal of the Air & Waste Management Association* 40, 296-304.

83. Garapon, C., Champeaux, C., Mugnier, J., Panczer, G., Marchet, P., Catherinot, A., Jacquier, B., 1996. Preparation of TiO_2 thin films by pulsed laser deposition for waveguiding applications. *Applied Surface Science* 96-98, 836-841.

84. Garrett, M.H., Hooper, M.A., Hooper, B.M., Rayment, P.R., Abramson, M.J., 1990. Increased risk of allergy in children due to formaldehyde exposure in homes. *Allergy* 54, 330-337.

85. Gerischer, H., Heller, A., 1992. Photocatalytic Oxidation of Organic-Molecules at TiO_2 Particles by Sunlight in Aerated Water. *Journal of the Electrochemical Society* 139, 113-118.

86. Gery, M.W., Fox, D.L., Kamens, R.M., Stockburger, L., 1987. Investigation of Hydroxyl Radical Reactions with Ortho-Xylene and Meta-Xylene in a Continuous Stirred Tank Reactor. *Environmental Science and Technology* 21, 339-348.

87. Gimeno, L., Marin, E., del Teso, T., Bourhim, S., 2001. How effective has been the reduction of SO_2 emissions on the effect of acid rain on ecosystems? *Science of the Total Environment* 275, 63-70.

88. Godish, T., 1989. Indoor Air Pollution Control. Leis Publishers, Michigan, USA.

89. Godish, T., 1990. Residential Formaldehyde - Increased Exposure Levels Aggravate Adverse Health-Effects. *Journal of Environmental Health* 53, 34-37.

90. Gold, D.R., 1992. Indoor air pollution. *Clinics in Chest Medicine* 13, 215-229.

91. Gomez, R., Lopez, T., Ortis-Islas, E., Navarrete, J., Sanchez, E., Tzompanztzi, F., Bokhimi, X., 2003. Effect of sulfation on the photoactivity of TiO_2 sol-gel derived catalysts. *Journal of Molecular Catalysis A-Chemical* 193, 217-226.

92. Goswami, D.Y., Trivedi, D.M., Block, S.S., 1997. Photocatalytic Disinfection of Indoor Air. *Journal of Solar Energy Engineering* 119, 92-97.

93. Graedel, T.E., 1978. Chemical Compounds in the Atmosphere, Academic Press, New York, p. 30.

94. Gratzel, M., Howe, R.F., 1990. Electron-Paramagnetic Resonance Studies of Doped TiO_2 Colloids. *Journal of Physical Chemistry*, 2566-2572.

95. Guo, H., Lee, S.C., Li, W.M., Cao, J.J., 2003. Source characterization of BTEX in indoor microenvironments in Hong Kong. *Atmospheric Environment* 37, 73-82.

96. Hager, S., Bauer, R., 1999. Heterogeneous photocatalytic oxidation of organics for air purification by near UV irradiated titanium dioxide. *Chemosphere* 38, 1549-1559.

97. Hager, S., Bauer, R., Kudielka, G., 2000. Photocatalytic oxidation of gaseous chlorinated organics over titanium dioxide. *Chemosphere* 41, 1219-1225.

98. Hanrahan, L.P., Dally, K.A., Anderson, H.A., Kanarek, M.S., Rankin, J., 1984. Formaldehyde Vapor in Mobile Homes - A Cross-Sectional Survey of Concentrations and Irritant Effects. *American Journal of Public Health* 74, 1026-1027.

99. Hashimoto, K., Wasada, K., Osaki, M., Shono, E., Adachi, K., Toukai, N., Kominami, H., Kera, Y., 2001. Photocatalytic oxidation of nitrogen oxide over titania–zeolite composite catalyst to remove nitrogen oxides in the atmosphere. *Applied Catalysis B: Environmental* 30, 429-436.

100. Hashimoto, K., Wasada, K., Toukai, Kominami, H., Kera, Y., 2001. Photocatalytic oxidation of nitrogen monoxide over titanium (IV) oxide nanocrystals large size areas. *Journal of Photochemistry and Photobiology A: Chemistry* 136, 103-109.

101. Hegg, D.A., Hobbs, P.V., 1978. Oxidation of Sulfur-Dioxide in Aqueous Systems with Particular Reference to Atmosphere. *Atmospheric Environment* 12, 241-253.

102. Heller, H.G., Langan, J.R., 1981. Photochromic heterocyclic fulgides. 3. the use of (e)-alpha-(2,5-dimethyl-3-furylethylidene) (isopropylidene)succinic anhydride as a simple convenient chemical actinometer. *Journal of the chemical society-perkin transactions 2*, 341-343.

103. Henry, J. G., Heinke, G.H., 1999. Environmental Science and Engineering, Prentice Hall, London, p. 122.

104. Herrmann, J.M., 1999. Heterogeneous photocatalysis: fundamentals and applications to the removal of various types of aqueous pollutants. *Catalysis Today* 53, 115-129.

105. Herrmann, J.M., Disdier, J., Pichat, P., 1984. Effect of Chromium Doping on the Electrical and Catalytic Properties of Powder Titania under UV and Visible Illumination. *Chemical Physics Letters* 108, 618-622.

106. Hines, A.L., Ghosh, T.K., Loyalka, S.K., Warder, R.C. (Eds.), 1993. Indoor Air-Quality and Control. Prentice-Hall, Englewood Cliffs, NJ.

107. Hishinuma, A., Goda, T., Kitaoka, M., Hayashi, S., Kawahara, H., 1991. *Applied Surface Science* 48/49, 405-408.

108. Ho, K.F., Lee, S.C., Louie, P.K.K., Zou, S.C., 2002. Seasonal variation of carbonyl compound concentrations in urban area of Hong Kong. *Atmospheric Environment* 36 1259-1265.

109. Ho, S.S.H., Yu, J.Z., 2002. Concentrations of formaldehyde and other carbonyls in environments affected by incense burning. *Journal of Environmental Monitoring* 4, 728-733.

110. Hodgson, M.J., Frohlinger, J., Permar, E., Tidwell, C., Traven, N.D., Olenchock, S.A., Karpf, M., 1991. Symptoms and microenvironmental measures in nonproblem buildings. *Journal of Occupational and Environmental Medicine* 33, 527-533.

111. Hoffmann, M.R., Martin, S.T., Choi, W., Bahnemann, D.W., 1995. Environmental applications of semiconductor photocatalysis. *Chemical Reviews* 95, 69-96.

112. Hong Kong Environmental Protection Department, 1997. Environment Hong Kong 1997.

113. Hong Kong Environmental Protection Department, 1997. Final Report for Consultancy Study on Indoor Air Pollution in Offices and Public Places in Hong Kong.

114. Hong Kong Environmental Protection Department, 2003. Guidance notes for the management of indoor air quality in offices and public places, Indoor Air Quality Management Group.

115. Hori, Y., Fujimoto, K., Suzuki, S., 1986. Rapid Oxidation of NO to NO_2 at ppm Concentration Level in a Heterogeneous Photocatalytic Reaction on Metal-Oxide Powders. *Chemistry Letters*, 1845-1848.

116. Horvath, E.P., 1997. Building-related illness and sick building syndrome: from the specific to the vague. *Cleveland Clinical Journal of Medicine* 64, 303-309.

117. Hu, Y., Zhang, J.L., Minagawa, M., Ayusawa, T., Matsuoka, M., Yamashita, H., Anpo, M., 2003. The origin of the decline in the photocatalytic activity of TiO_2 in the decomposition of NO: TPD spectra of the adsorbed NO species. *Research on Chemical Intermediates* 29, 125-135.

118. Hunter, C.A., Hull, A.V., Higham, D.F., Grimes, C.P., Lea, R.G., 1996. Fungi and bacteria. In: Berry, R.W., Brown, V.M., Coward, S.K.D. et al. (Eds.), Indoor Air Quality in Homes, the Building Research Establishment Indoor Environment Study, part 1. Construction Research Communications, London.

119. Hwang, S., Lee, M.C., Choi, W., 2003. Highly enhanced photocatalytic oxidation of CO on titania deposited with Pt nanoparticles: kinetics and mechanism. *Applied Catalysis B: Environmental* 46, 49-63.

120. Ibusuki, T., Takeuchi, K., 1986. Toluene oxidation on UV-irradiated titanium-dioxide with and without O_2, NO_2 or H_2O at ambient temperature. *Atmospheric Environment* 20, 1711-1715.

121. Ibusuki, T., Takeuchi, K., 1994. Removal of low concentration nitrogen-oxides through photoassisted heterogeneous catalysis. *Journal of Molecular Catalysis* 88, 93-102.

122. Ichiura, H., Kitaoka, T., Tanaka, H., 2003. Photocatalytic oxidation of NO_x using composite sheets containing TiO_2 and a metal compound. *Chemosphere* 51, 855-860.

123. Institute for Environment and Health (IEH). IEH assessment on indoor air quality in the home. Institute for Environment and Health, Leicester, UK, 1996.

124. Iwasaki, M., Hara, M., Kawada, H., Tada, H., Ito, S., 2000. Cobalt Ion-Doped TiO_2 Photocatalyst Response to Visible Light. *Journal of Colloid and Interface Science* 224, 202-204.

125. Jaffal, A.A., Banat, I.M., Mogheth, A.A., Nsanze, H., Bener, A., Ameen, A.S., 1997. Residential indoor airborne microbial populations in the United Arab Emirates. *Environment International* 23, 529-533.

126. Jarvis, D., Chinn, S., Luczynska, C., Burney, P., 1996. Association of respiratory symptoms and lung function in young adults with the use of domestic gas appliances. *Lancet* 1, 426-431.

127. Jin, H., Zheng, M., Mao, Y., Wan, H., Hang, Y., 1993. The effect of indoor pollution on human health. In: Jantunen, M., Kalliokoski, P., Kukkonen, E., Saarela, K., Seppanen, A., Vuorelma, H. (Eds.), Proceedings of the Sixth International Conference on Indoor Air Quality and Climate. Helsinki, Finland, pp. 477-482.

128. Jones, A.P., 1998. Asthma and domestic air quality. *Social Science and Medicine* 47, 755-764.

129. Jones, A.P., 1999. Indoor air quality and health. *Atmospheric Environment* 33, 4535-4564.

130. Kang, M., Lee, J.H., Lee, S.H., Chung, C.H., Yoon, K.J., Ogino, K., Miyata, S., Choung, S.J., 2003. Preparation of TiO_2 film by the MOCVD method and analysis for decomposition of trichloroethylene using in situ FT-IR spectroscopy. *Journal of Molecular Catalysis A: Chemical* 193, 273-283.

131. Karst, U., Binding, N., Cammann, K., Witting, U., 1993. Interferences of nitrogen-dioxide in the determination of aldehydes and ketones by sampling on 2,4-dinitrophenylhydrazine-coated solid sorbent. *Fresenius Journal of Analytical Chemistry* 345, 48-52.

132. Khan F.I., Ghoshal, A.K., 2000. Removal of volatile organic compounds from polluted air. *Journal of Loss Prevention in the Process Industries* 13, 527-545.

133. Kikuchi, Y., Sunada, K., Iyoda, T., Hashimoto, K., Fujishima, A., 1997. Photocatalytic bactericidal effect of TiO_2 thin films: dynamic view of the active oxygen species responsible for the effect. *Journal of Photochemistry and Photobiology A: Chemistry* 106, 51–56.

134. Kim, J.S., Joo, H.K., Lee, T.K., Itoh, K., Murabayashi, M., 2000. Photocatalytic activity of TiO_2 films preserved under different conditions: The gas-phase photocatalytic degradation reaction of trichloroethylene. *Journal of Catalysis* 192, 484-486.

135. Kim, S.B., Hong, S.C., 2002. Kinetic study for photocatalytic degradation of volatile organic compounds in air using thin film TiO_2 photocatalyst. *Applied Catalysis B: Environmental* 35, 305-315.

136. Kim, S.B., Hwang, H.T., Hong, S.C., 2002a. Photocatalytic degradation of volatile organic compounds at the gas-solid interface of a TiO_2 photocatalyst. *Chemosphere* 48, 437-444.

137. Ko, H.Y.Y., Mizuhata, M., Kajinami, A., Deki, S., 2003. Fabrication of high performance thin films from metal fluorocomplex aqueous solution by the liquid phase deposition. *Journal of Fluorine Chemistry* 120, 157-163.

138. Komazaki, Y., Shimizu, H., Tanaka, S., 1999. A new measurement method for nitrogen oxides in the air using an annular diffusion scrubber coated with titanium dioxide. *Atmospheric Environment* 33, 4363-4371.

139. Kotani, Y., Matsuda, A., Kogure, T., Tatsumisago, M., Minami, T., Umezawa, T., Kogure, T., 2000. Formation of anatase nanocrystals in sol-gel derived TiO_2-SiO_2 thin films with hot water treatment. *Journal of Sol-Gel Science and Technology* 19, 585-588.

140. Kotani, Y., Matsuda, A., Kogure, T., Tatsumisago, M., Minami, T., 2001. Effects of addition of poly(ethylene glycol) on the formation of anatase nanocrystals in SiO_2-TiO_2 gel films with hot water treatment. *Chemistry of Materials* 13, 2144-2149.

141. Kozlov, D.V., Vorontsov, A.V., Smirniotis, P.G., Savinov, E.N., 2003. Gas-phase photocatalytic oxidation of diethyl sulfide over TiO2: kinetic investigations and catalyst deactivation. *Applied Catalysis B: Environmental* 42, 77-87.

142. Kreiss, K., in Cone, J.E., and Hodson, M.J., (Ed.), Problem buildings:building-associated illness and the sick building syndrome, Hanley & Belfus, Philadelphia, 1985, p. 579.

143. Ku, Y., Ma, C.M., Shen, Y.S., 2001. Decomposition of gaseous trichloroethylene in a photoreactor with TiO_2-coated nonwoven fiber textile. *Applied Catalysis B: Environmental* 34, 181-190.

144. Kutsuna, S., Ebihara, Y., Nakamura, K., Ibusuki, T., 1993. Heterogeneous photochemical-reactions between volatile chlorinated hydrocarbons (trichloroethene and tetrachloroethene) and titanium-dioxide. *Atmospheric Environment Part A-General Topics* 27, 599-604.

145. Kwok, N.H., Lee, S.C., Guo H., Hung, W.T., 2003. Substrate effects on VOC emissions from an interior finishing varnish. *Building and Environment* 38, 1019-1026.

146. Lam, S., Lee, S.C., Ho, K.F., 2001. Characterization of VOCs, ozone, and PM_{10} emissions from office equipment in an environmental chamber. *Building and Environment* 36, *837*-842.

147. Lambert W.E., 1997. Combusiton pollution in indoor environments. Bardana, E.J., Montanaro, A. (Eds.), Indoor Air Pollution and Health. Marcel Dekker, New York.

148. Lambert, W.E., 1994. Urban exposures to carbon monoxide and myocardial ischemia in men with ischemic heart disease. Ph.D. Thesis, University of California.

149. Larson, S.A., Falconer, J.L., 1997. Initial reaction steps in photocatalytic oxidation of aromatics. *Catalysis Letters* 44, 57-65.

150. Larson, S.A., Widegren, J.A., Falconer, J.L., 1995. Transient studies of 2-propanol photocatalytic oxidation on titania. *Journal of Catalysis* 157, 611-625.

151. Leaderer, B.P., Stolwijk, J.A.J., Zagraniski, R.T., Qing-Shan, M., 1984. A field study of indoor air contaminant levels associated with unvented combustion sources. In: Proceedings of the 77th Annual Meeting of the Air Pollution Control Association, San Francisco, CA.

152. Leaderer, B.P., Stowe, M., Li, R., Sullivan, J., Koutrakis, P., Wolfson, M., Wilson, W., 1993. Residential levels of particle and vapor phase acid associated with combustion sources. In: Jantunen, M., Kalliokoski, P., Kukkonen, E., Saarela, K., SeppaK nen, A., Vuorelma, H. (Eds.), Proceedings of the Sixth International Conference on Indoor Air Quality and Climate. Helsinki, Finland, 147-152.

153. Leaderer, B.P., Zagraniski, R.T., Berwick, M., Stolwijk, J.A.J., 1986. Assessment of exposure to indoor air contaminants from combustion sources: methodology and application. *American Journal of Epidemiology* 124, 275-289.

154. Lee, B.Y., Park, S.H., Kang, M., Lee, S.C., Choung, S.J., 2003. Preparation of Al/TiO_2 nanometer photo-catalyst film and the effect of H_2O addition on photo-catalytic performance for benzene removal. *Applied Catalysis A: General* 253, 371-380.

155. Lee, S.C., Chan, L.Y., 1998. Indoor/Outdoor Air Quality Correlation and Questionnaire Survey at Two Staff Quarters in Hong Kong. *Environment International* 24, 729-737.

156. Lee, S.C., Chang, M., 1999. Indoor and outdoor air quality investigation at schools in Hong Kong. *Chemosphere* 41, 443-450.

157. Lee, S.C., Guo, H., Li, W.M., Chan, L.Y., 2002a. Inter-comparison of air pollutant concentrations in different indoor environments in Hong Kong. *Atmospheric Environment* 36, 1929-1940.

158. Lee, S.C., Kwok, N.H., Guo H., Hung, W.T., 2003a. The effect of wet film thickness on VOC emissions from a finishing varnish. *The Science of the Total Environment* 302, 75-84.

159. Lee, S.C., Li, W.M., Ao, C.H., 2002. Investigation of indoor air quality at residential homes in Hong Kong - case study. *Atmospheric Environment* 36, 225-237.

160. Lee, S.C., Li, W.M., Chan, L.Y., 2001. Indoor air quality at restaurants with different styles of cooking in metropolitan Hong Kong. *The Science of the Total Environment,* 279, 181-193.

161. Levesque, B., Dewailly, E., Lavoie, R., Prudhomme, D., Allaire, S., 1990. Carbon-Monoxide in Indoor Ice Skating Rinks - Evaluation of Absorption by Adult Hockey Players. *American Journal of Public Health* 80, 594-598.

162. Li, F.B., Li, X.Z.., 2002. Photocatalytic properties of gold/gold ion-modified titanium dioxide for wastewater treatment. *Applied Catalysis A-General* 228, 15-27.

163. Li, F.B., Li, X.Z.., 2002a. The enhancement of photodegradation efficiency using Pt-TiO_2 catalyst. *Chemosphere* 48, 1103-1111.

164. Li, K., Liu, S.Y.C., Khetarpal, S., Chen D.H., 1998. TiO_2 photocatalytic oxidation of toluene and PCE vapor in the air. *Journal of advanced oxidation technology* 3, 311-314.

165. Li, W.M., Lee, S.C., Chan, L.Y., 2001. Indoor air quality at nine shopping malls in Hong Kong. *The Science of the Total Environment* 273, 27-40.

166. Li, X.Z., Li, F.B., 2001. Study of Au/Au^{3+} TiO_2 photocatalysts toward visible photooxidation for water and wastewater treatment. *Environmental Science and Technology* 35, 2381-2387.

167. Li, X.Z., Li, F.B., Yang, C.L., Ge, W.K., 2001a. Photocatalytic activity of WO_x-TiO_2 under visible light irradiation. *Journal of Photochemistry and Photobiology A: Chemistry* 141, 209-217.

168. Lichtin, N.N., Avudaithai, M., Berman, E., Dong, J., 1994. Photocatalytic oxidative degradation of vapors of some organic compounds over TiO_2. *Research of Chemical Intermediates* 20, 755-781.

169. Lichtin, N.N., Avudaithai, M., Berman, E., Grayfer, A., 1996. TiO_2-photocatalyzed oxidative degradation of binary mixtures of vaporized organic compounds. *Solar Energy* 56, 377-385.

170. Lichtin, N.N., Sadeghi, M., 1998. Oxidative photocatalytic degradation of benzene vapor over TiO_2. *Journal of Photochemistry and Photobiology A: Chemistry* 113, 81-88.

171. Lim, T.H., Jeong, S.M., Kim, S.D., Gyenis, J., 2000. Photocatalytic decomposition of NO by TiO_2 particles. *Journal of Photochemistry and Photobiology A: Chemistry* 134, 209-217.

172. Lin, H., Kozuka, H., Yoko, T., 1998. Preparation of TiO_2 films on self-assembled monolayers by sol-gel method. *Thin Solid Films* 315, 111-117.

173. Linsebigler, A.L., Lu, G.Q., Yates, J.T., 1995. Photocatalysis on TiO_2 surfaces - principles, mechanisms, and selected results. *Chemical Reviews* 95, 735-758.

174. Litter, M.I., Navio, J.A., 1996. Photocatalytic properties of iron-doped titania semiconductors. *Journal of Photochemistry and Photobiology A: Chemistry* 93, 171-181.

175. Liu, J.B., Crittenden, J.C., Hand, D.W., Perram, D.L., 1996. Regeneration of adsorbents using heterogeneous photocatalytic oxidation. *Journal of Environmental Engineering-ACSE* 122, 707-713.

176. Lizzio, A.A., DeBarr, J.A., 1996. Effect of surface area and chemisorbed oxygen on the SO_2 adsorption capacity of activated char. *Fuel* 75, 1515-1522.

177. Luo, Y., Ollis, D.F., 1996. Heterogeneous photocatalytic oxidation of trichloroethylene and toluene mixtures in air: kinetic promotion and inhibition, time-dependent catalyst activity. *Journal of Catalysis* 163, 1-11.

178. Luo, Z., Gao, Q.H., 1992. Decrease in the photoactivity of TiO_2 pigment on doping with transition metals. *Journal of Photochemistry and Photobiology A: Chemistry* 63, 367-375.

179. Ma, Y., Qiu, J.B., Cao, Y.A., Guan, Z.S., Yao, J.N., 2001. Photocatalytic activity of TiO_2 films grown on different substrates. *Chemosphere* 44, 1087-1092.

180. Macher, J.M., Huang, F.Y., Flores, M., 1991. A two-year study of microbiological indoor air quality in a new apartment. Archives of Environmental Health 46, 25-29.

181. Maira, A.J., Yeung, K.L., Soria, J., Coronado, J.M., Belver, C., Lee, C.Y., 2001. Gas-phase photo-oxidation of toluene using nanometer-size TiO_2 catalysts. *Applied Catalysis B: Environmental* 29, 327-336.

182. Maroni, M., Seifert, B., Lindvall, T. (Eds.), 1995. Indoor Air Quality- a Comprehensive Reference Book. Elsevier, Amsterdam.

183. Martyanov, I.N., Klabunde, K.J., 2003. Photocatalytic Oxidation of Gaseous 2-Chloroethyl Ethyl Sulfide over TiO_2. *Environmental Science & Technology* 37, 3448-3453.

184. Maruska, H.P., Ghosh, A.K., 1979. Transition-Metal Dopants for Extending the Response of Titanate Photoelectrolysis Anodes. *Solar Energy Materials* 1, 237-249.

185. Matos, J., Laine, J., Herrmann, J.M., 1998. Synergy effect in the photocatalytic degradation of phenol on a suspended mixture of titania and activated carbon. *Applied Catalysis B: Environmental* 18, 281-291.

186. Matsuda, A., Kotani, Y., Kogure, T., Tatsumisago, M., Minami, T., 2001a. Photocatalytic decomposition of acetaldehyde with anatase nanocrystals-dispersed silica films prepared by the sol-gel process with hot water treatment. *Journal of Sol-Gel Science and Technology* 22, 41-46.

187. Matsuda, S., Hatano, H., Tsutsumi, A., 2001. Ultrafine particle fluidization and its application to photocatalytic NO_x treatment. *Chemical Engineering Journal* 82, 183-188.

188. Matthews, R.W., McEvoy, S.R., 1992. A comparison of 254 nm and 350 nm excitation of TiO_2 in simple photocatalytic reactors. *Journal of Photochemistry and Photobiology A: Chemistry* 66, 355-366.

189. Meller, J.R., Moortgat, G.K., 2000. Temperature dependence of the absorption cross sections of formaldehyde between 223 and 323 K in the wavelength range 225-375 nm. *Journal of Geophysical Research-Atmospheres* 105, 7089-7101.

190. Mendez-Roman, R., Cardona-Martinez, N., 1998. Relationship between the formation of surface species and catalyst deactivation during the gas-phase photocatalytic oxidation of toluene. *Catalysis Today* 40, 353-365.

191. Meszaros, E., 1981. Atmospheric Chemistry: Fundamental aspects, Elsevier Science Pub. Co., Amsterdam, p.141.

192. Metcalfe, I.S., 1997. Chemical Reaction Engineering: A First Course, Oxford University Press, New York, p.10.

193. Mikula, M., Brezova, V., Ceppan, M., Pach, L., Karpinsky, L., 1995. Comparison of Photocatalytic Activity of Sol-Gel TiO_2 and P25 TiO_2 Particles Supported on Commercial Fiberglass Fabric. *Journal of Materials Science Letters* 14, 615-616.

194. Milis, A., Peral, J., Domenech, X., 1994. Heterogeneous photocatalytic oxidation of nitrite over iron-doped TiO_2 sample. *Journal of Molecular Catalysis* 87, 67-74.

195. Mills, A., LeHunte, S., 1997. An overview of semiconductor photocatalysis. *Journal of Photochemistry and Photobiology A: Chemistry* 108, 1-35.

196. Mizushima, K., Tanaka, M., Asai, A., Iida, S., Goodenough, J.B., 1979. Impurity Levels of Iron-Group Ions in TiO_2. *Journal of Physics and Chemistry of Solids* 40, 1129-1140.

197. Mohseni, M., David, A., 2003. Gas phase vinyl chloride (VC) oxidation using TiO_2-based photocatalysis. *Applied Catalysis B: Environmental 46*, 219-228.

198. Montoya, I.A., Viveros, T., Dominguez, J.M., Canales, L.A., Schifter, I., 1992. On the Effects of the Sol-Gel Synthesis Parameters on Textural and Structural Characteristics of TiO_2. *Catalysis Letters* 15, 207-217.

199. Morgan, K.T., 1997. A brief review of formaldehyde carcinogenesis in relation to rat nasal pathology and human health risk assessment. *Toxicologic Pathology* 25, 291-307.

200. Morrison, B.M., Heicklen, J., 1981. The free-radical oxidation of CH_2O in the presence of NO_2 and NO. *Journal of Photochemistry* 15, 131-145.

201. Muggli, D.S., Ding, L.F., 2001. Photocatalytic performance of sulfated TiO_2 and Degussa P-25 TiO_2 during oxidation of organics. *Applied Catalysis B: Environmental* 32, 181-194.

202. Muralidharan, B.G., Agrawal, D.C., 1997. Sol-Gel Derived TiO_2-SiO_2 Fibres. *Journal of Sol-Gel Science and Technology* 9, 85-93.

203. Murata, Y., Tawara, H., Obata, H., Takeuchi, K., 1999. Air Purifying Pavement: Development of Photocatalytic Concrete Blocks. *Journal of Advanced Oxidation Technology* 4, 227-230.

204. Music, S., Gotic, M., Ivanda, M., Popovic, S., Turkovic, A., Trojko, R., Sekulic, A., Furic, K., 1997. Chemical and microstructural properties of TiO_2 synthesized by sol-gel procedure. *Materials Science and Engineering B-Solid State Materials for Advanced Technology* 47, 33-40.

205. Nagao, M., and Suda, Y., 1989. Adsorption of benzene, toluene, and chlorobenzene on titanium-dioxide. *Langmuir* 5, 42-47.

206. Nakamura, I., Negishi, N., Kutsuna, S., Ihara, T., Sugihara S., Takeuchi K., 2000. Role of oxygen vacancy in the plasma-treated TiO_2 photocatalyst with visible light activity for NO removal. *Journal of Molecular Catalysis A: Chemical* 161, 250-212.

207. Nam, W., Kim, J., Han, G., 2002. Photocatalytic oxidation of methyl orange in a three-phase fluidized bed reactor. *Chemosphere* 47, 1019-1024.

208. Navio, J.A., Macias, M., Gonzalezcatalan, M., Justo, A., 1992. Bulk and Surface Characterization of Powder Iron-Doped Titania Photocatalysts. *Journal of Materials Science* 27, 3036-3042.

209. Navio, J.A., Marchena, F.J., Roncel, M., Delarosa, M.A.., 1991. A Laser Flash-Photolysis Study of the Reduction of Methyl Viologen by Conduction-Band Electrons of TiO_2 and Fe-Ti Oxide Photocatalysts. *Journal of Photochemistry and Photobiology A:Chemistry* 55, 319-322.

210. Negishi, N., Takeuchi, K., Ibusuki, T., 1998. Surface structure of the TiO_2 thin film photocatalyst. *Journal of Materials Science* 33, 5789-5794.

211. Niemala, R., Vaino, H., 1985. Formaldehyde exposure in work and the general environment. *Scandinavian Journal of Work and Environmental Health* 7, 95-100.

212. Nishikawa, H., Takahara, Y., 2001. Adsorption and photocatalytic decomposition of odor compounds containing sulfur using TiO_2/SiO_2 bead. *Journal of Molecular Catalysis A-Chemical* 172, 247-251.

213. Noguchi, T., Fujishima, A., Sawunyama, P., Hashimoto, K., 1998. Photocatalytic degradation of gaseous formaldehyde using TiO_2 film. *Environmental Science and Technology* 32, 3831-3833.

214. Norback, D., Bjornsson, E., Janson, C., Widstrom, J., Boman, G., 1995. Asthmatic Symptoms and Volatile Organic-Compounds, Formaldehyde, And Carbon-Dioxide in Dwellings. *Occupational and Environmental Medicine* 52, 388-395.

215. Obee, T.N., 1996. Photooxidation of Sub-Parts-per-Million Toluene and Formaldehyde Levels on Titania Using a Glass-Plate Reactor. *Environmental Science and Technology* 30, 3578-3584.

216. Obee, T.N., Brown, R.T., 1995. TiO_2 photocatalysis for indoor air applications - effects of humidity and trace contaminant levels on the oxidation rates of formaldehyde, toluene, and 1,3-butadiene. *Environmental Science and Technology* 29, 1223-1231.

217. Obuchi, E., Sakamoto, T., Nakano, K., Shiraishi, F., 1999. Photocatalytic decomposition of acetaldehyde over TiO_2/SiO_2 catalyst. *Chemical Engineering Science* 54, 1525-1530.

218. Ohko, Y., Hashimoto, K., Fujishima, A., 1997. Kinetics of photocatalytic reactions under extremely low-intensity UV illumination on titanium dioxide thin film. *Journal of Physical Chemistry A* 101, 8057-8062.

219. Ohtani, B., Ogawam Y,, Nishimoto, S., 1997. Photocatalytic activity of amorphous-anatase mixture of titanium(IV) oxide particles suspended in aqueous solutions. *Journal of Physical Chemistry B* 101, 3746-3752.

220. Oikawa, K., Murano, K., Enomoto, Y., Wada, K., Inomata, T., 1994. Automatic Monitoring-System for Acid-Rain and Snow Based on Ion Chromatography. *Journal of Chromatography A* 671, 211-215.

221. Okimura, K., Maeda, N., Shibata, A., 1996. Characteristics of rutile TiO_2 films prepared by rf magnetron sputtering at a low temperature. *Thin Solid Films* 282, 247-430.

222. Ollis D.F., 2000. Photocatalytic purification and remediation of contaminated air and water. *Surface Chemistry and Catalysis* 3, 405-411.

223. Ollis, D.F., 1985. Contaminant degradation in water. *Environmental Science and Technology* 19, 480-484.

224. Orehek, J., Massari, J.P., Gayrard, P., Grimaud, C., Charpin, J., 1976. Effect of Short-Term, Low-Level Nitrogen-Dioxide Exposure on Bronchial Sensitivity of Asthmatic-Patients. *Journal of Clinical Investigation* 57, 301-307.

225. Otto, D., Hundell, H., House, D., Molhave, L., Counts, W., 1992. Exposure of humans to a volatile organic mixtures. I. Behavioral assessment. *Archives of Environmental Health* 47, 23-30.

226. Pagsberg, P., Bjergbakke, E., Ratajczak, E., Sillesen, A., 1997. Kinteics of the gas phase reaction OH+NO(+M)->HONO(+M) and the determination of the UV absorption cross sections of HONO. *Chemical Physics Letters* 272, 383-390.

227. Pandey, M.R., Smith, K.R., Boleij, J.S.M., 1989. Indoor air pollution in developing countries and acute respiratory infection in children. *Lancet* 1, 427-429.

228. Park, D.R., Zhang, J.L., Ikeue, K., Yamashita, H., Anpo, M., 1999. Photocatalytic oxidation of ethylene to CO_2 and H_2O on ultrafine powdered TiO_2 photocatalysts in the presence of O_2 and H_2O. *Journal of Catalysis* 185, 114-119.

229. Peat, J.K., Dickerson, J., Li, J., 1998. Effects of damp and mould in the home on respiratory health: a review of the literature. *Allergy* 53, 120-128.

230. Peiro, A.M., Peral, J., Domingo, C., Domenech, X., Ayllon, J.A., 2001. Low-temperature deposition of TiO_2 thin films with photocatalytic activity from colloidal anatase aqueous solutions. *Chemistry of Materials* 13, 2567-2573.

231. Peral, J., Domenech, X., Ollis, D.F., 1997. Heterogeneous photocatalysis for purification, decontamination and deodorization of air. *Journal of Chemical Technology and Biotechnology* 70, 117-140.

232. Peral, J., Ollis., D.F., 1992. Heterogeneous photocatalytic oxidation of gas-phase organics for air purification - acetone, 1-butanol, butyraldehyde, formaldehyde, and meta-xylene oxidation. *Journal of Catalysis* 136, 554-656.

233. Perry, R., Gee, I.L., 1994. Vehicle emissions and effects on air quality: indoors and outdoors. *Indoor Environment* 3, 224–236.

234. Pfeffer, H.U., 1994. Ambient air concentrations of pollutants at traffic-related sites in urban areas of North Rhine—Westphalia, Germany. *The Science of the Total Environment* 146/147, 263-273.

235. Pinceloup, S., Laverdet, G., Maguin, F., Doussin, J.F., Carlier, P., Bras, G.L., 2003. Laboratory investigation of the photooxidation of formaldehyde combining FTIR analysis of stable species and HO_2 detection by the chemical amplifier technique. *Journal of Photochemistry and Photobiology A: Chemistry* 157, 257-281.

236. Postlethwait, E.M., Bidani, A., 1990. Reactive Uptake Governs the Pulmonary Air Space Removal of Inhaled Nitrogen-Dioxide. *Journal of Applied Physiology* 68, 594-603.

237. Potter, W., Karst, U., 1996. Identification of chemical interferences in aldehyde and ketone determination using dual-wavelength detection. *Analytical Chemistry* 68, 3354-3358.

238. Powell, Q.H., Kodas, T.T., Anderson, B.M., 1996. Coating of TiO_2 particles by chemical vapor deposition of SiO_2. *Chemical Vapor Deposition* 2, 179.

239. Przepiorski J, Yoshizawa N, Yamada Y, 2001. Activated carbons containing TiO_2: Characterization and influence of a preparation method on the state of TiO_2 supported. J*ournal of Material Science* 36, 4249-4257.

240. Qin, Y.H., Zhang, X.M., Jin, H.Z., Liu, Y.Q., Fan, D.L., Cao, Z.J., 1993. Effects of indoor air pollution on respiratory illness of school children. In: Jantunen, M., Kalliokoski, P., Kukkonen, E., Saarela, K., SeppaK nen, A., Vuorelma, H. (Eds.), Proceedings of the Sixth International Conference on Indoor Air Quality and Climate. Helsinki, Finland, 477-482.

241. Raymundo-Piñero, E., Cazorla-Amorós, D., Linares-Solano, A., 2001. Temperature programmed desorption study on the mechanism of SO_2 oxidation by activated carbon and activated carbon fibres. *Carbon* 39, 231-242.

242. Richter, E., Kleinschmidt, R., Pilarczyk, E., Knoblauch, K., Juntgen, H., 1985. Thermal-Desorption of Nitrogen-Oxides from Activated Carbon. *Thermochemica Acta* 85, 311-314.

243. Ritchie, I.M., Lehnen, R.G., 1987. Formaldehyde-Related Health Complaints of Residents Living in Mobile and Conventional Homes. *American Journal of Public Health* 77, 323-328.

244. Roberts, J., Nelson, W.C., 1995. National Human Activity Pattern Survey Data Base. United States Environmental Protection Agency (USEPA), Research Triangle Park, NC.

245. Rosenstock L., 1987. Occupational medicine: state of the art reviews. Philadelphia: Hanley & Belfus.

246. Roughton, F.J.W., Darling, R.C., 1994. The effect of carbon monoxide on the oxyhemoglobin dissociation curve. *American Journal of Physiology* 141, 17-31.

247. Rubel A.M., Stencel, J.M., 1996. Effect of Pressure on NO_x Adsorption by Activated Carbons. *Energy & Fuels* 10, 704-708.

248. Ryan, P.B., Hemphill, C.P., Billick, I.H., Nagda, N.L., Koontz, M.D., Fortmann, R.C., 1989. Estimation of nitrogen dioxide concentrations in homes equipped with unvented gas space heaters. *Environment International* 15, 551-556.

249. Sakamoto, K., Tonegawa, Y., Ishitani, O., 1999. Destruction of Indoor Air Pollutants in TiO_2-Wall Coated Cylindrical Flow Reactor under 254 nm UV Irradiation. *Journal of Advanced Oxidation Technology* 4, 35-39.

250. Salome, C.M., Brown, N.J., Marks, G.B., Woolcock, A.J., Johnson, G.M., Nancarrow, P.C., Quigley, S., Tiong, J., 1996. Effect of nitrogen dioxide and other combustion products on asthmatic subjects in a home-like environment. *European Respiratory Journal* 9, 910-918.

251. Samet, J.M., Marbury, M.C., Spengler, J.D., 1987. Health-Effects and Sources of Indoor Air-Pollution: part 1. *American Review of Respiratory Disease* 136, 1486-1508.

252. Sampath, S., Uchida, H., Yoneyama, H., 1994. Photocatalytic degradation of gaseous pyridine over zeolite-supported titanium-dioxide. *Journal of Catalysis* 149, 189-194.

253. Sandmeyer, E.E., 1982. Aromatic hydrocarbons. In: Clayton, G.D., Clayton, F.E., (Eds.), Patty's Industrial Hygiene and Toxicology. Wiley, New York, pp. 3253-3431.

254. Sauer, M.L., Hale, M.A., Ollis, D.F., 1995. Heterogeneous photocatalytic oxidation of dilute toluene-chlorocarbon mixtures in air. *Journal of Photochemistry and Photobiology A: Chemistry* 88, 169-178.

255. Sauer, M.L., Ollis, D.F., 1996. Catalyst deactivation in gas-solid photocatalysis. *Journal of Catalysis* 163, 215-217.

256. Scheff, P.A., Wadden, R.A., 1993. Receptor modeling of volatile organic compounds. 1. Emission inventory and validation. *Environmental Science and Technology* 27, 617–625.

257. Schiavello, M., Rizzati, L., Bickley, R.I., Navio, A., Yue, P.L., 1984. Proceedings of VIII International Congress on Catalysis, Berlin.

258. Schleibinger, H., Ruden. H., 1999. Air filters from HVAC systems as possible source of volatile organic compounds (VOC) - laboratory and field assays. *Atmospheric Environment* 33, 4571-4577.

259. Schmitt, R. H.; Glove, E. L.; Brown, R. D., 1960. The Equivalent Conductance of the Hexafluorocomplexes of Group IV (Si, Ge, Sn, Ti, Zr, Hf). *Journal of the American Chemical Society* 82, 5292-5295.

260. Seinfeld, J.H., Pandis, S.N., 1998. Atmospheric Chemistry and Physics: From air pollution to climate change, Wiley, New York.

261. Seltzer, J.M., 1995. Effects of indoor environment on health. *Occupational Medicine* 10, 26-45.

262. Serpone, N., 1995. Brief introductory remarks on heterogeneous photocatalysis. *Solar Energy Materials and Solar Cells* 38, 369-379.

263. Serpone, N., Lawless, D., Khairutdinov, R., 1995. Size Effects on the Photophysical Properties of Colloidal Anatase TiO_2 Particles - Size Quantization or Direct Transitions in this Indirect Semiconductor. *Journal of Physical Chemistry* 99, 16646-16654.

264. Serpone, N., Pelizzetti, E., (Eds.), 1989. Photocatalysis: Fundamentals and Applications, John Wiley & Sons, U.S.

265. Shang, J., Zhu, Y.F., Du, Y.G., Xu, Z.L., 2002. Comparative studies on the deactivation and regeneration of TiO_2 nanoparticles in three photocatalytic oxidation systems: C_7H_{16}, SO_2, and C_7H_{16}-SO_2. *Journal of Solid State Chemistry* 166, 395-399.

266. Shen, Y.S., Ku, Y., 2002. Decomposition of gas-phase trichloroethene by the UV/TiO_2 process in the presence of ozone. *Chemosphere* 46, 101-107.

267. Shimizu, K., Imai, H., Hirashima, H., Tsukuma, K., 1999. Low-temperature synthesis of anatase thin films on glass and organic substrates by direct deposition from aqueous solutions. *Thin Solid Films* 351, 220-224.

268. Shin, E.M., Senthurchelvan, R., Munoz, J., Basak, S., Rajeshwar, K., Benglas-Smith, G., Howell, B.C., 1996. Photolytic and photocatalytic

destruction of formaldehyde in aqueous media. *Journal of the Electrochemical Society* 143, 1562-1570.

269. Shiraishi, F., Yamaguchi S., Ohbuchi, Y., 2003. A rapid treatment of formaldehyde in a highly tight room using a photocatalytic reactor combined with a continuous adsorption and desorption apparatus. *Chemical Engineering Science* 58, 929-934.

270. Sirju, A.P., Shepson, P.B., 1995. Laboratory and field investigation of the DNPH cartridge technique for the measurement of atmospheric carbonyl-compounds. *Environmental Science and Technology* 29, 384-392.

271. Smith, G.D., Molina, L.T., Molina, M.J., 2002. Measurement of radical quantum yields from formaldehyde photolysis between 269 and 339 nm. *Journal of Physical Chemistry A* 106, 1233-1240.

272. Sokmen, M., Ozkan, A., 2002. Decolourising textile wastewater with modified titania: the effects of inorganic anions on the photocatalysis. *Journal of Photochemistry and Photobiology A: Chemistry* 147, 77-81.

273. Sopyan, I., Watanabe, M., Murasawa, S., Hashimoto, K., Fujishima, A., 1996. An efficient TiO_2 thin-film photocatalyst: photocatalytic properties in gas-phase acetaldehyde degradation. *Journal of Photochemistry and Photobiology A: Chemistry* 98, 79-86.

274. Spengler, J.D., Dockery, D.W., Turner, W.A., Wolfson, J.M., Ferris, B.G., 1981. Long-Term Measurements of Respirable Sulfates and Particles inside and Outside Homes. *Atmospheric Environment* 15, 23-30.

275. Spicer, C.W., Kenny, D.V., Ward, G.F., Billick, I.H., 1993. Transformations, lifetimes, and sources of NO_2, HONO, and HNO_3 in

indoor environments. *Journal of the Air and Waste Management Association* 43, 1479-1485.

276. Sterling, T.D., 1991. Concentrations of nicotine, RSP, CO and CO_2 in non-smoking areas of offices ventilated by air recirculated from smoking designated areas. *American Industrial Hygiene Association Journal* 52, 564-565.

277. Stevens, L., Lanning, J.A., Anderson, L.G., Jacoby, W.A., Chornet, N., 1998. Investigation of the photocatalytic oxidation of low-level carbonyl compounds. *Journal of the Air & Waste Management Association* 48, 979-984.

278. Su, F., Calvert, J.G., Shaw, J.H., 1979. Mechanism of the photo-oxidation of gaseous formaldehyde. *Journal of Physical Chemistry* 83, 3185-3191

279. Sunada, K., Kikuchi, Y., Hashimoto, K., Fujishima, A., 1998. Bactericidal and detoxification effects of TiO_2 thin film photocatalysts. *Environmental Science and Technology* 32, 726–728.

280. Takahama, K., Sako, T., Yokoyama, M., Hirao, S., 1994. Preparation of Platinum-Loaded Supercritically-Dried TiO_2 Pillared Clays and Their Photocatalytic Activities in Oxidation of Carbon-Monoxide. *Nippon Kagaku Kaishi* 7, 613-618.

281. Takeda, N., Iwata, N., Torimoto, T., Yoneyama, H., 1998. Influence of carbon black as an adsorbent used in TiO_2 photocatalyst films on photodegradation behaviors of propyzamide. *Journal of Catalysis* 177, 240-246.

282. Takeda, N., Torimoto, T., Sampath, S., Kuwabata, S., Yoneyama, H., 1995. Effect of inert supports for titanium-dioxide loading on

enhancement of photodecomposition rate of gaseous propionaldehyde. *Journal of Physical Chemistry* 99, 9986-9991.n

283. Tanaka, K., Capule, M.F.V., Hisanaga, T., 1991. Effect of crystallinity of TiO_2 on its photocatalytic action. *Chemical Physics Letters* 187, 73-76.

284. Tanaka, K., Ohta, K., Haddad, P.R., Fritz, J.S., Lee, K.P., Hasebe, K., Ieuji, A., Miyanaga, A., 1999. *Journal of Chromatography A* 850, 311-317.

285. Tanaka, Y., Suganuma, M., 2001. Effects of heat treatment on photocatalytic property of sol-gel derived polycrystalline TiO_2. *Journal of Sol-Gel Science and Technology* 22, 83-89.

286. Tang Z., Zhang, J., Cheng, Z., Zhang, Z., 2002. Synthesis of nanosized rutile TiO_2 powder at low temperature. *Materials Chemistry and Physics* 77, 314-317.

287. Teichman, K.Y., 1995. Indoor air quality: research needs. *Occupational Medicine* 10, 217-227.

288. Teng, H.; Suuberg, E.M., 1993. Chemisorption of nitric-oxide on char.1. Reversible nitric-oxide sorption. *Journal of Physical Chemistry* 97, 478-493.

289. Torimoto T., Ito, S., Kuwabata, S., Yoneyama H., 1996. Effects of Adsorbents Used as Supports for Titanium Dioxide Loading on Photocatalytic Degradation of Propyzamide. *Environmental Science & Technology* 30, 1275-1281.

290. Torimoto T., Okawa, Y., Takeda, N., Yoneyama H., 1997. Effect of activated carbon content in TiO_2-loaded activated carbon on

photodegradation behaviors of dichloromethane. *Journal of Photochemistry and Photobiology A: Chemistry* 103, 153-157.

291. Toyoda, T., Hayakawa, T., Abe, K., Shigenari, T., Shen, Q., 2000. Photoacoustic and photoluminescence characterization of highly porous, polycrystalline TiO_2 electrodes made by chemical synthesis. *Journal of Luminescence* 87-89, 1237-1239.

292. Tsukuma, K., Akiyama, T., Yamada, N., Imai, H., 1998. Liquid phase deposition of a film of silica with an organic functional group. *Journal of Non-Crystalline Solids* 231, 161-168.

293. Tsumura, T., Kojitani, N., Umemura, H., Toyoda, M., Inagaki, M., 2002. Composites between photoactive anatase-type TiO_2 and adsorptive carbon. *Applied Surface Science* 196, 429-436.

294. U.S. Department of Energy. Specification for HEPA Filters used by DOE Contractors, http://tis.eh.doe.gov/hepa/standards.html.

295. U.S. Environmental Protection Agency, 1991. Air Quality Criteria for Carbon Monoxide. US Environmental Protection Agency, Washington, D.C.

296. U.S. Environmental Protection Agency, 1995. Characterizing air emissions from indoor sources. EPA Report EPA/600/F-95/005, Unites States Environmental Protection Agency, Washington, DC.

297. U.S. Environmental Protection Agency, 1999. Compendium method TO-11A, determination of formaldehyde in ambient air using adsorbent cartridge followed by high performance liquid chromatography (HPLC).

298. U.S. Environmental Protection Agency, 1999. Compendium method TO-14A, determination of volatile organic compounds (VOCs) in ambient air

using specially prepared canisters with subsequent analysis by gas chromatography.

299. Uchida, H., Itoh, S., Yoneyama, H., 1993. Photocatalytic Decomposition of Propyzamide Using TiO_2 Supported on Activated Carbon. *Chemistry Letters* 1995-1998.

300. Urano, K., Omori, S., Yamamoto, E., 1982. Prediction method for adsorption capacities of commercial activated carbons in removal of organic vapors. *Environmental Science & Technology* 16, 10-14.

301. Urban Air Pollution Control in China (UAPCC), 2001. China Science & Technology Press.

302. Van Winkle, M.R., Scheff, P.A., 2001. Volatile organic compounds, polycyclic aromatic hydrocarbons and elements in the air of ten urban homes. *Indoor Air* 11, 49-64.

303. VanOsdell D.M., Owen, M.K., Jaffe, L.B., Sparks L.E., 1996. VOC removal at low contaminant concentrations using granular activated carbon. *Journal of Air & Waste Management Association* 46, 883-890.

304. Vaughan, T.L., Strader, C., Davis, S., Daling, J.R., 1986. Formaldehyde and cancers of the pharynx, sinus, and nasal cavity: II. Residential exposures. *International Journal of Cancer* 38, 685-688.

305. Vega, E., Mugica, V., Carmona R., Valencia E., 2000. Hydrocarbon source apportionment in Mexico City using the chemical mass balance receptor model. *Atmospheric Environment* 34, 4121–4129.

306. Veyret, B., Lesclaux, R., Rayez, M.T., Rayez, J.C., Cox, R.A., Moortgat, G.K., 1989. Kinetics and Mechanism of the Photooxidation of

Formaldehyde .1. Flash-Photolysis Study. *Journal of Physical Chemistry* 93, 2368-2374.

307. Viegi, G., Carrozzi, L., Paoletti, P., Vellutini, M., DiViggiano, E., Baldacci, S., Modena, P., Pedreschi, M., Mammini, U., di-Pede, C., 1992. Effects of the home environment on respiratory symptoms of a general population sample in middle Italy. *Archives of Environmental Health* 47, 64-70.

308. Vogel, M., Buldt A., Karst, U., 2000. Hydrazine reagents as derivatizing agents in environmental analysis - a critical review. *Fresenius Journal of Analytical Chemistry* 366, 781-791.

309. Vorontsov, A. V., Savinov, E. N., Barannik, G. B., Troitsky, V. N., Parmon, V. N., 1997. Quantitative studies on the heterogeneous gas-phase photooxidation of CO and simple VOCs by air over TiO_2. *Catalysis Today* 39, 207-218.

310. Vorontsov, A. V., Savinov, E. N., Jin, Z.S., 1999. Influence of the form of photodeposited platinum on titania upon its photocatalytic activity in CO and acetone oxidation. *Journal of Photochemistry and Photobiology A: Chemistry* 125, 113-117.

311. Wallace, L., Nelson, W., Ziegenfus, R., Pellizzari, E., Michael, L., Whitemore, R., Zelon, H., Hartwell, T.Y., Perritt, R., Westerdahl, D., 1991. The Los Angeles team study: Personal exposures, indoor-outdoor air concentrations, and breath concentrations of 25 volatile organic compounds. *Journal of Exposure Analysis and Environmental Epidemiology* 1, 157-192.

312. Wallace, L.A., 1991. Personal exposure to 25 volatile organic compounds. EPA's 1987 team study in Los Angeles. California. *Toxicology and Industrial Health* 7, 203-208.

313. Wallace, L.A., 1991a. Comparison of risks from outdoor and indoor exposure to toxic chemicals. *Environmental Health Perspectives* 95, 7-13.

314. Wallace, L.A., 1997. Sick building syndrome. In:Bardana, E.J., Montanaro, A. (Eds.), Indoor Air Pollution and Health. Marcel Dekker, New York, 83-103.

315. Wamser, C.A., 1951. Equilibria in the System Boron Trifluoride--Water at 25°C. *Journal of the American Chemical Society* 82, 409-416.

316. Wang, D.X., Deng W., 2001. Atmospheric SO_2 pollution and acidity of rain in Changchun China. *Water Air and Soil Pollution* 130, 1631-1634.

317. Wang, J.H., Ray, M.B., 2000. Application of ultraviolet photooxidation to remove organic pollutants in the gas phase. *Separation and Purification Technology* 19, 11-20.

318. Wanner, H.U., 1993. Sources of pollutants in indoor air. *IARC Scientific Publications* 109, 19-30.

319. Weschler, C.J., Shields, H.C., Nalk, D.V., 1994. Indoor chemistry involving O_3, NO, and NO_2 as evidenced by 14 months of measurements at a site in southern California. *Environmental Science and Technology* 28, 2120-2132.

320. Wood, G.O., 2002. A review of the effects of covapors on adsorption rate coefficients of organic vapors adsorbed onto activated carbon from flowing gases. *Carbon* 40, 685-694.

321. World Health Organization, 1989. Indoor air quality: organic pollutants. WHO Regional Office for Europe (EURO Reports and Studies No. 111), Copenhagen.

322. Wright, G., Randall, P., Shepard, R.J., 1973. Carbon monoxide and driving skills. *Archives of Environmental Health* 27, 349-354.

323. Xie, Y., Yuan, C., 2004. Photocatalysis of neodymium ion modified TiO_2 sol under visible light irradiation. *Applied Surface Science* 221, 17-24.

324. Xu, Y., Langford, C.H., 1997. Photoactivity of Titanium Dioxide Supported on MCM41, Zeolite X and Zeolite Y. *Journal of Physical Chemistry B* 101, 3115-3121.

325. Xu, Y., Zheng, W., Liu, W., 1999. Enhanced photocatalytic activity of supported TiO_2: dispersing effect of SiO_2. *Journal of Photochemistry and Photobiology A:Chemistry* 122, 57-60.

326. Yamazaki S, Fujinaga N, Araki K., 2001. Effect of sulfate ions for sol-gel synthesis of titania photocatalyst. *Applied Catalysis A: General* 210, 97-102.

327. Yang, J.J., Li, D.X., Zhang, Z.J., Li, Q.L., Wang, H.Q., 2000. A study of the photocatalytic oxidation of formaldehyde on $Pt/Fe_2O_3/TiO_2$. *Journal of Photochemistry and Photobiology A:Chemistry* 137, 197-202.

328. Yoldas, B.E., 1989. Formation of Titania-Silica Glasses by Low-Temperature Chemical Polymerization. *Journal of Non-Crystalline Solids* 38-39, 81-86.

329. You, Y.S., Chung, K.H., Kim, J.H., Seo, G., 2001. Photocatalytic Oxidation of Toluene over TiO_2 Catalysts Supported on Glass Fiber. *Korean Journal of Chemical Engineering* 18, 924-929.

330. Yu, H.F., Wang, S.M., 2000. Effects of water content and pH on gel-derived TiO_2-SiO_2. *Journal of Non-Crystalline Solids* 261, 260-267.

331. Yu, J.C., Ho, W.K., Lin, J., Yip, K.Y., Wong, P.K., 2003a. Photocatalytic activity, antibacterial effect, and photoinduced hydrophilicity of TiO_2 films coated on a stainless steel substrate. *Environmental Science and Technology* 37, 2296-2301.

332. Yu, J.C., Yu, J.G., Ho, W.K., Jiang, Z.T., Zhang, L.Z., 2002b. Effects of F- doping on the photocatalytic activity and microstructures of nanocrystalline TiO_2 powders. *Chemistry of Materials* 14, 3808-3816.

333. Yu, J.C., Yu, J.G., Ho, W.K., Zhang, L.Z., 2001a. Preparation of highly photocatalytic active nano-sized TiO_2 particles via ultrasonic irradiation. *Chemical Communications*, 1942-1943.

334. Yu, J.C., Yu, J.G., Zhao, J.C., 2002. Enhanced photocatalytic activity of mesoporous and ordinary TiO_2 thin films by sulfuric acid treatment. *Applied Catalysis B: Environmental* 36, 31-43.

335. Yu, J.G., Yu, H.G., Cheng, B., Zhao, X.J., Yu, J.C., Ho, W.K., 2003. The Effect of Calcination Temperature on the Surface Microstructure and Photocatalytic Activity of TiO_2 Thin Films Prepared by Liquid Phase Deposition. *Journal of Physical Chemistry B* 107, 13871-13879.

336. Yu, J.G., Yu, J.C., Leung, M.P.K., Ho, W.K., B., Cheng, Zhao, X.J., Zhao, J.C., 2002a. Effects of acidic and basic hydrolysis catalysts on the photocatalytic activity and microstructures of bimodal mesoporous titania. *Journal of Catalysis* 217, 69-78.

337. Yu, J.G., Yu, J.C., Zhao, X.J., 2002b. The effect of SiO_2 addition on the grain size and photocatalytic activity of TiO_2 thin films. *Journal of Sol-Gel Science and Technology* 24, 95-103.

338. Yu, J.G., Zhao, X.J., 2001. Effect of surface treatment on the photocatalytic activity and hydrophilic property of the sol-gel derived TiO_2 thin films. *Materials Research Bulletin* 36, 97-107.

339. Yu, J.G., Zhao, X.J., Zao, Q.N., 2000. Effect of surface structure on photocatalytic activity of TiO_2 thin films prepared by sol-gel method. *Thin Solid Films* 379, 7-14.

340. Zhai, J.W., Zhang, J.Y., Yao, X., 1999. Effects of composition and temperature on gel-formed TiO_2/SiO_2 films. *Journal of Non-Crystalline Solids* 260, 160-163.

341. Zhang, J.L., Ayusawa, T., Minagawa, M., Kinugawa, K., Yamashita, H., Matsuoka, M., Anpo, M., 2001. Investigations of TiO_2 photocatalysts for the decomposition of NO in the flow system: The role of pretreatment and reaction conditions in the photocatalytic efficiency. *Journal of Catalysis* 198, 1-8.

342. Zhang, P., Liang, F., Y, Gang., Chen, Q., Zhu W., 2003. A comparative study on decomposition of gaseous toluene by O_3/UV, TiO_2/UV and O_3/TiO_2/UV. *Journal of Photochemistry and Photobiology A: Chemistry* 156, 189-194.

343. Zhang, Y., Crittenden, J.C., Hang, D.W., Perram, D.L., 1994. Fixed-Bed Photocatalysts for Solar Decontamination of Water. *Environmental Science and Technology* 28, 435-442.

344. Zhang, Z.B., Wang, C.C., Zakaria, R., Ying, J.Y., 1998. Role of Particle Size in Nanocrystalline TiO_2-Based Photocatalysts. *Journal of Physical Chemistry B* 102, 10871-10878.

345. Zhao, J., Yang, X.D., 2003. Photocatalytic oxidation for indoor air purification: a literature review. *Building and Environment* 38, 645-654.

346. Zhu, Y.F., Zhang, L., Wang, L., Fu, Y., Cao, L.L., 2001. The preparation and chemical structure of TiO_2 film photocatalysts supported on stainless steel substrates via the sol-gel method. *Journal of Materials Chemistry* 11, 1864-1868.

Appendix I Analytical equipments & procedures

1. Carbon monoxide (CO)

A gas filter correlation (GFC) spectrometer was used to analyze CO concentration continuously in this study. IR radiation is chopped and then passed through a gas filter alternating between CO and N_2 due to rotation of the filter wheel. The radiation then passed through a narrow band pass interference filter and entered a multiple optical passed cell where absorption by the sample gas occurred. The IR radiation then exited the sample cell and fell on an IR detector. CO concentration is obtained by comparing signal generated from CO (reference beam) & N_2 (measure beam) filter. The CO analyzer (Thermo Environmental Instruments Inc. Model 48) used in this study is shown in Fig. A1.

Figure A1 CO analyzer (Thermo Environmental Instruments Inc. Model 48)

2. Nitrogen monoxide (NO) and nitrogen dioxide (NO_2)

A chemiluminescence analyzer was used to analyze the NO and NO_2 concentrations continuously in this study. It utilizes the principle that NO reacts with O_3 and produces a characteristic luminescence with an intensity linearly proportional to the NO concentration. Infrared light emission results when electronically excited NO_2 molecules decay to lower energy states. A photomultiplier tube housed in a thermoelectric cooler detects the NO_2 luminescence. NO_2 is measured by converting to NO by a molybdenum NO_2-to-NO converter heated to about 325°C. The NO analyzer (Thermo Environmental Instruments Inc. Model 42c) used in this study is shown in Fig. A2.

Figure A2 NO-NO_2-NO_x analyzer (Thermo Environmental Instrument Inc., Model 42c).

3. *Sulfur dioxide (SO_2)*

A pulsed fluorescence analyzer was used to measure the SO_2 concentration continuously in this study. Pulsating ultraviolet (UV) light is filtered and focused into a fluorescence chamber. It excites SO_2 molecules into higher energy state. Owing to the excited SO_2 is very unstable, it rapidly decayed back to ground state and emitted a characteristic radiation. A second filter allowed only this radiation passed through a high sensitive photomultiplier tube (PMT). It is used to convert this light energy into electrical signal which is proportional to the SO_2 concentration. The SO_2 analyzer (Thermo Environmental Instruments Inc. Model 43b) used in this study is shown in Fig. A3.

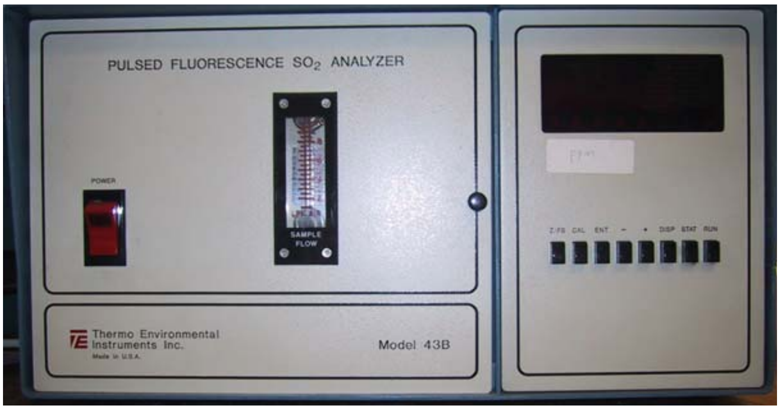

Figure A3 SO_2 analyzer (Thermo Environmental Instrument Inc., Model 43b).

4. Non-Methane Hydrocarbon (NMHC)

A back-flush gas chromatography (GC) system was used to measure the concentrations of methane and total hydrocarbons (NMHC) continuously in this study. It uses a read time flame ionization detector (FID) and a separation column. Methane moves faster than other organic compounds due to its low molecular weight and high volatility, and is the first to emerge from the end of the column. Once the methane peak has been detected, the direction of the carrier gas flow through the column is reversed and the NMHC are black-flushed out of the column and carried to the FID for measurement. Its signal is converted into a concentration by comparison with the signal produced by a calibration gas. The NMHC analyzer (Thermo Environmental Instruments Inc. Model 55c) used in this study is shown in Fig. A4.

Figure A4 NMHC analyzer (Thermo Environmental Instrument Inc., Model 43b).

5. *Volatile organic compounds (VOCs)*

USEPA Compendium Method TO-14A (USEPA, 1999) was used to analyze the VOCs concentration in this study. Samples were collected in a Summa canister (Fig A5). The systems consisted of a cryogenic concentration (Nutech 3550A, USA) with a gas chromatograph (GC) (HP 6980A) fitted with a mass selective detector (MSD) (HP 5973). 250 mL of the sample was loaded and concentrated in the cryogenic trap with liquid nitrogen. A capillary column (Restek RTX-1 column, 60m x 0.32mm, ID 0.3μm) was used for the GC/MS with an initial oven temperature of -30°C to 80°C at a heating rate of 10°C/min and finally raised to 220°C at a heating rate of 5°C/min.

VOCs were then identified by the mass spectra, retention time and fragmentation patterns. The VOCs was then quantified by multipoint calibration. The GC/MS used in this study is shown in Fig. A6.

Figure A5 Summer canister used for VOCs sampling.

Figure A6 GC/MS system used for VOCs analysis; (a) Nutech Cryogenic Concentrator; (b) Mass Selective Detector; (c) Gas Chromatography.

6. Aldehydes

USEPA Compendium Method TO-11A (USEPA, 1999a) was used to analyze the aldehydes concentration in this study. Samples were collected by a Desert Research

Institute standard carbonyl sampler (Fig. A7). The cartridge was eluted with 5 ml of acetonitrile (HPLC grade). The DNPH-carbonyl derivatives were analyzed by injecting 20 μl of the sample into a High Performance Liquid Chromatography (HPLC). The HPLC system consisted of a dual wavelength absorbance detector (Waters 2487) operating at 360 nm with a binary pump (Waters 1525) and an in-line degasser. A Nova-Pak (Waters) C_{18} reverse phase column (150mm x 3.9 mm) with a particle size of 4mm and pore size of 60Å was used to separate the hydrazones. The use of the reverse phase column is to facilitate the separation of formaldehyde from other aliphatic hydrazones since the hydrazones are eluted in the order of decreasing polarity (Potter and Karst, 1996). The mobile phase consisted of two solvent mixtures, namely mixture A: 6:3:1 (v/v) of water/acetonitrile/tetrahydrofuran; and mixture B: 4:6 (v/v) of water/acetonitrile. The gradient program was 100% A for 1 min, followed by a linear gradient from 100% A to 100% B in 16 min. The pumping rate was 1.5 mL/min. The GC/MS used in this study is shown in Fig. A8.

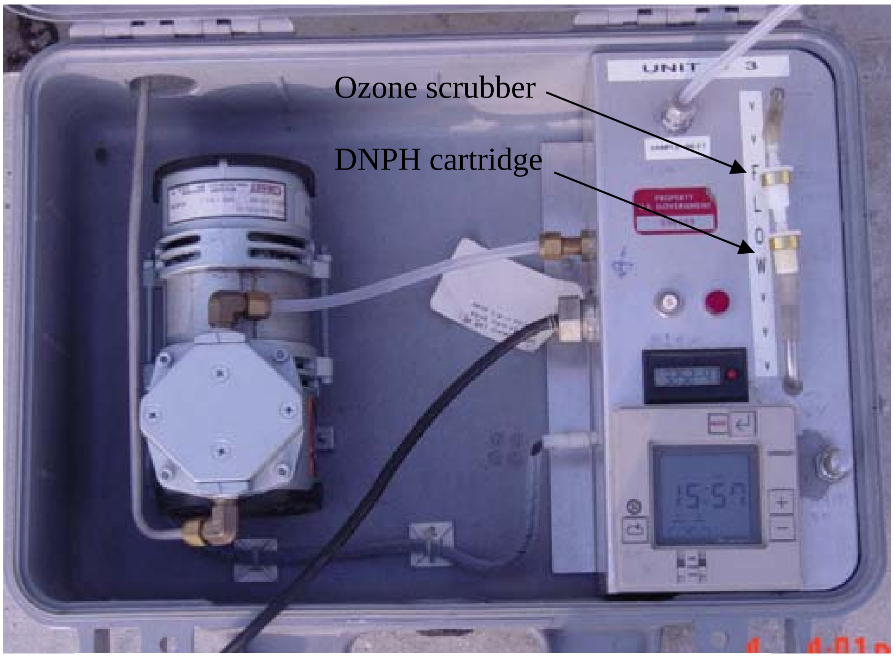

Figure A7 DRI standard carbonyl sampler.

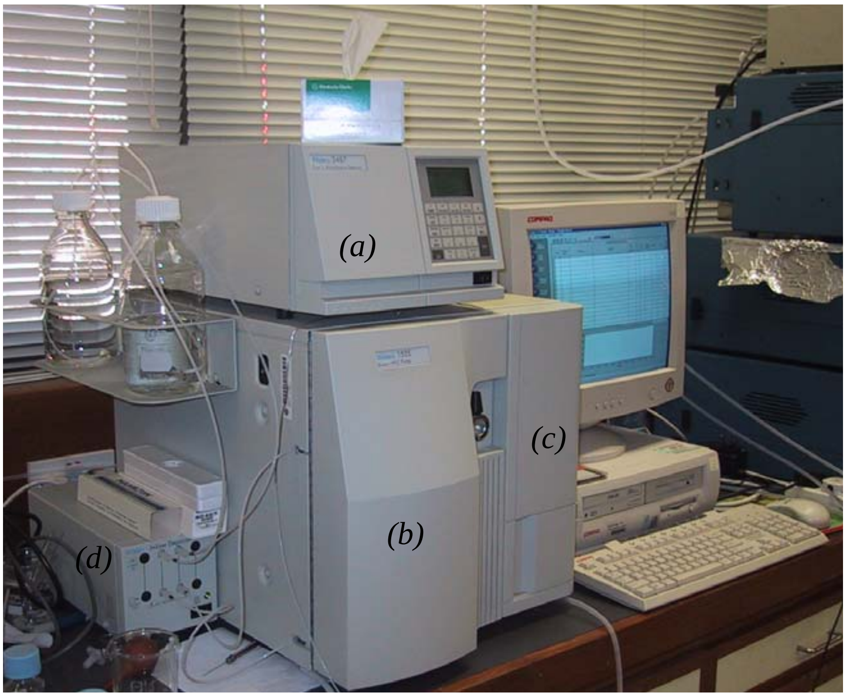

Figure A8 HPLC (Waters) for aldehydes analysis; (a) UV detector; (b) binary pump; (c) column; (d) in-line degasser.

7. Nitrate ion, sulfate ion and formic acid

Ion Chromatography (IC) was used to determine the concentrations of the formic acid, nitrate ion and sulfate ion by immersing the TiO_2 glass fiber filter into distilled deionized water for 24 hours. The solution was then filtered through a 0.45 μm filter to avoid clogging the column. It was then analyzed by a Dionex DX500 ion chromatograph with a conductivity detector. An AG11 guard column and an AS11 analytical column were used to separate the analytes. A Dionex ASRS-ultra anion self regenerating suppressor ensured the lowest possible background noise levels and detection limits. A sampling loop of 50μl was chosen. The eluent for these samples was 0.2-5 mM NaOH (gradient) and its flowrate during the analyses was equal to 2 mL/min.

8. Intermediates generated from the photodegradation of VOCs

Intermediates generated from the photodegradation of VOCs were identified by the following methods:

1. Gaseous phase intermediates (except aldehydes) were collected by the canister used for VOCs sampling and identified by GC/MS.
2. Gaseous phase intermediates of aldehydes were collected by the DNPH cartridge and analyzed by HPLC.

3. Intermediates accumulated on the TiO_2 filter was washed and immersed in ethanol. The solution was then filtered and analyzed by GC/MS.

Appendix II TiO$_2$ photocatalyst coated on stainless steel

1. Introduction

TiO$_2$ was also coated on metal surface such as stainless steel. Surface characterization methods such as FTIR, XRD, SEM, PL and XPS were used to characterize the TiO$_2$ coated on the stainless steel. NO was used as the target pollutant to evaluate the photocatalyst activity. An optimum NO conversion was obtained by modifying the synthetic parameters of the LPD process.

2. Characterization of photocatalyst

2.1 Fourier Transform Infrared Spectroscopy (FTIR)

Infrared absorption spectra were recorded for KBr disks containing powder sample obtained by scraping the films from the substrates with a FTIR spectrometer (Nialet –60SXB, American). FTIR spectra of the TiO$_2$ thin films are shown in Fig. B1. A broad absorption peak at 400 – 700 cm^{-1} wavelength range is clearly visible, which is attributed to the Ti-O stretching and Ti-O-Ti bridging stretching modes (Peiro et al., 2001). The absorption peak at 910 cm^{-1} is due to the vibration of Ti-F bond (Tsukuma et al., 1998). The peaks at 1419 cm^{-1} and at 1638 cm^{-1} can be ascribed to the bending vibrations of N-H bonds and O-H bonds, respectively (Yu et al., 2002b; Ko et al., 2003). A broad band is observed at 2800 – 3800 cm^{-1} wavelength range, which is assigned to the stretching modes of O-H bonds and of N-H bonds (Ko et al., 2003). The FTIR spectra of the sample dried at 100^{o}C reveals that the Ti-O, Ti-F, N-H, O-H groups exist in the as-prepared sample. Since LPD process was performed in the aqueous solution system, the samples easily absorbed the water molecules, NH_4^+ and F^- ions in the treatment solution. With increasing calcination temperature, the intensities of peaks related to the O-H, N-H, and Ti-F groups gradually decreased and the N-H and Ti-F groups then disappeared completely at 500^{o}C, while the intensities of peak related to Ti-O group increased. It has been shown that the removal of N-H, Ti-F and O-H groups promoted the rearrangement of Ti-O network and enhanced the crystallization of titania. When calcination temperature was over 500^{o}C, there were also some small vibration bands related to the O-H bonds, which was caused by the chemically absorbed water of Ti-OH. This means that the chemisorbed water is not completely removed even at the high-temperature calcination at 900^{o}C.

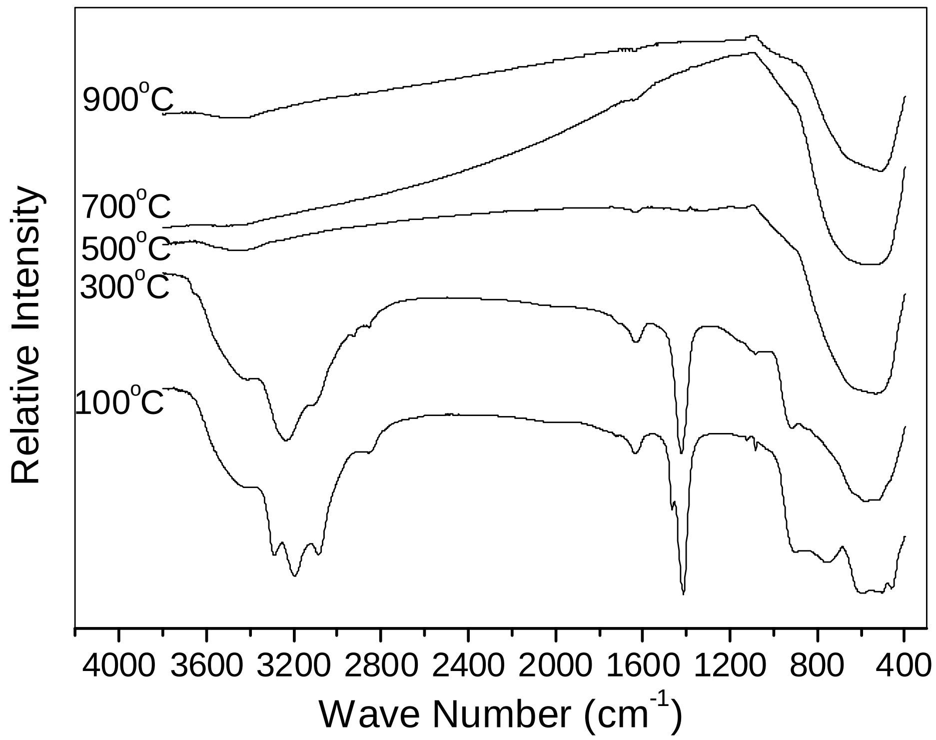

Figure B1 Infrared spectra of TiO_2 powder calcinated at 100, 300, 500, 700 and 900°C.

2.2 X-ray diffraction (XRD)

The X-ray diffraction (XRD) patterns obtained on a Bruker D8 Advance X-ray diffractometer using Cu-Kα radiation at a scan rate of 0.05° 2$\theta\cdot S^{-1}$ were used to determine the identity of crystalline phase and the crystallite size. The accelerating voltage and the applied current are 40 kV and 40 mA, respectively. XRD was used to investigate the phase constitutions and average crystallite size of the TiO_2 films. When calcination temperature was below 400°C, there was no diffraction peak, which was due to the fact that the thin films are amorphous. Fig. B2 shows the XRD patterns of the TiO_2 thin films calcinated at 400, 500, 700, and 900^{o}C. At 400^{o}C, a weak diffraction peak at $2\theta = 25.3^{o}$ was observed. This suggested that the phase transformation temperature from amorphous to anatase in the thin films was ca. 400^{o}C. With increasing calcination temperature, the peak intensity of anatase increased and the width of (101) peak of anatase became narrower, which was due to the enhancement of crystallization and the growth of crystallites. At 900^{o}C, the rutile phase began to form and became the main crystallite phase. Therefore, the phase transformation temperature of anatase to rutile was ca. 900^{o}C for the TiO_2 thin films prepared by LPD method, which was higher than that of the samples prepared by sol-gel method (ca. 700^{o}C) (Yu et al., 2001a; Yu et al., 2002;). The higher phase transformation temperature from anatase to rutile can be ascribed to the formation of Ti-O-Fe bonds in the thin film (as discussed below). The Fe-O species at the interface of TiO_2 crystallites inhibit the formation of rutile phase by preventing the nucleation that is necessary for the phase transformation to rutile. Therefore, it is necessary to provide greater heat to promote the phase transformation of anatase to rutile. Similar results were observed in the TiO_2 thin films deposited on the fused quartz by LPD method (Yu et al., 2003).

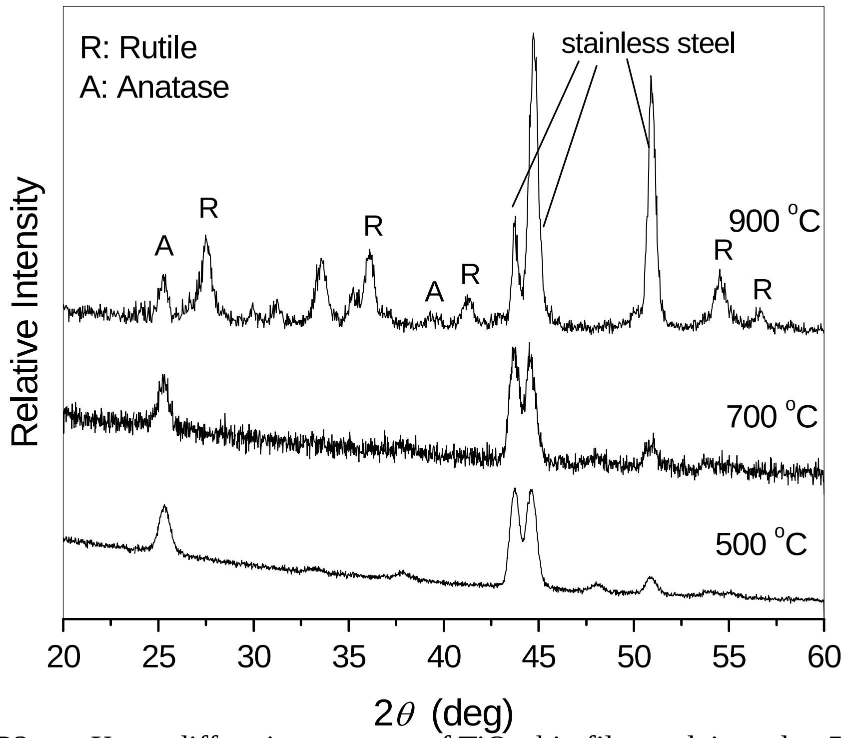

Figure B2 X-ray diffraction patterns of TiO_2 thin films calcinated at 500, 700, and 900°C.

2.3 Scanning Electron microscope (SEM)

Fig. B3 shows the SEM micrographs of the TiO_2 thin films calcinated at 100, 300, 500, 700 and 900°C. The surface morphologies and roughness of the TiO_2 thin films did not change significantly when calcination temperature was not over 700°C. With increasing calcination temperature, the cracks on the surface of films become wider and more cracks were observed, which was caused by the different thermal expansion coefficient between the TiO_2 and the stainless steel substrate. The stainless steel substrate has a higher coefficient (17×10^{-6} °C) of line thermal expansion than TiO_2 ($2.1\text{-}2.8\times10^{-6}$ °C) (Balasubramanian et al., 1983). The different thermal expansion coefficients between TiO_2 and the stainless steel substrate also cause interfacial stresses between the thin film and the substrates. During the heating or cooling, if the interfacial stresses were larger than the adhering stresses between thin film and substrate, the film would drop off from the substrate. In our samples, (there were no such the phenomena of dropping off for the thin film from the substrates) no such phenomenon was observed. The strong adhesion between the films and stainless steel was attributed to the formation of the chemical bonds of Ti-O-Fe at the interface of TiO_2 and substrate during calcination. Hence, heat treatment not only enhanced the crystallization of TiO_2 thin films but also improved the adherence between TiO_2 thin film and stainless steel substrate. At 900^{o}C, the surface morphology of TiO_2 thin film changed significantly. It can be seen from Fig. B3(e) that the width of cracks increased significantly and the TiO_2 film was composed of many large crystallites with a diameter of 200-400 nm. This is attributable to the fact that the phase transition from anatase to rutile accelerated the grain growth and sintering of TiO_2 crystallites by providing the heat of phase transformation. The thickness of TiO_2 thin films calcinated at 100, 500, 700 and 900^{o}C were ca. 400, 320, 250 and 230 nm, respectively, according to the SEM cross-section observation of the films.

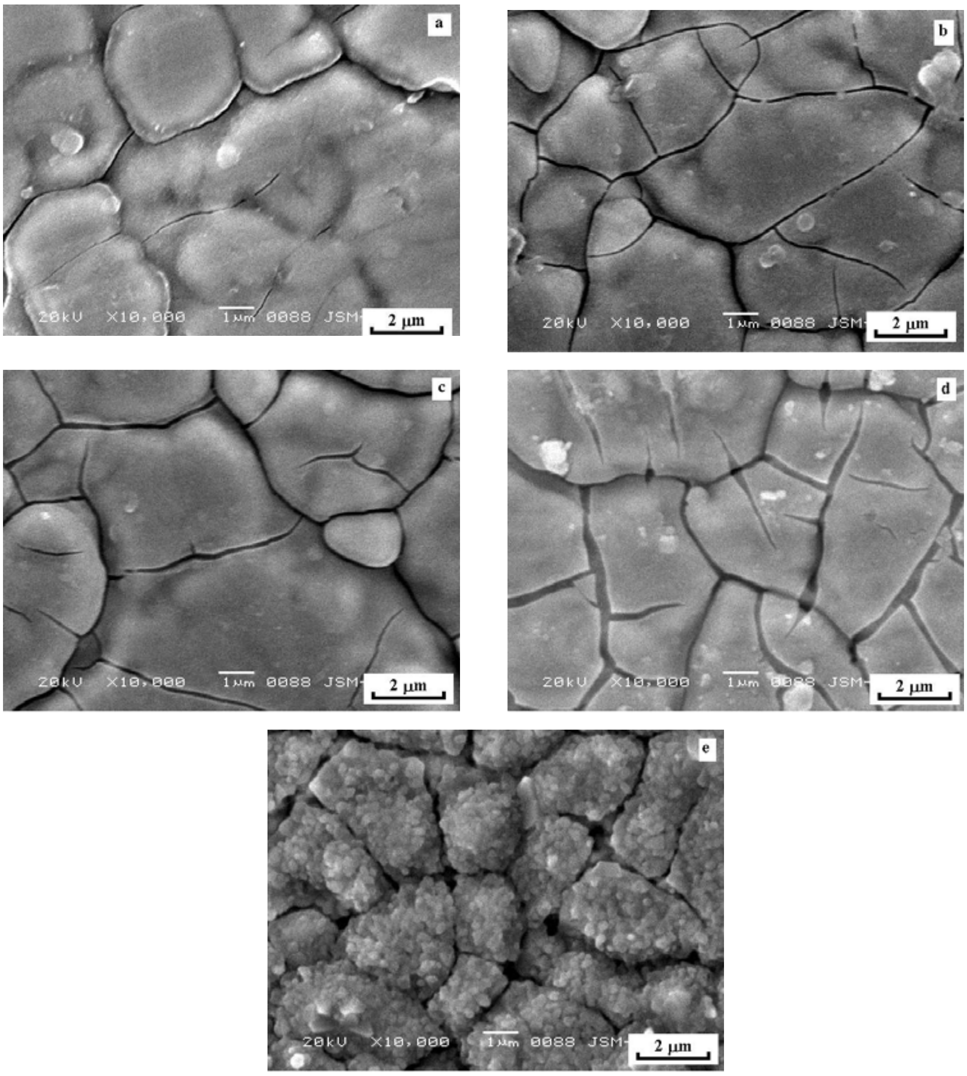

FigureB3 SEM micrographs of TiO_2 films calcinated at (a) 100, (b) 300, (c) 500, (d) 700 and (e) 900^{o}C.

2.4 Photoluminescence Spectra (PL)

The PL emission spectra can be used to investigate the efficiency of charge carrier trapping, immigration and transfer, and to understand the fate of photogenerated electrons and holes in semiconductor since PL emission results from the recombination of free carriers (Li and Li, 2001; Li and Li, 2002). Fig. B4 shows the room temperature PL spectra for TiO_2 thin films calcinated at 100, 300, 500, 700 and 900^{o}C in the range of 2.3-3.6 eV. Two main emission peaks appear at about 3.38 and 2.62 eV, which corresponds to the 367 and 473 nm wavelengths, respectively. The former is ascribed to the emission of band gap transition (Li and Li, 2002a). The latter is the emission signal originated from the charge-transfer transition from Ti^{3+} to oxygen anion in a TiO_6^{8-} complex (Li and Li, 2002a; Yu et al., 2002b). The difference of about 0.8 eV between the band gap energy (3.4 eV for anatase, as shown in Fig B.3) and the emission peak energy (2.6 eV) is caused by the Stokes shift due to the Franck-Condon effect (Li and Li, 2002a; Fujihara et al., 2002; Serpone et al., 1995). The variation of PL intensity may results from the change of defect states on the shallow level of film surface (Li and Li, 2002; Toyoda et al., 2000). Therefore, a lower PL intensity might show a lower recombination rate of photogenerated electrons and holes on the shallow level of film under light irradiation. It can be seen from Fig.B4 that the PL intensity decreased with increasing calcination temperature. At 500^{o}C, the PL intensity reaches the lowest value and then increased at a higher calcination temperature than 500^{o}C. The decrease of PL intensity was due to the decomposition of intermediates $(NH_4)_2TiF_{6-n}(OH)_n$, removal of other impurities, phase transformation of amorphous to anatase and enhancement of crystallization of anatase, leading to the decrease of defect sites or recombination centers.

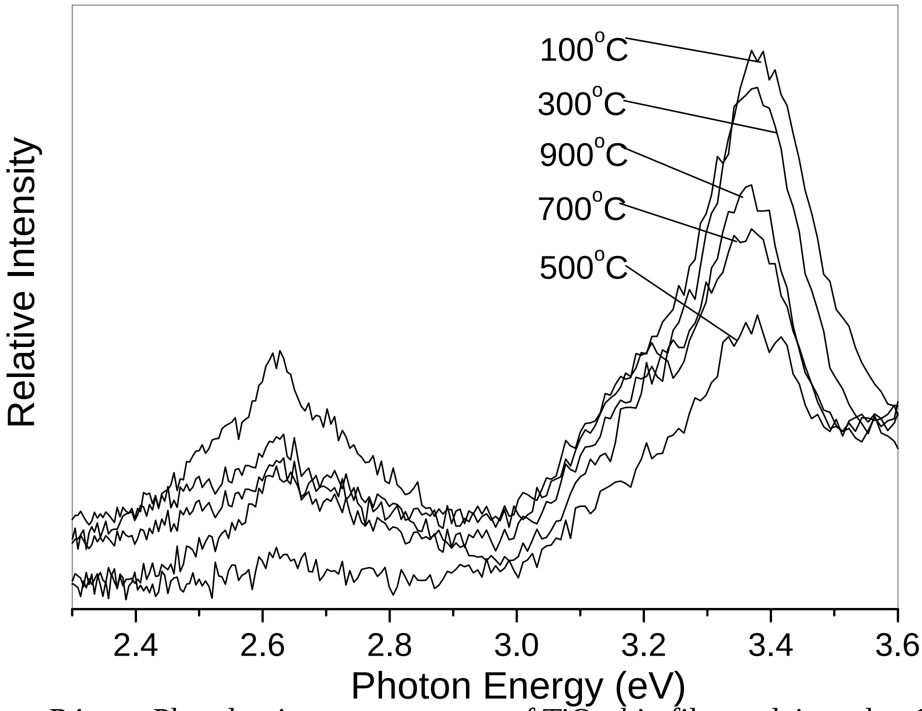

FigureB4 Photoluminescence spectra of TiO_2 thin films calcinated at 100, 300, 500, 700 and 900°C.

2.5 X-ray Photoelectron Spectroscopy (XPS)

Fig.B5 shows the XPS survey spectra of TiO_2 thin films calcinated at 100, 300, 500, 700 and 900°C. TiO_2 thin films deposited on stainless steel not only contained Ti and O elements, but also F, N and Fe elements. The XPS peak for C1s at E_b = 284.8 eV was observed due to the adventitious hydrocarbon from XPS instrument itself. The XPS peaks for F and N were also observed, which come from the residual elements in precursor solution. Table B1 shows the composition (at %) of TiO_2 thin films calcinated at various temperatures according to the XPS analysis. It can be seen that the amount of F and N elements in the film decreased with increasing calcination temperature and finally the F element disappeared completely at 500^{o}C. On the contrary, the amount of Fe element increased due to the diffusion of Fe^{3+} from the stainless steel substrate into the TiO_2 thin films.

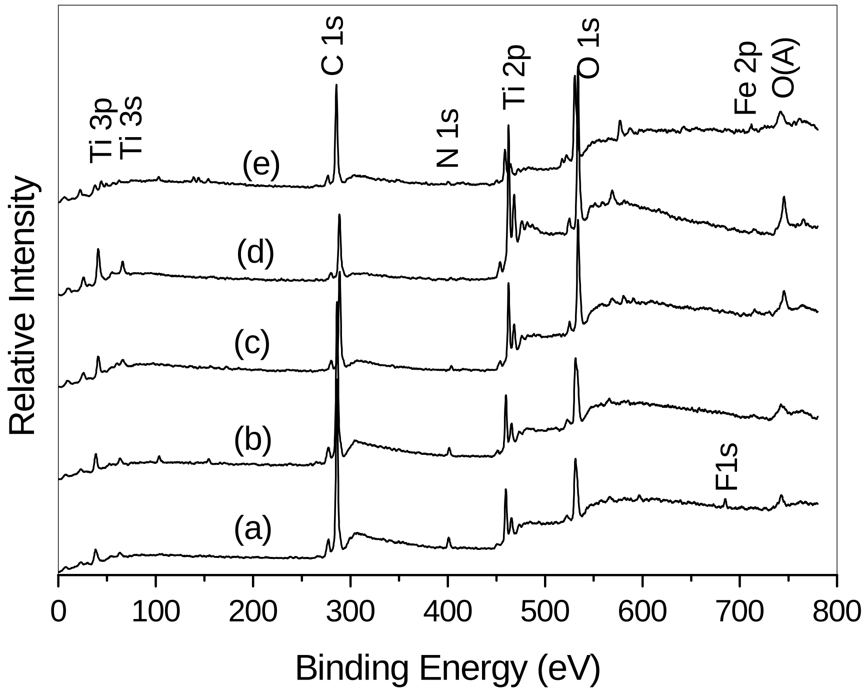

Figure B5 XPS survey spectra for the surface of TiO_2 films calcinated at (a) 100, (b) 300, (c) 500, (d) 700 and (e) 900^{o}C.

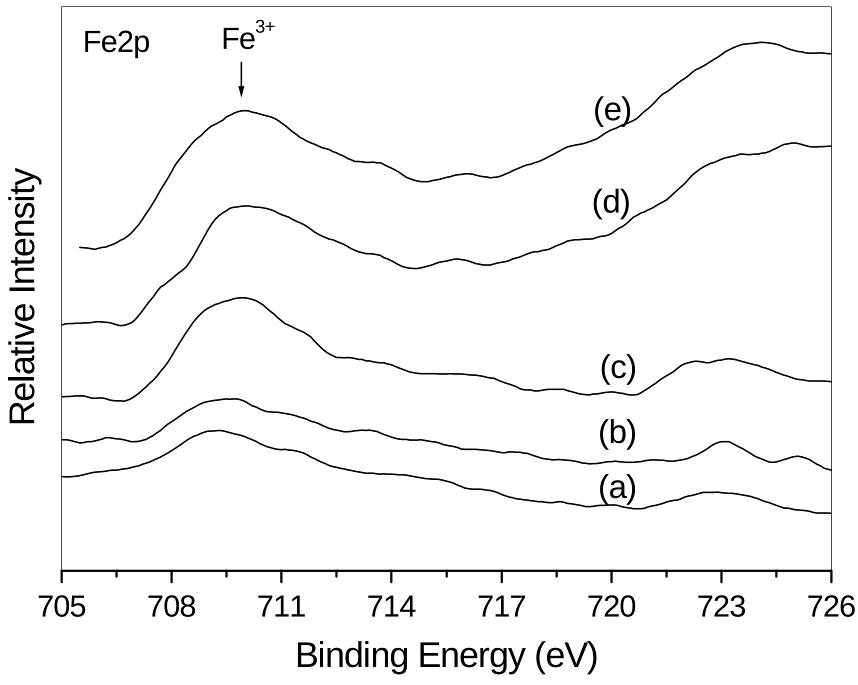

Figure B6 High-resolution XPS spectra of the Fe2p region of the TiO_2 thin films calcinated at (a) 100, (b) 300, (c) 500, (d) 700 and (e) 900^{o}C.

Fig. B6 shows the high-resolution XPS spectra of Fe2p region, taken on the surface of TiO_2 thin films calcinated at 100, 300, 500, 700 and 900^oC. It can be found that the peak for $Fe2p_{3/2}$ in each TiO_2 film was contributed to the Fe^{3+} (Kang et al., 2003; Zhang et al., 2003). It is well known that XPS is a surface probe detecting electrons that are generated from a depth of a few nm on the surface of sample. The thickness of TiO_2 thin films in our experiment was over 200 nm, which is much larger than the depth that XPS could detect. Moreover, the film sample calcinated at 100^oC was dense and did not fracture according to the previous SEM observation. It can be inferred that the photoelectron peaks for Fe2p come from the thin film itself, but not from the surface of stainless steel substrate.

Usually, it is impossible for Fe^{3+} to diffuse from stainless steel substrate into TiO_2 thin film at 100^oC, while the sample before calcination has also showed the photoelectron peaks for Fe2p on the XPS spectra. In the liquid phase deposition process, the ligand exchange equilibrium reactions of metal-fluorocomplex ions and consuming reaction F^- by boric acid as an F^- scavenger exist in the same reaction system as shown in the following equations (Toyoda et al., 2000; Schmitt et al., 1960):

$$[TiF_6]^{2-} + n\ H_2O \rightleftharpoons [TiF_{6-n}(OH)_n]^{2-} + n\ HF \qquad (B.1)$$

$H_3BO_3 + 4\ HF \rightleftharpoons BF_4^- + H_3O^+ + 2\ H_2O$ (B.2)

According to equations (B.1) and (B.2), HF and H^+ were produced in the treatment solution during deposition process. When stainless steel substrate was immersed into the treatment solution, the following reaction occurred:

$Fe + 6\ HF \longrightarrow [FeF_6]^{3-} + 3/2H_2 + 3\ H^+$ (B.3)

If the surface of stainless steel has been partly oxidized, the following reaction also occurred in the system:

$Fe_2O_3 + 12\ HF \longrightarrow 2\ [FeF_6]^{3-} + 3\ H_2O + 6\ H^+$ (B.4)

In the treatment solution, the Fe^{3+} were coordinated by fluorine ions to form $[FeF_6]^{3-}$. Also, there were other two-equilibrium reactions in the system as following (Wamser, 1951):

$[FeF_6]^{3-} + n\ H_2O \rightleftharpoons [FeF_{6-n}(OH)_n]^{3-} + n\ HF$ (B.5)

$[FeF_{6-n}(OH)_n]^{3-} + (6-n)\ H_2O \rightleftharpoons [Fe(OH)_6]^{3-} + (6-n)\ HF$ (B.6)

The ligand-exchange equilibrium reactions (equations (B.5) and (B.6)) shifted to the right-hand side when the consuming reaction of F^- (equation B.2) occurred by the addition of boric acid as an F^- scavenger to the treatment solution. Deki et al. (2003) observed that the deposition of TiO_2 thin film and precipitation of TiO_2 powder arose through the dehydration reaction of $[TiF_{6-n}(OH)_n]^{3-}$. In the present work, similar phenomenon also existed in the reaction system. The dehydration reaction between the $[FeF_{6-n}(OH)_n]^{3-}$ and $[TiF_{6-n}(OH)_n]^{2-}$ arose during the deposition and calcination process leading to the formation of Ti-O-Fe in the TiO_2 thin film. Since the radius of Fe^{3+} (0.64 A) and Ti^{4+} (0.68 A) are similar, the Fe^{3+} can be incorporated into the lattice of TiO_2 without any significant alteration of crystal structure during calcination process (Deki et al., 1997). Similar, Fe^{2+} also deposited onto the thin film when there was some Fe^{2+} in the treatment solution, but the Fe^{2+} was easily oxidized to Fe^{3+} during calcination process in air. Thus, the Fe element on the surface of TiO_2 thin films was mainly Fe^{3+}.

Films	O	Ti	F	Fe	N
100°C	65.8	23.3	5.0	1.2	4.7
300°C	69.8	23.8	0.7	1.4	4.3
500°C	70.2	23.8	0	2.2	3.8
700°C	68.9	24.5	0	3.4	2.9
900°C	72.8	20.7	0	4.0	2.5

Table B1 Composition (at %) of TiO_2 thin films calcinated at various temperatures according to XPS analysis.

From Table B1 and Fig. B6, the amount of Fe^{3+} increased significantly when calcination temperature was over 500°C. Zhu et al. (2001) and Yu et al. (2003) also prepared TiO_2 films on stainless steel substrate by sol-gel method. They found that there was some Fe element on the surface of the samples calcinated at 500°C, which is ascribed to the diffusion of Fe element from stainless steel into TiO_2 film. Herein, there also existed the diffusion phenomenon of Fe^{3+} for the samples calcinated at 500°C or a higher temperature.

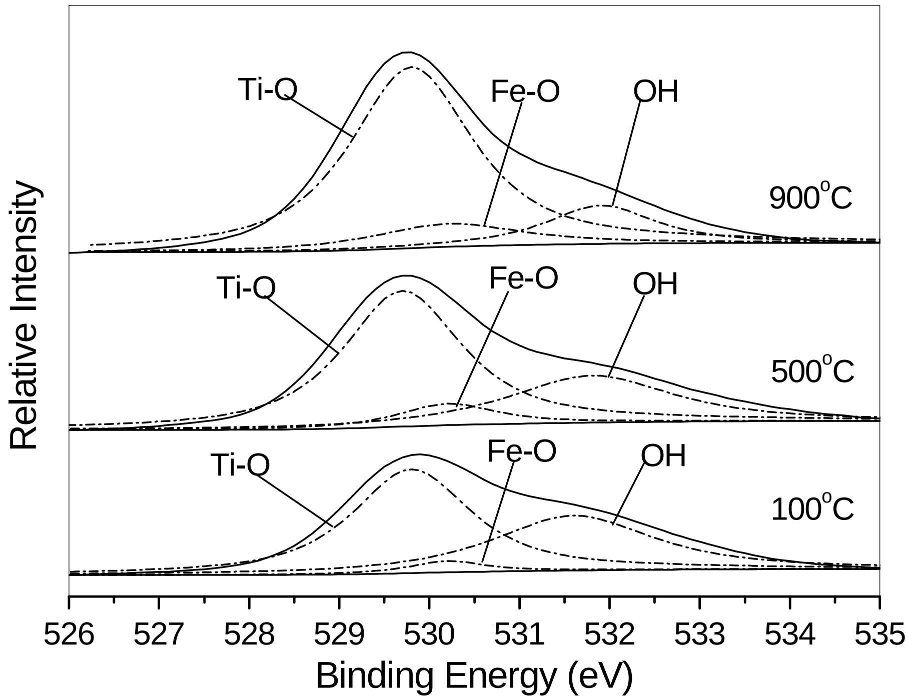

Figure B7 High-resolution XPS spectra of the O1s region of the TiO_2 thin films calcinated at 100, 500 and 900°C.

Fig. B7 shows the high-resolution XPS spectra of the O1s region, taken on the surface of TiO_2 thin films calcinated at 100, 500 and 900°C. It can be seen from Fig. B7 that the O1s region was fitted into three contributions. The main contribution was attributed to the Ti-O in TiO_2 and the other two kinds of oxygen contributions were ascribed to the OH in Ti-OH and the Fe-O, respectively. Although some H_2O was easily adsorbed on the surface of TiO_2 films, the physically absorbed H_2O on TiO_2 was easily desorbed under the ultra-high vacuum condition of the XPS system. Therefore, the hydroxyl groups can be attributed to the Ti-OH on the surface of thin films. Table B.2 lists the results of the curve fitting of XPS spectra for TiO_2 films samples calcinated at 100, 500 and 900^{o}C. As can be seen from Table B2 and Fig. B7, the hydroxyl content of samples decreased slightly with increasing calcination temperature, which is due to the fact that there is a reaction on the surface of TiO_2 thin films during calcination process: Ti-OH + HO-Ti $\rightarrow$ Ti-O-Ti + H_2O. According to Table B2, the amount of Fe-O in the TiO_2 thin films increased significantly when the calcination temperature was over 500^{o}C, which is attributed to the diffusion of Fe element from the surface of stainless steel to the TiO_2 thin films.

Films		O1s (Ti-O)	O1s (OH)	O1s(Fe-O)
TiO_2/steel+ (100℃)	E_b/eV	529.8	531.8	530.2
	r_i/%	60.67	35.44	3.89
TiO_2/steel + (500℃)	E_b/eV	529.8	531.8	530.2
	r_i/%	65.61	26.21	8.18
TiO_2/steel + (900℃)	E_b/eV	529.8	531.8	530.2
	r_i/%	73.66	14.86	11.48

TableB2 Results of Curve Fitting of High-Resolution XPS Spectra for the O1s Region of TiO_2 Thin Films.

3. *Photodegradation of NO by TiO_2 synthesized by LPD method*

The photocatalytic activity of TiO_2 thin films was evaluated by the photocatalytic degradation of NO in the gaseous phase. Under dark conditions, the concentration of NO did not change (for every measurement) using various TiO_2 thin films. UV illumination in the absence of TiO_2 films did not also result in the removal of NO. Therefore, the presence of both UV illumination and TiO_2 films are necessary for the effective degradation of NO. These results also suggested that the degradation removal of NO in the gaseous phase was caused by photocatalytic reactions on the surface of TiO_2 thin films under UV illumination. Similar results were obtained using TiO_2 (Degussa P25) as previously reported.

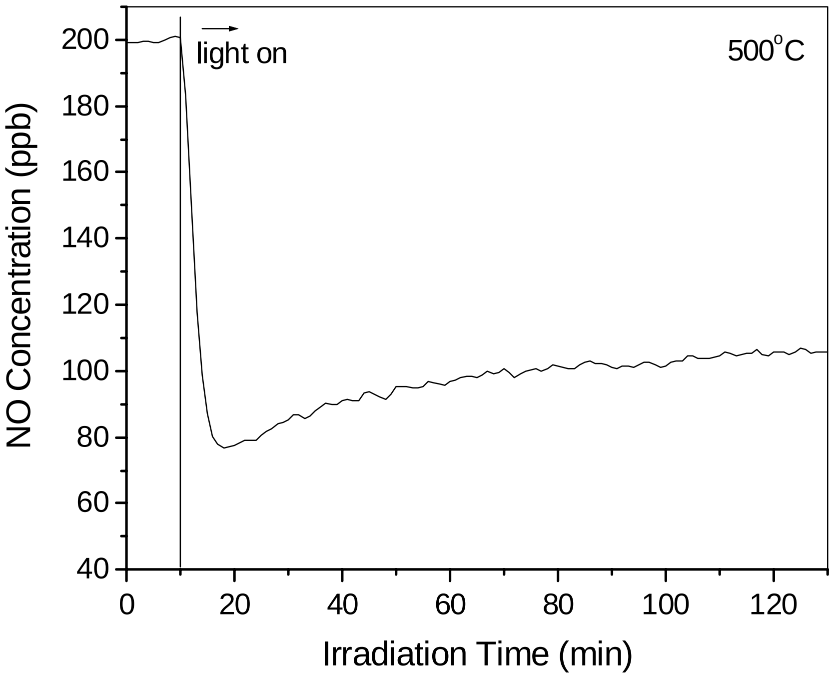

Figure B8 The photodegradation of NO for the TiO_2 thin film sample calcinated at 500°C. Experimental conditions: residence time 3.7 min, humidity levels 2,200 ppmv, 200 ppb NO.

Fig. B8 shows the photodegradation of 200 ppb NO for the TiO_2 thin film calcinated at 500°C. Prior to UV illumination, the adsorption and desorption had reached equilibrium. When UV lamp was turned on, the photodegradation reaction of NO was initiated. The concentration of NO dropped rapidly in the first 10 min and reached the lowest value of 76 ppb. After that, the concentration of NO increased slowly with increasing irradiation time, which was ascribed to the accumulation of a small amount of HNO_3 on the surface of the films, leading to the deactivation of TiO_2 thin films (Ibusuki and Yakeuchi, 1994). After 120 min, the concentration of NO steadily reached a photo-steady-state concentration of 105 ppb. The photodegradation profile is similar to that of using TiO_2 (Degussa P25) as the photocatalyst.

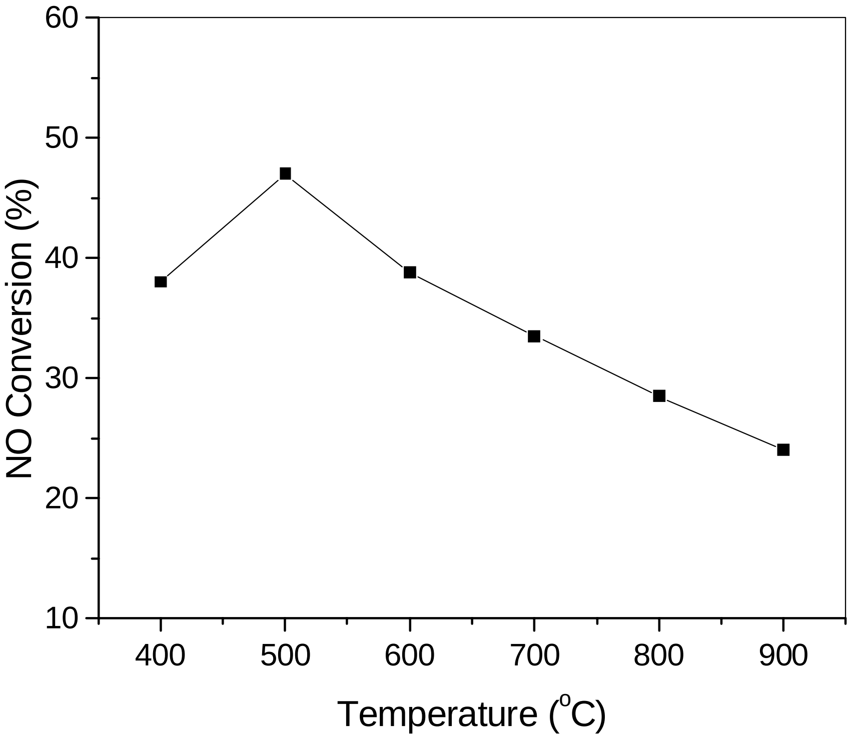

Figure B9 The removals of NO for the TiO_2 thin films calcinated at different calcination temperatures. Experimental conditions: residence time 3.7 min, humidity levels 2,200 ppmv, 200 ppb NO.

Fig. B9 shows the effects of calcination temperatures on the removal of NO for the TiO_2 films. There was no photocatalytic activity (or negligible) for the TiO_2 thin films when the calcination temperatures were below 400°C, which is due to the fact that the thin films were composed of amorphous TiO_2. At 400°C, the film showed obvious photocatalytic activity. With increasing calcination temperature, the photocatalytic activity of thin films increased obviously and reached a maximum value at 500°C. Then the photocatalytic activity steadily decreased with a further increase in calcination temperatures. At 900°C, the film showed the lowest photoreaction activity.

Under UV irradiation, photo-generated electrons and holes are produced in the conduction and valence bands of TiO_2, respectively.

$$TiO_2 + h\nu \longrightarrow h^+ + e^- \qquad (B.7)$$

The Ti^{4+} and O^{2-} sites in the TiO_2 lattice can trap the photo-generated electrons and holes, respectively (Yu et al., 2003; Gratzel and Howe, 1990). Meanwhile, the Fe^{3+} in the TiO_2 thin films can act not only as the trap sites for photo-generated electrons but also as trap sites for photo-generated holes (Gratzel and Howe, 1990; Litter and Navio, 1996; Sclafani et al., 1991; Soria et al., 1991; Choi et al., 1994).

$$Ti^{4+} + e^- \longrightarrow Ti^{3+} \qquad (B.8)$$

$$O^{2-} + h^+ \longrightarrow O^- \qquad (B.9)$$

$$Fe^{3+} + e^- \longrightarrow Fe^{2+} \qquad (B.10)$$

$$Fe^{3+} + h^+ \longrightarrow Fe^{4+} \qquad (B.11)$$

When an electron is excited from the valence band to the conduction band, the photo-generated free carrier will migrate to the surface of TiO_2 thin film. During the migration, there exists a multiple release-migration process for the free carrier. The photo-generated free carriers can be transferred between the different atoms (Litter and Navio, 1996; Choi et al., 1994). As for the Fe-doped TiO_2 thin film, except the intrinsic transferring process (as in the un-doped TiO_2), there also exist other release-migration processes at the Fe^{3+} sites for the photo-generated electrons and holes (Litter and Navio, 1996; Choi et al., 1994).

(*electron and hole pairs release and migration*)

$$Fe^{2+} + Ti^{4+} \rightleftharpoons Fe^{3+} + Ti^{3+} \qquad \text{(B.12)}$$

$$Fe^{4+} + O^{2-} \rightleftharpoons Fe^{3+} + O^{-} \qquad \text{(B.13)}$$

During the migration of free carriers from the internal onto the surface of TiO_2 thin films, the following recombination processes will also take place (Litter and Navio, 1996; Zhu et al., 2001).

(*electron and hole pairs recombination*)

$$Fe^{2+} + h^{+} \longrightarrow Fe^{3+} \qquad \text{(B.14)}$$

$$Fe^{4+} + e^{-} \longrightarrow Fe^{3+} \qquad \text{(B.15)}$$

$$Fe^{4+} + Fe^{2+} \longrightarrow 2Fe^{3+} \qquad \text{(B.16)}$$

When photo-generated electrons and holes migrate to the surface of TiO_2 films, they will initiate the following interfacial reactions.

(*electron and hole pairs interfacial reaction*)

$O_2 + e^- \longrightarrow O_2^-$ (B.17)

$OH^- + h^+ \longrightarrow OH\bullet$ (B.18)

The produced hydroxyl radical groups will initiate the photo-degradation reactions of NO. An increase in either the migration rate of charge carries or the interfacial electron-transfer rate constant is expected to reduce the recombination rate and results in higher quantum efficiencies. According to the viewpoint of crystal field theory, Fe^{4+} and Fe^{2+} ions are relatively unstable as compared to Fe^{3+} ions, which have half-filled d orbits (d^5) (Yu et al., 2003; Choi et al., 1994). Moreover, the energy levels of Fe^{3+}/Fe^{2+} and Fe^{4+}/Fe^{3+} are very close to the conduction band and valence band of TiO_2, respectively (Litter and Navio, 1996; Mizushima et al., 1979). Therefore, there is a tendency for the transfer of the trapped charges from Fe^{4+} and Fe^{2+} to the interface to initiate the following reactions (Yu et al., 2003; Choi et al., 1994):

$Fe^{4+} + OH^- \rightarrow Fe^{3+} + OH\bullet$ hole release (B.19)

$Fe^{2+} + O_2 \rightarrow Fe^{3+} + O_2^-$ electron release (B.20)

As a result, the increase in Fe^{3+} concentration in the film calcinated at 500°C is responsible for an enhancement in its photocatalytic activity. The PL results further confirmed that the sample calcinated at 500°C possessed the lowest recombination rate, which is due to not only better crystallization (compared to the samples calcinated at below 500°C), but also the increase in the amount Fe^{3+} ions.

Many investigations have shown that the photocatalytic activity of Fe-doped TiO_2 was strongly dependent on the dopant concentration, and more Fe^{3+} amount resulted in the increase of recombination rate of photo-generated electrons and holes and decrease of photocatalytic activity (Gratzel and Howe, 1990; Navio et al., 1991). When the Fe^{3+} concentration exceeded an optimal dopant concentration, the Fe^{3+} ions steadily became the recombination centers of photo-generated electrons and holes. This is ascribed to the fact that more Fe^{3+} sites would trap more photo-generated electrons and holes, but the trapped free carrier pairs easily recombined through quantum tunneling (Zhang et al., 1998). Moreover, when the amount of Fe^{3+} was large, there were more Fe^{3+} activity sites in the thin films, resulting in the shorter transferring distance between the two activity sites. Therefore, the chance of multiple trappings increased for a free carrier and the transferring time of free carriers became longer, leading to the increase of recombination rate. It is clear that the more the Fe^{3+} in the samples, the easier the reactions of recombination (equations B.14-B.16) happens.

Maruska et al. (1979) attributed the differences in photocatalytic activity between Fe^{3+}/TiO_2 and Cr^{3+}/TiO_2 to the different diffusion lengths of free carriers. They concluded that the diffusion length was longer for Fe^{3+}/TiO_2 than Cr^{3+}/TiO_2, which resulted in the higher photoactivity for the Fe^{3+}/TiO_2 sample. Thus, an optimal Fe^{3+} dopant concentration should be expected to exist in this case. Thus, it is not surprising that the photocatalytic activity of the sample decreased at 700^{o}C as compared with at 500^{o}C due to the increase of the Fe^{3+} dopant concentration, thought the films show better crystallization at 700^{o}C than at 500^{o}C. At 900^{o}C, the film showed the lowest photocatalytic activity, which is attributed to the results of the further increase of Fe^{3+} concentration, the phase transformation of anatase to rutile and the sintering and growth of TiO_2 crystallite (Yu et al., 2003).

3. Summary

By LPD method, the dense titania thin films could be deposited on stainless steel substrates. The as-prepared TiO_2 thin films contained not only Ti and O elements, but also a small amount of F, N and Fe elements. The F and N elements come from the precursor solution and their amount decreased with increasing calcination temperature. At 500^{o}C, the F element completely disappeared. The

Fe^{3+} in the TiO_2 thin films was divided into two contributions. One was from the $[FeF_{6-n}(OH)_n]^{3-}$ ions in the treatment solution, which was formed by a reaction between treatment solution and stainless steel substrate. The other was attributed to the diffusion of Fe element from the surface of stainless steel substrate into the thin films during calcination at 500°C or a higher temperature.

The photocatalytic activity of TiO_2 thin films deposited on stainless steel strongly depended on calcination temperature. When calcination temperature was below 400°C, there was no photocatalytic activity observed because the TiO_2 thin film was composed of amorphous TiO_2 or the amount of anatase TiO_2 in the film was too low. With increasing calcination temperature, the photocatalytic activity increased due to the enhancement of crystallization of anatase and the increase of Fe^{3+} concentration in the thin film. At 500°C, the film showed the highest photocatalytic activity. This was ascribed to the fact that an optimal Fe^{3+} concentration was obtained in the film, which effectually reduced the recombination of photogenerated free carriers. At 700°C, the photocatalytic activity of the film decreased. This was due to the fact that the increase of Fe^{3+} content in the film due to the diffusion of Fe^{3+} ions from the surface of stainless steel, which exceeded an optimal Fe^{3+} dopant concentration, and Fe^{3+} ions steadily became recombination centers of photo-generated electrons and holes.

At 900^{o}C, the TiO_2 thin film showed the lowest photocatalytic activity. This is attributed to the results of the further increase of Fe^{3+} concentration, the phase transformation from the anatase to rutile and the sintering and growth of TiO_2 crystallites.